

Electronic Thesis and Dissertation Repository

---

8-16-2012 12:00 AM

## Solar and Visible Light Driven Photocatalysis for Sacrificial Hydrogen Generation and Water Detoxification with Chemically Modified TiO<sub>2</sub>

Pankaj Chowdhury  
*The University of Western Ontario*

Supervisor

Dr. Ajay K. Ray  
*The University of Western Ontario* Joint Supervisor

Dr. Hassan Gomaa  
*The University of Western Ontario*

Graduate Program in Chemical and Biochemical Engineering

A thesis submitted in partial fulfillment of the requirements for the degree in Doctor of Philosophy

© Pankaj Chowdhury 2012

Follow this and additional works at: <https://ir.lib.uwo.ca/etd>

 Part of the [Catalysis and Reaction Engineering Commons](#), and the [Environmental Engineering Commons](#)

---

### Recommended Citation

Chowdhury, Pankaj, "Solar and Visible Light Driven Photocatalysis for Sacrificial Hydrogen Generation and Water Detoxification with Chemically Modified TiO<sub>2</sub>" (2012). *Electronic Thesis and Dissertation Repository*. 702.

<https://ir.lib.uwo.ca/etd/702>

This Dissertation/Thesis is brought to you for free and open access by Scholarship@Western. It has been accepted for inclusion in Electronic Thesis and Dissertation Repository by an authorized administrator of Scholarship@Western. For more information, please contact [wlsadmin@uwo.ca](mailto:wlsadmin@uwo.ca).

**SOLAR AND VISIBLE LIGHT DRIVEN PHOTOCATALYSIS FOR SACRIFICIAL  
HYDROGEN GENERATION AND WATER DETOXIFICATION WITH  
CHEMICALLY MODIFIED TiO<sub>2</sub>**

(Spine title: **Application of Solar and Visible Light Driven Photocatalysis**)

(Thesis format: Integrated Article)

by

**Pankaj Chowdhury** B.Tech. M.Tech.

Graduate Program in Engineering Science

**Department of Chemical and Biochemical Engineering**

A thesis submitted in partial fulfillment  
of the requirements for the degree of  
**Doctor of Philosophy**

The School of Graduate and Postdoctoral Studies  
The University of Western Ontario  
London, Ontario, Canada

© Pankaj Chowdhury 2012

**CERTIFICATE OF EXAMINATION**

Supervisors

\_\_\_\_\_  
Dr. Ajay K. Ray

\_\_\_\_\_  
Dr. Hassan Gomaa

Supervisory Committee

\_\_\_\_\_  
Dr. Hugo deLasa

\_\_\_\_\_  
Dr. Amarjeet Bassi

Examiners

\_\_\_\_\_  
Dr. Hugo deLasa

\_\_\_\_\_  
Dr. Lars Rehmann

\_\_\_\_\_  
Dr. Anand V. Singh

\_\_\_\_\_  
Dr. Ali Elkamel

The thesis by

**Pankaj Chowdhury**

entitled:

**SOLAR AND VISIBLE LIGHT DRIVEN PHOTOCATALYSIS FOR SACRIFICIAL  
HYDROGEN GENERATION AND WATER DETOXIFICATION WITH  
CHEMICALLY MODIFIED TiO<sub>2</sub>**

is accepted in partial fulfillment of the  
requirements for the degree of  
Doctor of Philosophy

\_\_\_\_\_  
Date

\_\_\_\_\_  
Chair of the Thesis Examination Board

## Abstract

Photocatalysis is a recognized approach where light energy is employed to excite the semiconductor material producing electron/hole pair which eventually involves in the detoxification of pollutants (in water or air) and water splitting. Existing photocatalysts suffer from poor activity or no activity in visible light irradiation which restricts them from solar light utilization. This work is focused on two key applications of photocatalysis (i) sacrificial hydrogen generation, and (ii) phenol degradation in visible and/or solar light.

Platinum was loaded on TiO<sub>2</sub> photocatalyst by solar photo-deposition method. Eosin Y dye was used as a sensitizer for sensitization of platinum loaded TiO<sub>2</sub> photocatalyst. The photocatalyst was irradiated from the top with a solar simulator. The light source was equipped with AM 1.5 G as well as a 420 nm cutoff filter to remove all the UV light.

A factorial design at two levels and four factors has been carried out in order to investigate the potential for hydrogen generation using Eosin Y-sensitized TiO<sub>2</sub>/Pt catalyst under visible solar light in presence of triethanolamine as electron donor. Experimental data were analyzed using both “Pareto analysis” as well as conventional regression analysis techniques. A regression function was proposed that satisfactorily predicts hydrogen generation as a function of various operating parameters.

Later, the photocatalytic behavior of the eosin Y-sensitized photocatalyst was studied in solar-UV (300-388 nm), solar-visible (420-650 nm) and full solar spectrum (300-650 nm) to explore the optimum reaction conditions such as (i) light intensity (100 mW cm<sup>-2</sup>), (ii) solution pH (7.0), (iii) platinum content (wt %) on TiO<sub>2</sub> (0.25 %), (iv) mass of eosin Y-TiO<sub>2</sub>/Pt (1-1.3 g L<sup>-1</sup>), (v) concentration of triethanolamine (0.25 M), and (vi) mass ratio of eosin Y to TiO<sub>2</sub>/Pt (1:10). The reaction mechanisms were different in solar and visible lights, although in both cases formaldehyde was detected as an intermediate product.

Studies in a pulsating flow reactor showed positive effects of pre-sonication, increased flow rate and bi-directional mixing mode in solar hydrogen generation.

A detailed study on the photocatalytic behavior of formaldehyde for sacrificial hydrogen generation was performed for better understanding of the process. Photocatalytic hydrogen generation from formaldehyde was influenced by solution pH, platinum content (wt %) on TiO<sub>2</sub>, catalyst concentration, light intensity, and initial formaldehyde concentration.

A Langmuir-type model was well fitted with the experimental data for photocatalytic hydrogen generation from both triethanolamine and formaldehyde as sacrificial agents.

Apparent quantum yield (QY) was much higher for UV light driven hydrogen generation. In solar and visible light the QYs were a function of the light intensity and the wavelength range considered for the calculation.

Phenol degradation with eosin Y-sensitized TiO<sub>2</sub>/Pt photocatalyst under solar-visible light was performed with triethanolamine as electron donor. About 93 % degradation of 40 ppm phenol solution was achieved within 90 minutes using Eosin Y-TiO<sub>2</sub>/Pt photocatalyst at optimum conditions (pH = 7.0, catalyst loading = 0.8 g L<sup>-1</sup>, triethanolamine concentration = 0.2 M, 0.5 % Pt loading on TiO<sub>2</sub>, visible solar light of 100 mW cm<sup>-2</sup>). Kinetic rate constant and adsorption equilibrium constant were determined and a Langmuir-Hinshelwood type equation was proposed to describe phenol degradation on TiO<sub>2</sub> at different visible light intensities. The model equation predicts experimental results quite well.

**Keywords:**

Dye, sensitization, solar, visible, hydrogen, sacrificial, TiO<sub>2</sub>, phenol, photoreactor, eosin Y, triethanolamine, formaldehyde.

## Co-Authorship Statement

Chapter 2 includes the work that is in progress for submission to “Chemical Reviews”. Chapter 3 and 6 include the work that has been published in the following articles. Chapter 4 and 5 incorporate the work those are in progress for submission to “Chemical Engineering Science” and “Industrial & Engineering Chemistry Research” respectively.

Chapter 2: Chowdhury, P.; Goma, H.; Ray, A. K.\* , A version of this chapter is in progress for submission to *Chemical Reviews*.

Chapter 3: Chowdhury, P.; Goma, H.; Ray, A. K.\* , Factorial design analysis for dye-sensitized hydrogen generation from water. *International Journal of Hydrogen Energy* **2011**, 36, (21), 13442-13451. Reproduced with permission from Elsevier.

Chapter 4: Chowdhury, P.; Housyn, M.; Goma, H.; Ray, A. K.\* , A version of this chapter is in progress for submission to *Chemical Engineering Science*.

Chapter 5: Chowdhury, P.; Ghodsieh, M.; Ray, M.; Ray, A. K.\* , A version of this chapter is in progress for submission to *Industrial & Engineering Chemistry Research*.

Chapter 6: Chowdhury, P.; Moreira, J.; Goma, H.; Ray, A. K.\* , Visible-solar-light-driven photocatalytic degradation of phenol with dye-sensitized TiO<sub>2</sub>: parametric and kinetic study. *Industrial & Engineering Chemistry Research* **2012**, 51, (12), 4523-4532. Reproduced with permission from American Chemical Society.

For each of these articles, the original draft of the manuscript was prepared by Pankaj Chowdhury, followed by revisions performed by Dr. Hassan Goma, Dr. Ajay K. Ray (corresponding author\*) and Pankaj Chowdhury.

## Acknowledgements

I express my deepest gratitude to a number of people, without whom it would have not been possible for me to undertake this rigorous academic program during my 4 years at Western.

I sincerely thank my thesis supervisors Dr Ajay K. Ray and Dr Hassan Gomaa for their continuous support, encouragement, and insightful guidance during the course of my doctoral studies at this University. I consider myself immensely fortunate and privileged to be able to work with them. I thank you Dr Ray and Dr Gomaa for your reasoning and constructive criticisms that motivated me to delve deeper into my research. Your contribution has made me an independent thinker and researcher.

I am indebted to you Dr Ray for your unconditional support in my personal life too. Working with you has been a life-time experience that I will continue to cherish for many years to come.

I would like to thank Natural Science and Engineering Research Council of Canada (NSERC), Western Engineering and UWO for providing me the financial support.

I am also thankful to my committee members, Dr Hugo deLasa and Dr Amarjeet Bassi for their guidance and insightful comments. I would like to thank you Dr deLasa for letting me use your laboratory facilities.

I thank Dr Mita Ray for her helpful comments in understanding and addressing several issues while I was working on the OCE project. I also thank you for all your help and moral support during the stressful periods of my life.

My thanks to Pastor Solano, Jose Munoz, Souheil Afara, Ying Zhang, and Fate Hashemi, for their technical support in my experimental work. I am also thankful to Yan Zhang and Enrique Solaices and for their guidance during the initial stage of my research.

I would like to thank my friends and colleagues Jesus, Ghodsieh, Noshin, Nil, and Housyn. Working with you in different projects has been a pleasurable experience.

I thank Bhavik, Gureet, Krupal and Anu for being such good friends and helping me both professionally and personally.

My sincere thanks to my dear friend Shital for motivating me towards pursuing an academic career. I am grateful to Anindo\_da for his unconditional support during the critical phase of my life. I consider myself fortunate to have Puskar, Rupma, and Anindya as my best friends forever. I thank you for being beside me in every step of my personal life.

I deeply thank my parents for their unconditional love and support, without which I would not have been able to succeed in this endeavor. I also thank my sisters, brother, grandmother, uncle and aunt for their encouragement. Finally I thank my wife Sharmistha for her continued support during the most difficult phase of my PhD.



## Dedication

I dedicate my dissertation to my beloved parents for all their love, care, and support throughout my life. Thank you Ma and Baba for being with me in every step of my life. Without you I would not have been able to succeed in my career.

# Table of Contents

<b>CERTIFICATE OF EXAMINATION</b> .....	ii
Abstract .....	iii
Co-Authorship Statement.....	v
Acknowledgements.....	vi
Dedication.....	viii
Table of Contents .....	ix
List of Tables .....	xvii
List of Figures .....	xix
Nomenclature .....	xxvi
Chapter 1 .....	1
1 General Introduction .....	1
1.1 Background & Motivation .....	1
1.1.1 Future fuel – hydrogen.....	1
1.1.2 Water pollution and water treatment.....	4
1.1.3 Heterogeneous photocatalysis – a single step solution for future fuel and water treatment.....	6
1.1.4 Solar energy – an abundant source .....	8
1.2 Problem Statement .....	10

1.3	Research Objectives .....	11
1.4	Thesis Overview.....	12
1.5	References .....	14
Chapter 2.....		18
2	Dye-Sensitized Photocatalyst - a Breakthrough in Green Energy and Environmental Detoxification .....	18
2.1	Introduction .....	18
2.2	Dye Sensitization.....	19
2.2.1	Theory of dye sensitization.....	19
2.2.2	Dye sensitization methodology.....	24
2.3	Incorporation of Noble Metal Co-catalyst on to Semiconductor .....	26
2.3.1	Platinum deposition methods.....	27
2.4	Application of Dye-Sensitized Photocatalyst for Water and Wastewater Detoxification .....	31
2.4.1	Aliphatic chlorinated hydrocarbon .....	32
2.4.2	Aromatic compounds .....	37
2.5	Application of Dye-Sensitized Photocatalyst for Hydrogen Generation .....	45
2.5.1	Basic requirement for hydrogen generation in visible light.....	45
2.5.2	Dye-sensitized photocatalytic hydrogen generation mechanism.....	46
2.5.3	Sensitization with different dyes for photocatalytic hydrogen generation ..	48

2.5.4	Effect of different parameters on the photocatalytic activity for hydrogen generation.....	51
2.6	Conclusions .....	56
2.7	References .....	58
Chapter 3.....		67
3	Factorial Design Analysis for Dye-sensitized Hydrogen Generation from Water ...	67
3.1	Introduction .....	67
3.2	Methodology .....	69
3.2.1	Experimental.....	69
3.2.2	Experimental design.....	71
3.3	Results and Discussion.....	72
3.3.1	Effect of solution pH.....	75
3.3.2	Pareto plot.....	78
3.3.3	Main effect plot (Set 2).....	79
3.3.4	Interaction effects plot (Set 2).....	82
3.3.5	Regression analysis.....	82
3.3.6	Prediction of hydrogen generation.....	83
3.3.7	Normal probability plot of residuals .....	85
3.4	Conclusions .....	86

3.5	References .....	87
Chapter 4.....		90
4	Sacrificial Hydrogen Generation from Aqueous Triethanolamine with Eosin Y-Sensitized TiO <sub>2</sub> /Pt Photocatalyst, in UV, Visible and Solar Light Irradiation .....	90
4.1	Introduction .....	90
4.2	Experimental .....	92
4.2.1	Reagents .....	92
4.2.2	Preparation of dye-sensitized photocatalyst.....	92
4.2.3	Photocatalyst characterization techniques .....	93
4.2.4	Reactor configuration for photocatalytic hydrogen generation .....	93
4.3	Results and Discussion.....	95
4.3.1	Photocatalyst characterization results .....	95
4.3.2	Sacrificial hydrogen generation in visible and solar light irradiation-parametric study.....	100
4.3.3	Discussion of reaction mechanism in visible and solar light irradiation ..	108
4.3.4	Hydrogen generation kinetics .....	115
4.3.5	Dependence of hydrogen evolution on light intensity .....	117
4.3.6	Photoluminescence (PL) study under UV, visible and solar light .....	119
4.3.7	Apparent quantum yield in UV, visible, and solar light .....	120
4.3.8	EY-sensitized hydrogen generation in flow-reactor in solar light .....	122

4.3.9	Modification of flow reactor by hydrodynamics study.....	128
4.4	Conclusions .....	130
4.5	References .....	132
Chapter 5	.....	137
5	Sacrificial Hydrogen Generation from Formaldehyde with TiO <sub>2</sub> /Pt Photocatalyst in Solar Radiation.....	137
5.1	Introduction .....	137
5.2	Experimental .....	139
5.2.1	Reagents.....	139
5.2.2	Preparation and characterization of photocatalyst .....	139
5.2.3	Light sources.....	140
5.2.4	Photocatalytic hydrogen generation.....	140
5.3	Results and Discussion.....	141
5.3.1	Characterization of TiO <sub>2</sub> /Pt photocatalyst .....	141
5.3.2	Effect of platinum deposition on the photocatalytic activity of TiO <sub>2</sub> .....	143
5.3.3	Effect of catalyst loading .....	144
5.3.4	Effect of initial pH of formaldehyde solution.....	146
5.3.5	Effect of initial concentration of formaldehyde.....	149
5.3.6	Effect of light intensity .....	150

5.4	Reaction Mechanism .....	151
5.5	Apparent Quantum Yield .....	153
5.6	Conclusions .....	154
5.7	References .....	155
Chapter 6.....		158
6	Visible-Solar-Light-Driven Photocatalytic Degradation of Phenol with Dye-Sensitized TiO <sub>2</sub> : Parametric and Kinetic Study .....	158
6.1	Introduction .....	158
6.2	Experimental Section .....	160
6.2.1	Materials .....	160
6.2.2	Instruments.....	160
6.2.3	Synthesis of eosin Y-sensitized TiO <sub>2</sub> /Pt photocatalyst.....	161
6.2.4	Photocatalytic phenol degradation.....	162
6.3	Catalyst Characterization .....	163
6.3.1	Brunauer–Emmett–Teller (BET) method.....	163
6.3.2	X-ray diffraction (XRD) .....	164
6.3.3	Energy-dispersive X-ray (EDX) and Transmission and electron microscopy (TEM) .....	165
6.3.4	Diffuse reflectance spectra (DRS) .....	166
6.4	Reaction Mechanism and Kinetic Rate Expression .....	167

6.4.1	Reaction mechanism .....	167
6.4.2	Reaction kinetics .....	170
6.5	Parametric Study .....	171
6.5.1	Effect of mass of TiO <sub>2</sub> .....	171
6.5.2	Effect of Pt content on TiO <sub>2</sub> .....	173
6.5.3	Effect of initial triethanolamine (TEOA) concentration.....	174
6.5.4	Effect of initial concentration of phenol .....	175
6.5.5	Effect of pH.....	177
6.5.6	Effect of light intensity .....	178
6.6	Phenol Degradation Kinetics.....	179
6.7	Conclusions .....	182
6.8	References .....	183
Chapter 7	.....	190
7	Conclusions and Recommendations .....	190
7.1	Major Contributions .....	190
7.2	Other Key Contributions .....	192
7.3	Recommendations for Future Work.....	194
APPENDIX	.....	196
A.	Appendix A: Dye Absorption Spectra .....	196



B. Appendix B: Calibration Plot –H <sub>2</sub> Gas .....	197
C. Appendix C: Details of Photoreactors .....	199
D. Appendix D: Eosin Y Degradation under Different Light Sources .....	202
E. Appendix E: Light Spectra of Solar Simulator .....	205
F. Appendix F: PL Spectra under UV, Visible and Solar light.....	206
G. Appendix G: Flow Reactor Modifications.....	207
H. Appendix H: Calibration Curves for Phenol.....	209
I. Appendix I: Copyright Informations .....	210
Chapter-1 copyright permission:.....	210
Chapter-2 copyright permission:.....	211
Chapter-3 copyright permission:.....	217
Chapter-6 copyright permission:.....	218
Curriculum Vitae .....	219

## List of Tables

Table 1.1 Different routes for hydrogen production.....	3
Table 2.1 Natural extracts used for dye-sensitization.....	25
Table 2.2. Exposure and regulatory limits of some organic pollutants (adapted from ATSDR, 1997, 2003, 2005, 2008, 1999).....	31
Table 2.3. Dye-sensitized photodegradation of organic compounds.....	39
Table 2.4 Dye-sensitized photodegradation of organic dyes.....	43
Table 2.5. Dye-sensitized photocatalytic hydrogen generation.....	53
Table 3.1 Coded and uncoded values of the factors for Set 1.....	72
Table 3.2 Coded and uncoded values of the factors for Set 2.....	73
Table 3.3 Uncoded design table for factors and response for Set 1.....	74
Table 3.4 Uncoded design table for factors and response for Set 2.....	75
Table 3.5 Estimated effects and coefficients for hydrogen generation <sup>a</sup> .....	83
Table 3.6 Experimental data points for validation.....	85
Table 4.1 Activity of TiO <sub>2</sub> and TiO <sub>2</sub> based photocatalyst for sacrificial H <sub>2</sub> generation..	100
Table 4.2 Comparison of formaldehyde formation with different catalyst in visible and solar light*.....	112
Table 4.3 Power law model constants and R <sup>2</sup> values.....	118
Table 4.4 Apparent quantum yield in UV, visible and solar light.....	121
Table 5.1 Effect of Pt deposition on TiO <sub>2</sub> P25.....	143

Table 6.1 Kinetics constant values.....	180
Table 6.2 Correlation coefficient values.....	180
Table 6.3 Comparison between experimental phenol concentration and model prediction values at 100 mWcm <sup>-2</sup> .....	181

## List of Figures

Figure 1.1 Global energy systems transition, 1850–2150. Reprinted with permission from Dunn. <sup>1</sup> (Copyright 2002 Elsevier) .....	2
Figure 1.2 Levels of wastewater treatment (Metcalf and Eddy <sup>12</sup> ). .....	5
Figure 1.3 Direct and global radiation .....	8
Figure 1.4 Diagram for air mass and solar components (adapted from Galvez et al. <sup>27</sup> ). ....	9
Figure 2.1 Dye sensitization principles for n-type semiconductor (adapted from Kalyanasundaram and Gratzel <sup>3</sup> ). .....	20
Figure 2.2 Possible binding mode of TiO <sub>2</sub> surface and –COOH. Reprinted with permission from Galoppini. <sup>8</sup> (Copyright 2004 Elsevier). .....	22
Figure 2.3 Energy level diagram of anodic dye sensitization process .....	23
Figure 2.4 Dye-sensitized photocatalytic H <sub>2</sub> generation from water (adapted from Chen et al. <sup>80</sup> ). .....	47
Figure 2.5 Scheme for visible light-driven hydrogen generation by dye-sensitized TiO <sub>2</sub> /Pt .....	48
Figure 3.1 Experimental Setup: Gastight photo-reactor for dye-sensitized hydrogen generation.....	71
Figure 3.2 Main effect plot for pH, dye and electron donor for % increment in hydrogen generation (Set 1).....	77
Figure 3.3 Interaction effect plot for pH, dye, and electron donor for % increment in hydrogen generation (Set 1).....	78

Figure 3.4 Pareto chart for standardized effects for hydrogen generation (Set 2) (Response is % increment in hydrogen generation, $\alpha=0.05$ ) .....	79
Figure 3.5 Main effects plot for Pt, dye, electron donor and irradiation time for % increment in hydrogen generation (Set 2).....	80
Figure 3.6 Interaction effect plot for Pt, dye, electron donor and irradiation time for % increment in hydrogen generation (Set 2).....	81
Figure 3.7 Percent increment in hydrogen generation: Comparison between experimental including independent validation data and model predicted value .....	84
Figure 3.8 Normal probability plot of the residuals for % increment in hydrogen generation.....	86
Figure 4.1 Flow reactor for sacrificial hydrogen generation. ....	94
Figure 4.2 Diffuse reflectance spectra of TiO <sub>2</sub> and EY-sensitized TiO <sub>2</sub> /Pt photocatalysts .....	95
Figure 4.3 N <sub>2</sub> adsorption-desorption isotherm (BJH poresize distribution) of EY- sensitized TiO <sub>2</sub> /Pt photocatalyst .....	96
Figure 4.4 XRD patterns of TiO <sub>2</sub> and EY-TiO <sub>2</sub> /Pt photocatalysts .....	97
Figure 4.5 FTIR spectrum of Eosin Y, TiO <sub>2</sub> and EY-TiO <sub>2</sub> /Pt.....	98
Figure 4.6 (a) EDX image of EY-TiO <sub>2</sub> /Pt (0.25 %) and EDX elemental area mapping: (b) Ti; (c) O; (d) Pt. ....	99
Figure 4.7 Effect of platinum wt % on photocatalytic hydrogen generation over EY-TiO <sub>2</sub> . (Experimental conditions: [TEOA] = 0.25 M, [EY-TiO <sub>2</sub> /Pt] = 1 g L <sup>-1</sup> , I = 100 mW cm <sup>-2</sup> , pH = 7, N <sub>2</sub> saturated, pre-sonicated, visible - 420 nm cutoff filter). ....	102

Figure 4.8 Effect of photocatalyst mass on hydrogen generation. (Experimental conditions: [TEOA] = 0.25 M, Pt in TiO <sub>2</sub> = 0.25%, I = 100 mW cm <sup>-2</sup> , pH = 7, N <sub>2</sub> saturated, pre-sonicated, visible - 420 nm cutoff filter).....	104
Figure 4.9 Comparison of immobilized and slurry photocatalyst for hydrogen generation in solar light. (Experimental conditions: [TEOA] = 0.25 M, I <sub>solar</sub> = 100 mW cm <sup>-2</sup> , pH = 7, N <sub>2</sub> saturated, pre-sonicated).....	106
Figure 4.10 Effect of EY to TiO <sub>2</sub> /Pt mass ratio on hydrogen generation rate. (Experimental conditions: [TEOA] = 0.25 M, TiO <sub>2</sub> /Pt(0.25%) = 1 g L <sup>-1</sup> , I = 100 mW cm <sup>-2</sup> , pH = 7, N <sub>2</sub> saturated, pre-sonicated, visible - 420 nm cutoff filter).....	107
Figure 4.11 Hydrogen generation in visible light. ....	109
Figure 4.12 Hydrogen generation in solar light. ....	110
Figure 4.13 Formation of formaldehyde in visible and solar light irradiation.....	113
Figure 4.14 H <sub>2</sub> generation and formaldehyde formation in visible light irradiation. (Experimental conditions: TiO <sub>2</sub> /Pt(0.25%) = 1 g L <sup>-1</sup> , [TEOA] = 0.25 M, I <sub>vis</sub> = 100 mW cm <sup>-2</sup> , pH = 7, N <sub>2</sub> saturated, pre-sonicated, visible - 420 nm cutoff filter). ....	114
Figure 4.15 H <sub>2</sub> generation and formaldehyde formation in solar light irradiation. (Experimental conditions: TiO <sub>2</sub> /Pt(0.25%) = 1 g L <sup>-1</sup> , [TEOA] = 0.25 M, I <sub>solar</sub> = 100 mW cm <sup>-2</sup> , pH = 7, N <sub>2</sub> saturated, pre-sonicated).....	115
Figure 4.16 Rate of hydrogen generation as a function of initial concentration of TEOA. (Experimental conditions: TiO <sub>2</sub> /Pt(0.25%) = 1 g L <sup>-1</sup> , E/T = 0.1, I <sub>vis</sub> = 100 mW cm <sup>-2</sup> , pH = 7, N <sub>2</sub> saturated, pre-sonicated, visible - 420 nm cutoff filter).....	116
Figure 4.17 Dependence of H <sub>2</sub> on light intensity of UV, visible and solar light. (Experimental conditions: TiO <sub>2</sub> /Pt(0.25%) = 1 g L <sup>-1</sup> , E/T = 0.05, I = 100 mW cm <sup>-2</sup> , [TEOA] = 0.25 M, pH = 7, N <sub>2</sub> saturated, pre-sonicated, visible - 420 nm cutoff filter, UV – long pass filter). ....	117

Figure 4.18 Comparison of PL for UV, vis and solar light irradiation. (Experimental conditions: $\text{TiO}_2/\text{Pt}$ (0.25%) = 1 g L <sup>-1</sup> , E/T=0.05, I = 50 mW cm <sup>-2</sup> , [TEOA] = 0.25 M, pH = 7, N <sub>2</sub> saturated, pre-sonicated, visible - 420 nm cutoff filter, UV -long pass filter)...	120
Figure 4.19 Effect of sonication on hydrogen generation for uni-directional flow. (Experimental conditions: EY-TiO <sub>2</sub> /Pt (0.25%) = 1 g L <sup>-1</sup> , [TEOA] = 0.25 M, I <sub>solar</sub> = 100 mW cm <sup>-2</sup> , pH = 7, N <sub>2</sub> saturated, flow = 1.62 L min <sup>-1</sup> , x-axis shows residence time inside reactor).....	124
Figure 4.20 Effect of sonication on hydrogen generation for bi-directional flow. (Experimental conditions: EY-TiO <sub>2</sub> /Pt(0.25%) = 1 g L <sup>-1</sup> , [TEOA] = 0.25 M, I <sub>solar</sub> = 100 mW cm <sup>-2</sup> , pH = 7, N <sub>2</sub> saturated, flow = 1.62 L min <sup>-1</sup> , x-axis shows residence time inside reactor).....	125
Figure 4.21 Effect of flow rate on H <sub>2</sub> generation for both uni- and bi-directional mixing. (Experimental conditions: EY-TiO <sub>2</sub> /Pt(0.25%) = 1 g L <sup>-1</sup> , [TEOA] = 0.25 M, I <sub>solar</sub> = 100 mW cm <sup>-2</sup> , pH = 7, N <sub>2</sub> saturated, pre-sonicated).....	126
Figure 4.22 Comparison of H <sub>2</sub> generation rate in batch and flow reactor. (Experimental conditions: EY-TiO <sub>2</sub> /Pt(0.25%) = 1 g L <sup>-1</sup> , [TEOA] = 0.25 M, I <sub>solar</sub> = 100 mW cm <sup>-2</sup> , pH = 7, N <sub>2</sub> saturated, pre-sonicated, batch reactor = 500 rpm, flow reactor = 1.62 L min <sup>-1</sup> )..	127
Figure 4.23 Flow pattern inside the flow reactor.....	129
Figure 5.1 XRD for TiO <sub>2</sub> and TiO <sub>2</sub> /Pt photocatalysts. ....	142
Figure 5.2 DRS for TiO <sub>2</sub> and TiO <sub>2</sub> /Pt photocatalysts. ....	142
Figure 5.3 Hydrogen generation rate versus platinum weight percent on TiO <sub>2</sub> . ....	144
Figure 5.4 Effect of catalyst concentration on the rate of hydrogen generation (r1); rate per unit mass of catalyst (r2). (Experimental conditions: [HCHO] = 0.1332 M, pH 6.7, Pt in TiO <sub>2</sub> = 0.25 %, I <sub>Solar</sub> = 100 mW cm <sup>-2</sup> , N <sub>2</sub> saturated, pre-sonicated).....	146

Figure 5.5 Photocatalytic reaction of formaldehyde on TiO <sub>2</sub> /Pt surface .....	147
Figure 5.6. Effect of initial pH of formaldehyde solution on the rate of hydrogen generation. (Experimental conditions: [HCHO] = 0.1332 M, [TiO <sub>2</sub> /Pt(0.25 %)] = 1 g L <sup>-1</sup> , I <sub>Solar</sub> = 100 mW cm <sup>-2</sup> , N <sub>2</sub> saturated, pre-sonicated).....	148
Figure 5.7. Effect of initial concentration of formaldehyde solution on the rate of hydrogen generation (both experimental rate and Langmuir type model rate). (Experimental conditions: pH 6.7-7.2,[TiO <sub>2</sub> /Pt]=1 g L <sup>-1</sup> , I <sub>Solar</sub> =100 mW cm <sup>-2</sup> , N <sub>2</sub> saturated, pre-sonicated). .....	150
Figure 5.8 Effect of light intensity on the rate of hydrogen generation. (Experimental conditions: [HCHO] = 0.1332 M, pH 6.7, [TiO <sub>2</sub> /Pt (0.25 %)] = 1 g L <sup>-1</sup> , I <sub>Solar</sub> = 100 mW cm <sup>-2</sup> , N <sub>2</sub> saturated, pre-sonicated). .....	151
Figure 6.1 Photo-reactor for phenol degradation .....	162
Figure 6.2 Isotherm plot (BJH pore size distribution) .....	163
Figure 6.3 XRD image for TiO <sub>2</sub> and EY-TiO <sub>2</sub> /Pt catalysts.....	164
Figure 6.4 (a) EDX image for EY-TiO <sub>2</sub> /Pt photocatalysts; (b) TEM image for EY-TiO <sub>2</sub> /Pt photocatalysts.....	165
Figure 6.5 DRS image for TiO <sub>2</sub> and EY-TiO <sub>2</sub> /Pt photocatalysts.....	166
Figure 6.6 Photo-degradation scheme of phenol under UV and visible photons. ....	169
Figure 6.7 Residual concentration vs irradiation time plot for phenol and intermediates. ....	170
Figure 6.8 Initial phenol degradation rate vs catalyst dosage.....	172
Figure 6.9 Residual phenol vs irradiation time plot at different platinum (wt %) on TiO <sub>2</sub> . ....	174



Figure 6.10 Residual phenol vs irradiation time plot at different concentration of TEOA. .....	175
Figure 6.11 Initial phenol conc. vs irradiation time plot.....	176
Figure 6.12 Residual phenol vs irradiation time plot at different solution pH. ....	178
Figure 6.13 Phenol photo-degradation profiles at different irradiation intensities for both experimental and model plots. ....	179
Figure A.1 UV-vis absorption spectrum of $9.65 \times 10^{-3}$ mM Eosin Y in aqueous solution .....	196
Figure B.1 TCD calibration curve for hydrogen.....	197
Figure C.1 Batch and flow reactor configuration under different light sources. ....	199
Figure C.2 Flow reactor for sacrificial hydrogen generation.....	200
Figure C.3 Flow reactor exploded view.....	201
Figure D.1 Eosin Y degradation under solar and visible light. Experimental conditions: [EY]= $3.86 \times 10^{-2}$ mM, I= $100 \text{ mW cm}^{-2}$ , [TEOA]=0.25 M.....	202
Figure D.2 Effect of UV light intensity on Eosin Y degradation. Experimental conditions: [EY]= $7.72 \times 10^{-2}$ mM, [TEOA]=0.25 M. ....	203
Figure D.3 Effect of visible light intensity on Eosin Y degradation. Experimental conditions: [EY]= $7.72 \times 10^{-2}$ mM, [TEOA]=0.25 M. ....	203
Figure D.4 Effect of solar light intensity on Eosin Y degradation. Experimental conditions: [EY]= $7.72 \times 10^{-2}$ mM, [TEOA]=0.25 M. ....	204
Figure E.1 Solar simulator light spectra at different intensities.....	205

Figure F.1 PL spectra EY-TiO<sub>2</sub>/Pt catalyst solution at different solar light intensities showing higher e<sup>-</sup>/h<sup>+</sup> recombination rate at higher light intensities. Experimental conditions: [EY]=7.72 x 10<sup>-2</sup> mM, [TEOA]=0.25 M. EY-TiO<sub>2</sub>/Pt (0.25 %)= 1g L<sup>-1</sup> ..... 206

Figure G.1 Proposed modified flow reactor with baffle. .... 207

Figure G.2 Modified flow reactor with minimum dead zones..... 208

Figure G.3 Particle tracking for modified flow reactor. .... 208

Figure H.1 Calibration curve for aqueous solution of phenol. .... 209

## Nomenclature

$C_0$	initial concentration ( $\text{g L}^{-1}$ )
$\text{Dye}^+$	oxidized form of dye
$e^-$	electron
$e^-_{\text{CB}}$	electron located in the conduction band
EY	eosin Y dye
$(\text{EY})_s$	adsorbed eosin Y on catalyst surface
$\text{EY}^+$	oxidized form of eosin Y dye
$\text{EY}^*$	eosin Y dye in excited state
$\Delta G$	change in Gibb's free energy
$\Delta H$	change in enthalpy
$h^+$	hole
$h^+_{\text{VB}}$	hole left in the valance band
$h$	Plank's constant
$\nu$	frequency ( $\text{s}^{-1}$ )
$I$	radiation intensity ( $\text{mW cm}^{-2}$ )
$k$	reaction rate constant
$K$	adsorption constant

$k_{app}$	apparent kinetic constant
$\lambda$	wavelength of radiation (nm)
$\lambda_{max}$	maximum wavelength at which the maximum fraction of light is adsorbed
$OH^{\bullet}_{ad}$	adsorbed hydroxyl radical
TEOA	triethanolamin
$TEOA^+$	oxidized form of triethanolamin
V	reactor volume
W	mass of catalyst
$\phi_{H_2}$	apparent quantum yield for hydrogen generation

### Acronyms

AM	air mass
ANOVA	analysis of variance
AOP	advanced oxidation process
CB	conduction band
DOE	design of experiment
E:T	eosin Y to $TiO_2/Pt$ mass ratio

# Chapter 1

## 1 General Introduction

### 1.1 Background & Motivation

#### 1.1.1 Future fuel – hydrogen

The world is moving from solid to liquid to gas fuels for future energy sources. The basic idea is decarbonization of the fuel. Coal has the lowest H:C ratio (0.5:1), for LPG the ratio goes up to 2.6:1 and for natural gas the ratio again increases to 4:1. Hydrogen is the fuel having H:C ratio of infinite. Hydrogen is the most abundant element in the universe found in water, life forms and hydrogen fuel.<sup>1</sup> The global energy systems transition is shown in Figure 1.1.

The driving forces for the energy transition towards hydrogen are many, but three major factors are i) growing energy demand, ii) oil scarcity in the near future and iii) risk of climate change. By 2050 world population will be 10 billion and the expected energy demand will be doubled.<sup>2</sup> Coal and oil are promising energy sources but still we need some other energy sources which are more abundant and can make up the future energy demand.

At the beginning stage of oil exploration (1859) the world petroleum supply was approximately 1.8 trillion barrel, and now we are left with only 0.9 trillion barrel petroleum with a current demand of 105 million barrel per day.<sup>2</sup> The fossil fuels are being consumed at a much faster rate than it is produced by the nature.<sup>3</sup> So a huge demand-supply gap is going to be created in the near future for oil.

Again with the declining oil reserve the extraction of the remaining oil will be more complicated considering the economical and technological difficulties, and consequently the energy requirement for obtaining oil will become significantly higher than the energy output from fuel.<sup>2</sup>

Another problem which is pushing the hydrogen transition is climate change. At the beginning of industrial revolution the atmospheric CO<sub>2</sub> level was 270 ppm which rose to 370 ppm during 20<sup>th</sup> century and the current level of CO<sub>2</sub> is 383 ppm. Different climate models suggest that a further increase of CO<sub>2</sub> level beyond 550 ppm would lead to a magnitude of warming equal to that of the cooling seen in the last ice age. So we would have the opportunity to experience a “steam age” in the near future.<sup>1,2</sup>

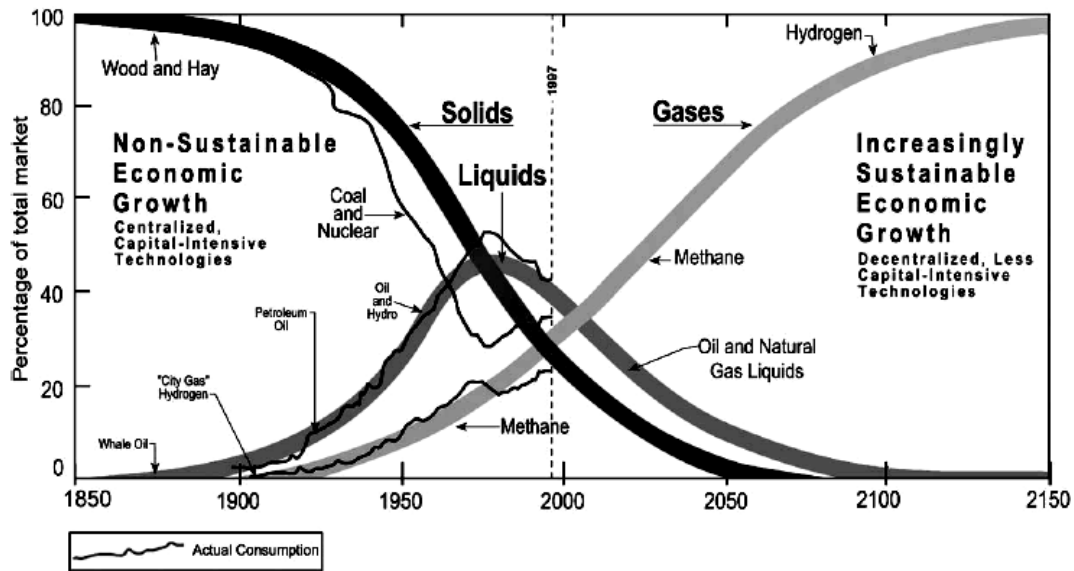


Figure 1.1 Global energy systems transition, 1850–2150. Reprinted with permission from Dunn.<sup>1</sup> (Copyright 2002 Elsevier)

Due to this, the world has progressively favored hydrogen atom over carbon atom. Between 1860 and 1990, the H:C ratio in fuel rose 6-fold. Right now the annual hydrogen production is 400 billion cubic meter. There are several routes for hydrogen production as mentioned in Table 1.1.<sup>1</sup> Among these processes, steam reforming is the most common and least expensive technique used today in oil refineries and in chemical industries, but it is an energy intensive process and contributes to huge amounts of greenhouse gases.

Therefore, the photoelectrochemical or photocatalytic water splitting would be the most promising technology for hydrogen generation from renewable water and sunlight.

**Table 1.1 Different routes for hydrogen production**

<b>Hydrogen production routes</b>	<b>Advantages</b>	<b>Disadvantages</b>
Steam reforming of methane	Least expensive (48 % of world hydrogen produced by this route)	Generation of greenhouse gases.
Gasification of coal	Only competitive with methane reforming where natural gas is expensive.	Generation of CO <sub>2</sub> ; Less efficient.
Gasoline and methanol reforming	Not mentioned.	Requirement of pure oxygen; Generation of more CO <sub>2</sub> than steam reforming.
From biomass	Less expensive raw materials.	Little contribution (4%) towards world H <sub>2</sub> production.
Electrolysis	Cost effective for production of extremely pure hydrogen in small amount.	Electrolysis is very much expensive at large scale.
Solar and wind power based electrolysis	Less expensive than conventional electrolysis.	Still in developing stage.

The unique solution for the problem is to use the abundant solar energy. To make a substantial contribution to the energy supply, solar energy needs to be captured, converted and stored, to overcome the daily cycle and the intermittency of solar radiation. The most fascinating approach for solar energy conversion and storage would be in the form of an energy carrier such as hydrogen. Following the conversion of solar radiation into hydrogen, it can be transported as well as stored for an extended period of time. Hydrogen is a clean energy carrier because the chemical energy stored in the H–H bond is easily released when it reacts with oxygen, producing only water.<sup>4, 5</sup>

### 1.1.2 Water pollution and water treatment

Water is the most precious natural resource in the world embracing over 70 % of the earth surface. In spite of this the accessibility of safe drinking water is a high priority issue for the survival of mankind as well as animals. This is because of the fact that water resources such as rivers, lakes and oceans are being contaminated by human beings through over-use and wastage. This affects natural environment as well as human health. Water pollutants are classified into two main groups namely i) point source (single source), and ii) non-point source (many sources) respectively.<sup>6</sup> Causes of water pollution are many but major sources can be categorized as industrial waste, sewage and wastewater, agricultural waste, oil spills, marine dumping and nuclear wastes. The World Health Organization (W.H.O) reported that in 2008 some 884 million people still relied upon unimproved water sources – 84% of whom were living in rural areas. Many more are surviving by drinking microbiologically unsafe water and experiencing the agony of waterborne diseases including typhoid, hepatitis, and cholera.<sup>7, 8</sup>

The removal of harmful matters from wastewater and detoxification of pollutants in surface water, and groundwater is a key issue in the world. Secondary treatment helps in organic matter decomposition to some extent, but major oxidation process occurs in tertiary treatment where wastewater is disinfected by  $\text{Cl}_2$ ,  $\text{O}_3$  or UV light. There are numerous methods under tertiary treatment which can be classified into biological, chemical or physical oxidation process. Biological oxidations are inexpensive but presence of toxic pollutants creates difficulties during the operation. Treatments of pollutant at high temperature (thermal treatment) are quite successful but not economically feasible. On the other hand, chemical oxidation with the help of several oxidants such as  $\text{H}_2\text{O}_2$ ,  $\text{O}_3$ ,  $\text{Cl}_2$ , and  $\text{ClO}_2$  do not experience such problem, although they could not afford complete mineralization of water pollutants.<sup>9</sup>

Stringent regulations have been set by USEPA over a much broader range of contaminants for wastewater discharge. To comply with those regulations, advanced oxidation processes (AOPs) have been introduced to eliminate different potentially



harmful compounds that could not be effectively removed by conventional treatment processes.<sup>10</sup> These AOPs include  $O_3/UV$ ,  $H_2O_2/UV$ ,  $O_3/H_2O_2/UV$  and  $TiO_2/UV$ .<sup>11</sup> Among the AOPs,  $TiO_2/UV$  based photocatalytic oxidation processes have received great attention in the recent years as an alternative for water detoxification. Common wastewater treatment scheme is shown in Figure 1.2.<sup>12</sup> To make the  $TiO_2$  based photooxidation process economical, solar light can be used as a potential replacement for commercial UV lamps. This again requires modification of  $TiO_2$  and  $TiO_2$  based photocatalysts for utilization of solar visible spectra.

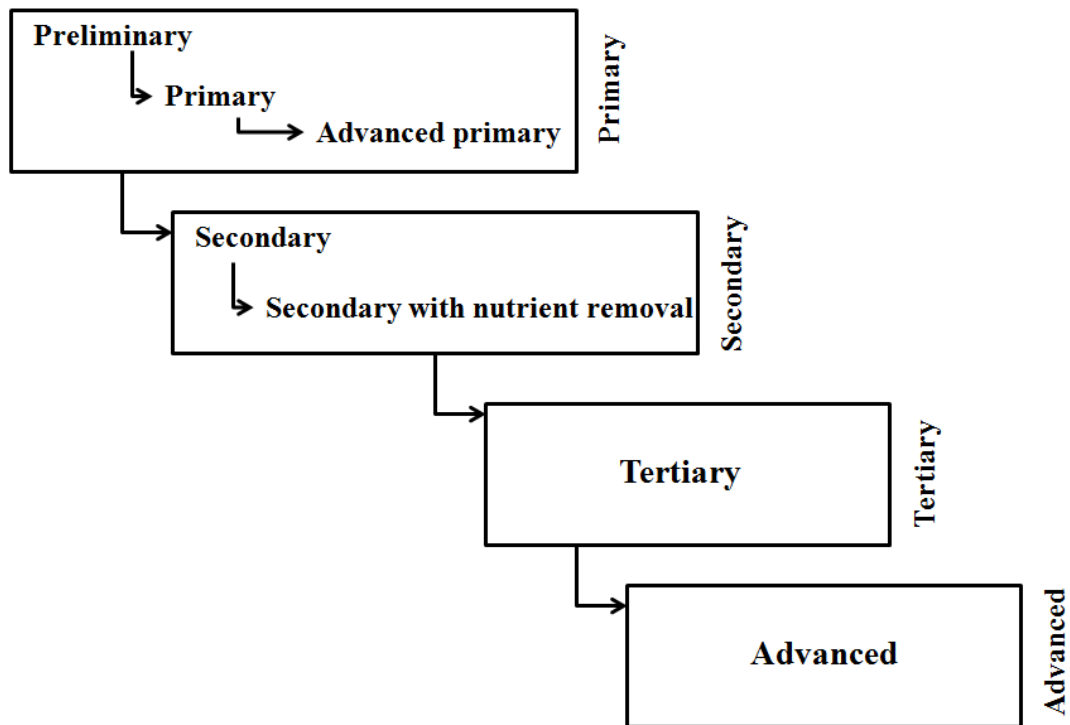


Figure 1.2 Levels of wastewater treatment (Metcalf and Eddy<sup>12</sup>).

### 1.1.3 Heterogeneous photocatalysis – a single step solution for future fuel and water treatment

#### 1.1.3.1 Application of photocatalysis in hydrogen generation

In the early 70s, Fujishima and Honda demonstrated water splitting for the 1<sup>st</sup> time using a TiO<sub>2</sub> electrode by UV light irradiation. Reduction of water molecule was achieved by the photogenerated electrons on a Pt counter electrode while oxidation of water was performed by the hole on the TiO<sub>2</sub> electrode. Additionally some external bias was employed by a power supply or pH difference between a catholyte and an anolyte.<sup>13</sup>

After that, remarkable progress has been seen in the last few decades using ultra-violet light.<sup>14</sup> The elements of group 4 (Ti and Zr), group 5 (Nb and Tc) and group 6 (W) acted as wide band gap photocatalytic materials for water splitting. Platinized TiO<sub>2</sub> photocatalyst, NiO loaded SrTiO<sub>3</sub>, Rh loaded SrTiO<sub>3</sub> were quite effective to decompose pure water into H<sub>2</sub> and O<sub>2</sub>. ZrO<sub>2</sub> was effective for water splitting without any co-catalyst because of its high conduction band level. K<sub>4</sub>Nb<sub>6</sub>O<sub>17</sub>, Rb<sub>4</sub>Nb<sub>6</sub>O<sub>17</sub>, Ca<sub>2</sub>Nb<sub>2</sub>O<sub>7</sub>, SrNb<sub>2</sub>O<sub>7</sub> and Ba<sub>5</sub>Nb<sub>4</sub>O<sub>15</sub> with layered structure showed high photocatalytic activities for water splitting. Alkali and alkaline earth tantalates also show good photocatalytic activity for water splitting.<sup>13</sup> In different studies TiO<sub>2</sub>-based photocatalysts such as Pt/TiO<sub>2</sub> and RuO<sub>2</sub>/TiO<sub>2</sub> were investigated.<sup>15, 16</sup> SrTiO<sub>3</sub>-based photocatalysts such as a reduced SrTiO<sub>3</sub> electrode with a platinum counterelectrode, platinized SrTiO<sub>3</sub>, SrTiO<sub>3</sub> powder modified by rhodium oxide, and nickel-loaded SrTiO<sub>3</sub> were also studied for improvement of their photocatalytic activities.<sup>14, 17-19</sup> Kim et al.<sup>20</sup> showed that layered perovskite, La<sub>2</sub>Ti<sub>2</sub>O<sub>7</sub> [110] was a good photocatalyst under ultraviolet light in water splitting reaction.

Nevertheless, such photocatalytic systems for water treatment as well as hydrogen generations are still experiencing a series of technical challenges. The basic difficulty with UV light is related to their narrow wavelength range (4 % of the solar spectrum) which is the driving force behind the utilization of the more abundant visible light (46 % of solar spectrum) for photocatalytic reactions. The photocatalyst used for above purposes must satisfy several functional requirements with respect to semiconducting and

electrochemical properties: i) suitable solar visible-light absorption capacity with a band gap around 2.0 – 2.2 eV and band edge potentials suitable for overall water splitting, ii) capacity for separating photoexcited electrons from reactive holes, iii) minimization of energy losses related to charge transport and recombination of photoexcited charges, iv) chemical stability against corrosion and photocorrosion in aqueous environment, v) kinetically suitable electron transfer properties from photocatalytic surface of water, and vi) easy synthesization and cost effective production.<sup>24</sup>

### 1.1.3.2 Application of photocatalysis in water treatment

The precise definition of the term ‘heterogeneous photocatalysis’ is a tricky one; particularly as in many cases the detailed mechanism of the ongoing reactions is uncertain. In case of photocatalytic reactions there is a light absorbing solid photocatalyst (semiconductor) which comes in contact with liquid or gas phase reactants and/or products.<sup>21</sup> All advanced oxidation processes operate through the formation of hydroxyl radical (OH<sup>•</sup>), which has very low selectivity. OH<sup>•</sup> radical can drive the oxidation process through complete mineralization of even less reactive pollutants. These radicals can even destroy biologically refractory pollutants that are characterized by high chemical stability.<sup>22</sup>

Heterogeneous photocatalysis utilizing different semiconductor photocatalysts such as ZnS, ZnO, TiO<sub>2</sub>, CdS, and GaP have established their effectiveness in pollutant degradation and eventually complete mineralization. Among them, TiO<sub>2</sub> is the most active photocatalyst under the photon energy of 300 nm <  $\lambda$  < 390 nm and also showed highest stability compared to other photocatalysts of similar class.<sup>23</sup> Moreover, TiO<sub>2</sub> has acquired extensive applications in photocatalytic water treatment as well as air purification and self cleaning surfaces due to its thermal and chemical stability, strong mechanical properties and low cost.<sup>24</sup>

Heterogeneous photocatalytic oxidation process became popular among the AOPs primarily because of the following reasons: (i) the processes can be carried out under

ambient condition (temperature and pressure), (ii) the oxidant is strong and less selective which leads to complete mineralization, (iii) the process do not consume any expensive oxidizing chemical, and iv) the photocatalyst are less expensive, non-hazardous, stable and reusable.<sup>6, 25</sup>

#### 1.1.4 Solar energy – an abundant source

Sun is a massive source of energy, from which the earth receives  $1.5 \times 10^{18}$  kWh per year, or approximately 28000 times world consumption for one year. World Meteorological Organization has recommended the solar constant value of  $1366.7 \text{ W m}^{-2}$  outside the atmosphere.<sup>26</sup> The solar radiation can be classified into two classes, direct and diffuse radiations. Direct radiation reaches the earth surface without being absorbed or scattered. On the other hand, if the radiation is dispersed before reaching earth surface, it is called diffuse radiation. Global radiation is basically the sum of direct and diffuse radiations (Figure1.3).

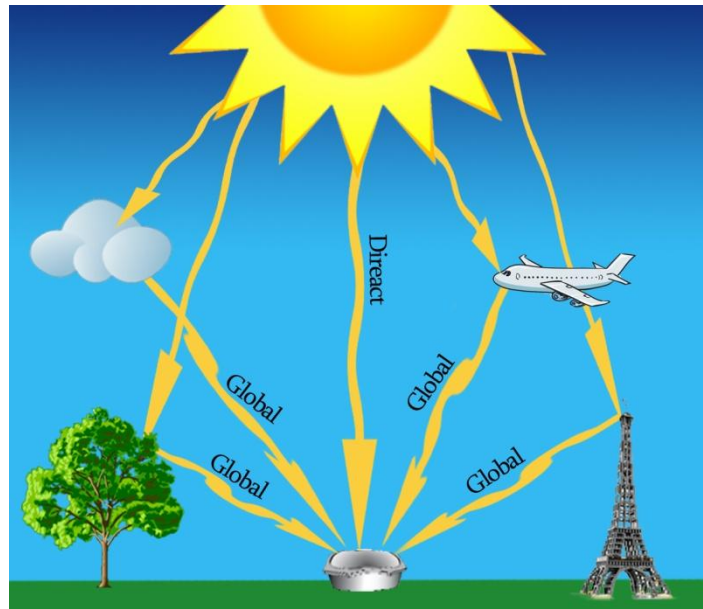


Figure 1.3 Direct and global radiation

The spectral irradiance data are generally acquired for the sun at a solar zenith angle of  $48.19^\circ$ . There is a term called air mass (AM), which is frequently used to express the direct optical path length through the atmosphere. It is a ratio of the direct beam solar-irradiance path length through the atmosphere at a certain solar zenith angle to the path length when the sun is in a vertical position (i.e.  $0^\circ$  zenith angles). Here, zenith angle of  $48.19^\circ$  corresponds to an air mass of 1.5. AM=1 when the sun is directly overhead (zenith). With increase in air mass, the direct beam passes through longer path lengths in the atmosphere that result in additional scattering and absorption of the direct beam and a lower percentage of direct-to-total radiation (Figure 1.4).<sup>27</sup> To simulate such system in photocatalysis laboratories, a solar simulator with 1.5 G (global) filter need to be used as light source.

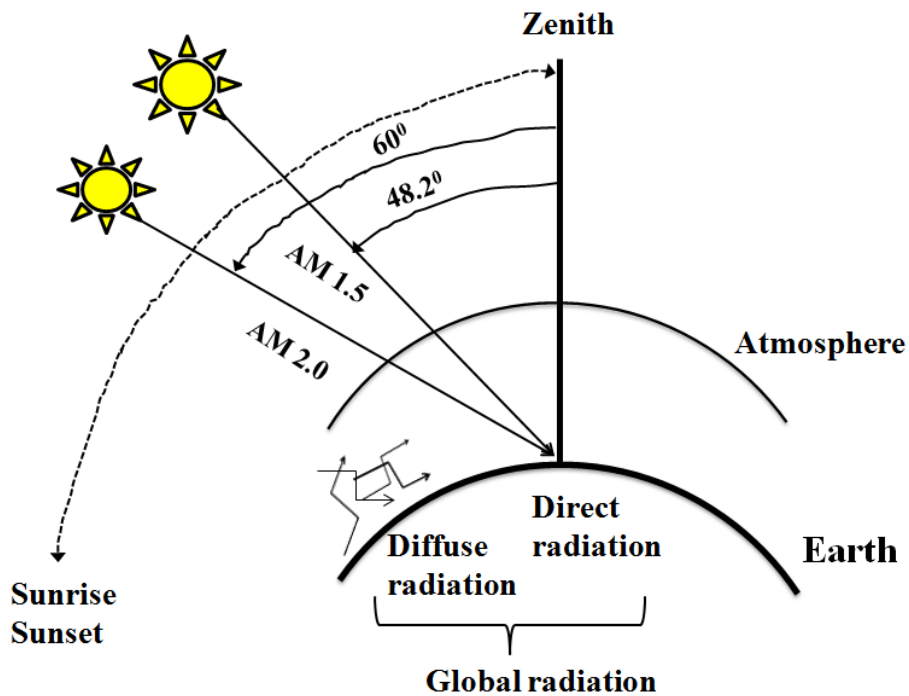


Figure 1.4 Diagram for air mass and solar components (adapted from Galvez et al.<sup>27</sup>).

## 1.2 Problem Statement

In order to use the entire solar spectra, especially visible one, and to improve the photocatalytic hydrogen generation and water treatment, several methods were undertaken to modify semiconductor photocatalyst. Metal/nonmetal doping was used to narrow down the band gap of photocatalyst.<sup>28-32</sup> Valance band controlled photocatalysts ( $\text{BiVO}_4$ ,  $\text{AgNbO}_3$  and  $\text{SnNb}_2\text{O}_6$ ),<sup>33-35</sup> and solid solution photocatalyst ( $\text{ZnS-CuInS}_2$ - $\text{AgInS}_2$ )<sup>36, 37</sup> were also applied to impose visible light activity in conventional photocatalyst. Composite semiconductor ( $\text{CdS-TiO}_2$ ,  $\text{CdS-ZnS}$ ),<sup>38, 39</sup> metal ion implantation and dye-sensitization were also reported as decent methods in such field.<sup>40</sup>

Dye-sensitization method is an inexpensive method compared to other methods applied in this field. Ruthenium based sensitizers were used extensively in dye sensitization field but because of their higher cost and toxicity, they are gradually replaced by non toxic organic dyes. Eosin Y dyes is a xanthane group dye which was used as sensitizer for different semiconductors due to its superior photocatalytic activity for sacrificial hydrogen production.<sup>41-46</sup> There is, however, lack of information on investigations of the key process parameters which affect sacrificial hydrogen generation based on robust experimental design methodology and statistical analysis.

Eosin Y-sensitized photocatalytic systems have provided plenty of information on visible-light-driven dye-sensitized hydrogen generation in presence of sacrificial electron donor. None of those, however, investigated the dye-sensitized process in complete solar spectrum, which is very essential for using a photocatalyst in real solar light applications. There is also inadequate information on the behavior of the electron donor and dye in presence of solar UV radiation. Intermediate analysis is also missing in those studies which would be useful in establishing the reaction mechanism. In photocatalytic reactions, mass transfer and light illumination are the two main factors that should be incorporated for efficient designing and scaling up of photo reactor. To the best of my knowledge, no studies so far have included the above two factors.

Eosin Y-sensitized photocatalytic system with triethanoamine electron donor is successful for hydrogen generation under nitrogen atmosphere but has not yet been applied for phenol degradation under aerated (or O<sub>2</sub>) systems. No study has yet been performed with such a system for phenol degradation under visible solar light. There is also inadequate information on the kinetics of this system.

### 1.3 Research Objectives

The objective of the present research is to investigate the sacrificial hydrogen generation in complete solar spectrum with Eosin Y sensitized platinum loaded TiO<sub>2</sub> (EY-TiO<sub>2</sub>/Pt) in aqueous triethanolamine solution. It also aims at exploring the dye-sensitization mechanism for phenol degradation under visible solar light with the same photocatalyst and electron donor. The specific objectives of this study are:

1. To perform a systemic experimental study on dye-sensitized hydrogen generation using design of experiment (DOE). This will be followed by a statistical analysis of the experimental data, analysis of variance (ANOVA), regression analysis, Pareto analysis, normal distribution, main effect plots and interaction effect plots.
2. To study the photocatalytic behavior in solar-UV (300-388 nm), solar-visible (420-650 nm) and full solar spectrum (300-650 nm) by varying reaction conditions including i) light intensity, ii) solution pH, iii) platinum content (wt %) on TiO<sub>2</sub>, iv) mass of EY-TiO<sub>2</sub>/Pt, v) concentration of triethanolamine, and vi) mass ratio of EY to TiO<sub>2</sub>/Pt.
3. To establish photocatalytic hydrogen generation mechanism in visible and solar light through intermediate and photoluminescence (PL) analysis.
4. To perform the parametric and kinetic study using the intermediate compound as electron donor for sacrificial hydrogen generation with Eosin Y-TiO<sub>2</sub>/Pt and triethanolamine.

5. To design a flow reactor considering the mass transfer limitations and preliminary hydrodynamics study for solar hydrogen generation with eosin Y-TiO<sub>2</sub>/Pt and triethanolamine.
6. To perform the parametric studies of (i) platinum content (wt %) on TiO<sub>2</sub>, (ii) triethanolamine concentration, (iii) solution pH, (iv) light intensity, and (v) catalyst mass, as well as reaction kinetics for phenol photodegradation in visible solar light.

## 1.4 Thesis Overview

This thesis has seven chapters including this one and follows the “integrated-article format” as mentioned in the Thesis Regulation Guide by the School of Graduate and Postdoctoral Studies (SGPS) of the Western University. The synopsis of the chapters are as follows.

Chapter 2 entitled “Dye-sensitized photocatalyst - a breakthrough in green energy and environmental detoxification” provides a critical review of dye sensitization theory, mechanism, metal ion deposition method, application in water treatment and hydrogen generation.

Chapter 3 is a research article entitled “Factorial design analysis for dye-sensitized hydrogen generation from water” published in International Journal of Hydrogen Energy. In this chapter factorial design analysis was used as a screening approach to identify the significant factors influencing sacrificial hydrogen generation from water with dye-sensitized photocatalyst. This method provides a quantitative assessment of the principal factors and effects that influence hydrogen generation performance.

Chapter 4 describes the preparation, and characterization of dye-sensitized TiO<sub>2</sub>/Pt photocatalysts followed by their applications in solar, visible and UV light. Optimization of various parameters related to sacrificial hydrogen generation is also presented. Effect of light intensity was studied for dye-sensitized photocatalytic hydrogen generation to



correlate UV, visible and solar radiation. Detailed intermediate analysis was also performed to understand the reaction mechanism. Finally it illustrates the development of flow reactor to overcome mass transfer limitation in solar hydrogen generation.

Chapter 5 investigates sacrificial hydrogen generation from formaldehyde (electron donor), which was detected as a major intermediate and product in solar (UV) and visible light irradiation respectively in chapter 5. The effects of different basic parameters were systematically studied with formaldehyde to understand the qualitative and quantitative effects as well as overall mechanism of the process.

Chapter 6 is a research article entitled “Visible-Solar-Light-Driven Photocatalytic Degradation of Phenol with Dye-Sensitized TiO<sub>2</sub>: Parametric and Kinetic Study”, which has been published in Industrial & Engineering Chemistry Research. Parametric studies were performed for the catalyst loading, initial triethanolamine concentration, initial phenol concentration, platinum content on TiO<sub>2</sub>, solution pH, and visible light intensity. The kinetic rate constant and adsorption equilibrium constant were determined, and a Langmuir–Hinshelwood-type equation was proposed to describe phenol degradation on TiO<sub>2</sub> at different visible light intensities.

Chapter 7 summarizes the key conclusions and suggests some directions for future research based on this study.

## 1.5 References

1. Dunn, S., Hydrogen futures: toward a sustainable energy system. *International Journal of Hydrogen Energy* **2002**, 27, (3), 235-264.
2. Grimes, C. A.; Varghese, O. K.; Ranjan, S., *Light, Water, Hydrogen – The Solar Generation of Hydrogen by Water Photoelectrolysis* Springer Science. NY, USA 2008; p 1-10.
3. Jain, I. P., Hydrogen the fuel for 21st century. *International Journal of Hydrogen Energy* **2009**, 34, (17), 7368-7378.
4. Lewis, N. S.; Nocera, D. G., Powering the planet: Chemical challenges in solar energy utilization. *Proceedings of the National Academy of Sciences of the United States of America* **2006**, 103, (43), 15729-15735.
5. Bockris, J., The origin of ideas on a hydrogen economy and its solution to the decay of the environment. *International Journal of Hydrogen Energy* **2002**, 27, (7-8), 731-740.
6. Mehrotra, K.; Yablonsky, G. S.; Ajay, K., Kinetic studies of photocatalytic degradation in a TiO<sub>2</sub> slurry system: Distinguishing working regimes and determining rate dependences. *Industrial & Engineering Chemistry Research* **2003**, 42, (11), 2273-2281.
7. Byrne, J. A.; Fernandez-Ibanez, P. A.; Dunlop, P. S. M.; Alrousan, D. M. A.; Hamilton, J. W. J., Photocatalytic enhancement for solar disinfection of water: a review. *International Journal of Photoenergy* **2011**, (Article ID 798051), 1-12. doi:10.1155/2011/798051.
8. *World Health Statistics 2011*; Publications of the World Health Organization: 20 Avenue Appia, 1211 Geneva 27, Switzerland.
9. Li, D.; Qu, J., The progress of catalytic technologies in water purification: A review. *Journal of Environmental Sciences* **2009**, 21, (6), 713-719.
10. Zhou, H.; Smith, D. W., Advanced technologies in water and wastewater treatment. *Canadian Journal of Civil Engineering* **2001**, 28, (Supplement 1), 49-66.
11. Legrini, O.; Oliveros, E.; Braun, A. M., Photochemical processes for water treatment. *Chemical Reviews* **1993**, 93, (2), 671-698.
12. *Metcalf & Eddy, Inc. Wastewater Engineering: Treatment and Reuse*. 4<sup>th</sup> ed.; McGraw Hill, NY: 2003.

13. Kudo, A.; Miseki, Y., Heterogeneous photocatalyst materials for water splitting. *Chemical Society Reviews* **2009**, 38, (1), 253-278.
14. Domen, K.; Kudo, A.; Onishi, T., Mechanism of photocatalytic decomposition of water into H<sub>2</sub> and O<sub>2</sub> over NiO---SrTiO<sub>3</sub>. *Journal of Catalysis* **1986**, 102, (1), 92-98.
15. Bulatov, A. V.; Khidekel, M. L., Decomposition of water under the effect of UV radiation in the presence of platinized titanium dioxide. *Russian Chemical Bulletin* **1976**, 25, (8), 1794.
16. Sato, S.; White, J. M., Photodecomposition of water over Pt/TiO<sub>2</sub> catalysts. *Chemical Physics Letters* **1980**, 72, (1), 83-86.
17. Wrighton, M. S.; Ellis, A. B.; Wolczanski, P. T.; Morse, D. L.; Abrahamson, H. B.; Ginley, D. S., Strontium titanate photoelectrodes. Efficient photoassisted electrolysis of water at zero applied potential. *Journal of the American Chemical Society* **1976**, 98, (10), 2774-2779.
18. Wagner, F. T.; Somorjai, G. A., Photocatalytic hydrogen production from water on Pt-free SrTiO<sub>3</sub> in alkali hydroxide solutions. *Nature (London, United Kingdom)* **1980**, 285, 559-560.
19. Lehn, J. M.; Sauvage, J. P.; Ziessel, R.; Hilaire, L., Water photocatalysis by UV irradiation of rhodium loaded strontium-titanate catalysts-relation between catalytic activity and nature of the deposit from combined photolysis and ESCA studies. *Israel Journal of Chemistry* **1982**, 22, (2), 168-172.
20. Kim, J.; Hwang, D. W.; Bae, S. W.; Kim, Y. G.; Lee, J. S., Effect of precursors on the morphology and the photocatalytic water-splitting activity of layered perovskite La<sub>2</sub>Ti<sub>2</sub>O<sub>7</sub>. *Korean Journal of Chemical Engineering* **2001**, 18, (6), 941-947.
21. Schiavello, M., *Heterogeneous photocatalysis*. John Wiley & Sons: 1997; Vol. 3, p 87-107.
22. Andreozzi, R.; Caprio, V.; Insola, A.; Marotta, R., Advanced oxidation processes (AOP) for water purification and recovery. *Catalysis Today* **1999**, 53, (1), 51-59.
23. Malato, S.; Fernandez-Ibanez, P.; Maldonado, M. I.; Blanco, J.; Gernjak, W., Decontamination and disinfection of water by solar photocatalysis: Recent overview and trends. *Catalysis Today* **2009**, 147, (1), 1-59.
24. Herrmann, J. M., Heterogeneous photocatalysis: fundamentals and applications to the removal of various types of aqueous pollutants. *Catalysis Today* **1999**, 53, (1), 115-129.

25. Chong, M. N.; Jin, B.; Chow, C. W. K.; Saint, C., Recent developments in photocatalytic water treatment technology: A review. *Water Research* **2010**, 44, (10), 2997-3027.
26. Brinker, D.; Curtis, H.; Flood, D. J.; Jenkins, P.; Scheiman, D., A summary of the international workshops on space solar cell calibration and measurement techniques. *Space Photovoltaic Research and Technology* **1996**, (SEE N 97- 10315 01-20), 186-190.
27. Galvez, J. B.; Rodriguez, S. M. *Solar Detoxification*; 9231039164; UNESCO: Plataforma Solar de Almeria, Spain, 2003.
28. Konta, R.; Ishii, T.; Kato, H.; Kudo, A., Photocatalytic activities of noble metal ion doped SrTiO<sub>3</sub> under visible light irradiation. *Journal of Physical Chemistry B* **2004**, 108, (26), 8992-8995.
29. Asahi, R.; Morikawa, T.; Ohwaki, T.; Aoki, K.; Taga, Y., Visible-light photocatalysis in nitrogen-doped titanium oxides. *Science* **2001**, 293, (5528), 269-271.
30. Umebayashi, T.; Yamaki, T.; Itoh, H.; Asai, K., Band gap narrowing of titanium dioxide by sulfur doping. *Applied Physics Letters* **2002**, 81, (3), 454-460.
31. Ohno, T.; Akiyoshi, M.; Umebayashi, T.; Asai, K.; Mitsui, T.; Matsumura, M., Preparation of S-doped TiO<sub>2</sub> photocatalysts and their photocatalytic activities under visible light. *Applied Catalysis A: General* **2004**, 265, (1), 115-121.
32. Mrowetz, M.; Balcerski, W.; Colussi, A. J.; Hoffmann, M. R., Oxidative power of nitrogen-doped TiO<sub>2</sub> photocatalysts under visible illumination. *Journal of Physical Chemistry B* **2004**, 108, (45), 17269-17273.
33. Kudo, A.; Ueda, K.; Kato, H.; Mikami, I., Photocatalytic O<sub>2</sub> evolution under visible light irradiation on BiVO<sub>4</sub> in aqueous AgNO<sub>3</sub> solution. *Catalysis Letters* **1998**, 53, (3), 229-230.
34. Kato, H.; Kobayashi, H.; Kudo, A., Role of Ag<sup>+</sup> in the band structures and photocatalytic properties of AgMO<sub>3</sub> (M: Ta and Nb) with the perovskite structure. *Journal of Physical Chemistry B* **2002**, 106, (48), 12441-12447.
35. Hosogi, Y.; Tanabe, K.; Kato, H.; Kobayashi, H.; Kudo, A., Energy Structure and Photocatalytic Activity of Niobates and Tantalates Containing Sn (II) with a 5s<sup>2</sup> Electron Configuration. *Chemistry Letters* **2004**, 33, (1), 28-29.
36. Tsuji, I.; Kato, H.; Kudo, A., Visible Light Induced H<sub>2</sub> Evolution from an Aqueous Solution Containing Sulfide and Sulfite over a ZnS-CuInS<sub>2</sub>-AgInS<sub>2</sub> Solid Solution Photocatalyst. *Angewandte Chemie* **2005**, 117, (23), 3631-3634.

37. Kudo, A.; Sekizawa, M., Photocatalytic H<sub>2</sub> evolution under visible light irradiation on Zn<sub>1-x</sub>Cu<sub>x</sub>S solid solution. *Catalysis Letters* **1999**, 58, (4), 241-243.
38. Chandra De, G.; Roy, A. M.; Bhattacharya, S. S., Effect of n-Si on the photocatalytic production of hydrogen by Pt-loaded CdS and CdS/ZnS catalyst. *International Journal of Hydrogen Energy* **1996**, 21, (1), 19-23.
39. Koca, A.; Sahin, M., Photocatalytic hydrogen production by direct sun light from sulfide/sulfite solution. *International Journal of Hydrogen Energy* **2002**, 27, (4), 363-367.
40. Ni, M.; Leung, M. K. H.; Leung, D. Y. C.; Sumathy, K., A review and recent developments in photocatalytic water-splitting using TiO<sub>2</sub> for hydrogen production. *Renewable and Sustainable Energy Reviews* **2007**, 11, (3), 401-425.
41. Chowdhury, P.; Gomaa, H.; Ray, A. K., Factorial design analysis for dye-sensitized hydrogen generation from water. *International Journal of Hydrogen Energy* **2011**, 36, (21), 13442-13451.
42. Zhang, X.; Jin, Z.; Li, Y.; Li, S.; Lu, G., Visible-light-induced hydrogen production over Pt-Eosin Y catalysts with high surface area silica gel as matrix. *Journal of Power Sources* **2007**, 166, (1), 74-79.
43. Kang, S. Z.; Chen, L.; Li, X.; Mu, J., Composite photocatalyst containing Eosin Y and multiwalled carbon nanotubes loaded with CuO/NiO: Mixed metal oxide as an active center of H<sub>2</sub> evolution from water. *Applied Surface Science* **2012**, 258, (16), 6029-6033.
44. Li, Q.; Lu, G., Visible-light driven photocatalytic hydrogen generation on Eosin Y-sensitized Pt-loaded nanotube Na<sub>2</sub>Ti<sub>2</sub>O<sub>4</sub>(OH)<sub>2</sub>. *Journal of Molecular Catalysis A: Chemical* **2007**, 266, (1), 75-79.
45. Sreethawong, T.; Junbua, C.; Chavadej, S., Photocatalytic H<sub>2</sub> production from water splitting under visible light irradiation using Eosin Y-sensitized mesoporous-assembled Pt/TiO<sub>2</sub> nanocrystal photocatalyst. *Journal of Power Sources* **2009**, 190, (2), 513-524.
46. Li, Y.; Xie, C.; Peng, S.; Lu, G.; Li, S., Eosin Y-sensitized nitrogen-doped TiO<sub>2</sub> for efficient visible light photocatalytic hydrogen evolution. *Journal of Molecular Catalysis A: Chemical* **2008**, 282, (1), 117-123.

## Chapter 2

# 2 Dye-Sensitized Photocatalyst - a Breakthrough in Green Energy and Environmental Detoxification

## 2.1 Introduction

Photocatalysis is a well known technology where light energy is utilized to excite the semiconductor material producing electron/hole pair which ultimately involves in the detoxification of pollutants and/or water splitting producing hydrogen. Pollutant degradation under UV light is already proven to be an effective method as reported by several researchers. At the same time, photocatalytic water splitting showed remarkable progress in the last few decades under UV light which started with the pioneer work of Fujishim and Honda.<sup>1</sup> The basic difficulty with UV light was related to its narrow wavelength ranges (4 % of the solar spectrum) which really drive the researcher to utilize the more profuse visible light (46 % of solar spectrum) for the excitation of semiconductor.

There are two significant impediments to visible light induced photocatalysis. First is the rapid recombination of electron/hole ( $e^-/h^+$ ) pair. The second is poor activation of semiconductor photocatalyst. Moreover, there is an additional problem of rapid backward reaction during water splitting. Efforts have been made to improve the photocatalytic activity and visible light response. This includes modification of semiconductor photocatalyst to expand their photo-response to visible region in several ways such as doping with cation/anion, sensitizing with dye, coupling with another small band gap semiconductor and implantation of metal ion.<sup>2</sup> Another approach, which attracts extensive industrial interest, is the field of dye-sensitization with possible applications in fields such as photography, photochromatic devices and photo lithography.<sup>3</sup>

Dye-sensitization of semiconductor is also a very popular concept that has been successfully utilized in solar cell for generating electricity. The same principle can be

applied to split the water molecule under visible light to produce hydrogen as well as to degrade toxic pollutants.

This review will first describe the basic phenomena for dye-sensitization and brief methodologies used for different semiconductor materials such as ZnO, TiO<sub>2</sub>, Cu<sub>2</sub>O etc. It will also discuss different methods for deposition of novel metals as co-catalyst on semiconductor surface. Finally dye-sensitization method will be elaborated with different semiconductors for hydrogen production and degradation of different organic pollutants.

## 2.2 Dye Sensitization

### 2.2.1 Theory of dye sensitization

The process of expanding the sensitivity of transparent semiconductor materials to the visible spectra is known as spectral sensitization. When the sensitization of a large band gap semiconductor to the visible region is achieved with a dye at the molecular level, it is called dye-sensitization.<sup>4</sup> The operating mechanism of dye in dye-sensitized semiconductor is similar to that in the field of photography.<sup>5</sup> Dye is adsorbed chemically onto the semiconductor surface by conventional adsorption process and the chemisorbed dye molecules play the role of spectral sensitizer which upon excitation with visible light inject electron into the conduction band of the semiconductor.<sup>5</sup> This phenomenon is also known as anodic sensitization. On the contrary, cathodic sensitization occurs when adsorbed dye molecule inject holes into valance band of the semiconductor.<sup>6</sup> This review only consider anodic sensitization of semiconductor.

Some early studies of spectral sensitization of semiconductors were conducted on ZnO and CdS. The first report discussed sensitization of pressed ZnO powder by adsorbed rhodamine B, eosin, erythrosine, and cyanine dyes.<sup>7</sup> But most of these early studies focused on organic dyes of interest to photographic industry. Gleria and Memming<sup>3</sup> performed the first experiment of sensitization using inorganic Ru metal based polypyridine complex dyes on SnO<sub>2</sub> electrodes.

Figure 2.1<sup>3</sup> demonstrates the dye-sensitization principles of an n-type semiconductor electrode such as TiO<sub>2</sub>. In the first step, the organic or inorganic dye molecule adsorb photon and results in the formation of excited state (equation 2.1). Then the excited dye molecule inject electron into the conduction band of the semiconductor (equation 2.2). The oxidized dye (S<sup>+</sup>) is consequently reduced to ground state (S) by an electron donor. Electron donor can be a molecule or a mediating redox couple in a regenerative cell. The injected electron flows through the semiconductor and then through the external circuit to the counter electrode where the reduction of the oxidized donor takes place. So, the photon of irradiated light drives an electron through the semiconductor and the external circuit, and this results in conversion of light to electrical energy.

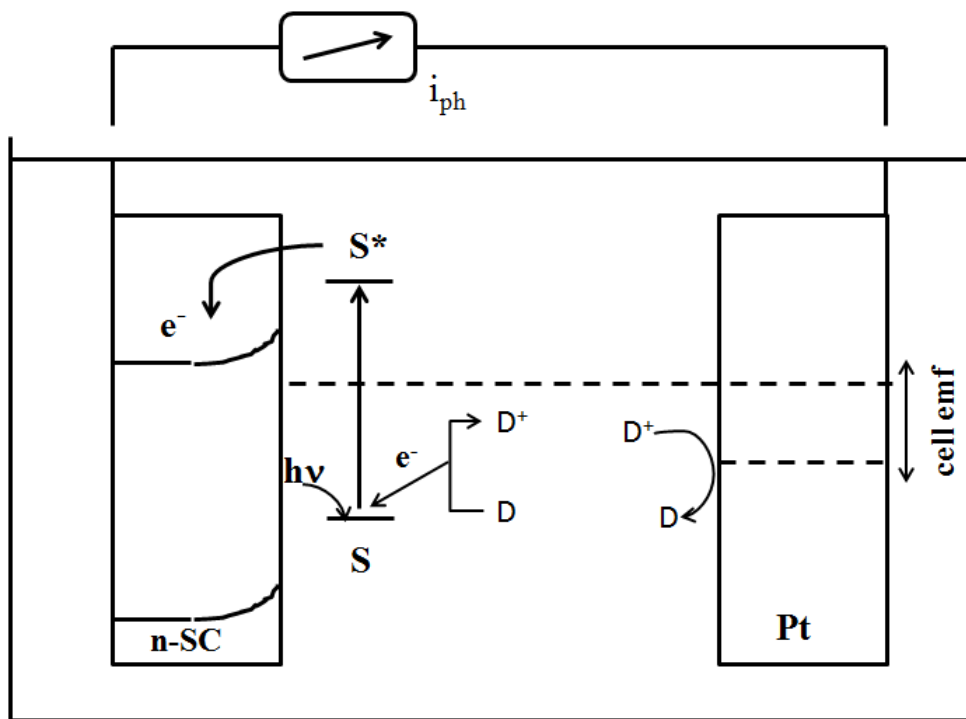


Figure 2.1 Dye sensitization principles for n-type semiconductor (adapted from Kalyanasundaram and Gratzel<sup>3</sup>).





The efficiency of the sensitization process can be expressed in terms of incident photon-to-current conversion efficiency (IPCE).

$$IPCE = \left[ \frac{\text{number of electrons generated by light in the external circuit}}{\text{number of incident photons (monochromatic)}} \right] \quad (2.3)$$

The IPCE value depends on the i) chemical nature of the dye, ii) mediating redox electrolyte, and iii) nature of the semiconductor and the interface of the electrolyte.<sup>3</sup> The excited states of most of the metal complexes and organic dyes have short life span. So the efficiency of charge injection process depends on those dyes molecules that are in close proximity of the semiconductor electrodes.<sup>3</sup>

The dye molecule should hold few basic properties regarding surface anchoring group, energy levels and ground state redox potential to undergo a successful electron injection. Anchoring groups, such as phosphonates or carboxylic acid derivatives form strong covalent bonds with the semiconductor surface and that covalent bond ultimately increases the strength of the electronic coupling between the molecular orbital of the dye and the semiconductor levels leading to fast electron injection rates.<sup>8</sup> Carboxylic and phosphoric acid groups show very good electron transfer process (80-90 %) as mentioned for some ruthenium complexes.<sup>4</sup> Different binding or interaction mode of TiO<sub>2</sub> surface and -COOH group is shown in Figure 2.2 as described by Galoppini.<sup>8</sup> The anchoring group can be arranged in the following order of reactivity: -P(O)(OH)<sub>2</sub> > -COOH > -COOR (R=alkyl group) > -COX (X=Cl, Br etc) > -COONH<sub>2</sub> ~ COOM (M=Na, K etc). There are few more functional groups such as silanes, ethers, acetylacetone and

salicylates that can also form bonds with metal oxide (semiconductor) by reacting with surface hydroxyl groups.

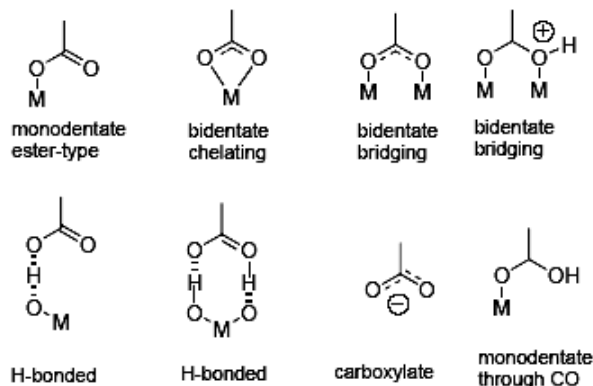


**Figure 2.2 Possible binding mode of  $\text{TiO}_2$  surface and  $-\text{COOH}$ .  
Reprinted with permission from Galoppini.<sup>8</sup> (Copyright 2004 Elsevier).**

Dye molecules in the bulk phase of the electrolyte solution undergo severe charge collection problem similar to that in photogalvanic cells. To overcome this problem dye molecules are fixed on the semiconductor surface either by chemisorptions or by some form of derivatization. Several approaches were adopted to attach dye molecule on semiconductor surface since the mid seventies. Matsumura et al.<sup>9</sup> investigated the possibility of chelate formation on the semiconductor surface. Fixation of xanthene dye to the surface was attempted either by etherification or by using a  $\text{Si}-\text{CH}_2-\text{CH}_2-\text{CH}_2-\text{NH}-\text{CO}$ -dye linkage. Visible light sensitization of ZnO was observed by certain azo dyes which form 1:1 Zn complex at the surface of ZnO powders. In another study, colloidal  $\text{TiO}_2$  sensitization was achieved by 8-hydroquinoline to generate hydrogen from water in visible light irradiation. 8-hydroquinoline experienced a chelation reaction with colloidal  $\text{TiO}_2$  that results in an active yellow complex during sensitization.<sup>3, 10</sup>

The type of sensitization (anodic or cathodic) mainly depends on the band position of the semiconductor and energy level of the dye. In anodic sensitization the energy level of the

dye molecule at excited state should be comparable with the lower level of semiconductor conduction band for better electron injection.<sup>5</sup> Here an electron excited from the lower singlet level ( $S_0$ ) to upper excited singlet level ( $S_1$ ) is transferred to conduction band (Figure 2.3). Moreover a higher value of ground state redox potential of the dye would be beneficial for rapid regeneration of exhausted dye in presence of suitable electrolyte such as  $I^-/IO_3^-$ . The best reported value of ground state oxidation potential is 0.5V vs SCE (Standard Calomel Electrode).<sup>4</sup>

The electron injection mechanism was explained by several authors but the most recent work by Willig's group enlightened the interfacial electron transfer (ET) mechanism in a proper way. They demonstrated the ET dynamics in dye- $TiO_2$  system and found that on leaving the dye, the electron was not trapped on the surface and certainly entered bulk  $TiO_2$ . Their observations with femtosecond laser spectroscopy was not in agreement with the usual model of electron transfer.<sup>11</sup>

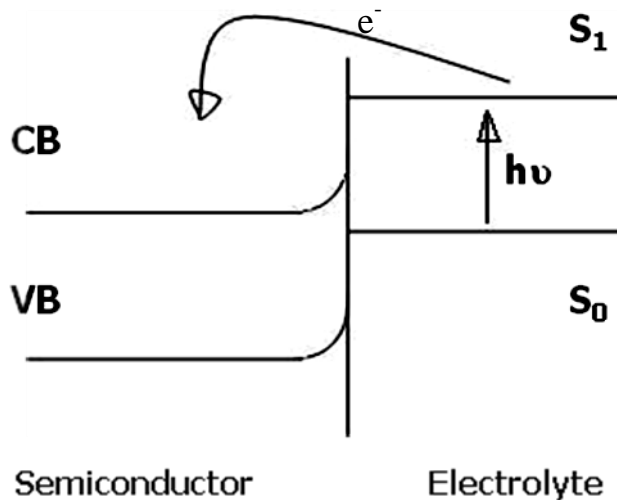


**Figure 2.3 Energy level diagram of anodic dye sensitization process**

## 2.2.2 Dye sensitization methodology

In dye sensitization the dye is adsorbed on to the semiconductor surface having a high surface area and forms a dye-sensitized semiconductor film which adsorbs the visible light efficiently. In common practice the semiconductor material (powder or immobilized form) is dipped into the dye solution for specified time interval under dark. Then the semiconductor material is separated from dye solution and washed with solvent (alcohol or water) to remove unadsorbed or loosely bound dye molecules from semiconductor surface. The final dye-sensitized material is obtained only after drying at some specific temperature in oven. Although the process is quite straight forward, wide variations are expected in sensitization with the change in dye type, dye concentration, semiconductor type, semiconductor surface morphology, solution pH and incorporation of electron donor into the system. Thus, the visible light absorption efficiency of dye-sensitized semiconductor is a function of all the above parameters.

### 2.2.2.1 Selection of dye

A group of semiconductor sensitizers such as porphyrins, coumarin, phalocyanines and carboxilate derivatives of anthracine are used by several authors. Among these photosensitizers, transition metal based sensitizers have been proved to be the best.<sup>12</sup> Transition metals such as Ru (II), Fe (II) and Os (II) form  $d^6$  complex and undergo intense charge transfer absorption across the entire visible range.<sup>12</sup> In dye sensitized solar cells mainly Ru (II) polypyridine complexes are used. In the field of dye-sensitized solar cell Gratzel reported the best sensitizer,  $\text{cis-}[\text{Ru}(\text{dcbH}_2)_2(\text{NCS})_2]$  (N3) where he applied thiocyanate ( $\text{NCS}^-$ ) as an ancillary ligand. Subsequently, several investigators attempted to substitute the  $\text{NCS}^-$  ligands which led to a variety of new photosensitizers, but the efficiency did not improve.<sup>5</sup>

The ruthenium polypyridyl complex contains heavy metals and thus it is not environment friendly. Moreover the process to synthesize the complex is complicated and costly. Recently few authors reported the use of natural dyes as an alternative for dye

sensitization. The natural dyes are generally found in fruits, flowers and leaves of plants. A list of several natural dyes is presented in Table 2.1.

**Table 2.1 Natural extracts used for dye-sensitization**

<b>Extract source</b>	<b>References</b>
Rosella	Wongcharee et al. <sup>13</sup>
Blue Pea	Wongcharee et al. <sup>13</sup>
Jaboticaba's skin	Polo and Iha <sup>14</sup>
Chaste tree fruit	Gracia et al. <sup>15</sup>
Mulberry	Gracia et al. <sup>15</sup>
Cabbage-palm fruit	Polo et al. <sup>12</sup>
Java Palm	Polo et al. <sup>12</sup>
Pomegranate seeds	Polo et al. <sup>12</sup>

### 2.2.2.2 Selection of semiconductor material

A range of semiconductors such as ZnO, TiO<sub>2</sub>, SrTiO<sub>3</sub>, SnO<sub>2</sub> and Cu<sub>2</sub>O have been studied with different dyes.<sup>16, 17</sup> TiO<sub>2</sub> became the semiconductor of choice because of several advantages such as i) low cost, ii) wide availability, iii) non-toxic nature, iv) high stability against photo-corrosion, and v) superior electronic energy band structure.<sup>5, 18</sup> The anatase form of TiO<sub>2</sub> (E<sub>g</sub>=3.2 eV) has been found to be the most active for photocatalysis. TiO<sub>2</sub> sensitization have also been studied with different dyes such as Ru(bpy)<sub>3</sub><sup>2+</sup>, RuL<sub>3</sub><sup>2+</sup> (L=2,2'-bipyridine-4,4'-dicarboxilate) and metal-quinolinol.<sup>16</sup> Composite semiconductors such as ZnO/SnO<sub>2</sub>, SnO<sub>2</sub>/MgO and Cds/MgO showed almost equal efficiencies as achieved with TiO<sub>2</sub> in solar cells.<sup>19</sup>

Semiconductor surface morphology and particle size are very important as these ultimately affect the e<sup>-</sup>/h<sup>+</sup> recombination and photocatalytic reaction rate.<sup>19</sup> Nanoporous

semiconductor film can be a solution to improve the process performance. There are several other methods to prepare the semiconductor material such as high temperature solidification methods from the elements in bulk form, or vapor phase and vacuum methods in the form of thin films.<sup>20</sup> High temperature processes are now replaced with cathodic electrodeposition to produce thin film of semiconductor in more economically efficient manner.<sup>21</sup> One step electrodeposition of ZnO/dye hybrid thin film was reported by Yoshida et al.,<sup>22</sup> where the morphology, the crystal size, and orientation of ZnO were significantly modified by the added dyes such as eosin Y, tetrabomophenol blue, and tetrasulfonated metallophthalocyanines. Sol-gel method is another widely used method for the preparation of nanocrystalline TiO<sub>2</sub> and ZnO.<sup>23-27</sup>

## 2.3 Incorporation of Noble Metal Co-catalyst on to Semiconductor

In the last few years interest has been shown in improving activity of TiO<sub>2</sub> by noble metal doping. Metal-ion-doped TiO<sub>2</sub> has been primarily studied to enhance the photocatalytic activity under UV radiation.<sup>28-30</sup> Choi et al.<sup>31</sup> reported increased UV photocatalytic degradation of chloroform with Fe<sup>3+</sup>, Ru<sup>3+</sup>, V<sup>4+</sup>, Mo<sup>5+</sup>, Os<sup>3+</sup>, Re<sup>5+</sup> and Rh<sup>3+</sup> ion doped TiO<sub>2</sub>. At the same time they observed decreased photoactivity in case of Co<sup>3+</sup> and Al<sup>3+</sup> ion doped TiO<sub>2</sub>.

Gas phase oxidation rate of ethanol,<sup>32</sup> acetone,<sup>33</sup> and acetaldehyde,<sup>34</sup> was improved with TiO<sub>2</sub>/Pt catalyst. It has been reported that in liquid phase, addition of Pt and other noble metals to TiO<sub>2</sub> improve photocatalytic performance for the degradation of different pollutants.<sup>35-37</sup> Platinum deposits on semiconductor assists better separation of photogenerated electron-hole pair.<sup>32</sup> Surface modification of TiO<sub>2</sub> by platinum is an effective method to increase its photoactivity for water and wastewater decontamination.<sup>38</sup> The generated electron hole pairs through band gap excitation undergo recombination after a finite amount of time, and this recombination rate is a critical factor to determine the overall photocatalytic efficiency of TiO<sub>2</sub>. Electron/hole recombination usually dominates semiconductor photosensitization, so the overall

process is often not very efficient with respect to photons.<sup>39</sup> Platinum metal consists of a Fermi levels lower than TiO<sub>2</sub> conduction band and could function as an electron trap centre to accelerate the discharge of photogenerated electrons from TiO<sub>2</sub>. This increases the lifespan of electron-hole pairs and thereby improves the photocatalytic activity of TiO<sub>2</sub>.<sup>40</sup>

### 2.3.1 Platinum deposition methods

Several methods are available for platinum deposition on catalyst surface, such as photo-deposition,<sup>41-43</sup> impregnation,<sup>37, 44, 45</sup> chemical vapor deposition,<sup>46</sup> chemical reduction of Pt salts,<sup>47, 48</sup> and atomic layer deposition.<sup>40, 49, 50</sup> They yield different degree of surface modification and subsequent catalytic efficiency. A brief summary of platinum deposition methods is illustrated in the following section.

#### 2.3.1.1 Photodeposition method

TiO<sub>2</sub> powder is suspended in a deaerated solution and dispersed by sonication. The solution contains a platinum precursor (e.g. H<sub>2</sub>PtCl<sub>6</sub>, K<sub>2</sub>PtCl<sub>6</sub>, H<sub>2</sub>Pt(OH)<sub>6</sub>, Pt(NH<sub>3</sub>)<sub>2</sub>(NO<sub>2</sub>)<sub>2</sub> etc.), water and a sacrificial organic reagent such as methanol, ethanol, propan-2-ol, 2-methylpropan-2-ol, and acetic acid.<sup>41</sup> The solution pH is adjusted to 3.0 before the reaction. The suspension is stirred and irradiated with either UV or solar light generated from Hg vapor lamp or Xe arc lamp. After 1-2 h irradiation, the color of the suspension changes from white to black owing to Pt deposition. Completion of photodeposition can be ascertained by an analysis of Pt species in the solution. In photodeposition method the platinum precursor Pt<sup>(IV)</sup>Cl<sub>6</sub><sup>2-</sup> is reduced by the photo generated electron at the valance band of TiO<sub>2</sub>, and the sacrificial organic reagent act as hole scavenger. According to Li et al.<sup>42</sup> Pt<sup>(IV)</sup>Cl<sub>6</sub><sup>2-</sup> is first adsorbed on TiO<sub>2</sub> surface, then reduced into Pt<sup>(II)</sup>Cl<sub>4</sub><sup>2-</sup> and Pt<sup>0</sup> or (Pt<sup>0</sup>)<sub>m</sub> (Pt metal cluster). They confirmed the presence of Pt, Pt(OH)<sub>2</sub>, and PtO<sub>2</sub> on the surface of TiO<sub>2</sub>. Yang et al.<sup>43</sup> also reported a mixture of Pt<sup>(II)</sup> and Pt<sup>0</sup> state even after 24 h of photoreduction, which could suggest the simultaneous agglomeration of Pt atoms and cathode-like reduction during the particle growth of Pt metal. They also suggested a particle growth mechanism of Pt on the basis of EXAFS and XPS results. Nakamatsu et

al.<sup>41</sup> reported the diameter of photodeposited platinum metal on TiO<sub>2</sub> particles in the range of 0.3-0.8 μm. XRD measurement showed that most of the TiO<sub>2</sub> particles were rutile and some were anatase (anatase (101)/rutile (110) peak ratio = 0.16). TEM and SEM analysis were carried out to identify the size distribution and orientation of the platinum deposits on TiO<sub>2</sub>. Dispersion of platinum deposit was dependent on sacrificial agent; the particle size decreased in the following order: acetic acid (100 nm) > 2-methylpropane-2-ol (100 nm) > methanol (30 nm) > propane-2-ol (30 nm) > ethanol (5 nm).

### 2.3.1.2 Impregnation

In impregnation process, metal complexes are dissolved in aqueous solution to allow the contact with a porous oxide catalyst support such as TiO<sub>2</sub>. In the aqueous solution the noble metal adsorbs onto the high surface area catalyst support. The catalyst slurry is then filtered if large excess solution has been employed, or just evaporated to dryness. Then it is treated further to transform the metal from its precursor state into its active form.<sup>44</sup> Platinum modified catalysts are synthesized by impregnation of anatase prepared from titanyl sulfate with aqueous solution of platinum nitrate. The mixture is evaporated to dryness and then calcined at 450°C for few hours. Then the deposited platinum salt is reduced to lower oxidation state in hydrogen atmosphere at 250°C. Kryukova et al.<sup>37</sup> reported 0.5-2 wt % platinum loading on TiO<sub>2</sub> surface, with specific surface area of around 170 m<sup>2</sup> g<sup>-1</sup> regardless of Pt loadings. Bavykin et al.<sup>45</sup> reported the impregnation of platinum metal on TiO<sub>2</sub> nanotube. In order to produce TiO<sub>2</sub>/Pt, the nanotube titanium dioxide was mixed with aqueous H<sub>2</sub>PtCl<sub>6</sub> solution. The process was very sensitive to humidity, so the reaction mixture was placed into a controlled humidity chamber for 7 days. Reduction of H<sub>2</sub>PtCl<sub>6</sub> in titanate nanotubes was carried out in a quartz U-tube with hydrogen at room temperature. This method allowed the deposition of nanowires of Pt metal inside nanotubes but resulted in very uneven distribution of platinum.



### 2.3.1.3 Chemical reduction of Pt salts

In this method inorganic or organic reducing agents are used to reduce platinum precursors. The use of formaldehyde and ethylene glycol (EG) as potential reducing agents were reported by Li et al.,<sup>47</sup> to deposit Pt on multiwalled carbon nanotube (MWNT) surface. Aqueous solution of  $\text{H}_2\text{PtCl}_6$  was employed as platinum precursor. The MWNT/Pt catalyst with a metal loading of 10 wt % was obtained. In case of formaldehyde reduction, Pt particles have a wide particle-size distribution ranging from 2 to 9 nm with a mean particle size of 3.4 nm. On the contrary, for EG reduction Pt particles had narrow size dispersion ranging from 2 to 5 nm with its peak centered at 2.6 nm. This observation explained a better interaction of platinum precursor with EG solvent to produce a high homogeneous dispersion of spherical Pt metal particles with a narrow particle size distribution. They also mentioned that surface modification of MWNTs and water content in EG solvent were found to be the key factors in controlling the particle size and distribution of Pt particles deposited on the MWNT support.

$\text{NaBH}_4$  can also be used as reducing agent to prepare Pt deposited surface. Mei et al.<sup>48</sup> mentioned about the immobilization of platinum nanoparticles on spherical polyelectrolyte brushes. After reduction of  $\text{H}_2\text{PtCl}_6$  by  $\text{NaBH}_4$  nanosized particles were formed. TEM analysis confirmed the formation of Pt nanoparticles with 2 nm diameter.

### 2.3.1.4 Chemical vapor deposition

There are wide applications of chemical vapor deposition (CVD) of noble metals in electronics, protective coating and catalyst industries. High volatility, thermal stability and clean decomposition of suitable precursors results in the effectiveness of CVD. Metal organic complexes are commonly used as precursors of noble metals in CVD. CVD method is applied to produce fine particles of platinum, which can be used to prepare catalysts. There are several precursors available for platinum CVD, such as  $\text{Pt}(\text{acac})_2$ ,  $\text{Pt}(\text{CO})_2\text{Cl}_2$ ,  $(\text{MeCp})\text{Pt}$ ,  $\text{Pt}(\text{allyl})_2$ ,  $(\text{Cp})\text{PtMe}_3$ , and  $(\text{MeCp})\text{PtMe}_3$ . The efficiency of CVD can be further improved by applying plasma or laser as an assisting energy source to CVD.<sup>46</sup>

### 2.3.1.5 Atomic layer deposition

It is a thin film growth technology which provides outstanding conformal and uniform growth with good control over both composition and thickness. It also follows sequential self-limiting surface reaction steps for metal deposition in an atomic layer-by-layer approach.<sup>50, 51</sup>

According to Floro et al.<sup>49</sup> the nucleation of precursors on surface sites in the early stages of atomic layer deposition (ALD) growth can be based on the Volmer–Weber growth mechanism. Volmer–Weber growth mode includes the following microstructural stages i) nucleation of discrete islands, ii) island growth, iii) island impingement and coalescence, iv) percolation of the island array, and v) channel filling to eventually form a continuous thin film. Variations in deposition temperatures can result in varying particle densities. Therefore, changes in the frequency of ALD cycles and deposition temperatures can control the loading and dispersion of platinum. Such characteristics enable ALD to produce both high-quality films and nanoparticles on the surfaces of flat or particulate substrates.

Zhou et al.<sup>40</sup> used fluidized bed reactor (FBR) for ALD of Pt nanoparticles on the surfaces of primary TiO<sub>2</sub>. They also described ALD as the best method in term of precise control the Pt deposition, to uniformly modify surfaces with small, highly dispersed Pt nanoparticles.

## 2.4 Application of Dye-Sensitized Photocatalyst for Water and Wastewater Detoxification

Table 2.2. Exposure and regulatory limits of some organic pollutants (adapted from ATSDR, 1997, 2003, 2005, 2008, 1999)

Compounds	Use/Exposure	Health effect	Maximum allowable contaminant level
Hydrazine	<ul style="list-style-type: none"> <li>i) rocket fuels,</li> <li>ii) chemical manufacturing,</li> <li>iii) boiler water treatment</li> </ul>	may cause nervous system effect, liver and kidney damage, human carcinogen	0.03-0.06 mg L <sup>-1</sup>
Trichloroethylene	<ul style="list-style-type: none"> <li>i) metal degreasing agent,</li> <li>ii) common ingredient in cleaning agents, paint and adhesive, varnishes and ink</li> </ul>	cause liver and lung damage, abnormal heartbeat, coma and possible death, human carcinogen	5 µg L <sup>-1</sup>
Carbon tetrachloride	<ul style="list-style-type: none"> <li>i) used in the production of refrigeration fluid and propellants for aerosol cans,</li> <li>ii) as a cleaning fluid and degreasing agent, in fire extinguishers, and in spot removers</li> </ul>	can damage the liver, kidney and nervous system, human carcinogen	5 µg L <sup>-1</sup>
Phenol	<ul style="list-style-type: none"> <li>i) used in the manufacture of phenolic resins nylon and other synthetic fiber,</li> <li>ii) used as a disinfectant and antiseptic</li> </ul>	high amount can produce skin burns, liver damage, dark urine, and even death, not a human carcinogen	2 mg L <sup>-1</sup>

---

	<p>iii) it is found in aqueous effluent from industries such as petroleum refining, steel production,</p> <p>coal gasification, textile, tannery, pulp and paper, pesticides, pharmaceuticals and food processing</p>		
Chlorophenols	<p>i) used in pesticides and antiseptics,</p> <p>ii) produced in pulp and paper industry in bleaching process with chlorine,</p> <p>iii) formed as a result of chlorination of humic matter during the chlorination of drinking water</p>	high levels can cause damage to liver and immune system	0.04-0.05 mg L <sup>-1</sup>

---

## 2.4.1 Aliphatic chlorinated hydrocarbon

### 2.4.1.1 Carbon tetrachloride (CCl<sub>4</sub>) degradation

The sensitized degradation of CCl<sub>4</sub> in water was successfully demonstrated by several authors under visible light illumination ( $\lambda > 420$  nm).<sup>52-55</sup> Ruthenium based dyes have very good potential to sensitize TiO<sub>2</sub> photocatalyst as well as non ionic surfactant (Brij-35). Cho et al.<sup>54</sup> studied the effect of different parameters such as solution pH, dissolved oxygen and number of dye layer on TiO<sub>2</sub> surface as a function of CCl<sub>4</sub> dechlorination rate. Tris (4,4-dicarboxy-2,2-bipyridyl) ruthenium (II) complex dye was used as sensitizer under visible light with 2-propanol as an electron donor. The pyrolysis rate was dependent on pH due to the strong pH dependence of the sensitizer adsorption on TiO<sub>2</sub>

surface with a maximum degradation rate achieved at pH 3.0. The photolysis rate of CCl<sub>4</sub> showed a maximum at a sensitizer surface coverage of 30 % monolayer.

Dissolved oxygen showed negative effect towards dechlorination as oxygen competed for conduction band electrons. Similar result was observed by Cho et al.<sup>52</sup> where they used [Ru<sup>II</sup> (bpy)<sub>3</sub>] photosensitizer with nonionic surfactant. With increase in each concentration of surfactant, sensitizer or CCl<sub>4</sub> the corresponding CCl<sub>4</sub> dechlorination rate progressively increased to reach saturation at the concentration of 0.4 g L<sup>-1</sup> (surfactant), 5 mM (sensitizer) or 30 mM (CCl<sub>4</sub>) respectively. With the ruthenium sensitizer alone in the absence of the surfactant, the dechlorination rate is negligible as the photoinduced electron transfer from the excited sensitizer to CCl<sub>4</sub> takes place only in the presence of the surfactant which concentrates both reactants within a micelle.

Fung et al.<sup>53</sup> anchored a Ru(II) photosensitizer onto the surface of anatase TiO<sub>2</sub> particles via in situ silylation. The silyl linkage displayed excellent stability in both aqueous media, over a wide pH range, and in common organic solvents. The silyl linkage also enabled electronic coupling between the photosensitizer and TiO<sub>2</sub> and mediated injection of electrons from the photosensitizer to the conduction band of TiO<sub>2</sub> upon photoexcitation. The photosensitized TiO<sub>2</sub> material TiO<sub>2</sub>-[Ru<sup>II</sup>(py-pz-Si)<sub>3</sub>] was able to mediate photodegradation of CCl<sub>4</sub> in the presence of electron donor in aqueous medium under both aerobic and anaerobic conditions. The degradation kinetics obeys Langmuir-Hinshelwood type rate law indicating the surface adsorption of CCl<sub>4</sub> on TiO<sub>2</sub> surface during degradation.

#### 2.4.1.2 Trichloroethylene (TCE) degradation

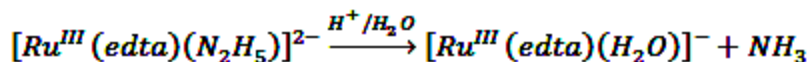
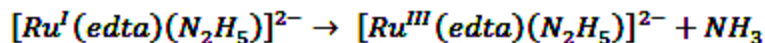
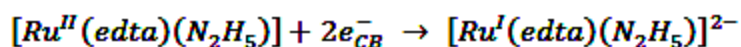
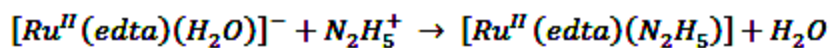
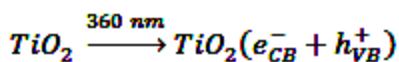
Alexander et al. examined the photo oxidation of TCE using buoyant TiO<sub>2</sub> coated microspheres, which was sensitized using natural anthocyanine dyes obtained from fruits. The dye-sensitized system provided excellent remediation with 93 % of the TCE removal in 12 h. A drawback to the photo-oxidative remediation technique is the significant drop in pH associated with the conversion of TCE to hydrochloric acid which would make this method unacceptable to some sensitive aquatic environments.<sup>56</sup>

### 2.4.1.3 Pesticides degradation

Muszkat et al. suggested accelerated photocatalytic oxidation of pesticides in water by dye sensitization. They studied two widely applied herbicides, bromacil (5-bromo-3-sec-butyl-6-methyluracil) and metribuzin (4-amino-6-tert-butyl-4,5-dihydro-3-methylthio-1,2,4-triazine-5-one). In absence of TiO<sub>2</sub>, different reaction patterns of photo-oxidation were shown by the above mentioned pesticides. Oxygen had a distinct effect on the rate of photo-oxidation of metribuzin while the influence of H<sub>2</sub>O<sub>2</sub> was quite moderate. On the contrary, in presence of H<sub>2</sub>O<sub>2</sub>, photo-oxidation of bromacil improved a lot although oxygen showed nominal effect. In dye-sensitized system, bromacil (BR) degradation was observed in presence of small amount of methylene blue (MB) and red 22 (R) dyes in UV and natural sun light respectively. Degradation of BR in UV light was slightly higher than that of sun light. The photo-oxidation mechanism of the reaction seems to happen in presence of dual oxidant. First one was hydroxyl radicals produced by band gap excitation of semiconductor and subsequent formation of electron/hole pair. Second one was singlet oxygen formed through dye-sensitization process.<sup>57</sup>

### 2.4.1.4 Hydrazine degradation

Chatterjee, studied the reduction of hydrazine to ammonia via dye-sensitized photocatalysis with Pt/TiO<sub>2</sub>-[Ru<sup>III</sup>(EDTA)(H<sub>2</sub>O)] - system. The reaction mechanism was explained by the formation of [Ru<sup>III</sup>(EDTA)(N<sub>2</sub>H<sub>5</sub>)] species (adsorbed on TiO<sub>2</sub> surface) which experienced a two-electron transfer reduction followed by cleavage of the N-N bond of coordinated hydrazine as described below:



The rate controlling step of the photocatalytic process was the surface chemical step (electron transfer) which could be coupled with adsorption of reactants and desorption of ammonia molecule.<sup>58</sup>

#### 2.4.1.5 Dye degradation

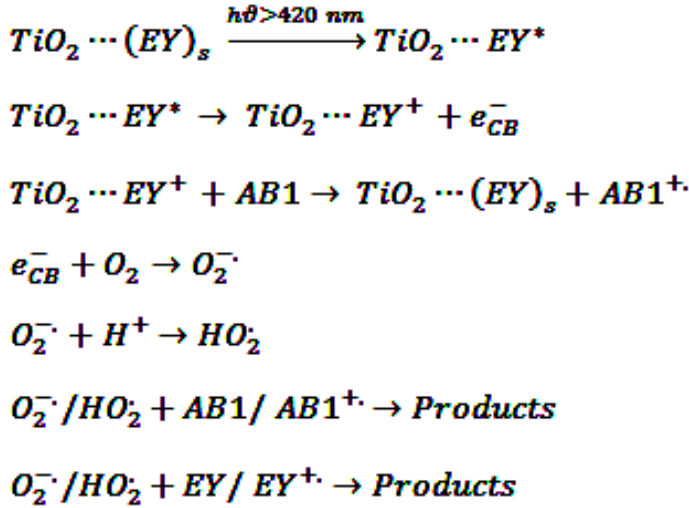
A non-sensitizing dye (e.g. acid blue1 (AB1)) in an effluent can be degraded by just mixing with another effluent containing sensitizing dye (eosin Y or thionine) and subjecting the mixture of effluent to visible light and aqueous suspensions of TiO<sub>2</sub>. However, the sensitizing dye also degrades gradually due to self-sensitized degradation mechanism.<sup>59</sup>

Different dye degradation such as bromothymol blue, acid blue 1, methylene blue, eosin Y, thionine, and chrysoidine Y were reported in recent literatures.<sup>59-63</sup> Degradation rates are strongly influenced by several factors such as solution pH, catalyst concentration, substrate concentration, type of electron acceptor and semiconductor type. Degussa TiO<sub>2</sub> P25 showed highest efficiency compared to Hombikat UV100, PC 500, TTP and ZnO.<sup>60</sup> Solution pH is an important parameter in the photocatalytic reactions, since it influences the surface charge of the catalyst and therefore the adsorption behavior of the pollutants. The efficiency of bromothymol blue degradation was found to be more or less similar in pH range of 4-9. Formation of reaction intermediate was also confirmed by new absorption peak at pH 9. At pH 2, slightly lower mineralization rates were observed.<sup>60</sup> In case of chrysoidine Y, maximum degradation was found at pH 9. At alkaline pH, high concentration of HO<sup>-</sup> ion facilitated the formation of hydroxyl radicals, which finally diffused away and degraded the dye molecule in the bulk solution.<sup>61</sup>

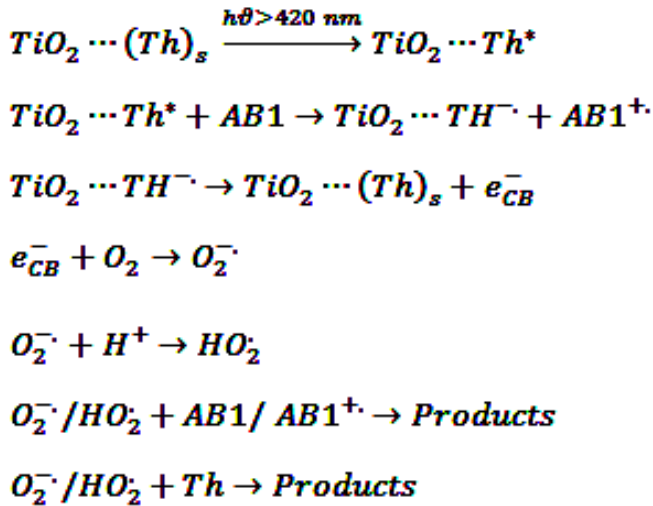
Simultaneous photocatalytic degradation of AB1, eosin Y and thionine in air equilibrated aqueous suspension of TiO<sub>2</sub> photocatalyst has been achieved by Chatterjee et al.<sup>59</sup> They also proposed the formation of reactive  $\bullet\text{O}_2/\bullet\text{HO}_2$  as a major route of dye degradation. Degradation mechanism of AB1 in presence of eosin Y and thionine is quite different. Thionine accepts electron at the excited state whereas eosin Y usually releases electron. So, thionine can oxidize AB1 to AB1<sup>+</sup> even in the absence of TiO<sub>2</sub> and in the process it is

converted into a colorless species, semithionine. However, eosin Y cannot undergo such oxidation (AB1 to AB1<sup>+</sup>) upon irradiation in absence of TiO<sub>2</sub>. Scheme 1 and Scheme 2 were proposed for the degradation of AB1-EY and AB1-Th.<sup>59</sup>

**Scheme 1:**



**Scheme 2:**





In case of dye-sensitized TiO<sub>2</sub> photocatalyst, the dye molecules were only adsorbed on TiO<sub>2</sub> surface and no stable chemical bonds were formed between them. As a result, the dye molecules were easily desorbed from TiO<sub>2</sub> surface during photocatalytic process, which could decrease its photocatalytic activity. Jing et al. synthesized a dye modified TiO<sub>2</sub> using Chrysoidine G (CG), tolylene-2,4-diisocyanate (TDI) and Degussa P25 as raw materials. TDI linked together TiO<sub>2</sub> and CG via –NHCOOTi and –NHCONH– bonds to produce a dye modified TiO<sub>2</sub> catalyst. The dye modified TiO<sub>2</sub> showed strong absorption in visible region and improved adsorption capacity to methylene blue (MB) As a result, the photocatalytic degradation of MB by dye-modified TiO<sub>2</sub> showed much higher activity than bare TiO<sub>2</sub>.<sup>63</sup>

## 2.4.2 Aromatic compounds

### 2.4.2.1 Phenol degradation

Photodegradation of phenol with dye-sensitized TiO<sub>2</sub> showed promising results under visible light irradiation.<sup>64, 65</sup> Grandos et al. utilized Zn(II) and Co(II) tetracarboxyphthalocyanine (TcPcM) to sensitize TiO<sub>2</sub> and TiO<sub>2</sub>/Pt for the degradation of phenol in visible light. They expressed the degradation of phenol with TcPcM/TiO<sub>2</sub> in terms of photonic efficiency [ $\eta = (kC_0/I_0)$ ]; where C<sub>0</sub> was the initial phenol concentration and I<sub>0</sub> was the incident photonic flow per unit volume. The photonic efficiencies ( $\eta$ ) of phenol degradation were 4.3% and 3.3% on TcPcCo/TiO<sub>2</sub> and TcPcZn/TiO<sub>2</sub> respectively. Again, photodeposition of platinum on TcPcM/TiO<sub>2</sub> enhanced reaction photo-efficiency up to  $\eta \cong 0.1$ .<sup>64</sup>

Chowdhury et al.,<sup>65</sup> also reported eosin Y-sensitized TiO<sub>2</sub>/Pt catalyst for the degradation of phenol in visible light. About 93% degradation of phenol (C<sub>0</sub> = 40 mg L<sup>-1</sup>) was achieved within 90 minutes under optimum reaction conditions such as pH 7.0, catalyst loading of 0.8 g L<sup>-1</sup>, electron donor (triethanolamine) concentration of 0.2 M, 0.5% Pt loading on TiO<sub>2</sub>, and visible solar light intensity of 100 mW cm<sup>-2</sup>. They considered the formation of superoxide ( $\bullet\text{O}_2^-$ ) ions followed by HO $\bullet$ , which subsequently proceeded to the complete mineralization of phenol and other intermediates. They also found a

significant effect of the Pt loading on phenol degradation. Eosin Y-sensitized TiO<sub>2</sub> without Pt metal can degrade phenol (~ 67 %) in visible light, but with the incorporation of Pt (0.5 %) on TiO<sub>2</sub>, complete degradation was achieved.

#### 2.4.2.2 Chlorophenol degradation

Ghosh et al.<sup>66</sup> reported the degradation of 4-chlorophenol in aqueous medium with coumerine (C-343,  $\lambda_{\text{max}} = 446$  nm) sensitized TiO<sub>2</sub> photocatalyst using 436 nm LED based photoreactor. LEDs offer high electrical to light energy conversion with slight heat production, forward directed output facilitating delivery to a target, extended lifetime, and operation on DC which may facilitate its use in remote locations. Additionally, the LED reactor efficiency for 4-chlorophenol degradation was fairly comparable with a conventional multi-lamp reactor or sun light. The coumarin dye can harvest a larger fraction of energy from the well-matched LED. The reaction rate fitted approximately to first order kinetics and moved towards a limiting value at a quite high catalyst concentration (3 g L<sup>-1</sup>). They mentioned about HO<sup>•</sup> radical initiated reaction mechanism although the formation of chlorocatechol was not reported. The only supporting fact regarding this was HO<sup>•</sup> radical scavenging experiment. Formation of superoxide ion (<sup>•</sup>O<sub>2</sub><sup>-</sup>) was also assumed, which would involve the attack to benzene ring with loss of chlorine from chlorophenol.<sup>66, 67</sup>

#### 2.4.2.3 Benzyl alcohol degradation

The photocatalytic oxidation of benzyl alcohol has been investigated by Hussein and Alkateeb, under natural weathering conditions (sunlight and oxygen) in presence of TiO<sub>2</sub> or sensitized TiO<sub>2</sub>. Sensitization of TiO<sub>2</sub> was achieved by the impregnation of riboflavin (RF), safranin O (SO), methyl red (MR), eosin B (EB), and methyl blue (MB) on anatase (TiO<sub>2</sub> P25). Benzaldehyde was identified as the only reaction product through HPLC, FTIR, and spectrophotometric analysis. The photo-oxidation of benzyl alcohol was found to follow the sequence: RF > SO > naked TiO<sub>2</sub> > MR > EB > MB. The formation of benzaldehyde during the photocatalytic reaction was studied by using FTIR, HPLC and spectrophotometric measurements.<sup>68</sup>

**Table 2.3. Dye-sensitized photodegradation of organic compounds**

No	Organic compounds	Initial substrate concentration	Sensitizer/ Photocatalyst	Light source and accessories	Other experimental details	Results/ comments	Reference
1.	CCl <sub>4</sub>	10 mM	Ruthenium bipyridyl complex (Ru <sup>II</sup> (bpy) <sub>3</sub> )/nonionic surfactant Brij-35 .	450 W Xe arc lamp (Oriel); 10 cm IR water filter; UV cutoff filter ( $\lambda > 420$ nm)	Irradiation time 120 min; Air equilibrated.	i) CCl <sub>4</sub> degradation rate was enhanced in absence of O <sub>2</sub>	Cho et al. <sup>52</sup>
2.	CCl <sub>4</sub>	3 – 4 ppm	Silylated [Ru <sup>II</sup> (py-pzH) <sub>3</sub> ] <sup>2+</sup> /TiO <sub>2</sub> .  py-pzH $\equiv$ 3-(2'-pyridyl)	100 W tungsten lamp (Oriel) ( $\lambda > 450$ nm);  IR filter.	Irradiation time 30 min; pH 6.5-7.0; purged with air (for 15 min); I <sup>-</sup> as sacrificial electron donor.	i) Silyl linkage is highly stable in extreme pH range (pH 1.0 – 12.0).	Fung et al. <sup>53</sup>
3.	CCl <sub>4</sub>	1 mM	Tris (4, 4'-dicarboxy-2,2'-bipyridyl) ruthenium (II) chloride	450 W Xe-arc lamp (Oriel); 10 cm IR water filter; UV cut off filter ( $\lambda > 420$ nm).	Irradiation time 6 h; N <sub>2</sub> saturated system; TiO <sub>2</sub> =0.5g L <sup>-1</sup> ; pH 3; 2-propanol as electron donor.	Quantum yield of CCl <sub>4</sub> dechlorination 10 <sup>-3</sup>	Cho et al. <sup>54</sup>

4.	i) CCl <sub>4</sub> ii) trichloroacetate (TCA)	i) 1 mM ii) 1 mM	Tris (4, 4'-dicarboxy-2, 2'-bipyridyl)-ruthenium (II) complex.	450 W Xe-arc lamp (Oriel); 10 cm IR water filter; UV cut off filter ( $\lambda > 420$ nm).	Irradiation time 1 h (CCl <sub>4</sub> ) and 2 h (TCA); O <sub>2</sub> was removed by N <sub>2</sub> sparging before reaction; pH 3	Photocatalyst was completely inactive in presence of dissolved oxygen.	Bae and Choi <sup>55</sup>
5.	Trichloroethylene (TCE)	2-500 ppm	Natural anthocyanine dye (obtained from fruits)/buoyant TiO <sub>2</sub> coated microsphere.	150 W Xe lamp;	Irradiation time 15 - 1440 min	i) Mineralization product: HCl; ii) 93 % TCE degradation was reported.	Alexander and Rosentreter <sup>56</sup>
6.	Pesticides (bromacil (BR))	30-100 ppm	Methylene blue (MB), Red 22 (R).	UV: HBO 200 W; natural sunlight	TiO <sub>2</sub> concentration 100 mg L <sup>-1</sup> ; MB/BR molar ratio varied from 0.05-0.2 ; R/BR molar ratio was 0.143	Highest enhancement factor (EF) 2.27 was achieved at MB/BR molar ratio of 0.1	Muszkat et al. <sup>57</sup>

7.	Hydrazine	1 mmol	$\text{Ru}^{\text{III}}(\text{EDTA})(\text{H}_2\text{O})^-$ /Pt/TiO <sub>2</sub> P25	250 W Xe lamp	Irradiation time 8 h; pH 3.1; Temperature 25 <sup>0</sup> C.	i) Hydrazine is reduced to ammonia;  ii) Yield of ammonia production 1.98×10 <sup>-5</sup> mol h <sup>-1</sup> .  ii) Declined yield after 5 h	Chatterjee <sup>58</sup>
8.	Phenol	100 ppm	Zn(II) and Co(II) tetracarboxphthalo cyanine/Pt/TiO <sub>2</sub> .	100 W halogen lamp (Osram); 1M K <sub>2</sub> Cr <sub>2</sub> O <sub>7</sub> as UV filter.	Irradiation time 60 min; Temperature 20±2 <sup>0</sup> C; Air supply into reaction medium.	i) 33 % phenol degradation with TcPcZn/TiO <sub>2</sub> /Pt  ii) 65 % phenol degradation with TcPcCo/TiO <sub>2</sub> /Pt.	Granados O et al. <sup>64</sup>
9.	4- chlorophenol (4ClPh)	40 ppm	Coumarin- 343/TiO <sub>2</sub> P25	81 Gilway “super bright” (Peabody, MA) E472 μW (max output); 1mM K <sub>2</sub> Cr <sub>2</sub> O <sub>7</sub> in 0.22 M Na <sub>2</sub> CO <sub>3</sub> aqueous solution as UV filter.	Irradiation time 8 – 10 h; Temperature 20±2 <sup>0</sup> C;	i) Reaction intermediate: 1,2,4 -benzenetriol and d  ihydroxymaleic acid;  ii) First order reaction kinetics	Ghosh et al. <sup>66</sup>

---

						followed.	
10	i) Chlorophenol ii) 1,2-dichloroethane iii) 1,4-dichlorobenzene iv) trichloroethylene	i) 1 mmol ii) 1 mmol iii) 0.1 mmol iv) 1 mmol	Thionine, Eosin Y, Rhodamine B, methylene Blue, Nileblue A, Safranin O/ TiO <sub>2</sub> .	150 W Xenon lamp (Oriental Instruments); UV filter solution (NaNO <sub>3</sub> +CuSO <sub>4</sub> +NH <sub>4</sub> OH).	O <sub>2</sub> was bubbled in the photoreactor.	i) Product of CO <sub>2</sub> , Cl <sup>-</sup> ; ii) 55-72 % degradation of pollutant was achieved.	Chatterjee et al. <sup>59</sup>
11	Benzyl alcohol		Riboflavin (RF), Safranin O (SO), Methyl red (MR), Eosin B (EB), Methylene blue (MB)/TiO <sub>2</sub> P25	Sunlight	Irradiation time 75 min; Temperature 316-321 K; Reaction volume 150 cm <sup>3</sup> .	i) Benzaldehyde was the photooxidation product; ii) The sequence of dye in the following superiority order: RF>SO>naked TiO <sub>2</sub> >MR>EB>MB;	Hussein et al. <sup>68</sup>

---

**Table 2.4 Dye-sensitized photodegradation of organic dyes**

No.	Organic dyes	Initial substrate concentration	Sensitizer/ Photocatalyst	Light source and accessories	Other experimental details	Results/ Comments	Reference
1.	Methylene blue	50 ppm	Chrysoidine G/TiO <sub>2</sub> P25.	250 W metal halide lamp (Philips); UV cut off filter.	Irradiation time 12 h.	special organic complexes were formed on the TiO <sub>2</sub> surface via stable $\pi$ -conjugated chemical bonds between TiO <sub>2</sub> and dye molecules	Jiang et al. <sup>63</sup>
2.	Bromothymol blue (BTB)	0.25 mM	TiO <sub>2</sub> P25	125 W medium pressure mercury lamp; IR and UV filter.	Catalyst dose 1 g L <sup>-1</sup> ; Irradiation time 90 min; electron acceptor (KBrO <sub>3</sub> , H <sub>2</sub> O <sub>2</sub> etc).	Electron acceptors showed positive effect on BTB degradation	Haque and Muneer <sup>60</sup>
3.	Acid blue 1 (AB1)	25 ppm	Eosin Y, Thionine/TiO <sub>2</sub> .	150 W Xenon lamp (Oriel Instruments); Copper sulfate and ammonium hydroxide as UV filter ( $\lambda > 420$ nm).	Irradiation time 5 h; O <sub>2</sub> was bubbled in photoreactor; pH 5.0.	decoloration of eosinY (EY) or thionine (Th) due to self-sensitized degradation was also noticed	Chatterjee et al. <sup>59</sup>

---

4.	Chrysoidine Y	0.25 mM	Chrysoidine Y/TiO <sub>2</sub> P25.	125 W medium pressure Hg lamp.	Irradiation time 120 min; O <sub>2</sub> purging and stirring; pH 3.0-9.0.	Degussa P25 was more efficient than that of ZnO	Qamar et al. <sup>61</sup>
----	---------------	---------	-------------------------------------	--------------------------------	--	---	----------------------------

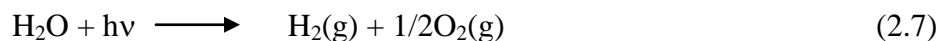
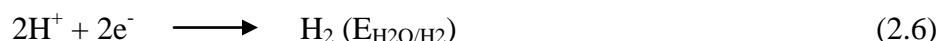
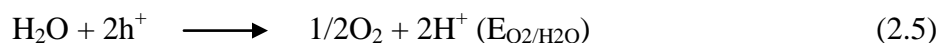
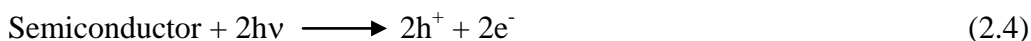
---



## 2.5 Application of Dye-Sensitized Photocatalyst for Hydrogen Generation

### 2.5.1 Basic requirement for hydrogen generation in visible light

When a semiconductor material is illuminated with photons having an energy  $h\nu$  equal to or larger than the semiconductor band gap, the result is formation of electronic charge carriers, electrons in the conduction band and holes in the valance band.



The photoelectrons and holes reduce and oxidize water to produce the stoichiometric 2:1 mixture of  $\text{H}_2$  and  $\text{O}_2$  by the above reaction (2.4-2.7).<sup>69</sup>

The Gibb's free energy ( $\Delta G$ ) at STP is positive for water splitting reaction (equation (2.7)). Such a non-spontaneous reaction will be possible if the energy of the incident photon's energy is equivalent to the change in the Gibb's free energy ( $\Delta G$ ) of the reaction and that must be supplied. Under standard conditions water can be electrolyzed reversibly into hydrogen and oxygen (2:1) at a potential of 1.23 V which is derived from the equation of Gibb's free energy:

$$\Delta G^0 = - nF ((\Delta E^0)) \quad (2.8)$$

Where,  $\Delta G^0$  and  $\Delta E^0$  are standard Gibbs free energy change and standard electrical potential of the reaction. The standard Gibbs free energy change ( $\Delta G^0$ ) is the negative value of maximum electrical work corresponding to  $237.14 \text{ kJ mol}^{-1}$  or  $2.46 \text{ eV}$  for equation (2.7). Since this is a two electron redox process, photocatalytic water splitting is

possible if the semiconductor photocatalyst possess a band gap energy ( $E_g$ ) greater than 1.23 eV.<sup>70, 71</sup>

Now the semiconductor photocatalyst will be visible light active if the band gap energy is less than 3.0 eV. In addition, the band position is also an important parameter for visible light excitation. Therefore, the photocatalytic materials for visible light water splitting should have proper band position and suitable band gap energy ( $1.23 \text{ eV} < E_g < 3.0 \text{ eV}$ ).<sup>70</sup> Oxides such as  $\text{TiO}_2$ ,  $\text{ZnO}$  and  $\text{SnO}_2$  have large band gap (3-3.8 eV) and absorb only ultra-violet part of the solar emission and so has low conversion efficiencies. The adsorbed dye is photo excited and then inject electron to the conduction band of semiconductor.

Dye sensitization to photocatalyst is an excellent method to broaden its absorbance range. Remarkable increases in visible-light absorption ability were observed after dye sensitization without compromising the photocatalyst structure. Abe et al.<sup>72</sup> reported maximum improvement in visible light absorption for N3- $\text{TiO}_2/\text{Pt}$  (Ru complex N3) followed by M- $\text{TiO}_2/\text{Pt}$  (merocyanine NK2045) and C- $\text{TiO}_2/\text{Pt}$  (coumarine C343). Nanotube  $\text{Na}_2\text{Ti}_2\text{O}_4(\text{OH})_2$ ,<sup>73</sup> has a absorption band edge of about 390 nm, which was expanded to 670 nm by sensitization with eosin Y dye. Sensitizations with eosin Y dye were also reported for N-doped  $\text{TiO}_2/\text{Pt}$ ,<sup>74</sup> silane-coupled  $\text{TiO}_2$ ,<sup>75</sup> mesoporous  $\text{TiO}_2/\text{Pt}$ ,<sup>76</sup> TS-1 zeolite,<sup>77</sup> and silica gel H<sup>78</sup>. In all cases a red-shift of the absorption band edge to about 600 nm were observed. Li et al.<sup>79</sup> prepared multilayer-eosin Y- $\text{TiO}_2$  through linkage of  $\text{Fe}^{3+}$  and achieved similar improvement in visible light absorption.

## 2.5.2 Dye-sensitized photocatalytic hydrogen generation mechanism

Dye-sensitized photocatalytic hydrogen evolution from water is pointed out in Figure 2.5.<sup>80</sup> Light excitation of sensitizer is followed by electron transfer into the conduction band of the photocatalyst and is channeled to the platinum site, where hydrogen evolution occurs.<sup>16</sup>

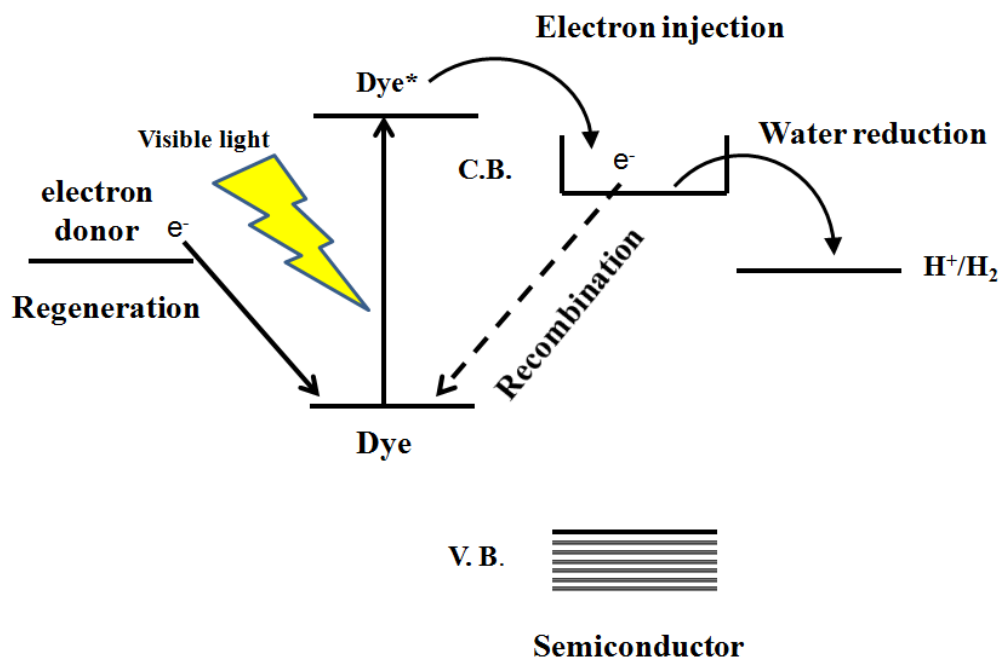
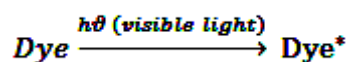


Figure 2.4 Dye-sensitized photocatalytic H<sub>2</sub> generation from water (adapted from Chen et al.<sup>80</sup>).

Dye sensitization followed by photocatalytic hydrogen generation process can be expressed in few consecutive steps i) visible light absorption by dye molecule and excitation, ii) sensitization of semiconductor (TiO<sub>2</sub>) with excited dye species, iii) hydrogen generation with the assistance of co-catalyst (Pt), iv) regeneration of dye with the help of electron donor.

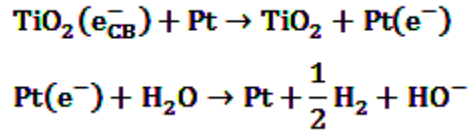
i) Light absorption:



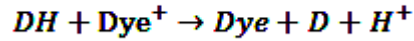
ii) Sensitization of TiO<sub>2</sub>:



iii) Hydrogen generation:



iv) Dye regeneration:



The summarized scheme is give in Figure 2.6, which shows that the overall mechanism induced by light is reduction of water and oxidation of the third component employed as an electron donor.

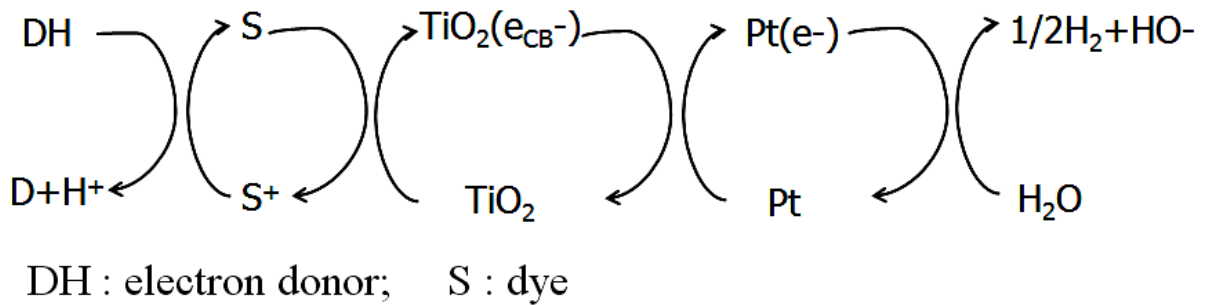


**Figure 2.5 Scheme for visible light-driven hydrogen generation by dye-sensitized TiO<sub>2</sub>/Pt**

### 2.5.3 Sensitization with different dyes for photocatalytic hydrogen generation

Different types of dye molecules have been used so far as sensitizer generating hydrogen in visible light. In early studies, Ru(bpy)<sub>3</sub><sup>2+</sup> and its derivatives were used as sensitizer for Pt/RuO<sub>2</sub>-loaded TiO<sub>2</sub> particles for overall water cleavage.<sup>81-83</sup> Sacrificial hydrogen generation was also reported for Ru(bpy)<sub>3</sub><sup>2+</sup> and Ru<sup>II</sup>(acid)<sub>3</sub> sensitized TiO<sub>2</sub>/Pt in visible

light using EDTA as electron donor. Activities of Tris(2,2'-bipyridine-4,4'-dicarboxylic acid) ruthenium(II) ( $\text{Ru}(\text{dcbpy})_3$ ) and  $\text{Ru}(\text{bpym})_3^{2+}$  were better for hydrogen generation in visible light compared to  $\text{Ru}(\text{bpy})_3^{2+}$ .<sup>84</sup> Enhanced dye adsorption on the photocatalyst surface was mainly projected as the explanation of such improvement. Strongly bound dye molecule can be stabilized near semiconductor surfaces, which leads to fast electron-injection of the excited dye into substrate. The photocatalytic activity and stability of  $\text{Ru}(\text{bpy})_3^{2+}$ -sensitized  $\text{TiO}_2$  depends on surface anchoring group. According to Bae et al.<sup>85</sup> phosphonate group based sensitizer exhibited higher photocatalytic activity for hydrogen production from water than carboxylate group based sensitizer. Anchoring through phosphonate group assisted faster regeneration and thus acted as better ruthenium sensitizer linkage to the  $\text{TiO}_2$  surface in aqueous solution.

Again, close proximity of dye molecule and substrate also increases the probability of electron/oxidized dye recombination reaction. Kajiwara et al.<sup>86</sup> also believed that the thermal re-orientational motion of the loosely attached molecules was responsible for enhanced electron transfer. Peng et al.<sup>87</sup> did a comparative photosensitizing activity study with three kinds of dyes, having different terminal groups that can attach to  $\text{TiO}_2$  through firm or loose linkage. Among them, N719 [ $(\text{n-Bu}_4\text{N})_2\text{-cis-Ru}(\text{dcbpy})_2(\text{SCN})_2$ ], one of the best sensitizer for DSSCs with the same structure as N3 dye.  $\text{Ru}(\text{bpy})_2(\text{him})_2\text{-NO}_3$  and  $\text{Ru}_2(\text{bpy})_4\text{L}_1\text{-PF}_6$  have no terminal group like N719 and can just loosely link with  $\text{TiO}_2$ .  $\text{Ru}_2(\text{bpy})_4\text{L}_1\text{-PF}_6$  showed more steady and higher increases in  $\text{H}_2$  generation with extended irradiation time than the strongly linked N719. Therefore, the dynamic equilibrium between the ground state dye- $\text{TiO}_2$  attachment and oxidized dye- $\text{TiO}_2$  detachment played a crucial role in the photochemical behavior during the photocatalyst sensitization process.<sup>88</sup>

Higher cost constrains and toxicity of metal based dyes (especially Ru based dyes) forced researchers to use less expensive organic dyes for dye sensitization. Photosensitization activity of five different dyes namely acriflavin, eosin blue, fluorescein, rhodamine B, rose bengal, was examined for hydrogen production by  $\text{SnO}_2/\text{Pt}$ .<sup>89</sup> Among them eosin blue provided the maximum efficiency to sensitize  $\text{SnO}_2$  and produced a greater amount

of hydrogen, even higher than  $\text{Ru}(\text{bpy})_3^{2+}$ . Photosensitization abilities of eosin Y dye for sacrificial hydrogen generation were studied extensively by several authors.<sup>73-79</sup> Sreethawong et al.<sup>76</sup> synthesized mesoporous-assembled  $\text{TiO}_2/\text{Pt}$  by a single step sol-gel process with the aid of structure-directing surfactant. The activity of the photocatalyst with eosin Y sensitization was studied in diethanolamine (30 vol %) aqueous solution. Platinum loaded (0.6 wt %)  $\text{TiO}_2$  calcined at  $500^\circ\text{C}$  showed highest photocatalytic performance for hydrogen generation from aqueous diethanolamine solution containing 2 mM eosin Y. Li et al.<sup>74</sup> prepared a nitrogen-doped  $\text{TiO}_2/\text{Pt}$  ( $\text{N-TiO}_2$ ) by calcination of the hydrolysis product of  $\text{Ti}(\text{SO}_4)_2$  with aqueous ammonia followed by platinum loading. Then,  $\text{N-TiO}_2/\text{Pt}$  was sensitized with anhydrous ethanol solution of eosin Y and used for hydrogen generation in presence of triethanolamine. Nitrogen doping created surface oxygen defects which facilitated the adsorption of eosin Y. Thus, under similar experimental conditions eosin Y- $\text{N-TiO}_2/\text{Pt}$  showed higher photocatalytic activity compared to that of eosin Y- $\text{TiO}_2/\text{Pt}$ . A chemical fixation of eosin Y on  $\text{TiO}_2/\text{Pt}$  was tried by Abe et al.,<sup>75</sup> with silane-coupling in order to get steady hydrogen generation from aqueous triethanolamine solution. The turnover number was quite high ( $10^4$ ), which represented high catalyst stability, although the initial hydrogen generation rate was low, compared to that of physically mixed system of eosin Y and  $\text{TiO}_2/\text{Pt}$ . The quantum yield at 520 nm was found to be about 10 %. Eosin Y-sensitized platinum loaded nanotube  $\text{Na}_2\text{Ti}_2\text{O}_4(\text{OH})_2$ , with a quantum yield up to 14.97 %, showed good photocatalytic stability for hydrogen production over 100 h after 10 consecutive runs. Li et al.<sup>79</sup> prepared a multilayer-eosin Y-sensitized  $\text{TiO}_2$  through  $\text{Fe}^{3+}$  coupling between  $\text{TiO}_2$ -eosin Y and different eosin Y molecule. The photocatalyst had very high light harvesting efficiency and photocatalytic activity for visible light driven hydrogen generation from aqueous triethanolamine solution. The apparent quantum yield for hydrogen evolution was 19.1 %. Eosin Y-sensitized TS-1 zeolite,<sup>77</sup> silica gel H,<sup>78</sup> and multiwalled carbon nanotube/Pt,<sup>90</sup> were also able to generate hydrogen from aqueous triethanolamine solution in visible light with apparent quantum efficiency of 9.4 %, 10.4 % and 12.4 % respectively.

## 2.5.4 Effect of different parameters on the photocatalytic activity for hydrogen generation

### 2.5.4.1 Effect of co-catalyst loading

Till date platinum has shown the highest photocatalytic activity as co-catalyst in water splitting system in visible light. There are few other noble metals from group 8-11 in periodic table (Ru, Rh, Pd, Ag and Au) which have also been reported as effective co-catalyst for such system. Higher electron flow from semiconductor to metal can be achieved with the smaller Schottky barrier height at the metal/semiconductor junction which leads to higher photocatalytic activity for hydrogen production.<sup>91</sup>

### 2.5.4.2 Effect of electron donor

In case of band UV photocatalysis or band gap excitation process sacrificial agents are used to stop  $e^-/h^+$  pair recombination. They are basically electron donors or hole scavengers. These react irreversibly with the photo-generated valance band hole and can enhance the  $e^-/h^+$  pair separation and provide higher quantum efficiency. Aliphatic organic compounds such as ethylenediamine tetra-acetic acid (EDTA), carboxylic acids, aldehydes, and alcohols are mostly used as sacrificial agents to enhance hydrogen production.<sup>2</sup> The degree of enhancement capability was found in the following order by Nada et al.<sup>92</sup>: EDTA > methanol > ethanol > lactic acid. Inorganic ions such as  $S^{2-}/SO_3^{2-}$ ,  $IO_3^-/I^-$  and  $Ce^{4+}/Ce^{3+}$  were also used as sacrificial agent for hydrogen production.<sup>93-95</sup> In dye-sensitized system under visible light, practically no hole is present. In this case the function of electron donor may be viewed in light of its dual function since it could quench the oxidized form of the dye ( $dye^+$ ) or it could extend its lifetime in the photosensitized system providing long-term hydrogen generation. Different electron donors such as EDTA, acetonitrile, methanol, isopropanol,  $IO_3^-/I^-$ , diethanolamine, triethanolamine, chloroacetic acid, and oxalic acid etc. can be used.

### 2.5.4.3 Effect of solution pH

Solution pH has immense influence on photocatalytic reaction which takes place over the photocatalyst surface. In aqueous slurry of TiO<sub>2</sub> the catalyst surface is embraced with plenty of hydroxyl groups and thus the ionization of TiO<sub>2</sub> is greatly affected by solution pH. Moreover, the ionization of the electron donor and regeneration of dye are also influenced by solution pH. Chowdhury et al.<sup>96</sup> reported that dye (eosin Y) molecule showed stronger interaction with solution pH in comparison with the electron donor-pH interaction. Different optimum pH was reported for dye-sensitized photocatalytic system ranging from 3 to 11. With Ru (II) based sensitizer and methyl viologen (MV<sup>2+</sup>) the optimum pH was in acidic range.<sup>81, 82</sup> In case of EDTA and triethanolamine based systems the optimum pH were 7.<sup>73, 75, 84</sup> On the contrary, with diethanolamine based system the optimum pH was alkaline (11.5).<sup>76</sup>



**Table 2.5. Dye-sensitized photocatalytic hydrogen generation**

No	Aqueous mixture details	Capacity/ Concentration	Sensitizer/ Photocatalyst	Light source and accessories	Other experimental details	Results/ Comments	Reference
1.	Water, methyl viologen (MV <sup>2+</sup> )	25 mL/ dye: 10 <sup>-4</sup> – 5x10 <sup>-5</sup> M.	[Ru(bpy) <sub>3</sub> ] <sup>2+</sup> ; Rhodamine B /TiO <sub>2</sub> sol loaded with Pt and RuO <sub>2</sub> (Pt 1mg, RuO <sub>2</sub> 0.2 mg)	450 W –Xe lamp, 420 nm cutoff filter	N <sub>2</sub> saturated; pH 3; TiO <sub>2</sub> 1g L <sup>-1</sup> .	Quantum yield (QY) 30 %	Duonghong et al. <sup>81</sup>
2.	Water, methyl viologen (MV <sup>2+</sup> )	25 mL/ 10 <sup>-4</sup> M dye; 5x10 <sup>-3</sup> M MV <sup>2+</sup>	[Ru(bpy) <sub>3</sub> ] <sup>2+</sup> /colloidal TiO <sub>2</sub> -Pt-RuO <sub>2</sub> (Pt 40 mg/L)	450 W Xe lamp, IR filter, 400 nm cut off filter	N <sub>2</sub> saturated; pH 4.7; TiO <sub>2</sub> 0.5g/L, 4% Nb <sub>2</sub> O <sub>5</sub> , 0.1% RuO <sub>2</sub>	rate of H <sub>2</sub> = 2(rate of O <sub>2</sub> ) only after saturation of TiO <sub>2</sub> adsorption sites	Borgarello et al. <sup>82</sup>
3.	Water- EDTA (electron donor)	3 mL water; EDTA 0.01 M	[Ru(bpy) <sub>3</sub> ] <sup>2+</sup> /TiO <sub>2</sub> P25/Pt and TiO-5/Pt (0.3 wt %).	500 W Xe lamp, UV cutoff filter L42	pH 7 ; TiO <sub>2</sub> (TiO-5): 0.05g	rate H <sub>2</sub> ~5.73μmol min <sup>-1</sup>	Hirano et al. <sup>84</sup>
4.	Water	40 mL/10 <sup>-4</sup> M dye	[Ru(dcbpy) <sub>2</sub> (dpq)] <sup>2+</sup> /TiO <sub>2</sub> P25/Pt (0.4wt %); ZnO/Pt (0.4wt %)	250 W tungsten halogen lamp; IR filter	N <sub>2</sub> saturated; pyrogallol solution to remove O <sub>2</sub> ; cat dose 1g L <sup>-1</sup> ;	rateH <sub>2</sub> : 4.16x10 <sup>-3</sup> mL H <sub>2</sub> /min (TiO <sub>2</sub> /Pt), 5x10 <sup>-4</sup> mL H <sub>2</sub> /min (ZnO/Pt)	Dhanalakshmi et al. <sup>16</sup>
5.	Water-	100m L/ water 5	Merocyanine (M),	300 W Xe	Cat dose 0.5 g	Q.Y (%): N3-	Abe et al. <sup>72</sup>

	acetonitrile , NaI (I <sub>3</sub> <sup>-</sup> /I)	%; NaI 0.1 M	Coumarin (C), Ru complex (N3) dye/TiO <sub>2</sub> /Pt (0.5 wt %)	lamp, 410 nm cut off filter	L <sup>-1</sup>	Pt/TiO <sub>2</sub> :4.5 ; C- Pt/TiO <sub>2</sub> :1.8 ; M- Pt/TiO <sub>2</sub> 2.5.	
6.	Water- methanol (MeOH) (electron donor); Water- triethanolamine (TEOA) (electron donor)	100 mL / 20 ml electron donor	N719, Ru(bpy) <sub>2</sub> (him) <sub>2</sub> - NO <sub>3</sub> , Ru <sub>2</sub> (bpy) <sub>4</sub> L <sub>1</sub> - PF <sub>6</sub> /TiO <sub>2</sub> /Pt ( 1wt %)	500 W-Xe arc lamp, 420 cutoff filter, outer radiation type photo reactor	Degassed before reaction; Cat dose 0.4g L <sup>-1</sup>	Highest H <sub>2</sub> generation rate was observed with Ru <sub>2</sub> (bpy) <sub>4</sub> L <sub>1</sub> - PF <sub>6</sub> ;  rateH <sub>2</sub> : 0.58 μmol H <sub>2</sub> /min (with TEOA) and 0.04μmol H <sub>2</sub> /min (with methanol )	Peng et al. <sup>87</sup>
7.	Water- MeOH (electron donor)	100 mL /20 ml MeOH	N719, Ru(bpy) <sub>2</sub> (him) <sub>2</sub> - NO <sub>3</sub> , Ru <sub>2</sub> (bpy) <sub>4</sub> L <sub>1</sub> - PF <sub>6</sub> /mesoporous TiO <sub>2</sub> /Pt (1 wt%)	250 W Xe lamp 420 nm cutoff filter, outer radiation type photo reactor	Degassed before reaction; Cat dose 0.4g L <sup>-1</sup>	rateH <sub>2</sub> :  0.24 μmol min <sup>-1</sup>  (300 <sup>0</sup> C calcination);  0.16 μmol min <sup>-1</sup>  (500 <sup>0</sup> C calcination )	Peng et al. <sup>88</sup>
8.	Water-TEOA	80 mL /TEOA	Eosin Y/	300 W tungsten	N <sub>2</sub> saturated;	rateH <sub>2</sub> :1.26	Li et al. <sup>73</sup>

	(electron donor)	15 vol%,	nanotube Na <sub>2</sub> Ti <sub>2</sub> O <sub>4</sub> (OH) <sub>2</sub> /Pt (0.5wt %)	halogen lamp, 420 nm cut off filter	dye:cat mass=1:1; pH 7; Cat dose: 0.5g L <sup>-1</sup> ;	μmol/min; QY:14.97 %	
9.	Water-TEOA (electron donor)	80 mL/ TEOA 0.79 M	Eosin Y/N-TiO <sub>2</sub> /Pt (0.5 wt%)	400 W high pressure Hg lamp; 420 nm cut off filter	N <sub>2</sub> saturated; pH 7; Cat dose: 1.25 g L <sup>-1</sup>	rateH <sub>2</sub> ~1.33 μmol min <sup>-1</sup> ;	Li et al. <sup>74</sup>
10.	Water-TEOA (electron donor)	250 mL/ TEOA	Eosin Y/TiO <sub>2</sub> / Pt (0.1 wt%) (fixed with silane coupling agent )	300 W Xe lamp; 460 nm cut off filter;	N <sub>2</sub> saturated; pH 7; Cat dose: 1.2g L <sup>-1</sup> ;	rateH <sub>2</sub> ~11.6 μmol min <sup>-1</sup> ; QY:10 %	Abe et al. <sup>75</sup>
11.	Water- diethanolamine (electron donor)	150 mL/ diethanolamine 30vol %	Eosin Y/ mesoporous- assembled TiO <sub>2</sub> /Pt (0.6 wt%)	300 W Xe arc lamp; 400 nm cut off filter;	N <sub>2</sub> saturated; pH 11.5; Cat dose: 3.33g L <sup>-1</sup> ;	rate H <sub>2</sub> ~ 0.033 ml min <sup>-1</sup>	Sreethawong et al. <sup>76</sup>
12.	Water-TEOA (electron donor)	60 mL/ TEOA 15wt %	Eosin Y/TS-1 zeolite/Pt (1 wt%)	300 W tungsten halogen lamp; 420 nm cut off filter;	N <sub>2</sub> saturated; pH 7; dye:cat mass=1:8; Cat dose: 0.6g L <sup>-1</sup> ;	rate H <sub>2</sub> : 0.56 μmol /min; QY:9.4 %	Zhang et al. <sup>77</sup>
13.	Water-TEOA (electron donor)	60 mL/ TEOA 15wt %	Eosin Y/silica gel/Pt	300 W tungsten halogen lamp; 420 nm cut off filter;	N <sub>2</sub> saturated; pH 7; dye:cat mass=1:3; Cat dose: 1g L <sup>-1</sup> ;	rate H <sub>2</sub> : 0.72 μmol min <sup>-1</sup> ; QY:10.4 %	Zhang et al. <sup>78</sup>
14.	Water-TEOA (electron donor)	80 mL/ TEOA 0.79 M	Eosin Y/ TiO <sub>2</sub> /Pt (1 wt%) (linkage via Fe <sup>3+</sup> coupling)	400 W metal halide lamp; 420 nm filter;	N <sub>2</sub> saturated; pH 7; Cat dose:1.25g L <sup>-1</sup>	rate H <sub>2</sub> : 4.58 μmol /min; QY:19.1 %	Li et al. <sup>79</sup>

## 2.6 Conclusions

In this review the basic principle of dye-sensitization and effect of different parameters on the process were discussed. Surface anchoring group, energy level and ground state redox potential of dye molecule were recognized as the most important parameters for successful electron injection to the conduction band of semiconductor. Ruthenium based sensitizers were used extensively in dye sensitization field but because of their higher cost and toxicity, future researchers are gradually focusing on non-toxic organic dyes as well as natural dyes from fruits, flowers and vegetables.

The presence of novel metals on semiconductor surface was crucial for hydrogen generation and also had positive effect on organic degradation. Different methods of co-catalyst loading have been discussed in details. Among the five methods, atomic layer deposition (ALD) was described as the best method in terms of precise control over both composition and thickness of loaded metal. This however is an expensive method, and further research is needed to find a simpler method such as photodeposition that can utilize solar radiation instead of UV lamps to minimize the operation cost.

Finally, the applications of different dye-sensitized photocatalysts under visible light were presented for treatment of organic compounds and hydrogen generation. Ru (II) based dye-sensitized photocatalysts were able to degrade carbon tetrachloride ( $\text{CCl}_4$ ) and hydrazine in high acidic pH. They also performed water splitting in visible light with high quantum yield. Organic and natural dye-sensitized photocatalysts were efficient for the degradation of pesticides, trichloroethylene, phenol and chlorophenols. Excellent hydrogen generation activity was observed for metal free dyes such as xanthane dyes, merocyanine dyes and coumarin dyes in visible light.

Although extensive work in this field has been carried out, several topics are yet to be explored. Natural dyes need to be studied properly for dye sensitization purpose. We need to consider the utilization of complete solar spectrum rather than only visible light in those experiments. Effect of light intensity has not been studied for dye-sensitized

photocatalytic hydrogen generation. If the effect of light intensity on hydrogen generation is not properly selected, a large portion of photons energy will be dissipated in the form of heat.

## 2.7 References

1. Fujishima, A.; Honda, K., Electrochemical Photolysis of Water at a Semiconductor Electrode. *Nature (London)* **1972**, 238, 37-38.
2. Ni, M.; Leung, M. K. H.; Leung, D. Y. C.; Sumathy, K., A review and recent developments in photocatalytic water-splitting using TiO<sub>2</sub> for hydrogen production. *Renewable and Sustainable Energy Reviews* **2007**, 11, (3), 401-425.
3. Kalyanasundaram, K.; Gratzel, M., *Photosensitization and photocatalysis using inorganic and organometallic compounds*. Kluwer Academic Publishers: **1993**; Vol. 14, p 247-271.
4. Bard, A. J.; Stratmann, M., *Encyclopedia of Electrochemistry, Vol. 6*. Wiley-VCH: Germany, **2002**; p 393-495.
5. Gratzel, M., Dye-sensitized solar cells. *Journal of Photochemistry and Photobiology C: Photochemistry Reviews* **2003**, 4, (2), 145-153.
6. Tennakone, K.; Kumarasinghe, A. R.; Sirimanne, P. M., Dye sensitization of low-bandgap semiconductor electrodes: cuprous oxide photocathode sensitized with methyl violet. *Semiconductor Science and Technology* **1993**, 8, 1557-1560.
7. Putzeiko, E. K.; Terenin, A. N., Photosensitization of the internal photoeffect in zinc oxide and other semiconductors by adsorbed dyes. *Zhurnal Fizicheskoi Khimii* **1949**, 23, 676-688.
8. Galoppini, E., Linkers for anchoring sensitizers to semiconductor nanoparticles. *Coordination Chemistry Reviews* **2004**, 248, (13), 1283-1297.
9. Matsumura, M.; Nomura, Y.; Tsubomura, H., Dye-sensitization on the Photocurrent at Zinc Oxide Electrode in Aqueous Electrolyte Solution. *Bulletin of the Chemical Society of Japan* **1977**, 50, (10), 2533-2537.
10. Houlding, V. H.; Gratzel, M., Photochemical hydrogen generation by visible light. Sensitization of titanium dioxide particles by surface complexation with 8-hydroxyquinoline. *Journal of the American Chemical Society* **1983**, 105, (17), 5695-5696.
11. Duncan, W. R.; Prezhdo, O. V., Theoretical studies of photoinduced electron transfer in dye-sensitized TiO<sub>2</sub>. *Annual Review of Physical Chemistry* **2007**, 58, 143-184.
12. Polo, A. S.; Itokazu, M. K.; Murakami Iha, N. Y., Metal complex sensitizers in dye-sensitized solar cells. *Coordination Chemistry Reviews* **2004**, 248, (13), 1343-1361.

13. Wongcharee, K.; Meeyoo, V.; Chavadej, S., Dye-sensitized solar cell using natural dyes extracted from rosella and blue pea flowers. *Solar Energy Materials and Solar Cells* **2007**, 91, (7), 566-571.
14. Polo, A. S.; Murakami Iha, N. Y., Blue sensitizers for solar cells: Natural dyes from Calafate and Jaboticaba. *Solar Energy Materials and Solar Cells* **2006**, 90, (13), 1936-1944.
15. Garcia, C. G.; Polo, A. S.; Murakami Iha, N. Y., Fruit extracts and ruthenium polypyridinic dyes for sensitization of TiO<sub>2</sub> in photoelectrochemical solar cells. *Journal of Photochemistry and Photobiology A: Chemistry* **2003**, 160, (1-2), 87-91.
16. Dhanalakshmi, K. B.; Latha, S.; Anandan, S.; Maruthamuthu, P., Dye sensitized hydrogen evolution from water. *International Journal of Hydrogen Energy* **2001**, 26, (7), 669-674.
17. Nian, J. N.; Hu, C. C.; Teng, H., Electrodeposited p-type Cu<sub>2</sub>O for H<sub>2</sub> evolution from photoelectrolysis of water under visible light illumination. *International Journal of Hydrogen Energy* **2008**, 33, (12), 2897-2903.
18. Nada, A. A.; Hamed, H. A.; Barakat, M. H.; Mohamed, N. R.; Veziroglu, T. N., Enhancement of photocatalytic hydrogen production rate using photosensitized TiO<sub>2</sub>/RuO<sub>2</sub>-MV<sup>2+</sup>. *International Journal of Hydrogen Energy* **2008**, 33, (13), 3264-3269.
19. Mane, R. S.; Lee, W. J.; Pathan, H. M.; Han, S. H., Nanocrystalline TiO<sub>2</sub>/ZnO thin films: fabrication and application to dye-sensitized solar cells. *Journal of Physical Chemistry B* **2005**, 109, (51), 24254-24259.
20. Lincot, D., Electrodeposition of semiconductors. *Thin Solid Films* **2005**, 487, (1), 40-48.
21. Karuppuchamy, S.; Nonomura, K.; Yoshida, T.; Sugiura, T.; Minoura, H., Cathodic electrodeposition of oxide semiconductor thin films and their application to dye-sensitized solar cells. *Solid State Ionics* **2002**, 151, (1), 19-27.
22. Yoshida, T.; Pauporte, T.; Lincot, D.; Oekermann, T.; Minoura, H., Cathodic Electrodeposition of ZnO/Eosin Y Hybrid Thin Films from Oxygen-Saturated Aqueous Solution of ZnCl<sub>2</sub> and Eosin Y. *Journal of the Electrochemical Society* **2003**, 150, (9), C608-C615.
23. Wang, C. C.; Ying, J. Y., Sol-gel synthesis and hydrothermal processing of anatase and rutile titania nanocrystals. *Chemistry of Materials* **1999**, 11, (11), 3113-3120.
24. Mao, L.; Li, Q.; Dang, H.; Zhang, Z., Synthesis of nanocrystalline TiO<sub>2</sub> with high photoactivity and large specific surface area by sol-gel method. *Materials Research Bulletin* **2005**, 40, (2), 201-208.

25. Venkatachalam, N.; Palanichamy, M.; Murugesan, V., Sol-gel preparation and characterization of nanosize TiO<sub>2</sub>: Its photocatalytic performance. *Materials Chemistry and Physics* **2007**, 104, (2-3), 454-459.
26. Ristic, M.; Music, S.; Ivanda, M.; Popovic, S., Sol-gel synthesis and characterization of nanocrystalline ZnO powders. *Journal of Alloys and Compounds* **2005**, 397, (1), L1-L4.
27. Rani, S.; Suri, P.; Shishodia, P. K.; Mehra, R. M., Synthesis of nanocrystalline ZnO powder via sol-gel route for dye-sensitized solar cells. *Solar Energy Materials and Solar Cells* **2008**, 92, (12), 1639-1645.
28. Choi, W.; Termin, A.; Hoffmann, M. R., The role of metal ion dopants in quantum-sized TiO<sub>2</sub>: correlation between photoreactivity and charge carrier recombination dynamics. *Journal of Physical Chemistry* **1994**, 98, (51), 13669-13679.
29. Karakitsou, K. E.; Verykios, X. E., Effects of altrivalent cation doping of titania on its performance as a photocatalyst for water cleavage. *Journal of Physical Chemistry* **1993**, 97, (6), 1184-1189.
30. Soria, J.; Conesa, J. C.; Augugliaro, V.; Palmisano, L.; Schiavello, M.; Sclafani, A., Dinitrogen photoreduction to ammonia over titanium dioxide powders doped with ferric ions. *Journal of Physical Chemistry* **1991**, 95, (1), 274-282.
31. Choi, J.; Park, H.; Hoffmann, M. R., Effects of single metal-ion doping on the visible-light photoreactivity of TiO<sub>2</sub>. *Journal of Physical Chemistry C* **2010**, 114, (2), 783-792.
32. Kennedy, J. C.; Datye, A. K., Photothermal heterogeneous oxidation of ethanol over Pt/TiO<sub>2</sub>. *Journal of Catalysis* **1998**, 179, (2), 375-389.
33. Vorontsov, A. V.; Stoyanova, I. V.; Kozlov, D. V.; Simagina, V. I.; Savinov, E. N., Kinetics of the photocatalytic oxidation of gaseous acetone over platinized titanium dioxide. *Journal of Catalysis* **2000**, 189, (2), 360-369.
34. Falconer, J. L.; Magrini-Bair, K. A., Photocatalytic and thermal catalytic oxidation of acetaldehyde on Pt/TiO<sub>2</sub>. *Journal of Catalysis* **1998**, 179, (1), 171-178.
35. He, C.; Xiong, Y.; Zhu, X.; Li, X., A platinised TiO<sub>2</sub> film with both photocatalytic and non-photocatalytic activities towards the oxidation of formic acid. *Applied Catalysis A: General* **2004**, 275, (1), 55-60.
36. Kraeutler, B.; Bard, A. J., Heterogeneous photocatalytic preparation of supported catalysts. Photodeposition of platinum on titanium dioxide powder and other substrates. *Journal of the American Chemical Society* **1978**, 100, (13), 4317-4318.



37. Kryukova, G. N.; Zenkovets, G. A.; Shutilov, A. A.; Wilde, M.; Gunther, K.; Fassler, D.; Richter, K., Structural peculiarities of TiO<sub>2</sub> and Pt/TiO<sub>2</sub> catalysts for the photocatalytic oxidation of aqueous solution of Acid Orange 7 Dye upon ultraviolet light. *Applied Catalysis B: Environmental* **2007**, 71, (3), 169-176.
38. Sivalingam, G.; Nagaveni, K.; Hegde, M. S.; Madras, G., Photocatalytic degradation of various dyes by combustion synthesized nano anatase TiO<sub>2</sub>. *Applied Catalysis B: Environmental* **2003**, 45, (1), 23-38.
39. Mills, A.; Lee, S. K., Platinum group metals and their oxides in semiconductor photosensitisation. *Platinum Metals Review* **2003**, 47, (1), 2-12.
40. Zhou, Y.; King, D. M.; Liang, X.; Li, J.; Weimer, A. W., Optimal preparation of Pt/TiO<sub>2</sub> photocatalysts using atomic layer deposition. *Applied Catalysis B: Environmental* **2010**, 101, (1), 54-60.
41. Nakamatsu, H.; Kawai, T.; Koreeda, A.; Kawai, S., Electron-microscopic observation of photodeposited Pt on TiO<sub>2</sub> particles in relation to photocatalytic activity. *Journal of Chemical Society, Faraday Transactions* **1986**, 82, (2), 527-531.
42. Li, F. B.; Li, X. Z., The enhancement of photodegradation efficiency using Pt-TiO<sub>2</sub> catalyst. *Chemosphere* **2002**, 48, (10), 1103-1111.
43. Yang, J. C.; Kim, Y. C.; Shul, Y. G.; Shin, C. H.; Lee, T. K., Characterization of photoreduced Pt/TiO<sub>2</sub> and decomposition of dichloroacetic acid over photoreduced Pt/TiO<sub>2</sub> catalysts. *Applied Surface Science* **1997**, 121, 525-529.
44. Spieker, W. A.; Regalbuto, J. R., A fundamental model of platinum impregnation onto alumina. *Chemical Engineering Science* **2001**, 56, (11), 3491-3504.
45. Bavykin, D. V.; Lapkin, A. A.; Plucinski, P. K.; Torrente-Murciano, L.; Friedrich, J. M.; Walsh, F. C., Deposition of Pt, Pd, Ru and Au on the surfaces of titanate nanotubes. *Topics in Catalysis* **2006**, 39, (3), 151-160.
46. Garcia, J. R. V.; Goto, T., Chemical vapor deposition of iridium, platinum, rhodium and palladium. *Materials Transactions* **2003**, 44, (9), 1717-1728.
47. Li, W.; Liang, C.; Zhou, W.; Qiu, J.; Zhou, Z.; Sun, G.; Xin, Q., Preparation and characterization of multiwalled carbon nanotube-supported platinum for cathode catalysts of direct methanol fuel cells. *Journal of Physical Chemistry B* **2003**, 107, (26), 6292-6299.
48. Mei, Y.; Sharma, G.; Lu, Y.; Ballauff, M.; Drechsler, M.; Irrgang, T.; Kempe, R., High catalytic activity of platinum nanoparticles immobilized on spherical polyelectrolyte brushes. *Langmuir* **2005**, 21, (26), 12229-12234.

49. Floro, J. A.; Hearne, S. J.; Hunter, J. A.; Kotula, P.; Chason, E.; Seel, S. C.; Thompson, C. V., The dynamic competition between stress generation and relaxation mechanisms during coalescence of Volmer - Weber thin films. *Journal of Applied Physics* **2001**, 89, 4886.
50. Liang, X.; George, S. M.; Weimer, A. W.; Li, N. H.; Blackson, J. H.; Harris, J. D.; Li, P., Synthesis of a novel porous polymer/ceramic composite material by low-temperature atomic layer deposition. *Chemistry of Materials* **2007**, 19, (22), 5388-5394.
51. Hakim, L. F.; King, D. M.; Zhou, Y.; Gump, C. J.; George, S. M.; Weimer, A. W., Nanoparticle coating for advanced optical, mechanical and rheological properties. *Advanced Functional Materials* **2007**, 17, (16), 3175-3181.
52. Cho, Y.; Park, Y.; Choi, W., Ruthenium bipyridyl complex-sensitized dechlorination of CCl<sub>4</sub> in aqueous micellar solutions under visible light. *Journal of Industrial and Engineering Chemistry* **2008**, 14, (3), 315-321.
53. Fung, A. K. M.; Chiu, B. K. W.; Lam, M. H. W., Surface modification of TiO<sub>2</sub> by a ruthenium (II) polypyridyl complex via silyl-linkage for the sensitized photocatalytic degradation of carbon tetrachloride by visible irradiation. *Water Research* **2003**, 37, (8), 1939-1947.
54. Cho, Y.; Choi, W.; Lee, C. H.; Hyeon, T.; Lee, H. I., Visible light-induced degradation of carbon tetrachloride on dye-sensitized TiO<sub>2</sub>. *Environmental Science & Technology* **2001**, 35, (5), 966-970.
55. Bae, E.; Choi, W., Highly enhanced photoreductive degradation of perchlorinated compounds on dye-sensitized metal/TiO<sub>2</sub> under visible light. *Environmental Science & Technology* **2003**, 37, (1), 147-152.
56. Alexander, M. V.; Rosentreter, J. J., Photocatalytic oxidation of aqueous trichloroethylene using dye sensitized buoyant photocatalyst monitored via micro-headspace solid-phase microextraction gas chromatography/electron capture detection and mass spectrometry. *Microchemical Journal* **2008**, 88, (1), 38-44.
57. Muszkat, L.; Feigelson, L.; Bir, L.; Muszkat, K. A., Photocatalytic degradation of pesticides and bio-molecules in water. *Pest Management Science* **2002**, 58, (11), 1143-1148.
58. Chatterjee, D., Photocatalytic reduction of hydrazine to ammonia catalysed by [Ru<sup>III</sup>(edta)(H<sub>2</sub>O)]<sup>-</sup> complex in a Pt/TiO<sub>2</sub> semiconductor particulate system. *Journal of Molecular Catalysis A: Chemical* **2000**, 154, (1), 1-3.
59. Chatterjee, D.; Dasgupta, S.; Dhodapkar, R. S.; Rao, N. N., Simultaneous degradation of non-emissive and emissive dyes on visible light illuminated TiO<sub>2</sub> surface. *Journal of Molecular Catalysis A: Chemical* **2006**, 260, (1), 264-268.

60. Haque, M. M.; Muneer, M., TiO<sub>2</sub>-mediated photocatalytic degradation of a textile dye derivative, bromothymol blue, in aqueous suspensions. *Dyes and Pigments* **2007**, *75*, (2), 443-448.
61. Qamar, M.; Saquib, M.; Muneer, M., Semiconductor-mediated photocatalytic degradation of anazo dye, chrysoidine Y in aqueous suspensions. *Desalination* **2005**, *171*, (2), 185-193.
62. Kojima, M.; Takahashi, K.; Nakamura, K., Cationic Dye-sensitized Degradation of Sodium Hyaluronate Through Photoinduced Electron Transfer in the Upper Excited State¶. *Photochemistry and Photobiology* **2001**, *74*, (3), 369-377.
63. Jiang, D.; Xu, Y.; Wu, D.; Sun, Y., Visible-light responsive dye-modified TiO<sub>2</sub> photocatalyst. *Journal of Solid State Chemistry* **2008**, *181*, (3), 593-602.
64. Granados O, G.; Paez M, C. A.; Martinez O, F.; Paez-Mozo, E. A., Photocatalytic degradation of phenol on TiO<sub>2</sub> and TiO<sub>2</sub>/Pt sensitized with metallophthalocyanines. *Catalysis Today* **2005**, *107-108*, 589-594.
65. Chowdhury, P.; Moreira, J.; Gomaa, H.; Ray, A. K., Visible Solar Light Driven Photocatalytic Degradation of Phenol with Dye-sensitized TiO<sub>2</sub>: Parametric and Kinetic Study. *Industrial & Engineering Chemistry Research* **2012**, *51*, (12), 4523-4532.
66. Ghosh, J. P.; Langford, C. H.; Achari, G., Characterization of an LED based photoreactor to degrade 4-chlorophenol in an aqueous medium using coumarin (C-343) sensitized TiO<sub>2</sub>. *Journal of Physical Chemistry A* **2008**, *112*, (41), 10310-10314.
67. Li, X.; Cabbage, J. W.; Tetzlaff, T. A.; Jenks, W. S., Photocatalytic degradation of 4-chlorophenol. 1. The hydroquinone pathway. *Journal of Organic Chemistry* **1999**, *64*, (23), 8509-8524.
68. Hussein, F. H.; Alkhateeb, A. N., Photo-oxidation of benzyl alcohol under natural weathering conditions. *Desalination* **2007**, *209*, (1), 350-355.
69. Salvador, P., Thermodynamic and kinetic considerations about water splitting and competitive reactions in a photoelectrochemical cell. *New Journal of Chemistry* **1988**, *12*, (1), 35-43.
70. Lee, J. S., Photocatalytic water splitting under visible light with particulate semiconductor catalysts. *Catalysis Surveys from Asia* **2005**, *9*, (4), 217-227.
71. Grimes, C. A.; Varghese, O. K.; Ranjan, S., *Light, Water, Hydrogen – The Solar Generation of Hydrogen by Water Photoelectrolysis* Springer Science. NY, USA **2008**; p 1-10.

72. Abe, R.; Sayama, K.; Sugihara, H., Effect of Water/Acetonitrile Ratio on Dye-Sensitized Photocatalytic H<sub>2</sub> Evolution under Visible Light Irradiation. *Journal of Solar Energy Engineering* **2005**, 127, 413-416.
73. Li, Q.; Lu, G., Visible-light driven photocatalytic hydrogen generation on Eosin Y-sensitized Pt-loaded nanotube Na<sub>2</sub>Ti<sub>2</sub>O<sub>4</sub>(OH)<sub>2</sub>. *Journal of Molecular Catalysis A: Chemical* **2007**, 266, (1), 75-79.
74. Li, Y.; Xie, C.; Peng, S.; Lu, G.; Li, S., Eosin Y-sensitized nitrogen-doped TiO<sub>2</sub> for efficient visible light photocatalytic hydrogen evolution. *Journal of Molecular Catalysis A: Chemical* **2008**, 282, (1), 117-123.
75. Abe, R.; Hara, K.; Sayama, K.; Domen, K.; Arakawa, H., Steady hydrogen evolution from water on Eosin Y-fixed TiO<sub>2</sub> photocatalyst using a silane-coupling reagent under visible light irradiation. *Journal of Photochemistry and Photobiology A: Chemistry* **2000**, 137, (1), 63-69.
76. Sreethawong, T.; Junbua, C.; Chavadej, S., Photocatalytic H<sub>2</sub> production from water splitting under visible light irradiation using Eosin Y-sensitized mesoporous-assembled Pt/TiO<sub>2</sub> nanocrystal photocatalyst. *Journal of Power Sources* **2009**, 190, (2), 513-524.
77. Zhang, X.; Jin, Z.; Li, Y.; Li, S.; Lu, G., Photocatalytic hydrogen generation over Eosin Y-Sensitized TS-1 zeolite. *Applied Surface Science* **2008**, 254, (15), 4452-4456.
78. Zhang, X.; Jin, Z.; Li, Y.; Li, S.; Lu, G., Visible-light-induced hydrogen production over Pt-Eosin Y catalysts with high surface area silica gel as matrix. *Journal of Power Sources* **2007**, 166, (1), 74-79.
79. Li, Y.; Guo, M.; Peng, S.; Lu, G.; Li, S., Formation of multilayer-Eosin Y-sensitized TiO<sub>2</sub> via Fe<sup>3+</sup> coupling for efficient visible-light photocatalytic hydrogen evolution. *International Journal of Hydrogen Energy* **2009**, 34, (14), 5629-5636.
80. Chen, X.; Shen, S.; Guo, L.; Mao, S. S., Semiconductor-based photocatalytic hydrogen generation. *Chemical Reviews* **2010**, 110, (11), 6503-6570.
81. Duonghong, D.; Borgarello, E.; Graetzel, M., Dynamics of light-induced water cleavage in colloidal systems. *Journal of the American Chemical Society* **1981**, 103, (16), 4685-4690.
82. Borgarello, E.; Kiwi, J.; Pelizzetti, E.; Visca, M.; Graetzel, M., Sustained water cleavage by visible light. *Journal of the American Chemical Society* **1981**, 103, (21), 6324-6329.
83. Borgarello, E.; Kiwi, J.; Pelizzetti, E.; Visca, M.; Gratzel, M., Photochemical cleavage of water by photocatalysis. *Nature* **1981**, 289, 158-160.

84. Hirano, K.; Suzuki, E.; Ishikawa, A.; Moroi, T.; Shiroishi, H.; Kaneko, M., Sensitization of TiO<sub>2</sub> particles by dyes to achieve H<sub>2</sub> evolution by visible light. *Journal of Photochemistry and Photobiology A: Chemistry* **2000**, 136, (3), 157-161.
85. Bae, E.; Choi, W.; Park, J.; Shin, H. S.; Kim, S. B.; Lee, J. S., Effects of surface anchoring groups (carboxylate vs phosphonate) in ruthenium-complex-sensitized TiO<sub>2</sub> on visible light reactivity in aqueous suspensions. *Journal of Physical Chemistry B* **2004**, 108, (37), 14093-14101.
86. Kajiwarra, T.; Hashimoto, K.; Kawai, T.; Sakata, T., Dynamics of luminescence from Ru (bpy)<sub>3</sub>Cl<sub>2</sub> adsorbed on semiconductor surfaces. *Journal of Physical Chemistry* **1982**, 86, (23), 4516-4522.
87. Peng, T.; Dai, K.; Yi, H.; Ke, D.; Cai, P.; Zan, L., Photosensitization of different ruthenium (II) complex dyes on TiO<sub>2</sub> for photocatalytic H<sub>2</sub> evolution under visible-light. *Chemical Physics Letters* **2008**, 460, (1), 216-219.
88. Peng, T.; Ke, D.; Cai, P.; Dai, K.; Ma, L.; Zan, L., Influence of different ruthenium (II) bipyridyl complex on the photocatalytic H<sub>2</sub> evolution over TiO<sub>2</sub> nanoparticles with mesostructures. *Journal of Power Sources* **2008**, 180, (1), 498-505.
89. Gurunathan, K.; Maruthamuthu, P.; Sastri, M. V. C., Photocatalytic hydrogen production by dye-sensitized Pt/SnO<sub>2</sub> and Pt/SnO<sub>2</sub>/RuO<sub>2</sub> in aqueous methyl viologen solution. *International Journal of Hydrogen Energy* **1997**, 22, (1), 57-62.
90. Li, Q.; Chen, L.; Lu, G., Visible-light-induced photocatalytic hydrogen generation on dye-sensitized multiwalled carbon nanotube/Pt catalyst. *Journal of Physical Chemistry C* **2007**, 111, (30), 11494-11499.
91. Gurunathan, K., Photocatalytic hydrogen production using transition metal ions-doped [gamma]-Bi<sub>2</sub>O<sub>3</sub> semiconductor particles. *International Journal of Hydrogen Energy* **2004**, 29, (9), 933-940.
92. Nada, A. A.; Barakat, M. H.; Hamed, H. A.; Mohamed, N. R.; Veziroglu, T. N., Studies on the photocatalytic hydrogen production using suspended modified TiO<sub>2</sub> photocatalysts. *International Journal of Hydrogen Energy* **2005**, 30, (7), 687-691.
93. Koca, A.; Sahin, M., Photocatalytic hydrogen production by direct sun light from sulfide/sulfite solution. *International Journal of Hydrogen Energy* **2002**, 27, (4), 363-367.
94. Abe, R.; Sayama, K.; Domen, K.; Arakawa, H., A new type of water splitting system composed of two different TiO<sub>2</sub> photocatalysts (anatase, rutile) and a IO<sup>3-</sup>/I shuttle redox mediator. *Chemical Physics Letters* **2001**, 344, (3), 339-344.

95. Bamwenda, G. R.; Arakawa, H., The photoinduced evolution of O<sub>2</sub> and H<sub>2</sub> from a WO<sub>3</sub> aqueous suspension in the presence of Ce<sup>4+</sup>/Ce<sup>3+</sup>. *Solar Energy Materials & Solar Cells* **2001**, 70, (1), 14.
96. Chowdhury, P.; Goma, H.; Ray, A. K., Factorial design analysis for dye-sensitized hydrogen generation from water. *International Journal of Hydrogen Energy* **2011**, 36, (21), 13442-13451.

## Chapter 3

### 3 Factorial Design Analysis for Dye-sensitized Hydrogen Generation from Water

#### 3.1 Introduction

The pressing need to find viable alternatives to fossil fuels combined with the growing requirement for environmentally friendly industrial processes motivates a dramatic paradigm shift from fossil fuels (which also require carbon capture and sequestration) to reliable, clean, and efficient fuels.<sup>1</sup> The long sought after shift from solid (coal) to liquid (oil) to gas (hydrogen) fuel based system is not a local phenomenon, it is happening on a global scale, and a technology that can shift the balance would be quickly pursued worldwide. The basic idea is decarbonization of the fuel. Coal has the lowest H/C ratio (0.5), for LPG the ratio goes up to 2.67 and for natural gas the ratio again increased to 4. Hydrogen is perceived as an ideal energy carrier<sup>2</sup> having H/C ratio of infinite. Hydrogen has the potential to meet the requirements as a clean nonfossil fuel in the future if it can be produced using the world's most abundant sources, the sun and water. The driving forces for the energy transition toward hydrogen are many, but three major reasons are (i) growing energy demand, (ii) oil shortage in near future and (iii) threat of climate change.<sup>3</sup> Hydrogen is a top energy storage candidate because it has a high energy content, low environmental impact, and can be stored or produced on demand.

The world is gradually favoring hydrogen over carbon atom. Between 1860 and 1990, the H/C ratio in fuel rose 6-folds. As of 2002, the annual hydrogen production was close to 400 billion cubic meters.<sup>4</sup> Hydrogen is an ideal fuel<sup>4</sup>: when burned, the product is energy and water. This suggests visions of a world in which cars and other machines leave behind only plumes of water rather than clouds of smog. Unlike fossil fuels, hydrogen cannot simply be obtained from previous deposits; there are no hydrogen "mines". This means that energy must be expended to remove hydrogen from other materials, and currently, most hydrogen produced is generated and used on-site in the chemical and

petroleum industries through natural gas reforming, coal gasification, thermal water splitting, and electrolysis.<sup>5</sup> These processes require huge infrastructure, large energy input and come with a high environmental cost. Even more energy is required to distribute hydrogen if it is not generated on-site. Hydrogen can also be produced from biomass, but the basic feedstock is limited and would also need considerable energy input. Photoelectrical and photobiological hydrogen production methods exist<sup>6</sup> but the technologies involved are currently at a very early stage of development, and it is unclear whether they will be a viable source. However, our planet is covered with an abundant, clean carbon free source of hydrogenewater. The planet is also bathed in an abundant, clean source of energy-sunlight. The vision and focus of our work is to use the green energy of the sun to split water into hydrogen using nanotechnology.<sup>7, 8</sup> If such a system can be made inexpensive, efficient, and stable, it would provide a practical method of producing high-purity hydrogen. Currently this is not achievable<sup>9</sup> and new photocatalytic nanomaterials and methods are required to reach this goal.

Recent reviews of hydrogen production with visible light photocatalyst discussed various barriers of the process such as rapid recombination of photo-generated electron/hole pair ( $e^-/h^+$ ) and poor activation of semiconductor photocatalyst. Dye-sensitization technique has been reported as an innovative technology that could play an important role in developing efficient and cost effective semiconductor photocatalyst in the near future.<sup>9, 10</sup> Solar cell applications based on dye-sensitized  $TiO_2$  is among the most popular and successful till date<sup>11-14</sup> which has also been applied to visible light induced hydrogen generation.<sup>9, 15-18</sup> The quintessence of dye-sensitization is the electron injection from the excited dye to the conductionband (CB) of  $TiO_2$  and the subsequent interfacial electron transfer.<sup>19-23</sup> Eosin Y-sensitized systems have been extensively studied owing to its superior photocatalytic activity for hydrogen production from water splitting.<sup>17, 24-28</sup> There is however, lack of information on investigations of the key process parameters which affect sacrificial hydrogen generation based on robust experimental design methodology and statistical analysis.



The main objective of this investigation is to fill such gap, by developing a methodology based on factorial design analysis to screen the significant factors that influence the hydrogen generation from water with Eosin Y-sensitized TiO<sub>2</sub> catalyst under visible solar light. Another objective is to define the optimum conditions for hydrogen generation within the investigated operating parameters space domain.

## 3.2 Methodology

### 3.2.1 Experimental

#### 3.2.1.1 Reagents

All reagents were analytical grade and were used without further treatment. Aeroxide TiO<sub>2</sub> P25 (80-20% anatase to rutile) from Evonik Degussa Corporation was used as catalyst. Eosin Y dye (99.0%, SigmaAldrich Canada Ltd) was used as sensitizer for TiO<sub>2</sub>; triethanolamine (98.0%) and hydrogen hexachloroplatinate (IV) solution (8 wt %) were also purchased from SigmaAldrich Canada Ltd. Ultra pure water (18MU) was prepared from an in-house EASYPure® RODI system (Thermo Scientific, Canada).

#### 3.2.1.2 Instruments

The simulated Air Mass (AM) 1.5 solar light was generated using solar simulator (Model: SS1 KW, Sciencetech, ON, Canada with a 1000-W Xe arc lamp and an AM 1.5G filter). It produces identical simulated 1 SUN irradiance of 100 mW cm<sup>-2</sup> at full power that matches the global solar spectrum at sea level. Spectral analysis of the irradiation from solar simulator with StellarNet EPP 2000C-25LT16 Spectrometer for UV-VIS-NIR showed 6.5% UV, 64.5% visible while the rest NIR light. The generated Hydrogen gas was quantified using gas chromatography (Shimadzu GC 2014, HeyeSep D packed column: 10 m length, 2 mm ID, 2 mm film thickness and thermal conductivity detector (TCD)). All the spectrophotometric studies were done using UV-VIS-NIR Spectrophotometer (Shimadzu UV-3600). An integrating sphere was utilized in order to measure the diffuse reflectance absorption spectra of the catalyst. pH measurement was carried out using a pH meter (780-Metrohm Ltd).

### 3.2.1.3 Synthesis of eosin Y-sensitized TiO<sub>2</sub>/Pt photocatalyst

Platinum was loaded on TiO<sub>2</sub> catalyst by solar photodeposition method. TiO<sub>2</sub> powder was stirred in an aqueous ethanol solution (ethanol: water = 1.0: 99.0 by volume) containing the required amount of hydrogen hexachloroplatinate (IV) solution and irradiated under the solar simulator (AM 1.5G filter) for 3 h. Photoreduction of Pt<sup>IV</sup> (H<sub>2</sub>PtCl<sub>6</sub>) to Pt<sup>0</sup> (platinum particles) occurred, and highly dispersed Pt particles were deposited on the TiO<sub>2</sub> surface.<sup>16</sup> After filtering and washing with water, the powder was dried at 150<sup>0</sup>C for 2 h and milled in a mortar. Eosin Y dye was adsorbed onto TiO<sub>2</sub>/Pt by stirring 0.5 g of the catalyst powder in a mixture of Eosin Y and anhydrous ethanol solvent (4.6 x 10<sup>-4</sup> M to 4.6 x 10<sup>-3</sup> M) at room temperature for 12 h in the dark. This was followed by filtration and washing with anhydrous ethanol and drying at 100<sup>0</sup>C for 2 h. The obtained sample was kept under dark to avoid catalyst deactivation. The Eosin Y-sensitized TiO<sub>2</sub>/Pt photocatalyst showed a broad absorption from 410 nm to 640 nm.

### 3.2.1.4 Photocatalytic hydrogen generation

Photocatalytic reactions were carried out in a gastight Pyrex glass reactor (600 mL) with a flat window at top for illumination. Figure 3.1 shows a schematic diagram of the photocatalytic reactor (11 cm diameter, 6.3 cm height) used in this investigation. The catalyst powder (Eosin Y-TiO<sub>2</sub>/Pt) was suspended in 100 mL trietanolamine (TEOA) solution (0.05 M-0.5 M) after pH adjustment with 1:1 HCl. The catalyst suspension was dispersed for 5 min in an ultrasonic bath and then the system was degassed by bubbling ultra pure nitrogen gas for 40 min. Very gentle stirring was performed using magnetic stirrer. The photocatalyst was irradiated with a solar simulator from the top. The light source was equipped with AM 1.5 G as well as a 420 nm cut-off filter (Omega optical, USA) to remove all the UV light. The water layer above the catalyst itself acted as an IR filter. The gas sampling port in the reactor was sealed with a silicone rubber septum, and sampling was made intermittently through the septum during the experiments. Hydrogen was analyzed by Shimazu GC 2014 (TCD, ultra pure N<sub>2</sub> as carrier gas and HeyeSep D column).

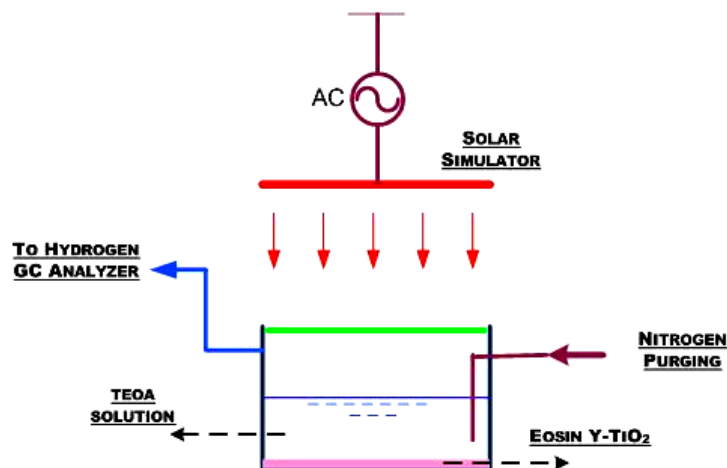


**Figure 3.1 Experimental Setup: Gastight photo-reactor for dye-sensitized hydrogen generation**

### 3.2.2 Experimental design

To evaluate the main factors that influence the hydrogen generation with dye-sensitized TiO<sub>2</sub> photocatalyst, two different sets of full factorial design were performed to investigate the response in terms of percentage increment in hydrogen generation with dye-sensitized TiO<sub>2</sub>. In the first set a two levels three factors full factorial design approach was applied, where three factors such as solution pH, initial dye concentration for dye-sensitization (Eosin Y), and electron donor concentration (TEOA) were chosen. In the second set, a two levels four factors full factorial design was implemented in which four factors including platinum content (wt %) in TiO<sub>2</sub> (Pt), visible light irradiation time (I-time), initial dye concentration for dye-sensitization (Eosin Y), and electron donor concentration (TEOA), were chosen.

Each factor was studied at both low-and high-level. To analyze the factorial design, the original measurement units for the experimental factors (uncoded units) were transformed

into coded units.<sup>29</sup> The factor levels were coded as -1 (low) and +1 (high). The responses were expressed in terms of percent increment in hydrogen generation (calculated relative to reference center point experimental values as mentioned in Tables 3 and 4).

In a two levels three factors full factorial design (set 1), the minimum number of experimental runs equals  $2^3 = 8$  runs. With two replicates, the number of test runs increases to 16. Similarly in a two level four factors full factorial design (set 2) the minimum number of experimental runs =  $2^4 = 16$ ; with two replicates, the total number is 32 runs.<sup>30</sup> Minitab 15 software was used to create and analyze the experimental data. Coded and uncoded values for set 1 and set 2 are presented in Tables 3.1 and Table 3.2.

### 3.3 Results and Discussion

The design table for the factors and the response in terms of percent change in hydrogen generation for set 1 and 2 are shown in Tables 3.3 and Table 3.4 respectively. Experiments in set 1 were performed to identify an optimum pH for further study. It also gave an idea of interaction among pH, dye molecule and electron donor. For set 2, a detailed statistical analysis (normal probability plot) of the data in terms of standardized residual was performed to confirm the normality of the data. A regression analysis was also conducted for the experimental data using least square technique. The effects of the different parameters are systematically discussed through Pareto chart, main effect plot and interaction effect plot in the following sections.

**Table 3.1 Coded and uncoded values of the factors for Set 1**

<b>Factors</b>	<b>Coded low level</b>	<b>Corresponding uncoded low value</b>	<b>Coded high level</b>	<b>Corresponding uncoded high value</b>
Eosin Y concentration for dye-sensitization (Eosin Y)	-1	$4.6 \times 10^{-4}$ M	+1	$4.6 \times 10^{-3}$ M
Electron donor concentration (TEOA)	-1	0.05 M	+1	0.5 M
pH	-1	4.0	+1	10.0

**Table 3.2 Coded and uncoded values of the factors for Set 2**

<b>Factors</b>	<b>Coded low level</b>	<b>Corresponding uncoded low value</b>	<b>Coded high level</b>	<b>Corresponding uncoded high value</b>
Electron donor concentration (TEOA)	-1	0.05 M	+1	0.5 M
Initial Eosin Y concentration for dye-sensitization (Eosin Y)	-1	$4.6 \times 10^{-4}$ M	+1	$4.6 \times 10^{-3}$ M
Platinum content (wt%) in TiO <sub>2</sub> (Pt)	-1	0.25 %	+1	2.5 %
Visible solar light irradiation time (I-time)	-1	60 min	+1	180 min

**Table 3.3 Uncoded design table for factors and response for Set 1**

Run	Eosin Y (M)	TEOA (M)	pH	% increment in H <sub>2</sub> generation <sup>a</sup>	
				Replicate 1	Replicate 2
1	-1	-1	-1	-87.39	-88.89
2	1	-1	-1	-71.53	-72.09
3	-1	1	-1	-73.60	-76.13
4	1	1	-1	-71.31	-71.35
5	-1	-1	1	8.29	7.22
6	1	-1	1	51.97	48.73
7	-1	1	1	40.35	44.87
8	1	1	1	83.47	80.18

<sup>a</sup>Results in this column is based on relative increase/decrease with respect to experiment performed at reference centre point value corresponding to [Eosin Y] =  $2.5 \times 10^{-3}$  M; [TEOA] = 0.275 M; Pt% in TiO<sub>2</sub> = 0.25%; pH = 7.0.

### 3.3.1 Effect of solution pH

The 2 levels 3 factors Full Factorial Design (set 1) was performed to determine the interaction of the solution pH with the dye molecule and the electron donor. The solution pH seems to be a crucial parameter as it shows good interaction with both dye and electron donor. The main effect plot and interaction effect plot of pH are shown in Figures 3.2 and Figure 3.3 respectively. These are fairly consistent with the results of Li et al.,<sup>25</sup> for the effect of the solution pH on the existing state of the dye and the electron donor as well as the change of the oxidation-reduction potential of semiconductor. From Figure 3.2 it is evident that the pH had a positive effect on sacrificial hydrogen generation from water. The Dye molecule showed stronger interaction with the pH as compared to the electron donor-pH interaction due to the stronger dependency of the dye regeneration rate on the pH.<sup>27</sup> As can be seen from the results, an alkaline pH (10.0) results in much higher hydrogen generation compared to an acidic pH (4.0). This can be attributed to the fact that TEOA can more rapidly donate electrons to the oxidized sensitizer (Eosin Y<sup>+</sup>) in an alkaline solution than in an acidic solution due to the more protonated form.<sup>27, 31</sup> The advantage of operating at higher pH however, was found to be offset by its negative impact on the catalyst integrity where deterioration to the dye-sensitized TiO<sub>2</sub> occurred at such high pH values. Based on that, it was decided to maintain the solution pH at 7.0.

**Table 3.4 Uncoded design table for factors and response for Set 2**

Run	TEOA	Eosin Y	Pt	I-time	% increment in H <sub>2</sub> generation <sup>a</sup>	
	(M)	(M)	(%)	(min)	Replicate 1	Replicate 2
1	-1	-1	-1	-1	-68.93	-69.91
2	1	-1	-1	-1	-59.01	-59.97
3	-1	1	-1	-1	-48.79	-49.87
4	1	1	-1	-1	-41.94	-40.12

5	-1	-1	1	-1	-86.81	-86.62
6	1	-1	1	-1	-86.75	-87.44
7	-1	1	1	-1	-65.40	-65.23
8	1	1	1	-1	-65.19	-65.27
9	-1	-1	-1	1	12.89	13.17
10	1	-1	-1	1	54.43	51.56
11	-1	1	-1	1	56.09	56.37
12	1	1	-1	1	87.36	92.49
13	-1	-1	1	1	-56.17	-56.44
14	1	-1	1	1	-52.59	-52.33
15	-1	1	1	1	-18.05	-19.70
16	1	1	1	1	11.88	12.40

<sup>a</sup>Results in this column is based on relative increase/decrease with respect to experiment performed at reference centre point value corresponding to [Eosin Y] =  $2.5 \times 10^{-3}$  M; [TEOA] = 0.275 M; Pt% in TiO<sub>2</sub> = 1.375%; visible light irradiation time = 120 min; pH = 7.0.



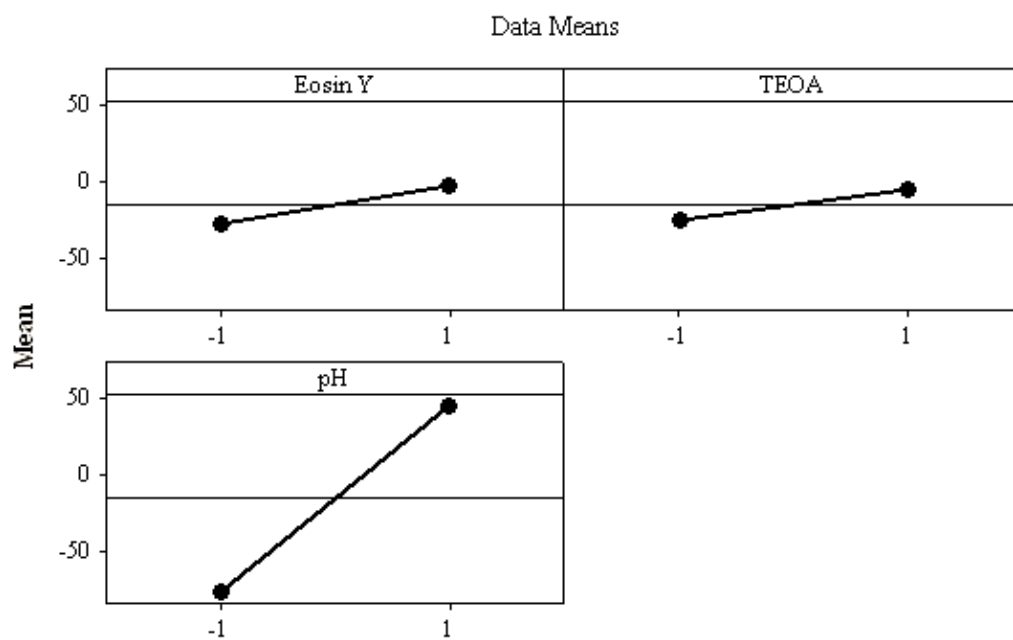


**Figure 3.2 Main effect plot for pH, dye and electron donor for % increment in hydrogen generation (Set 1)**

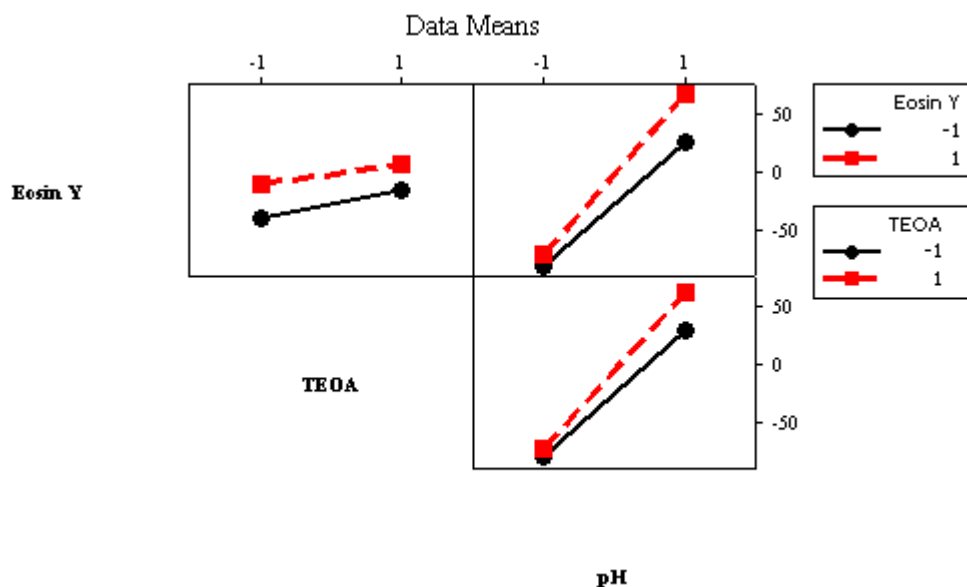
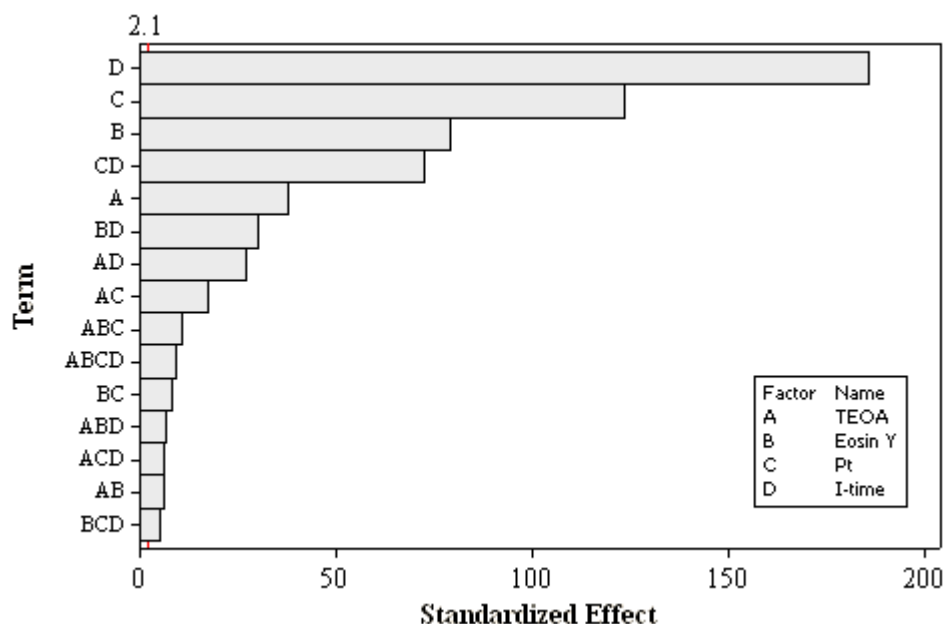


Figure 3.3 Interaction effect plot for pH, dye, and electron donor for % increment in hydrogen generation (Set 1)

### 3.3.2 Pareto plot

Pareto analysis uses the Pareto principle, which is also called the “80-20” rule for data analysis. The numbers 80 and 20 are not meant to be absolute but a great majority of problems (80 %) are produced by a few key causes (20 %). If we can rectify these few key causes, we will have a better probability of success. Pareto plots are graphical tools used in Pareto analysis.<sup>32</sup> A Pareto plot is a bar chart that displays the relative importance of factors in a format that is very easy to interpret. This plot visually represents the absolute values of the effects of the main factors and the effects of their interaction. The most important factor is represented by the tallest bar; the next important problem is represented by next tallest bar, and so on. It also draws a reference line to indicate that these factors extending past this line are potentially important.<sup>33</sup> It can be seen from Figure 3.4 that visible light irradiation time has highest effect followed by Pt content and initial dye concentration.



**Figure 3.4 Pareto chart for standardized effects for hydrogen generation (Set 2) (Response is % increment in hydrogen generation,  $\alpha=0.05$ )**

### 3.3.3 Main effect plot (Set 2)

The main effect is considered present when the mean response changes across the level of factor. The sign of the main effect indicates the direction of the effect.<sup>30</sup> Figure 3.5 shows that the platinum content (Pt %) in  $\text{TiO}_2$  has negative effect on hydrogen generation whereas the other three factors, initial dye concentration (Eosin Y), electron donor concentration (TEOA) and visible light irradiation time (I-time) all have positive effects. In this reaction system, Eosin Y molecules adsorbs on the surface of  $\text{TiO}_2/\text{Pt}$ . Under visible light irradiation, it absorbs visible light and the electron is excited from the HOMO (highest occupied molecular orbital) to LUMO (lowest unoccupied molecular orbital) state. The excited electron is trapped by  $\text{TiO}_2$  conduction band, and then transfers to the surface of the Pt nanoparticles directly, which then participates in the photocatalytic water reduction for hydrogen production.<sup>25</sup> The decrease in photocatalytic

activity as well as hydrogen generation with the increase in Pt content may be at least partly, due to more Pt cluster on  $\text{TiO}_2$  which would decrease adsorption sites for dye and would scatter the visible light.<sup>34</sup> Eosin Y concentration also plays a key role in the number of electrons transported from the excited Eosin Y to  $\text{TiO}_2$  conduction band, resulting in enhancement of the photocatalytic hydrogen production activity.<sup>25, 27</sup> Electron donor (TEOA) concentration, actually plays an important role in regenerating the electron-deficient sensitizer (Eosin  $\text{Y}^+$ ) after injecting electrons into the  $\text{TiO}_2$  conduction band. Sreethawong et al.,<sup>27</sup> showed the increased rate of photocatalytic hydrogen production rate with increasing electron donor (diethanolamine) concentration for Eosin Y-mesoporous assembled Pt/ $\text{TiO}_2$  nanocrystal system.

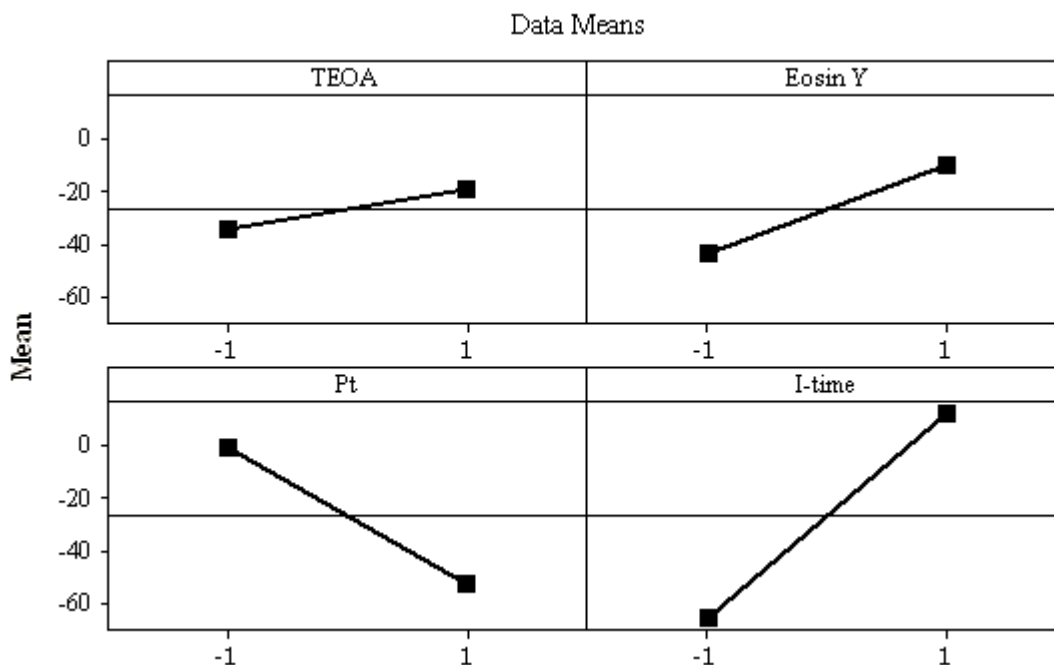


**Figure 3.5 Main effects plot for Pt, dye, electron donor and irradiation time for % increment in hydrogen generation (Set 2)**

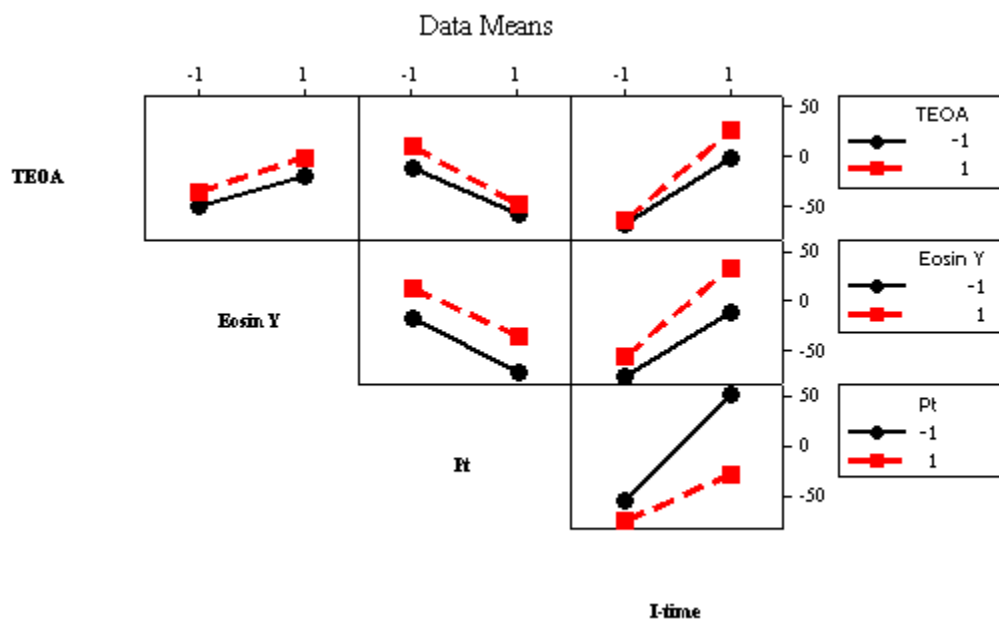


**Figure 3.6 Interaction effect plot for Pt, dye, electron donor and irradiation time for % increment in hydrogen generation (Set 2)**

### 3.3.4 Interaction effects plot (Set 2)

The interaction effects plot is shown in Figure 3.6 for the sacrificial hydrogen generation from water. The plot provides the mean response of two factors at all possible combinations of their settings. If the lines are not parallel, it is an indication of interaction between the two factors.<sup>30, 33</sup> The interaction plot showed that the visible light irradiation time interacts strongly with all other factors which indicate its maximum influence on hydrogen generation. With time more photons are absorbed by dye molecules for its excitation as evident from the height interaction of Eosin Y and irradiation time. The oxidized dye molecules (Eosin Y<sup>+</sup>) are regenerated by electron donor (TEOA) whereas TEOA gradually spent out with time. Pt content also shows very good interaction with irradiation time. Minor interactions were observed in Eosin Y-Pt and Eosin Y-TEOA pairs.

### 3.3.5 Regression analysis

Regression analysis illustrates the statistical relationship between one or more predictors and the response variable to predict new observations. In this investigation, data analysis was achieved using Minitab 15 software which uses ordinary least squares method to derive a regression function. Regression results specify the statistical significance, direction and size of the relationship between a predictor and response. Sign of each coefficient indicates the direction of the relationship. The coefficients represent the mean change in the response for one unit of change in the predictor while holding other predictors in the model constant. The p-value for each coefficient tests the null hypothesis that the coefficient is equal to zero (no effect). Therefore, low p-values suggest the predictor is a meaningful addition to the proposed function.<sup>29</sup> The regression results shown in Table 3.5 reveal that all the four predictors are significant because of their low p-values. For each 1 M increase in the initial Eosin Y concentration (for dye-sensitization) the percentage of increment of hydrogen generation increased by 16.5 %. Again for each 1 min visible light irradiation time and each 1 M TEOA concentration increment, the percentage of increment of hydrogen generation increased by 38.8 % and

7.9 % respectively. On the other hand for each 1 % increase in Pt content in TiO<sub>2</sub>, percentage of increment of hydrogen generation decreased by 25.8 %.

**Table 3.5 Estimated effects and coefficients for hydrogen generation <sup>a</sup>**

Predictor	Regression coefficient	Standardized effect (T)	p-Value
Constant	-26.68	-32.52	0.000
TEOA	7.90	9.63	0.000
Eosin Y	16.49	20.10	0.000
Pt	-25.80	-31.43	0.000
I-time	38.77	47.24	0.000
TEOA x Eosin Y	1.23	1.50	0.148
TEOA x Pt	-3.58	-4.36	0.000
TEOA x I-time	5.66	6.90	0.000
Eosin Y x Pt	1.66	2.03	0.056
Eosin Y x I-time	6.27	7.64	0.000
Pt x I-time	-15.16	-18.48	0.000

<sup>a</sup>Standard error coefficient for all cases = 0.8207; (R<sup>2</sup> = 99.2 %)

### 3.3.6 Prediction of hydrogen generation

Using the experimentally measured results in Minitab 15, a regression function is generated which could be used to predict the % increment in hydrogen generation rate with confidence level of 95 %. TEOA-Eosin Y and Eosin Y-Pt interaction effects were not considered because of their high (>0.05) p-values.

The regression function obtained is:

$$\begin{aligned} \text{Hydrogen generation (\% increment)} = & - 26.7 + 7.90 \times (\text{TEOA}) + 16.5 \times (\text{Eosin Y}) - 25.8 \\ & \times (\text{Pt}) + 38.8 \times (\text{I-time}) - 3.58 \times (\text{TEOA}) \times (\text{Pt}) + 5.66 \times \\ & (\text{TEOA}) \times (\text{I-time}) + 6.27 \times (\text{Eosin Y}) \times (\text{I-time}) - 15.2 \times \\ & (\text{Pt}) \times (\text{I-time}). \end{aligned}$$

Figure 3.7 shows a comparison between the experimental values and those predicted by the regression function (square symbols), which as can be seen is very satisfactory (R<sup>2</sup> = 0.99). The figure also shows comparison of few other independent experimental data

(Table 3.6) obtained under different experimental conditions that were not used in the regression analysis, with model predicted values (triangle symbol).

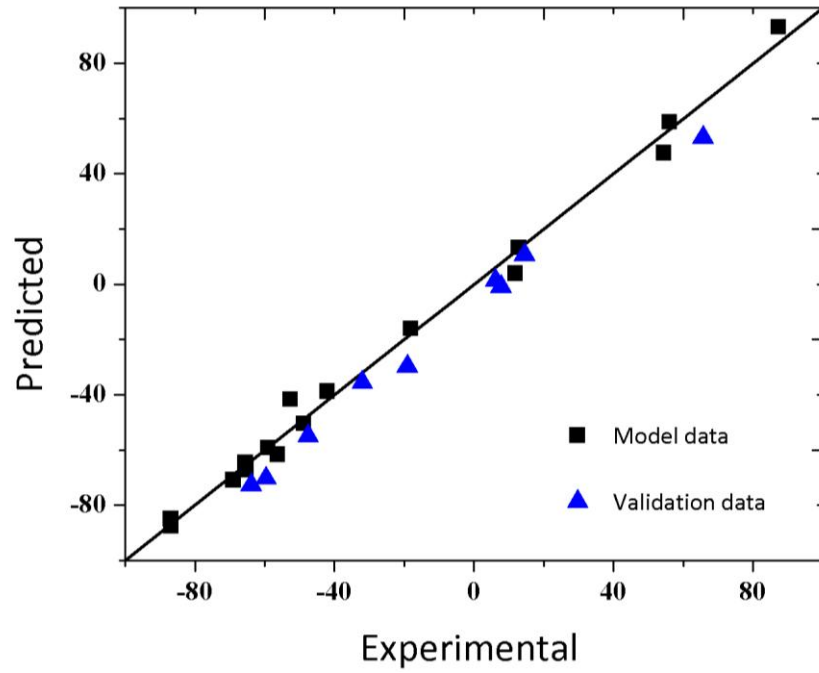


**Figure 3.7 Percent increment in hydrogen generation: Comparison between experimental including independent validation data and model predicted value**



**Table 3.6 Experimental data points for validation**

<b>SL. No.</b>	<b>TEOA (M)</b>	<b>Eosin Y (M)</b>	<b>Pt (%)</b>	<b>Time (min)</b>	<b>Experimental Value (% increment in H<sub>2</sub> generation)</b>	<b>Predicted Value (% increment in H<sub>2</sub> generation)</b>
1.	0.254	4.6X10 <sup>-4</sup>	1.0	60	-63.88	-72.57
2.	0.254	4.6X10 <sup>-4</sup>	1.0	120	-32.05	-35.58
3.	0.254	4.6X10 <sup>-4</sup>	1.0	180	6.17	1.40
4.	0.254	4.6X10 <sup>-4</sup>	0.75	60	-59.65	-70.24
5.	0.254	4.6X10 <sup>-4</sup>	0.75	120	-19.16	-29.81
6.	0.254	4.6X10 <sup>-4</sup>	0.75	180	14.49	10.61
7.	0.275	2.54x10 <sup>-3</sup>	0.25	60	-47.48	-54.90
8.	0.275	2.54x10 <sup>-3</sup>	0.25	120	-7.70	-0.90
9.	0.275	2.54x10 <sup>-3</sup>	0.25	180	65.64	53.1

### 3.3.7 Normal probability plot of residuals

Residual plots are used to examine the goodness of a fit in regression analysis and ANOVA (analysis of variance). Typically, residual plots are used to determine if the ordinary least squares assumptions are satisfactory to produce unbiased coefficient estimates with minimum variance. One of the key assumptions for the statistical analysis of data for experiments is that the data come from a normal distribution.<sup>33</sup> The normal probability plot (residual) for hydrogen generations are presented in Figure 3.8. It is clear that all the points are fairly close to the straight line. Therefore, the data from the experiment (set 2) satisfies a normally distributed population.<sup>30</sup>

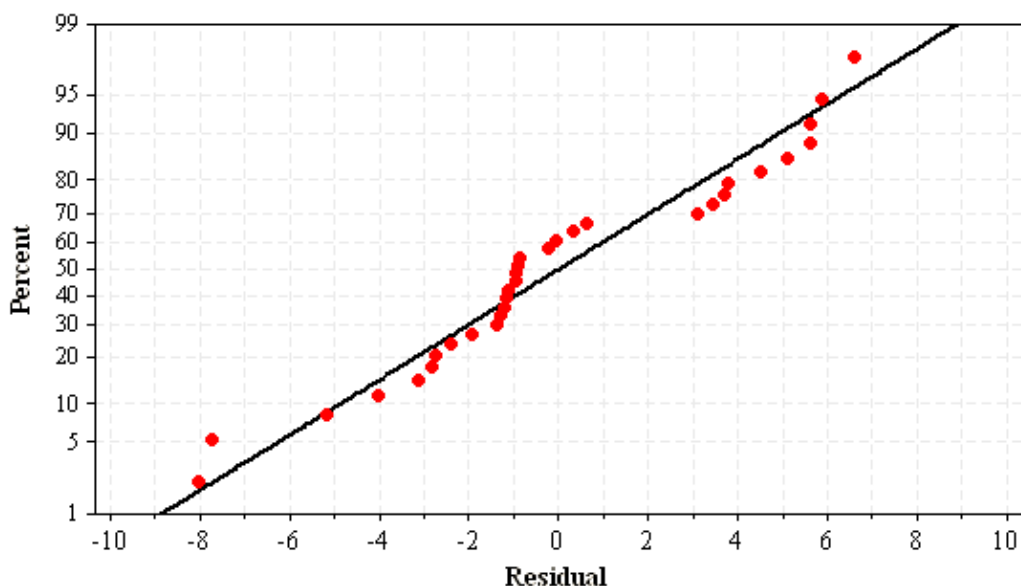


**Figure 3.8 Normal probability plot of the residuals for % increment in hydrogen generation**

### 3.4 Conclusions

The factorial design analysis can be used as a screening approach to identify the significant factors influencing sacrificial hydrogen generation from water with dye-sensitized photocatalyst. This method provides a quantitative assessment of the principal factors and effects that influence hydrogen generation performance. Based on data analysis the following is concluded: (a) Solution pH is a significant parameter as it interacts with both Eosin Y and triethanolamine as well as affects the stability of dye-sensitized TiO<sub>2</sub>/Pt, (b) Visible light irradiation time is the most influential factor in hydrogen generation. The second most significant factor is platinum content in TiO<sub>2</sub>. The interaction between these two factors has also considerable influence on hydrogen generation. The Pt content (wt %) has a negative effect, whereas visible light irradiation time has positive effect on hydrogen generation, and (c) Eosin Y concentration and TEOA concentration have shown moderate positive effect on hydrogen generation although their interaction effect is insignificant compared to other parameters.

### 3.5 References

1. Kudo, A., Recent progress in the development of visible light-driven powdered photocatalysts for water splitting. *International Journal of Hydrogen Energy* **2007**, 32, (14), 2673-2678.
2. Lee, S. H. D.; Applegate, D. V.; Ahmed, S.; Calderone, S. G.; Harvey, T. L., Hydrogen from natural gas: part I--autothermal reforming in an integrated fuel processor. *International Journal of Hydrogen Energy* **2005**, 30, (8), 829-842.
3. Bak, T.; Nowotny, J.; Rekas, M.; Sorrell, C. C., Photo-electrochemical hydrogen generation from water using solar energy. Materials-related aspects. *International Journal of Hydrogen Energy* **2002**, 27, (10), 991-1022.
4. Dunn, S., Hydrogen futures: toward a sustainable energy system. *International Journal of Hydrogen Energy* **2002**, 27, (3), 235-264.
5. Rosen, M. A.; Scott, D. S., Comparative efficiency assessments for a range of hydrogen production processes. *International Journal of Hydrogen Energy* **1998**, 23, (8), 653-659.
6. Willner, I.; Steinberger-Willner, B., Solar hydrogen production through photobiological, photochemical and photoelectrochemical assemblies. *International Journal of Hydrogen Energy* **1988**, 13, (10), 593-604.
7. Nada, A. A.; Barakat, M. H.; Hamed, H. A.; Mohamed, N. R.; Veziroglu, T. N., Studies on the photocatalytic hydrogen production using suspended modified TiO<sub>2</sub> photocatalysts. *International Journal of Hydrogen Energy* **2005**, 30, (7), 687-691.
8. Kudo, A., Development of photocatalyst materials for water splitting. *International Journal of Hydrogen Energy* **2006**, 31, (2), 197-202.
9. Ni, M.; Leung, M. K. H.; Leung, D. Y. C.; Sumathy, K., A review and recent developments in photocatalytic water-splitting using TiO<sub>2</sub> for hydrogen production. *Renewable and Sustainable Energy Reviews* **2007**, 11, (3), 401-425.
10. Dhanalakshmi, K. B.; Latha, S.; Anandan, S.; Maruthamuthu, P., Dye sensitized hydrogen evolution from water. *International Journal of Hydrogen Energy* **2001**, 26, (7), 669-674.
11. O'Regan, B.; Gratzel, M., A low-cost, high-efficiency solar cell based on dye-sensitized colloidal TiO<sub>2</sub> films. *Nature* **1991**, 353, (6346), 737-740.
12. Bach, U.; Lupo, D.; Comte, P.; Moser, J. E.; Weissortel, F.; Salbeck, J.; Spreitzer, H.; Gratzel, M., Solid-state dye-sensitized mesoporous TiO<sub>2</sub> solar cells with high photon-to-electron conversion efficiencies. *Nature* **1998**, 395, (6702), 583-585.

13. Karuppuchamy, S.; Nonomura, K.; Yoshida, T.; Sugiura, T.; Minoura, H., Cathodic electrodeposition of oxide semiconductor thin films and their application to dye-sensitized solar cells. *Solid State Ionics* **2002**, 151, (1), 19-27.
14. Mane, R. S.; Lee, W. J.; Pathan, H. M.; Han, S. H., Nanocrystalline TiO<sub>2</sub>/ZnO thin films: fabrication and application to dye-sensitized solar cells. *Journal of Physical Chemistry B* **2005**, 109, (51), 24254-24259.
15. Abe, R.; Sayama, K.; Arakawa, H., Efficient hydrogen evolution from aqueous mixture of I<sup>-</sup> and acetonitrile using a merocyanine dye-sensitized Pt/TiO<sub>2</sub> photocatalyst under visible light irradiation. *Chemical Physics Letters* **2002**, 362, (5), 441-444.
16. Abe, R.; Sayama, K.; Arakawa, H., Dye-sensitized photocatalysts for efficient hydrogen production from aqueous I<sup>-</sup> solution under visible light irradiation. *Journal of Photochemistry and Photobiology A: Chemistry* **2004**, 166, (1), 115-122.
17. Nada, A. A.; Hamed, H. A.; Barakat, M. H.; Mohamed, N. R.; Veziroglu, T. N., Enhancement of photocatalytic hydrogen production rate using photosensitized TiO<sub>2</sub>/RuO<sub>2</sub>-MV<sup>2+</sup>. *International Journal of Hydrogen Energy* **2008**, 33, (13), 3264-3269.
18. Peng, T.; Ke, D.; Cai, P.; Dai, K.; Ma, L.; Zan, L., Influence of different ruthenium (II) bipyridyl complex on the photocatalytic H<sub>2</sub> evolution over TiO<sub>2</sub> nanoparticles with mesostructures. *Journal of Power Sources* **2008**, 180, (1), 498-505.
19. Ellingson, R. J.; Asbury, J. B.; Ferrere, S.; Ghosh, H. N.; Sprague, J. R.; Lian, T.; Nozik, A. J., Dynamics of electron injection in nanocrystalline titanium dioxide films sensitized with [Ru (4, 4'-dicarboxy-2, 2'-bipyridine)<sub>2</sub> (NCS)<sub>2</sub>] by infrared transient absorption. *Journal of Physical Chemistry B* **1998**, 102, (34), 6455-6458.
20. Galoppini, E., Linkers for anchoring sensitizers to semiconductor nanoparticles. *Coordination Chemistry Reviews* **2004**, 248, (13), 1283-1297.
21. Gratzel, M., Solar energy conversion by dye-sensitized photovoltaic cells. *Inorganic Chemistry* **2005**, 44, (20), 6841-6851.
22. Duncan, W. R.; Prezhdo, O. V., Theoretical studies of photoinduced electron transfer in dye-sensitized TiO<sub>2</sub>. *Annual Review of Physical Chemistry* **2007**, 58, 143-184.
23. Kim, W.; Tachikawa, T.; Majima, T.; Choi, W., Photocatalysis of Dye-Sensitized TiO<sub>2</sub> Nanoparticles with Thin Overcoat of Al<sub>2</sub>O<sub>3</sub>: Enhanced Activity for H<sub>2</sub> Production and Dechlorination of CCl<sub>4</sub>. *Journal of Physical Chemistry C* **2009**, 113, (24), 10603-10609.
24. Abe, R.; Hara, K.; Sayama, K.; Domen, K.; Arakawa, H., Steady hydrogen evolution from water on Eosin Y-fixed TiO<sub>2</sub> photocatalyst using a silane-coupling

reagent under visible light irradiation. *Journal of Photochemistry and Photobiology A: Chemistry* **2000**, 137, (1), 63-69.

25. Li, Q.; Chen, L.; Lu, G., Visible-light-induced photocatalytic hydrogen generation on dye-sensitized multiwalled carbon nanotube/Pt catalyst. *Journal of Physical Chemistry C* **2007**, 111, (30), 11494-11499.

26. Li, Y.; Xie, C.; Peng, S.; Lu, G.; Li, S., Eosin Y-sensitized nitrogen-doped TiO<sub>2</sub> for efficient visible light photocatalytic hydrogen evolution. *Journal of Molecular Catalysis A: Chemical* **2008**, 282, (1), 117-123.

27. Sreethawong, T.; Junbua, C.; Chavadej, S., Photocatalytic H<sub>2</sub> production from water splitting under visible light irradiation using Eosin Y-sensitized mesoporous-assembled Pt/TiO<sub>2</sub> nanocrystal photocatalyst. *Journal of Power Sources* **2009**, 190, (2), 513-524.

28. Li, Y.; Guo, M.; Peng, S.; Lu, G.; Li, S., Formation of multilayer-Eosin Y-sensitized TiO<sub>2</sub> via Fe<sup>3+</sup> coupling for efficient visible-light photocatalytic hydrogen evolution. *International Journal of Hydrogen Energy* **2009**, 34, (14), 5629-5636.

29. Minitab 15 for windows. USA: Minitab Inc.; **2007**.

30. Srinivasan, A.; Viraraghavan, T., Oil removal from water by fungal biomass: A factorial design analysis. *Journal of Hazardous Materials* **2010**, 175, (1-3), 695-702.

31. Durr, H.; Bossmann, S.; Beuerlein, A., Biomimetic approaches to the construction of supramolecular catalysts: titanium dioxide--platinum antenna catalysts to reduce water using visible light. *Journal of Photochemistry and Photobiology A: Chemistry* **1993**, 73, (3), 233-245.

32. Leavengood, S.; Reeb, J. E. *Statistical process control: part 3, starting a program: pereto analysis. Ext. Serv. EM 8771*; Oregon State University: **2001**; p 9.

33. Antony, J., *Design of experiments for engineers and scientist*. New York: Butterworth-Heinemann: **2003**.

34. Li, Y.; Lu, G.; Li, S., Photocatalytic hydrogen generation and decomposition of oxalic acid over platinized TiO<sub>2</sub>. *Applied Catalysis A: General* **2001**, 214, (2), 179-185.

## Chapter 4

# 4 Sacrificial Hydrogen Generation from Aqueous Triethanolamine with Eosin Y-Sensitized TiO<sub>2</sub>/Pt Photocatalyst, in UV, Visible and Solar Light Irradiation

## 4.1 Introduction

Photocatalytic water splitting for hydrogen production has drawn attention due to its potential to generate green fuel from water. Fujishima and Honda reported the photocatalytic water splitting over a TiO<sub>2</sub> single crystal in 1972,<sup>1</sup> following which a remarkable progress was witnessed in the last decade under ultra-violet light.<sup>2, 3</sup> In different studies Pt/TiO<sub>2</sub>, RuO<sub>2</sub>/TiO<sub>2</sub>, reduced SrTiO<sub>3</sub> electrode with a platinum counter electrode, platinized SrTiO<sub>3</sub>, SrTiO<sub>3</sub> powder modified by rhodium oxide, and nickel-loaded SrTiO<sub>3</sub> were also investigated for improvement of their photocatalytic activities.<sup>2, 4-8</sup>

The primary problem with UV photocatalysis was its limited solar spectrum of 4% compared (46 %) for visible light. For visible light water splitting, the photocatalytic materials should have proper band position and suitable band gap energy ( $1.23 \text{ eV} < E_g < 3.0 \text{ eV}$ ).<sup>9</sup> Oxides such as TiO<sub>2</sub>, ZnO and SnO<sub>2</sub> have large band gap (3-3.8 eV) and absorb only ultra-violet part of the solar radiation and so has low conversion efficiencies. Only few chalcogenides (CdS, CdSe etc.) have band gap within 1.23 eV and 3.0 eV, which can be activated with visible light. These catalysts, however, can't be used because of severe photo corrosion problem.

Semiconductor photocatalyst can be modified to expand the photo-response to visible region in several ways such as doping with cation/anion, spectral sensitization using dye or polymer, coupling with another small band gap semiconductor and implantation of metal ions.<sup>10</sup> To harvest solar visible light, spectral sensitization of broad band gap semiconductors such as TiO<sub>2</sub>, ZnO etc by adsorbed dye molecule have been studied for sacrificial hydrogen generation with several electron donors.<sup>11</sup> Organic dyes, inorganic

sensitizers and coordination metal complexes were mostly studied for sacrificial hydrogen generation. Ruthenium-based dyes are very expensive and toxic which would not be economical in large scale application. On the contrary, organic dyes are less toxic, less expensive and can be used for dye sensitization process. Several organic dyes such as eosin Y, rose bengal, merocyanine, crystal violet and riboflavin have been utilized for spectral sensitization of semiconductors.<sup>12</sup>

In dye sensitization process, sacrificial electron donors play a vital role, as the dye regeneration and electron injection to semiconductor are assisted by the electron donor. By choosing an industrial organic effluent as electron donor we can make the hydrogen generation process self sustained. Literature showed plenty of electron donors such as EDTA, acetonitrile, methanol, isopropanol, IO<sup>3-</sup>/I<sup>-</sup>, diethanolamine, triethanolamine, chloroacetic acid, and oxalic acid etc for such applications. Among these we have chosen triethanolamine as the electron donor which can be achieved easily from industrial effluents related to dry cleaning, cosmetics, shampoo, detergents, surfactant, textile and water repellents.<sup>13, 14</sup> Among the dyes used, eosin Y (EY) and triethanolamine (TEOA) were proven to be a very good dye-electron donor couple for sacrificial hydrogen generation.<sup>15</sup> EY showed a good absorption in solar visible spectrum and was studied with a wide variety of materials such as i) TS-1 zeolite,<sup>16</sup> silica gel,<sup>17</sup> multiwalled carbon nanotubes,<sup>18, 19</sup> nanotube Na<sub>2</sub>Ti<sub>2</sub>O<sub>4</sub>(OH)<sub>2</sub>,<sup>20</sup> sol-gel TiO<sub>2</sub>,<sup>21</sup> N-doped sol-gel TiO<sub>2</sub>,<sup>22</sup> and silane coupled-TiO<sub>2</sub>.<sup>15</sup>

Although these studies have provided plenty of information on visible-light-driven dye-sensitized hydrogen generation in presence of sacrificial electron donor, none of them have investigated the dye-sensitized process in complete solar spectrum which is very essential for using the photocatalyst in real solar light applications. Furthermore there is also insufficient information about the characteristics of the electron donor and dye in presence of solar UV radiation as well as lack of intermediate analysis to assist in establishing the reaction mechanism.

In this present work, we aim to explore the sacrificial hydrogen generation in complete solar spectrum with EY sensitized platinum loaded TiO<sub>2</sub> in aqueous TEOA solution. The photocatalytic behavior has been systematically studied in solar-UV (300-388 nm), solar-visible (420-650 nm) and full solar spectrum (300-650 nm) by varying reaction conditions including i) light intensity, ii) solution pH, iii) platinum content (wt %) on TiO<sub>2</sub>, iv) mass of EY-TiO<sub>2</sub>/Pt, v) concentration of TEOA, and vi) mass ratio of EY to TiO<sub>2</sub>/Pt. We also aim at investigating mass transfer and light intensity effects, which are essential parameters in designing flow photoreactor. To the best of our knowledge, studies of those factors are limited, thus, information gained in this investigation would be helpful for developing proper design and scale up methodologies for solar hydrogen generation photoreactors.

## 4.2 Experimental

### 4.2.1 Reagents

All reagents were analytical grade and were used without further treatment. Aeroxide TiO<sub>2</sub> P25 (80-20% anatase to rutile) from Evonik Degussa Corporation was used as catalyst. Eosin Y dye (99.0%, Sigma-Aldrich Canada Ltd) was used as sensitizer for TiO<sub>2</sub>; triethanolamine (98.0%) and hydrogen hexachloroplatinate (IV) solution (8 wt%) were also purchased from Sigma-Aldrich Canada Ltd. Ultra pure water (18 MΩ) was prepared from an in-house EASYPure® RODI system (Thermo Scientific, Canada).<sup>23</sup>

### 4.2.2 Preparation of dye-sensitized photocatalyst

Platinum was loaded on TiO<sub>2</sub> catalyst by a solar photodeposition method. TiO<sub>2</sub> powder was stirred in an aqueous ethanol solution (ethanol/water = 10/90 by volume) with hexachloroplatinate (IV) solution (H<sub>2</sub>PtCl<sub>6</sub>), the amount of which corresponded to platinum loadings of 0.05, 0.25, 0.5, 0.75, 1, and 1.5 wt %. Then, the solution was irradiated under the solar simulator (at 1 sun) for 3 h. Photoreduction of H<sub>2</sub>PtCl<sub>6</sub> (Pt<sup>IV</sup>) occurred, and highly dispersed Pt particles were deposited on the TiO<sub>2</sub> surface. After



being filtered and washed with water, the powder was dried at 150 °C for 2 h and milled in a mortar resulting in platinum loaded TiO<sub>2</sub> (TiO<sub>2</sub>/Pt).

Eosin Y (EY) sensitization was achieved by two different methods. In first method, EY was adsorbed on TiO<sub>2</sub>/Pt in anhydrous ethanol solution as described in our earlier work.<sup>24</sup> This photocatalyst is abbreviated as EY-TiO<sub>2</sub>/Pt.

In second method, EY was mixed with TiO<sub>2</sub>/Pt in aqueous TEOA solution, sonicated and then purged with nitrogen gas. This photocatalyst is abbreviated as EY:TiO<sub>2</sub>/Pt.

### 4.2.3 Photocatalyst characterization techniques

Diffuse reflection spectra (DRS) were collected using UV-3600 (Shimadzu, Japan) equipped with DR integrated sphere coated with barium sulfate. Barium sulfate is also considered suitable standards by the CIE. The spectra were recorded at room temperature in the range of 200-750 nm. The Merck DIN 5033 barium sulfate powder standard (EM Industries Inc., Hawthorne, NY) has an absolute reflectance of 0.973 to 0.988 in the 380- to 750-nm wavelength range, and > 0.95 in the 750- to 1500-nm wavelength range. The XRD data were obtained using a Rigaku–MiniFlex II, powder diffractometer (Japan), using CuK $\alpha$  ( $\lambda$  for K $\alpha$  = 1.54059 Å) over the desired  $2\theta$  range with step width of 0.05° with a counting time of 2s for each step. Scanning electron micrographs (SEM) and Energy Dispersive X-ray (EDX) were performed with Hitachi S-4500 field emission SEM with a Quartz XOne EDX system. Surface area was measured by Micromeritics ASAP 2010 instrument. FTIR study was performed with Nicolet 6700 FT-IR spectrophotometer.

### 4.2.4 Reactor configuration for photocatalytic hydrogen generation

Photocatalytic reactions were carried out in a gastight Pyrex glass made batch reactor (530 mL) with a flat window at top for illumination (Appendix C). The catalyst powder (EY-TiO<sub>2</sub>/Pt) was suspended in 100 mL TEOA solution (0.05 M to 0.5 M) after pH adjustment with 1:1 HCl. The catalyst suspension was dispersed for 5 min in an ultrasonic bath and then the system was degassed by bubbling ultra pure nitrogen gas for

40 min. Reaction mixture was stirred (500 rpm) using a magnetic stirrer. The photocatalyst was irradiated with a solar simulator from the top. The light source was equipped with AM 1.5 G as well as a 420 nm cut-off filter (Omega optical, USA) to remove all the UV light. A long pass filter was used to cut the visible and NIR light for UV operation only. The lamp and reactor was attached with cooling fans to avoid heating up.

The gas sampling port in the reactor was sealed with a silicone rubber septum, and the sampling was made intermittently through the septum during the experiments. Hydrogen was analyzed by Shimazu GC 2014 (TCD, ultra pure N<sub>2</sub> as carrier gas and HeyeSep D column). A flow reactor (Figure 4.1) was also used for better understanding the effect of mass transfer and future scale up of the solar hydrogen photo reactor. Details of the flow reactor are described in the Appendix C.

The data show mean values from two to three independent experiments with standard deviation of less than 5 percent.

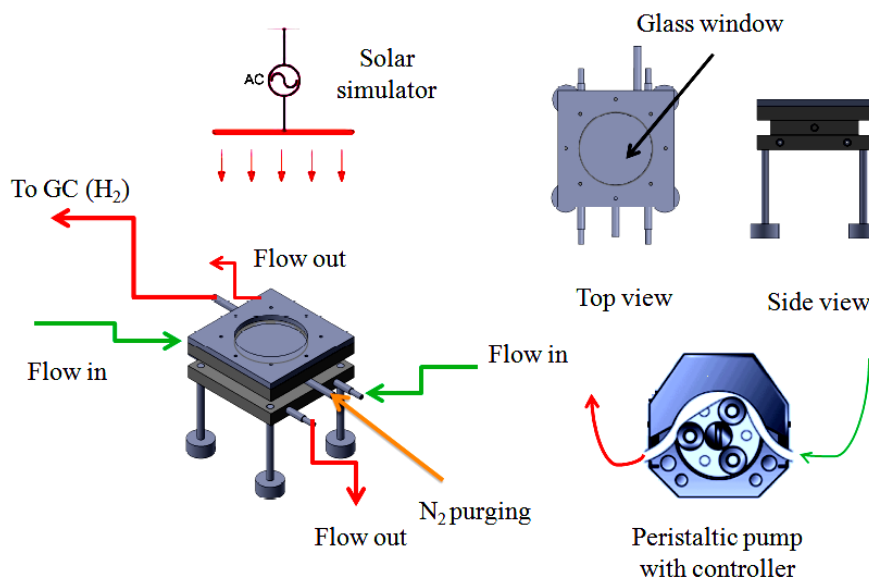


**Figure 4.1** Flow reactor for sacrificial hydrogen generation.

## 4.3 Results and Discussion

### 4.3.1 Photocatalyst characterization results

#### 4.3.1.1 Diffuse reflectance spectra (DRS)

Diffuse reflectance spectra of TiO<sub>2</sub> P25 and EY-sensitized TiO<sub>2</sub>/Pt are shown in Figure 4.2. It is clearly observed that the absorption band of TiO<sub>2</sub> is in the UV light range of 200-400 nm, and after platinum loading and EY sensitization the absorption edges shifted towards longer wavelength. A broad spectrum of 450–600 nm can be seen from the figure below. EY dye mainly absorbs visible light with a maximum absorption at 514 nm (Appendix A) and thus can provide visible light activity to the resulting photocatalyst.

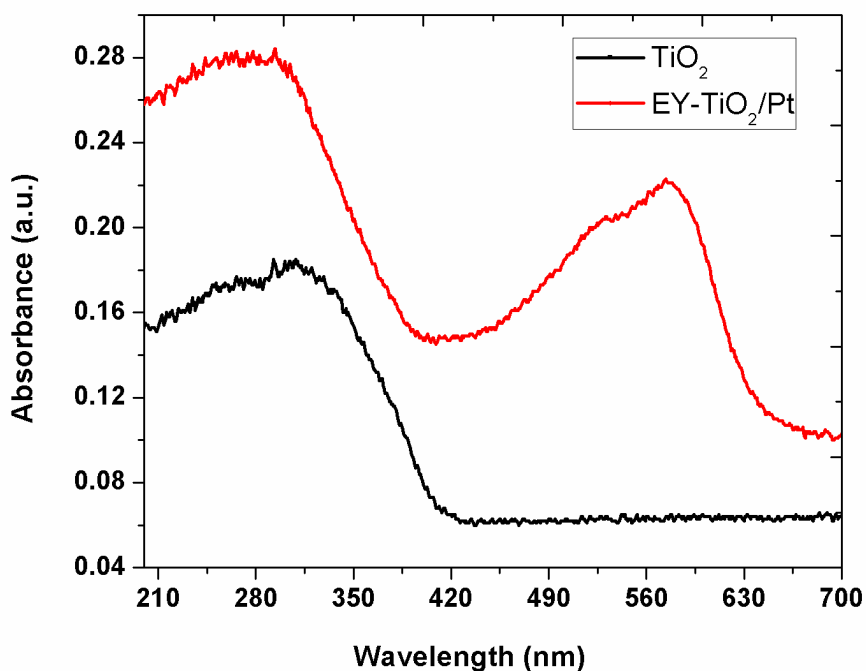
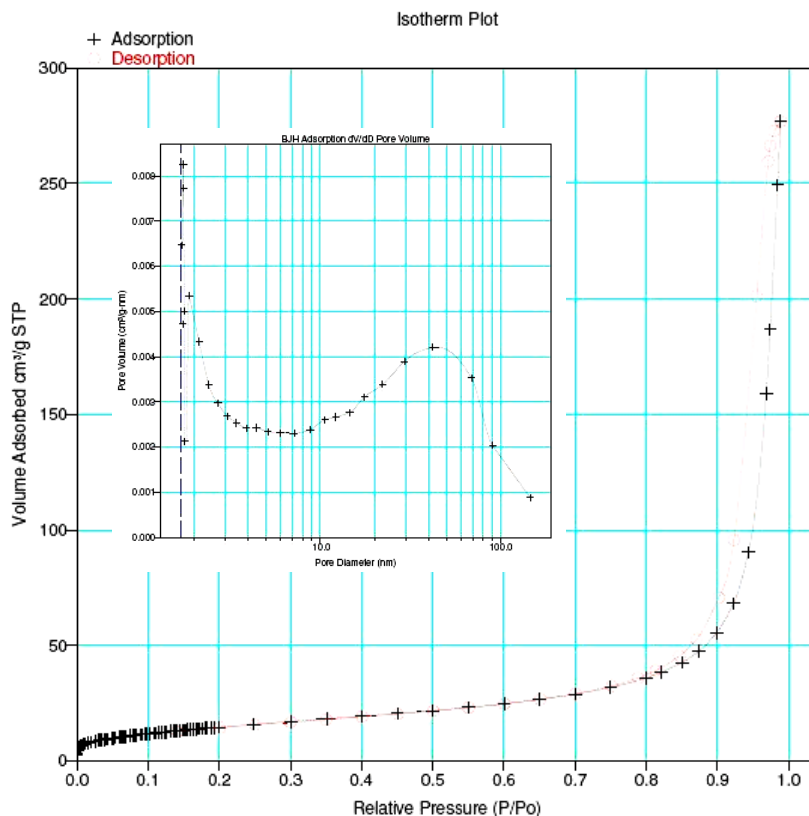


Figure 4.2 Diffuse reflectance spectra of TiO<sub>2</sub> and EY-sensitized TiO<sub>2</sub>/Pt photocatalysts

### 4.3.1.2 Brunauer–Emmett–Teller (BET) method

Figure 4.3 shows the representative Barrett–Joyner– Halenda (BJH) pore size distribution and adsorption–desorption isotherm plot (inset) of the EY-sensitized Pt-loaded TiO<sub>2</sub> catalyst. The determined BET surface area was found to be 55 m<sup>2</sup> g<sup>-1</sup>, which is comparable to that of TiO<sub>2</sub> P25 (50 m<sup>2</sup> g<sup>-1</sup>). This indicates that platinum loading and dye adsorption did not significantly affect the catalyst total surface area.



**Figure 4.3 N<sub>2</sub> adsorption-desorption isotherm (BJH poresize distribution) of EY-sensitized TiO<sub>2</sub>/Pt photocatalyst**

### 4.3.1.3 X-ray diffraction (XRD)

The XRD pattern (Figure 4.4) of  $\text{TiO}_2$  and EY- $\text{TiO}_2/\text{Pt}$  were investigated to identify the crystalline phase of the sample. Several dominant peaks at  $2\theta$  of about 25.2, 37.9, 48.3, 53.8, 62.7, 68.9 and 73.5° were observed. These represented the indices of (101), (103), (200), (105), (213), (116), and (107) planes respectively and showed the crystalline structure of pure anatase phase.<sup>21</sup> The XRD pattern was similar to the standard crystal structure of  $\text{TiO}_2$ , with no diffraction peaks associated with Pt metal in the EY- $\text{TiO}_2/\text{Pt}$  sample. This suggests that the platinum loading process did not produce separate impurity phases and that the Pt nanoparticles can be considered as fully dispersed in the  $\text{TiO}_2$  lattice. The only difference in the Pt loaded EY-sensitized sample is the reduced peak intensity of anatase phase at 25.2° compared to that of pure  $\text{TiO}_2$ .

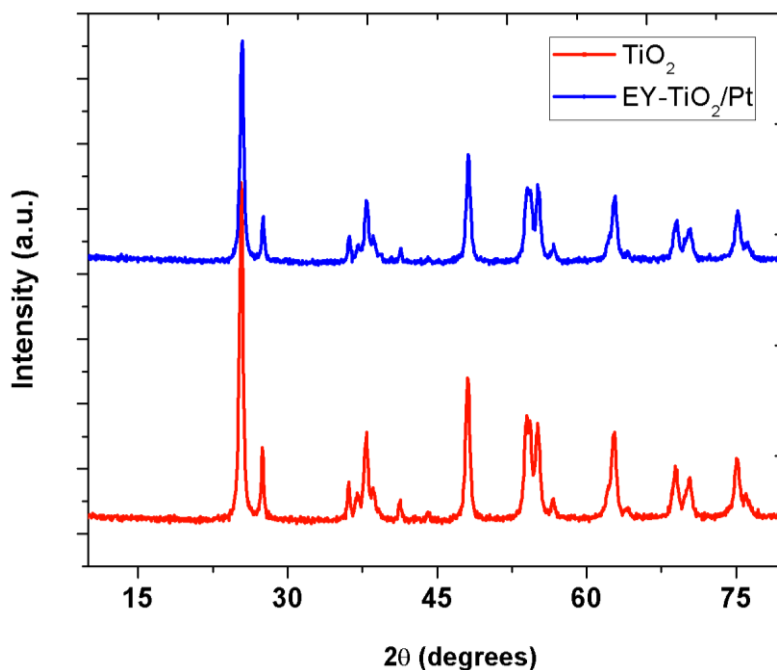


Figure 4.4 XRD patterns of  $\text{TiO}_2$  and EY- $\text{TiO}_2/\text{Pt}$  photocatalysts

#### 4.3.1.4 Fourier Transform Infrared (FTIR) spectroscopy

Figure 4.5 shows the FTIR spectrum of EY, TiO<sub>2</sub> and EY-sensitized TiO<sub>2</sub>/Pt samples. In all cases a broad peak was observed around 3200 cm<sup>-1</sup>, which may be due to surface –OH group of TiO<sub>2</sub> or –COOH group of EY. The –C=O stretch band was observed at 1750 cm<sup>-1</sup> for EY samples, but pure TiO<sub>2</sub> and EY-sensitized TiO<sub>2</sub>/Pt did not show such peak. The ester C-C(O)-C linkage appeared at around 1170 cm<sup>-1</sup> as broad multiple peaks. Therefore the dye could be anchored on to TiO<sub>2</sub>/Pt through ester-like linkage or carboxylate linkage.<sup>16, 25</sup>

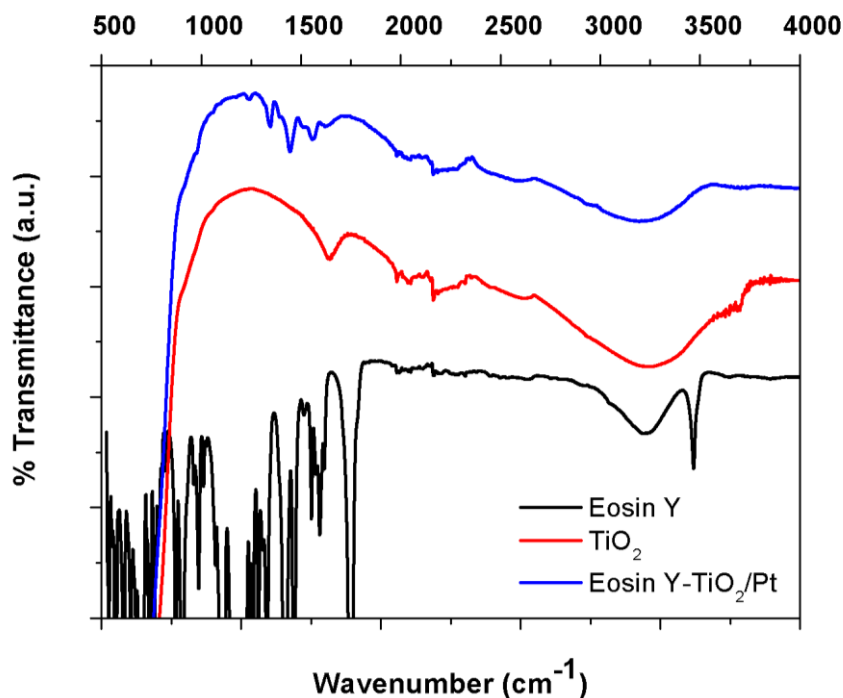
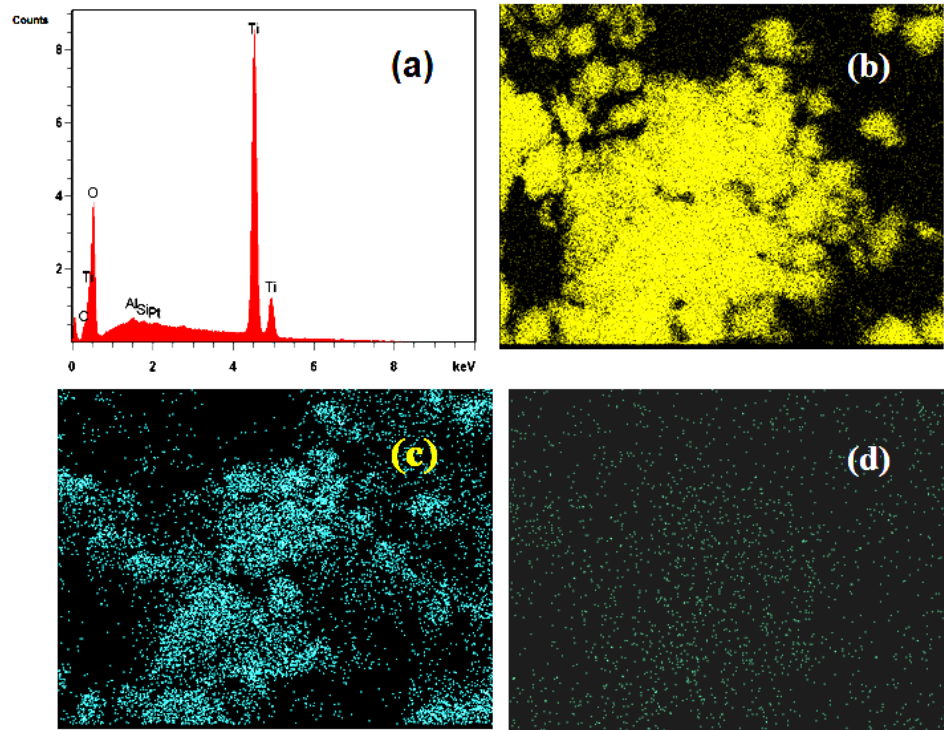


Figure 4.5 FTIR spectrum of Eosin Y, TiO<sub>2</sub> and EY-TiO<sub>2</sub>/Pt

#### 4.3.1.5 Energy-dispersive X-ray (EDX)

The EDX (Figure 4.6a) image clearly shows the existence of platinum metal on EY-TiO<sub>2</sub>. The elemental distribution of the platinum loaded EY-TiO<sub>2</sub> was also examined using EDX analysis by elemental area mapping of each component. It is clear from the mapping diagram that platinum was well dispersed on the photocatalyst surface.



**Figure 4.6 (a) EDX image of EY-TiO<sub>2</sub>/Pt (0.25 %) and EDX elemental area mapping: (b) Ti; (c) O; (d) Pt.**

### 4.3.2 Sacrificial hydrogen generation in visible and solar light irradiation- parametric study

Initially several dye solutions were used for dye-sensitization of Pt loaded TiO<sub>2</sub> with different electron donor in visible light irradiation. EY-TEOA system showed highest performance for dye-sensitized hydrogen generation. The higher LUMO (lowest unoccupied molecular orbital) of EY (-0.92 V) than E<sub>CB</sub> (-0.5 V) of TiO<sub>2</sub> and lower HOMO (+1.15 V) than E<sub>(TEOA+/TEOA)</sub> (+0.82 V) fulfills the thermodynamics for both electron injection and EY regeneration.<sup>26</sup>

#### 4.3.2.1 Comparison of TiO<sub>2</sub> and EY-sensitized TiO<sub>2</sub> based photocatalysts for hydrogen generation in solar and visible light irradiation

TiO<sub>2</sub> P25 and TiO<sub>2</sub>/Pt showed no activity in visible light irradiation. This was because of the higher band gap energy of TiO<sub>2</sub> and TiO<sub>2</sub>/Pt. On the contrary, EY-sensitized TiO<sub>2</sub>P25 and TiO<sub>2</sub>/Pt showed hydrogen generation activity in visible light irradiation. In solar light irradiation all of them showed hydrogen generation activity as shown in Table 4.1.

**Table 4.1 Activity of TiO<sub>2</sub> and TiO<sub>2</sub> based photocatalyst for sacrificial H<sub>2</sub> generation**

Photocatalyst	Hydrogen Generation (μmol g <sup>-1</sup> )*	
	Visible Light	Solar Light
TiO <sub>2</sub>	0	775
EY-TiO <sub>2</sub>	42	1047
TiO <sub>2</sub> /Pt	0	3629
EY-TiO <sub>2</sub> /Pt	1181	4297

(\* Experimental conditions: H<sub>2</sub> generation reported for 3h interval, [Catalyst]=1 g L<sup>-1</sup>, [TEOA]=0.25 M, I=100 mW cm<sup>-2</sup>, N<sub>2</sub> saturated, pre-sonicated.)



EY can incorporate visible light activity in both TiO<sub>2</sub> and TiO<sub>2</sub>/Pt. In solar light also hydrogen generation increased by 1.4 and 1.2 times by EY sensitization on TiO<sub>2</sub> and TiO<sub>2</sub>/Pt respectively. Platinum had significant effect on hydrogen generation. In visible light a huge improvement in hydrogen generation was achieved compared to EY-TiO<sub>2</sub> alone. In solar light platinum loading on both TiO<sub>2</sub> and EY-TiO<sub>2</sub> gave 4.7 and 4.1 times increment in hydrogen generation respectively.

#### 4.3.2.2 Dependence of photocatalytic activity of hydrogen evolution on platinum loading (wt %) over EY-TiO<sub>2</sub> in visible and solar light

Photocatalytic hydrogen generation from EY-TiO<sub>2</sub> with various platinum loadings (0.05–1.5 wt %) was studied in aqueous solution of TEOA, in solar and visible light irradiation. In visible light, EY accepts photon and is excited to higher energy level from where it can inject electron to the conduction band of TiO<sub>2</sub>. Photogenerated conduction band electron then transferred to H<sup>+</sup> forming gaseous hydrogen. In solar light the photocatalytic reaction initiates with the formation of electron/hole (e<sup>-</sup>/h<sup>+</sup>) pairs. With platinum on EY-TiO<sub>2</sub> photocatalyst, platinum can confine electrons and hydrogen can be produced on platinum particles.<sup>27</sup>

The amount of hydrogen generation increased with irradiation time during 3 h reaction period. However, the rate of hydrogen generation in first hour was highest and decreased gradually with time due to backward reactions of gaseous products in the system.<sup>28</sup> The rate of hydrogen production is presented as a function of platinum loading in both visible and solar light irradiation (Figure 4.7).

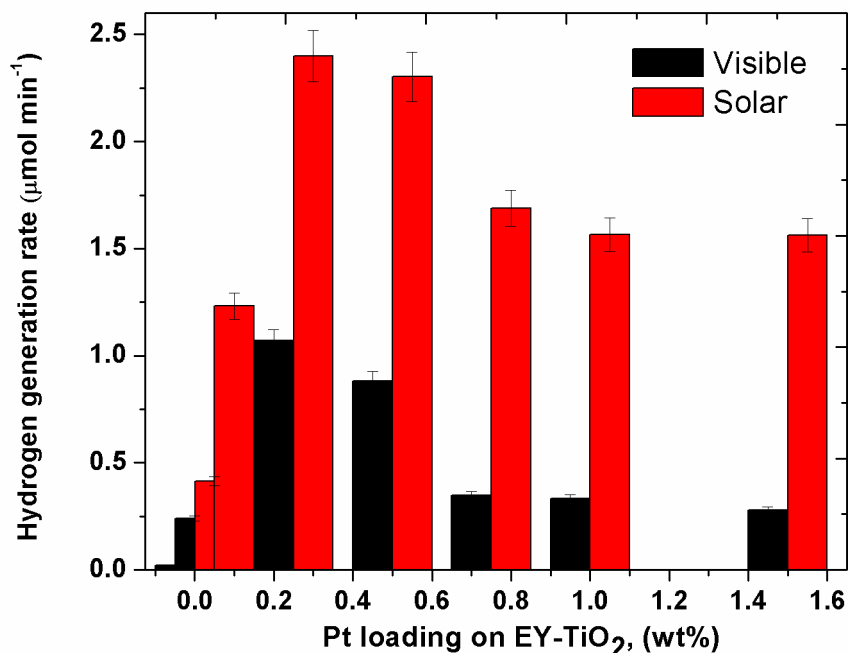


**Figure 4.7 Effect of platinum wt % on photocatalytic hydrogen generation over EY-TiO<sub>2</sub>.** (Experimental conditions: [TEOA] = 0.25 M, [EY-TiO<sub>2</sub>/Pt] = 1 g L<sup>-1</sup>, I = 100 mW cm<sup>-2</sup>, pH = 7, N<sub>2</sub> saturated, pre-sonicated, visible - 420 nm cutoff filter).

The rate of hydrogen generation initially increased as the platinum content increased from 0.05% to 0.25%, but further increment of platinum did not show any positive effect. Over loading of platinum metal beyond the optimum value resulted in lower hydrogen generation rate. The reasons may be the following:

i) more light scattering and lower light absorption due to excessive Pt nanoclusters on TiO<sub>2</sub>, and ii) at very high metal loading they act as recombination centres.<sup>29</sup>

#### 4.3.2.3 Dependence of hydrogen evolution on solution pH in visible and solar light

Solution pH had notable effect on hydrogen generation over EY-TiO<sub>2</sub>/Pt as discussed in our earlier study.<sup>23</sup> Acidic pH was not very helpful in hydrogen generation compared to alkaline pH. According to Li and Lu,<sup>20</sup> EY molecule has carboxylic acid group that can

interact with the hydroxyl groups on TiO<sub>2</sub>/Pt surface and thereby form an ester like linkage in TEOA solution. Again from zeta potential point of view, TiO<sub>2</sub> has zero surface charge in between pH 5.6-6.8.<sup>24, 30</sup> Hence, at alkaline pH (pH 10.0), the TiO<sub>2</sub> surface is negatively charged, and at acidic pH (pH 4.0), the surface is positively charged. Therefore, the pH value has a significant effect on the adsorption–desorption properties at the EY–TiO<sub>2</sub>/Pt surface.

Moreover, the ionization of oxidized form of triethanolamine (TEOA<sup>+</sup>) in aqueous solution depends on solution pH. At alkaline pH (pH = 9) TEOA<sup>+</sup> deprotonates to yield a neutral radical with the unpaired electron in alpha-position to either the amino or alcohol group. Such species are expected to exhibit reduction instead of oxidation properties. In acidic pH, the acid base equilibrium of TEOA<sup>+</sup> seems to favor the protonated form of the radical. In neutral solution both protonated and unprotonated forms coexist. The protonated form is less favorable as electron donor compared to the unprotonated form, thus unprotonated form of the amine is effective as reducing agent.<sup>31</sup>

Comparable initial rate of hydrogen generation was found in our experiment for both neutral (pH = 7) and alkaline (pH = 10) solutions, although after a while the rate of hydrogen generation dropped considerably for alkaline pH. Lower rate of hydrogen generation at alkaline pH is also reported by Zhang et al.<sup>17</sup>. As described by Li and Lu,<sup>20</sup> at strong basic solution a part of hydroxyl group on catalyst surface (TiO<sub>2</sub>/Pt) first reacts with H<sup>+</sup> and then leaves a basic group with negative charge. Because of the electrostatic repulsion force, carboxylic acid group of EY are difficult to adsorb on the TiO<sub>2</sub>/Pt surface, which prevents the electron transfer from excited dye (EY\*) to the TiO<sub>2</sub> conduction band. In solar light irradiation, experiments were also performed at pH 7.

#### 4.3.2.4 Dependence of hydrogen evolution on catalyst mass in visible and solar light

To explore the effects of catalyst mass on hydrogen generation, a series of batch experiments were performed with TiO<sub>2</sub>/Pt (0.25%) catalyst, in which the catalyst mass varied between 0.2 and 1.5 g L<sup>-1</sup>. In all cases natural pH (7.0) was maintained and all

other parameters such as initial concentration of TEOA, platinum content on TiO<sub>2</sub> and light intensity were identical. The rate of hydrogen production (r) in visible light irradiation is shown as a function of catalyst loading (g L<sup>-1</sup>) (Figure 4.8). The rate increased with catalyst loading in a linear manner, in particular at low catalyst loadings.

The rate of hydrogen generation increased initially up to 1.3 g L<sup>-1</sup> then reached a plateau. This can be explained by the concept of active site. At a low concentration of photocatalyst slurry, the photocatalytic reaction is mainly controlled by active sites which are accessible for adsorption of light and reactant.<sup>32, 33</sup> With gradual increment of photocatalyst slurry concentration the solution turbidity increases which, in turn, raises light scattering.

In solar light, similar experiments were also performed to achieve the optimum catalyst concentration for hydrogen generation. The optimum catalyst concentration was 1 g L<sup>-1</sup>. This concentration was little lower than the optimum concentration obtained in visible light (Figure 4.8).

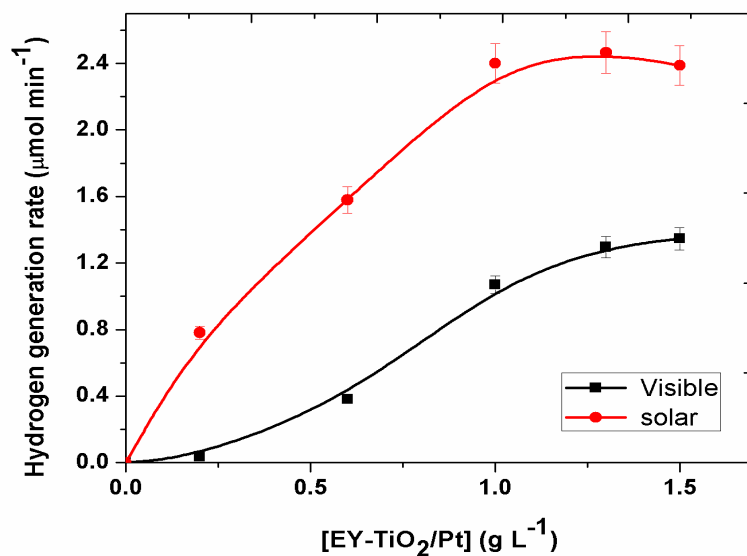


**Figure 4.8 Effect of photocatalyst mass on hydrogen generation.**

(Experimental conditions: [TEOA] = 0.25 M, Pt in TiO<sub>2</sub> = 0.25%, I = 100 mW cm<sup>-2</sup>, pH = 7, N<sub>2</sub> saturated, pre-sonicated, visible - 420 nm cutoff filter).

#### 4.3.2.5 Comparison of immobilized and slurry photocatalyst for hydrogen generation in solar light

##### 4.3.2.5.1 Preparation of immobilized EY-TiO<sub>2</sub>/Pt/PAM photocatalyst

A EY-TiO<sub>2</sub>/Pt/PAM composite was synthesized by solution polymerization method as described by Tang et al.<sup>34</sup> Cross linked polyacrylamide (PAM) is a superabsorbent polymer which is able to absorb hundreds to thousands times water of its own mass to form a stable hydrogel.

At first 0.13 g EY-TiO<sub>2</sub>/Pt catalyst was mixed with 3 gm acrylamide and 4 ml of deionized water. The mixture was sonicated for 5 min and then 0.0012 g cross linker was added. Again it was sonicated for 5 min and degassed under vacuum for 30 min. Then the mixture was heated in water bath (80<sup>0</sup>C) for 15 min with continuous stirring. Initiator was added (0.018 g) and the mixture was stirred a while. Finally the whole mixture was cooled down at room temperature.

##### 4.3.2.5.2 Hydrogen generation and stability of immobilized and slurry based EY-TiO<sub>2</sub>/Pt

To compare the activity of immobilized versus slurry form of EY-TiO<sub>2</sub>/Pt catalyst, batch experiments were performed in solar light. Experiments were run up to 12 h, and at every 3 h interval hydrogen gas was evacuated by nitrogen purging. This enabled us to obtain the consecutive hydrogen generation rates (Figure 4.9). During the reaction EY-TiO<sub>2</sub>/Pt/PAM absorbed huge amount of water and formed hydrogel. The reaction rate of slurry catalyst was much higher compared to immobilized catalyst. The main reason of lower activity of immobilized catalyst could be low illuminated surface and mass transfer.

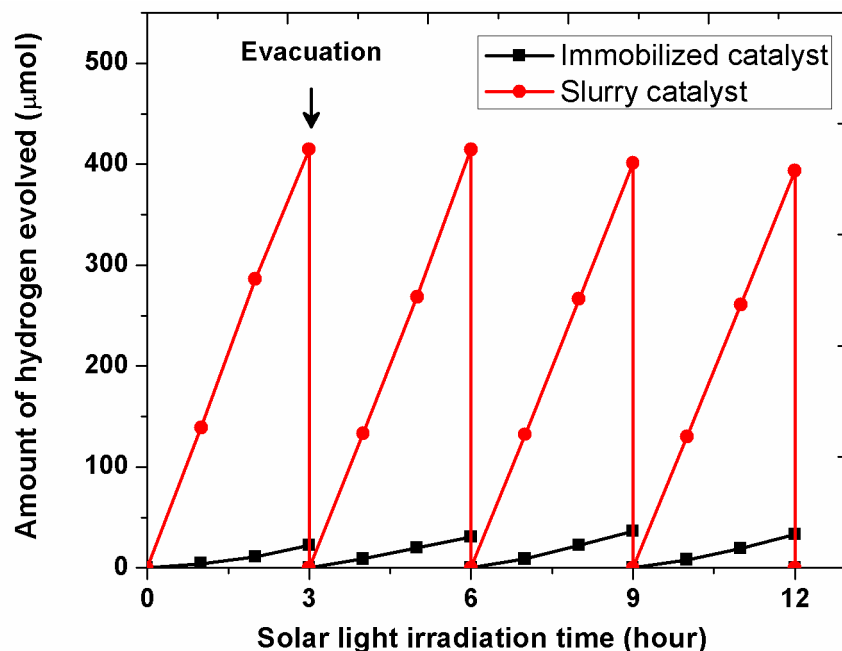


**Figure 4.9 Comparison of immobilized and slurry photocatalyst for hydrogen generation in solar light.** (Experimental conditions:  $[\text{TEOA}] = 0.25 \text{ M}$ ,  $I_{\text{solar}} = 100 \text{ mW cm}^{-2}$ ,  $\text{pH} = 7$ ,  $\text{N}_2$  saturated, pre-sonicated).

#### 4.3.2.6 Dependence of hydrogen generation on EY to $\text{TiO}_2/\text{Pt}$ mass ratio

The concentration of EY has a leading role in improving the number of excited electrons and thereby increasing the photocatalytic activity. Again, the dye adsorption and photocatalytic activities are both related to the active sites (or surface area) of the semiconductor catalyst. So, it was necessary to investigate the effect of the dye and semiconductor catalyst together. In earlier studies people reported different optimum EY: $\text{TiO}_2/\text{Pt}$  (EY:T) ratio for hydrogen generation in visible light. Li and Lu<sup>20</sup> reported EY:T mass ratio of 1:1 as optimum for  $\text{Na}_2\text{TiO}_4(\text{OH})_2/\text{Pt}$  nanotubes in visible light. Zhang et al.<sup>16</sup> reported an optimum mass ratio (EY:T) of 1:8 for TS-1 zeolite.

Our former method of dye sensitization using alcoholic solution of EY was time consuming and expensive. So, we switched to a simpler method to study the effect of EY concentration, where EY was mixed with the TiO<sub>2</sub>/Pt catalyst just before the reaction; sonicated and then purged with nitrogen gas. We found an optimum mass ratio (EY:T) of 1:10 and 1:13.3 in visible and solar light respectively (Figure 4.10).

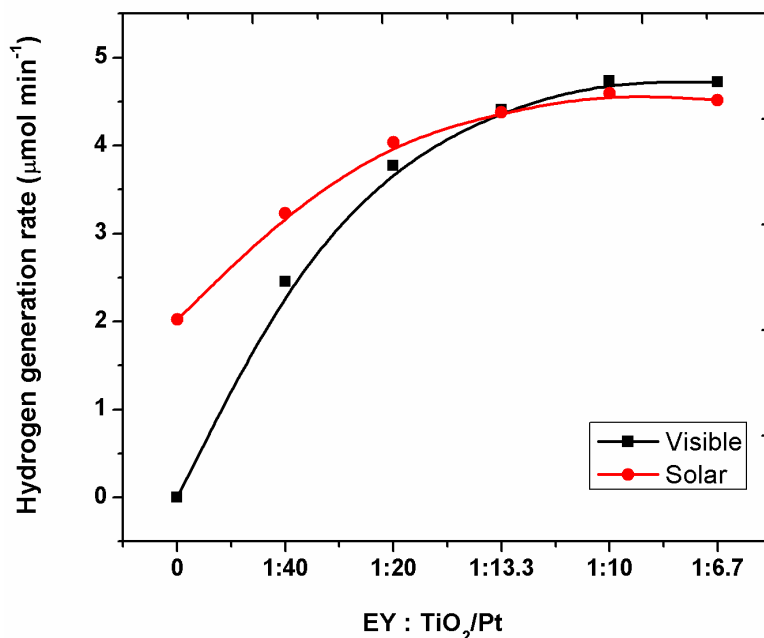


**Figure 4.10 Effect of EY to TiO<sub>2</sub>/Pt mass ratio on hydrogen generation rate.** (Experimental conditions: [TEOA] = 0.25 M, TiO<sub>2</sub>/Pt(0.25%) = 1 g L<sup>-1</sup>, I = 100 mW cm<sup>-2</sup>, pH = 7, N<sub>2</sub> saturated, pre-sonicated, visible - 420 nm cutoff filter).

#### 4.3.2.7 Dependence of hydrogen generation on initial TEOA concentration

TEOA played a vital role in dye-sensitized process for hydrogen generation. In absence of TEOA, EY-TiO<sub>2</sub>/Pt was unable to produce any hydrogen. TEOA has three different roles i) electron donor, ii) extend the dye stability and iii) act as a buffer. As an electron

donor it can reduce the  $EY^+$  species to give it back to its ground state and also enhance the stability of EY through the Vander-Walls interaction with oxidized dye radicals.<sup>17</sup> Moreover, aqueous solution of TEOA had a natural pH of 10.4 and it actually acted as a buffer solution throughout the reaction. Initial concentration of TEOA correlates the hydrogen generation rate by Langmuir-type isotherm as discussed in section 4.3.4.

### 4.3.3 Discussion of reaction mechanism in visible and solar light irradiation

In the photosensitization system, a photochemically excited molecule may donate or accept electron depending on the presence of electron acceptor or electron donor respectively.<sup>35</sup> In case of dye sensitization, dye serves dual role, i) sensitizer for semiconductor and ii) molecular bridge between semiconductor and electron donor.<sup>12</sup> Till date most of the papers discussed application of dye-sensitized photocatalyst in visible light. We have used EY-sensitized Pt loaded  $TiO_2$  catalyst in solar light which includes both UV and visible spectrum. Results showed that the hydrogen production increased drastically in solar light with TEOA as electron donor. Probable explanation is that, in solar UV light band gap excitation produce  $e^-/h^+$  pairs on  $TiO_2$ . Positive  $h^+$  reacts with water to produce  $HO^\bullet$  radical which oxidizes TEOA to HCHO and  $NH_3$ . HCHO is further oxidized to produce  $H_2$  and  $CO_2$ . Blank experiments were performed with only  $TiO_2/Pt$  (without dye) separately in visible light and solar light in presence of aqueous solution of TEOA to verify the reaction mechanism.

#### 4.3.3.1 Reactions in visible light

In visible light ( $\lambda > 420$  nm) the energy of photon is lower than the band gap of  $TiO_2/Pt$  but higher than the band gap of dye molecule. So, the adsorbed EY molecules on the surface of semiconductor are excited with visible photons and then inject electron to the conduction band of  $TiO_2$ . After the electron injection EY is converted to its oxidized form ( $EY^+$ ) and the electron can reduce  $H^+$  to  $H_2$  on the platinum site over the  $TiO_2$ . The proposed mechanism is shown below:



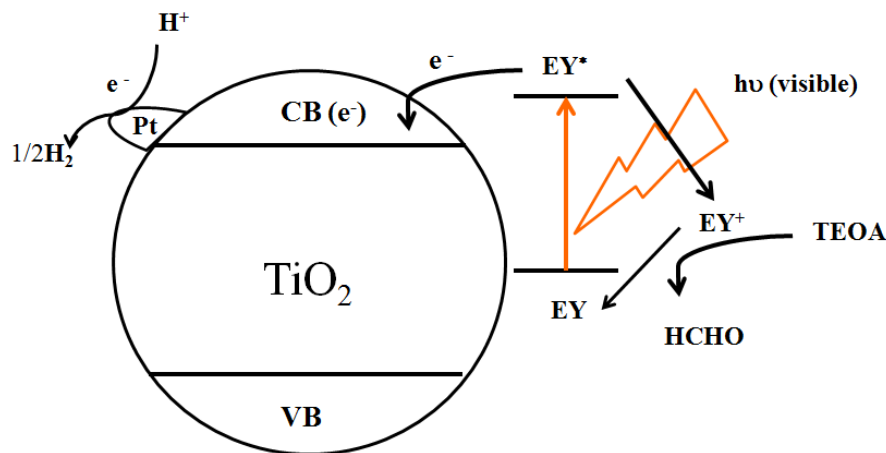
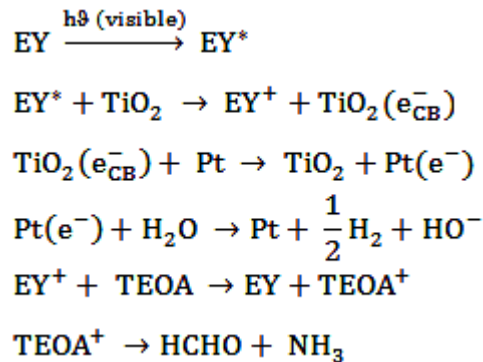


Figure 4.11 Hydrogen generation in visible light.

#### 4.3.3.2 Reactions in solar light

Solar light irradiation includes both UV and visible spectrum. UV light can excite  $\text{TiO}_2$  and produce  $e^-/h^+$  pair by conventional band gap excitation process. At the same time EY dye is also sensitized in solar light. TEOA oxidation might occur in presence of  $h^+$  /or  $\text{HO}^\bullet$  radical as evident from the formation of formaldehyde as an intermediate. Oxidation of triethanolamine can be achieved in presence of several oxidants such as periodate, hypochlorous acid, chlorine dioxide, and hexacyanoferrate (III). But in those cases further oxidation of formaldehyde was not reported or the oxidation of the formaldehyde was extremely slow and, therefore, formaldehyde was the end product.<sup>36</sup> In our case we

noticed further oxidation of formaldehyde to hydrogen in solar light. This fact was confirmed by increased hydrogen generation and decreased formaldehyde concentration compared to visible light. This also confirms much higher oxidizing capability of HO• radical compared to above mentioned oxidants.

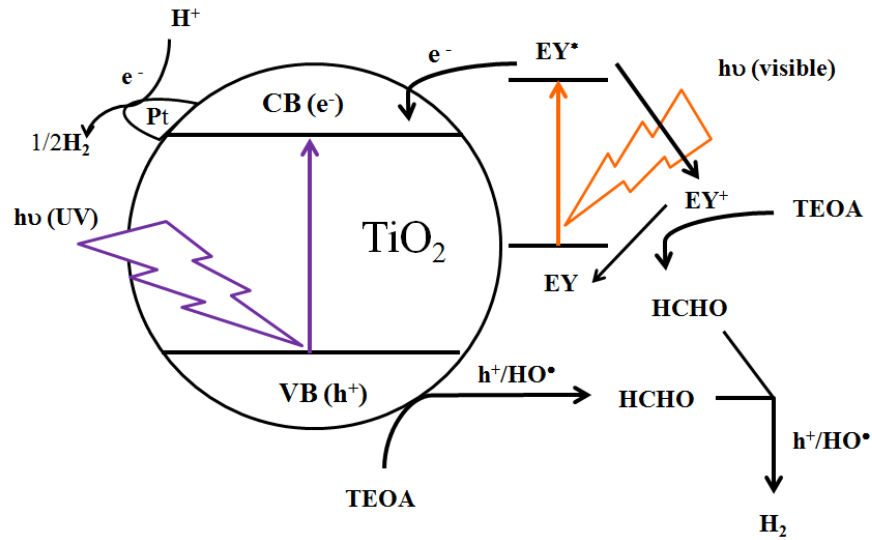
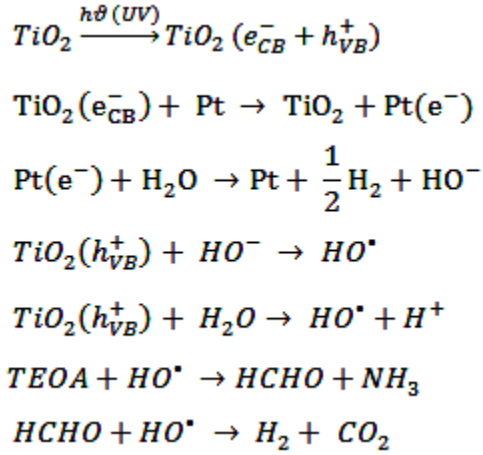
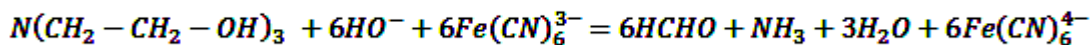


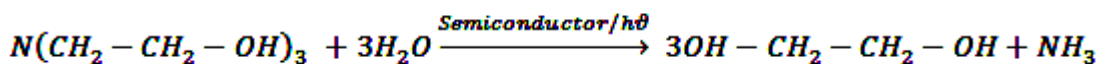
Figure 4.12 Hydrogen generation in solar light.

#### 4.3.3.3 Oxidation of TEOA: formation of formaldehyde

Shukla et al.<sup>36</sup> reported the oxidation kinetics of TEOA with alkaline hexacyanoferrate (III) in aqueous media. The oxidation reaction is shown below:



Naman and Gratzel<sup>37</sup> have studied the colloidal suspension of vanadium sulfide with different percentage of ethanolamine (mono-, di-, and triethanolamine) in water as a sweetening mixture of H<sub>2</sub>S. Trace amount of ethylene glycol was formed in the system, but further oxidation of ethylene glycol was not reported.



In another study, the photodegradation of ethanolamine did not report any ethylene glycol formation, but formaldehyde formation was mentioned as a major intermediate.<sup>38</sup> In our case formaldehyde was detected and quantified as an intermediate product in both visible and solar light driven reactions using both semi-quantitative and quantitative methods. Table 4.2 shows the formaldehyde formation with different photocatalyst in solar and visible light irradiation.

**Table 4.2 Comparison of formaldehyde formation with different catalyst in visible and solar light\***

<b>Photocatalyst</b>	<b>Light sources</b>	<b>HCHO (mg L<sup>-1</sup>)</b>
<b>TiO<sub>2</sub></b>	Visible	nil
<b>TiO<sub>2</sub></b>	Solar	15
<b>TiO<sub>2</sub>/Pt</b>	Visible	nil
<b>TiO<sub>2</sub>/Pt</b>	Solar	28
<b>EY-TiO<sub>2</sub>/Pt</b>	Visible	80
<b>EY-TiO<sub>2</sub>/Pt</b>	Solar	78

(\*Formaldehyde concentration was determined by MBTH method. Experimental conditions: Catalyst = 1 g L<sup>-1</sup>, I = 100 mW cm<sup>-2</sup>, pH = 7, N<sub>2</sub> saturated, pre-sonicated, visible - 420 nm cutoff filter).

In case of visible light, only dye sensitization mechanism is possible. So, TEOA is being oxidized by EY<sup>+</sup> species. However, in presence of solar light, TEOA oxidation was also initiated by the valance band hole (h<sub>VB</sub><sup>+</sup>). This is evident by the fact that, under similar reaction conditions visible light generates more formaldehyde than solar light. Figure 4.13 shows the plot of EY:T mass ratio vs intermediate (formaldehyde) formation in solar and visible light. With the increase in dye to photocatalyst ratio the photocatalytic hydrogen generation rate is increased. At the same time formaldehyde formation is also increased. In solar light formaldehyde molecule is further oxidized to hydrogen which is not possible in visible light. Figure 4.14 and Figure 4.15 shows the plot of H<sub>2</sub> and formaldehyde formation at different EY:T ratio in visible and solar light, respectively.

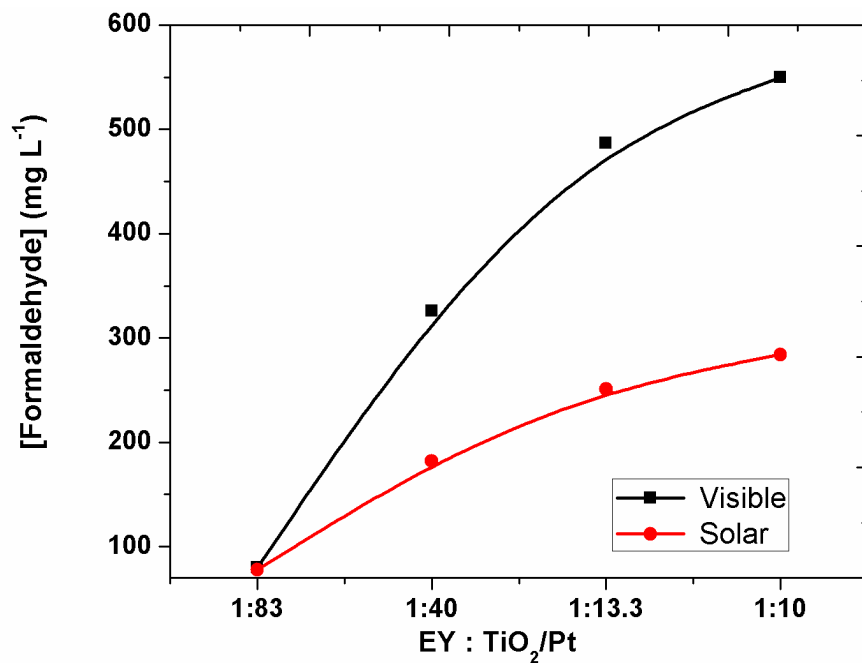
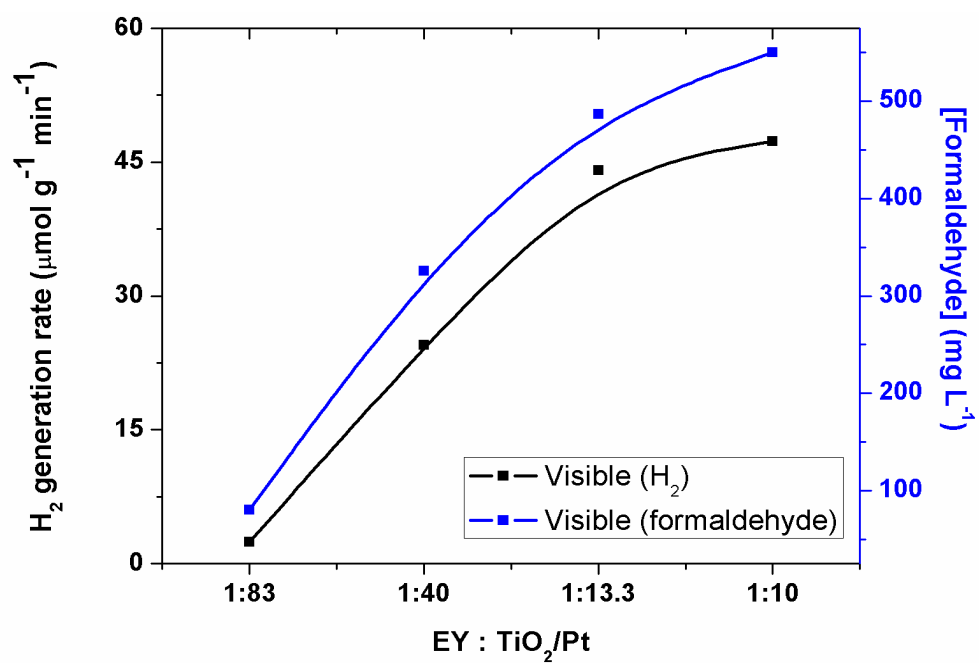
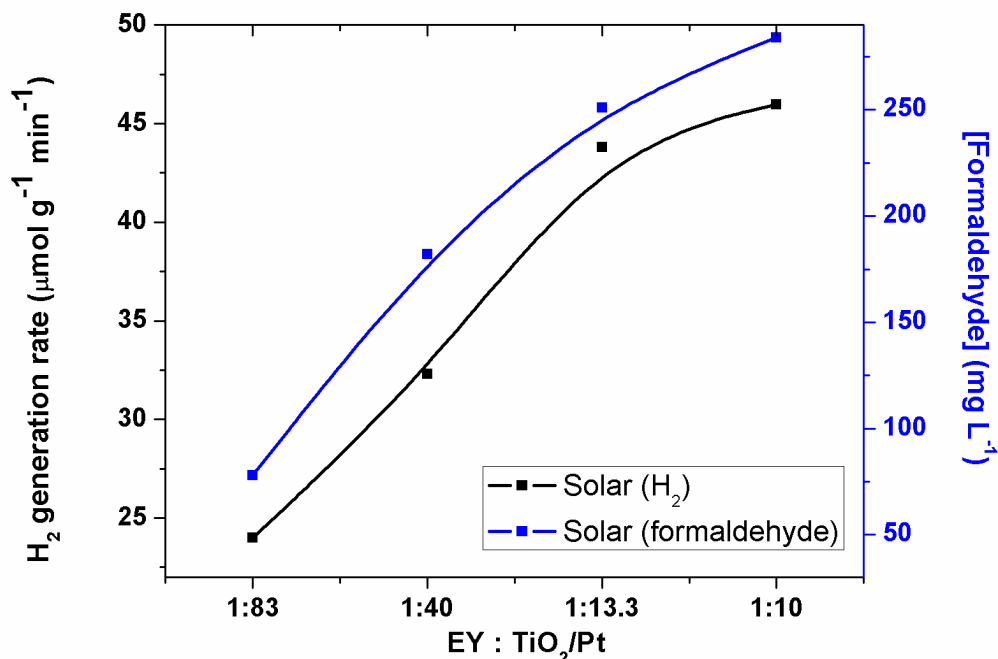


Figure 4.13 Formation of formaldehyde in visible and solar light irradiation.



**Figure 4.14 H<sub>2</sub> generation and formaldehyde formation in visible light irradiation.** (Experimental conditions: TiO<sub>2</sub>/Pt(0.25%) = 1 g L<sup>-1</sup>, [TEOA] = 0.25 M, I<sub>vis</sub> = 100 mW cm<sup>-2</sup>, pH = 7, N<sub>2</sub> saturated, pre-sonicated, visible - 420 nm cutoff filter).



**Figure 4.15 H<sub>2</sub> generation and formaldehyde formation in solar light irradiation.** (Experimental conditions: TiO<sub>2</sub>/Pt(0.25%) = 1 g L<sup>-1</sup>, [TEOA] = 0.25 M, I<sub>solar</sub> = 100 mW cm<sup>-2</sup>, pH = 7, N<sub>2</sub> saturated, pre-sonicated).

#### 4.3.4 Hydrogen generation kinetics

TEOA reacts with the photogenerated h<sup>+</sup> and/or HO<sup>•</sup> and degrades to different compounds. Thus the concentration of TEOA continuously changes throughout the reaction. To determine the effect of initial concentration of TEOA on hydrogen generation, we have chosen 60 minutes time interval, as the change of reactant or product can be well determined during this time interval. Figure 4.16 describes the effect of TEOA concentration on the rate of hydrogen evolution. A significant improvement of hydrogen generation was observed as the concentration of TEOA increased from 0.05 to 0.25 M. However, the hydrogen generation rate was found almost independent after 0.25 M of TEOA concentration. Therefore, the rate varies as a function of TEOA concentration according to Langmuir-type isotherm as described below<sup>39</sup>:

$$r = \frac{dC_{H_2}}{dt} = \frac{kKC_o}{1 + KC_o} \quad (4.1)$$

Where,  $r$  is the initial rate of hydrogen generation,  $k$ , the reaction rate constant, and  $K$  the adsorption constant of triethanolamine on to EY-TiO<sub>2</sub>/Pt photocatalyst. According to the Langmuir - type plot  $k = 6.7723 \times 10^{-6} \text{ mol min}^{-1}$  and  $K = 14.44798 \text{ M}^{-1}$ .

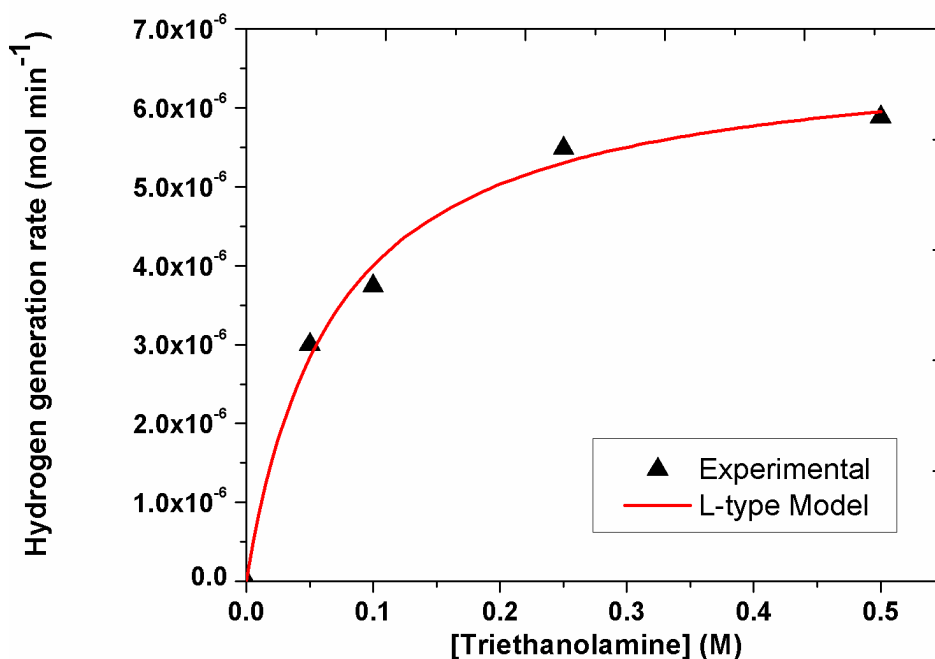


**Figure 4.16** Rate of hydrogen generation as a function of initial concentration of TEOA. (Experimental conditions: TiO<sub>2</sub>/Pt(0.25%) = 1 g L<sup>-1</sup>, E/T = 0.1, I<sub>vis</sub> = 100 mW cm<sup>-2</sup>, pH = 7, N<sub>2</sub> saturated, pre-sonicated, visible - 420 nm cutoff filter).



### 4.3.5 Dependence of hydrogen evolution on light intensity

The incident light intensity is expected to be one of the rate controlling parameters. In order to illustrate this effect, experiments were performed under four levels of light intensity and the hydrogen generation rates were compared. To achieve pure UV light from solar simulator we used a long pass filter placed above the reactor with an external attachment. To receive visible light we placed an UV cutoff filter inside the solar simulator. We have studied the effect of UV, visible, and solar light at different intensities such as 30  $\text{mW cm}^{-2}$ , 50  $\text{mW cm}^{-2}$ , 70  $\text{mW cm}^{-2}$  and 100  $\text{mW cm}^{-2}$  (Figure 4.17).

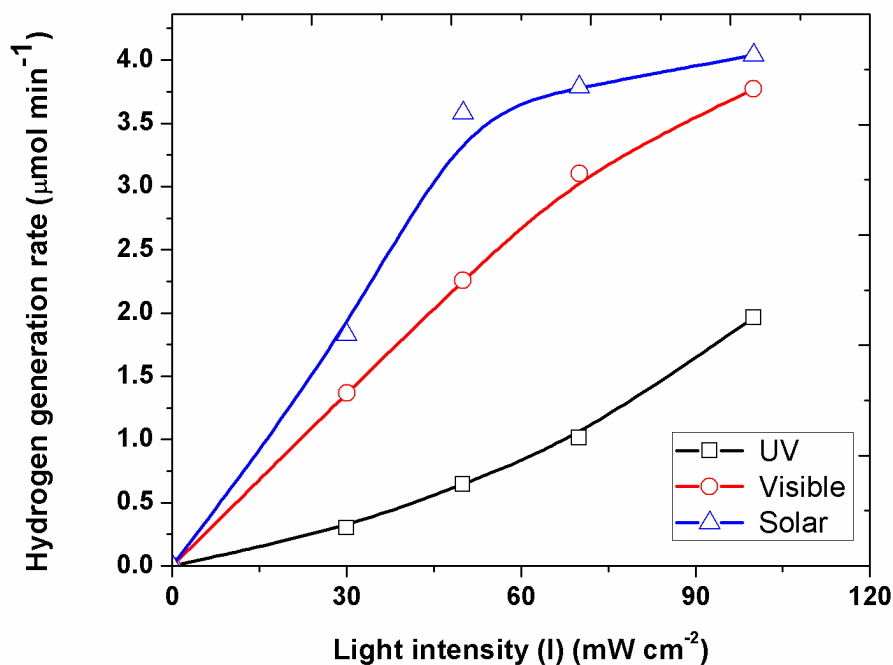


**Figure 4.17** Dependence of  $\text{H}_2$  on light intensity of UV, visible and solar light. (Experimental conditions:  $\text{TiO}_2/\text{Pt}(0.25\%) = 1 \text{ g L}^{-1}$ ,  $E/T = 0.05$ ,  $I = 100 \text{ mW cm}^{-2}$ ,  $[\text{TEOA}] = 0.25 \text{ M}$ ,  $\text{pH} = 7$ ,  $\text{N}_2$  saturated, pre-sonicated, visible - 420 nm cutoff filter, UV – long pass filter).

The reaction rate constant  $k$ , typically follows power-law dependence on light intensities.<sup>40</sup> The hydrogen generation rate constants were evaluated as a function of UV, visible and solar light intensities ( $I_{UV}$ ,  $I_{vis}$ ,  $I_{solar}$ ), keeping all other parameters fixed. In UV and visible radiation, the data fitted well with the power law model ( $k(I)=aI^b$ ) compared to that of solar light. The constants and  $R^2$  values are presented in the Table 4.3.

**Table 4.3 Power law model constants and  $R^2$  values**

Light source	a	b	$R^2$
UV	$9.3078 \times 10^{-4}$	1.66	0.996
Visible	0.09794	0.799	0.992
Solar	0.30169	0.598	0.943

Solar light contains both UV and visible spectrum, so it may be assumed that the hydrogen generation rate in solar light could be predicted from UV and visible light assisted hydrogen generation. So, we tried modeling the solar hydrogen generation with the following function combining UV and visible rate constant data:

$$k(I_{solar}) = \beta(k(I_{UV})) + (1 - \beta)(k(I_{vis})) \quad (4.2)$$

$$k(I_{solar}) = \beta(9.3078 \times 10^{-4} I_{UV}^{1.66}) + (1 - \beta)(0.09794 I_{vis}^{0.8}) \quad (4.3)$$

Where,  $\beta$  is the fraction of UV light contributed to solar hydrogen generation. Unfortunately, this model was not able to predict the hydrogen generation in solar light. On the contrary, solar hydrogen generation follow the simple power law model as described by the equation below.

$$k(I_{solar}) = 0.30169(I_{solar}^{0.6}) \quad (4.4)$$

The main reason behind the failure of the above model is the different excitation mechanism in UV and visible light. In both cases TEOA oxidation occurs with either  $EY^+$  or  $h^+$ . Therefore in solar light there is always a competition for TEOA.

#### 4.3.6 Photoluminescence (PL) study under UV, visible and solar light

Photoluminescence (PL) technique is a very good means to assess the electron transfer performance in semiconductor. We have studied the PL of EY sensitized  $TiO_2/Pt$  photocatalyst in UV, visible and solar light irradiation (Figure 4.18). The excitation wavelength of the light source was 490 nm and the emission peaks were observed in the range of 525-540 nm. The emission peaks attributed the electron/ $EY^+$  or electron/hole recombination processes. UV and solar light showed lower PL intensities ( $6 \times 10^5$  -  $7 \times 10^5 \text{ s}^{-1}$ ) compared to visible light ( $13 \times 10^5 \text{ s}^{-1}$ ). Higher PL value for visible light indicates higher electron/ $EY^+$  recombination process. Again, the charge recombination process also increased with increasing light intensity for all three kind of light sources (Appendix F).

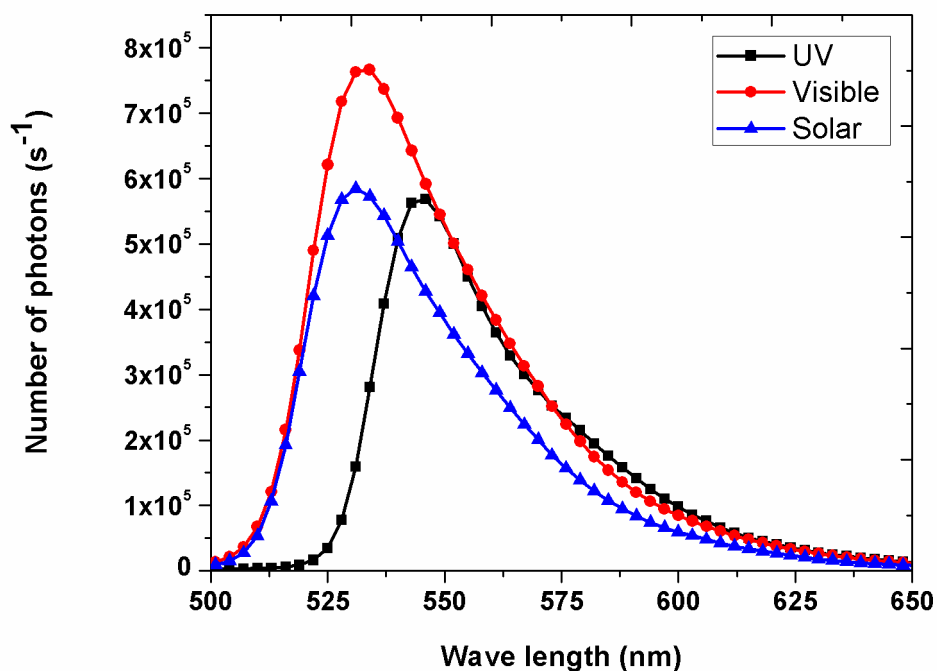


**Figure 4.18 Comparison of PL for UV, vis and solar light irradiation.**  
 (Experimental conditions:  $\text{TiO}_2/\text{Pt}$  (0.25%) = 1 g L<sup>-1</sup>, E/T=0.05, I = 50 mW cm<sup>-2</sup>, [TEOA] = 0.25 M, pH = 7, N<sub>2</sub> saturated, pre-sonicated, visible - 420 nm cutoff filter, UV -long pass filter).

#### 4.3.7 Apparent quantum yield in UV, visible, and solar light

Figure 4.2 shows the DRS of pure TiO<sub>2</sub> and EY sensitized TiO<sub>2</sub>/Pt photocatalyst. Compared to pure TiO<sub>2</sub>, the EY sensitized photocatalyst showed good visible light absorption which was also confirmed by its hydrogen generation capability in visible light. Apparent quantum yields were evaluated for hydrogen generation over EY sensitized TiO<sub>2</sub>/Pt (0.25 %) according to the formulae below (equation 4.5).<sup>41</sup> Incident light intensities were measured with StelerNET instrument. Table 4.4 shows the apparent quantum yield values at different light intensities for UV, visible, and solar light. Apparent quantum yield was highest (9.58 %) in UV light whereas in both visible and solar light, the values were pretty low (2.15 - 2.39 %) at 1 sun considering full spectrum.

At 100 mW cm<sup>-2</sup> the photon flux values implied the simulated sun light, which were higher than the previously reported values by several authors. At lower intensity the apparent quantum yields were much higher due to reduced e<sup>-</sup>/h<sup>+</sup> recombination rate. Again at lower light intensity (30 mW cm<sup>-2</sup>), if only 300 – 520 nm range of wavelengths were considered we achieved higher apparent quantum yields (11.33 – 12.23 %) than that of UV light (10.82 %).

The quantum yield ( $\phi$ ) will certainly be higher than the apparent quantum yield, as the adsorbed photons are a certain fraction of the incident photons.

$$\begin{aligned} \phi > \text{apparent quantum yield, } \phi_{H_2} (\%) &= \frac{\text{number of } e^- \text{ or } h^+}{\text{number of incident photons}} \times 100 \\ &= \frac{\text{number of } H_2 \text{ molecule evolved}}{\text{number of incident photons}} \times 100 \end{aligned} \tag{4.5}$$

**Table 4.4 Apparent quantum yield in UV, visible and solar light**

Light source		Apparent Quantum Yield (%)			
		30 mW cm <sup>-2</sup>	50 mW cm <sup>-2</sup>	70 mW cm <sup>-2</sup>	100 mW cm <sup>-2</sup>
Wavelength (nm)					
UV	300-388	10.82	10.65	10.42	9.58
Visible	420-650	5.16	3.88	3.26	2.39
Visible	420-520	12.23	9.38	8.23	5.73
Solar	300-650	5.81	5.23	3.32	2.15
Solar	300-520	11.33	10.39	6.69	4.19

## 4.3.8 EY-sensitized hydrogen generation in flow-reactor in solar light

### 4.3.8.1 Reactor configuration

In the small batch reactor, a high ratio of illuminated surface of catalyst to the effective reactor volume can be achieved and low mass transfer limitation exists since the maximum diffusion resistance is very small due to the use of ultrafine photocatalyst particles. In batch reactor with magnetic stirring the convective mass transfer is enhanced; but mechanical attrition and dye wash out are more likely. To overcome these problems and to scale-up of a slurry photocatalytic reactor we introduced a peristaltic pump in the reactor. The peristaltic pump is connected with a pump controller.<sup>42</sup>

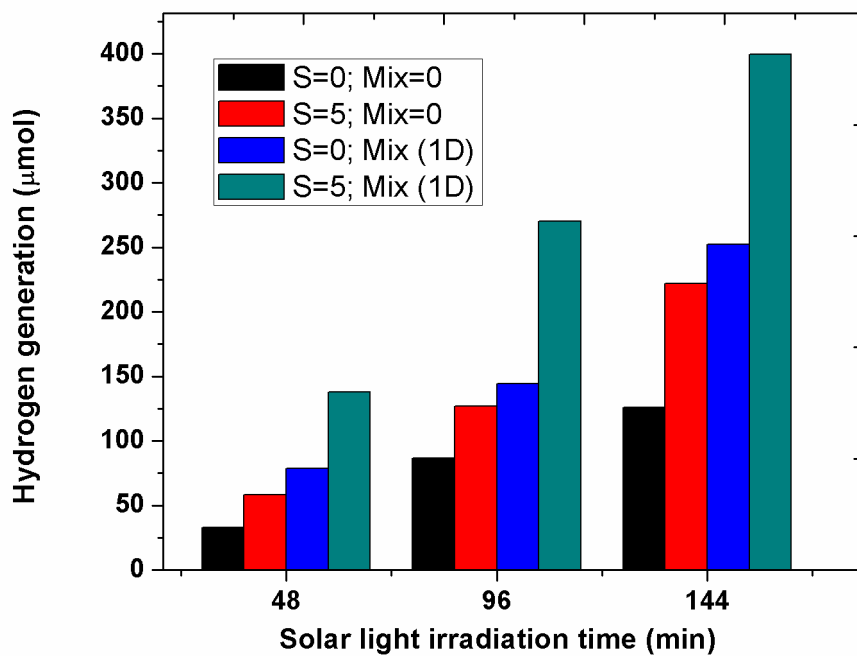
The flow reactor has two inlet and two outlet ports positioned diagonally to each other. It has one nitrogen purging line located at the middle of the reactor. A quartz glass plate is located at the top of the gas-tight reactor to allow illumination from the top. The gas collecting port is located on the opposite side of the nitrogen purging line.

Figure 4.1 shows a schematic diagram of the flow reactor. Both unidirectional flow and/or bi-directional flows (pulsation flow) can be achieved with the help of a pump controller. Flow rate can be varied between 0 and  $0.027 \text{ L s}^{-1}$ . In case of unidirectional operation, this is just like conventional peristaltic pump. However, in case of bi-directional operation, the controller switches the inlet and outlet ports at regular time intervals. Bi-directional flow is quite similar as oscillating/pulsating type flow. The use of oscillatory motion is known to be an effective method for enhancing the performance of mass and heat transfer processes.<sup>43-46</sup> In our case we have introduced this pulsating flow to achieve higher mass transfer rates which could not be achieved by conventional mixing. We have studied the effects of sonication, flow rate and both uni- and bi-directional mixing modes on hydrogen generation under solar light irradiation.

#### 4.3.8.2 Effect of pre-sonication of photocatalyst on hydrogen generation

Sonication is a tool for obtaining a better dispersion of solid in liquid medium. In sonication the progression of a sound wave in liquid phase causes the molecule to oscillate about their mean position. During this process cavitation bubbles form, and implosion of the cavitation bubbles generate high energy shock waves.<sup>47</sup> These effects usually lead to the reduction of particle size and better dispersion.

In our experiment we have used a sonicator (330 W, 60 Hz) to disperse the solid photocatalyst in aqueous TEOA solution. We varied the sonication between 0-8 min and found 5 min sonication time as optimum for our reaction. Figure 4.19 and Figure 4.20 show the effect of sonication in uni- and bi-directional operations, respectively. Sonication showed around 1.8 times improvement in hydrogen generation for zero mixing condition, whereas 1.6 and 1.4 times improvement for uni- and bi-directional mixing conditions (144 min residence time).



**Figure 4.19** Effect of sonication on hydrogen generation for uni-directional flow. (Experimental conditions: EY-TiO<sub>2</sub>/Pt (0.25%) = 1 g L<sup>-1</sup>, [TEOA] = 0.25 M, I<sub>solar</sub> = 100 mW cm<sup>-2</sup>, pH = 7, N<sub>2</sub> saturated, flow = 1.62 L min<sup>-1</sup>; x-axis shows residence time inside reactor).



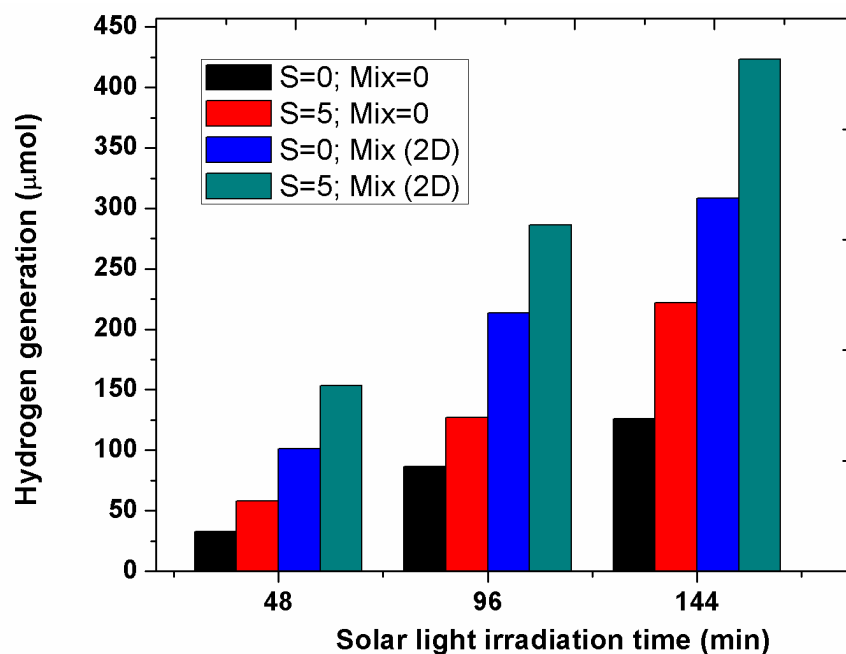


**Figure 4.20 Effect of sonication on hydrogen generation for bi-directional flow.** (Experimental conditions: EY-TiO<sub>2</sub>/Pt(0.25%) = 1 g L<sup>-1</sup>, [TEOA] = 0.25 M, I<sub>solar</sub> = 100 mW cm<sup>-2</sup>, pH = 7, N<sub>2</sub> saturated, flow = 1.62 L min<sup>-1</sup>, x-axis shows residence time inside reactor).

#### 4.3.8.3 Effect of flow rate and different mixing mode on hydrogen generation

Besides the process kinetic issues, significant mass transfer limitations are present in most heterogeneous photocatalytic reactors. Photocatalytic reactor design requires the presence of high catalyst surface area, illumination, and reactant species in close proximity. Immobilized photocatalysts face significant mass transfer limitations compared to slurry photocatalysts as observed in Figure 4.9. Again, photocatalyst in slurry form also experience similar mass transfer limitations as the suspended

photocatalyst tends to be present as micrometer-size agglomerates rather than discrete nano-size particles.

We have studied the effects of both uni- and bi-directional flows in the flow reactor with variable flow rates (0, 0.84, and 1.62 L min<sup>-1</sup>). Figure 4.21 shows the effect of flow rate in uni- and bi-directional operations.

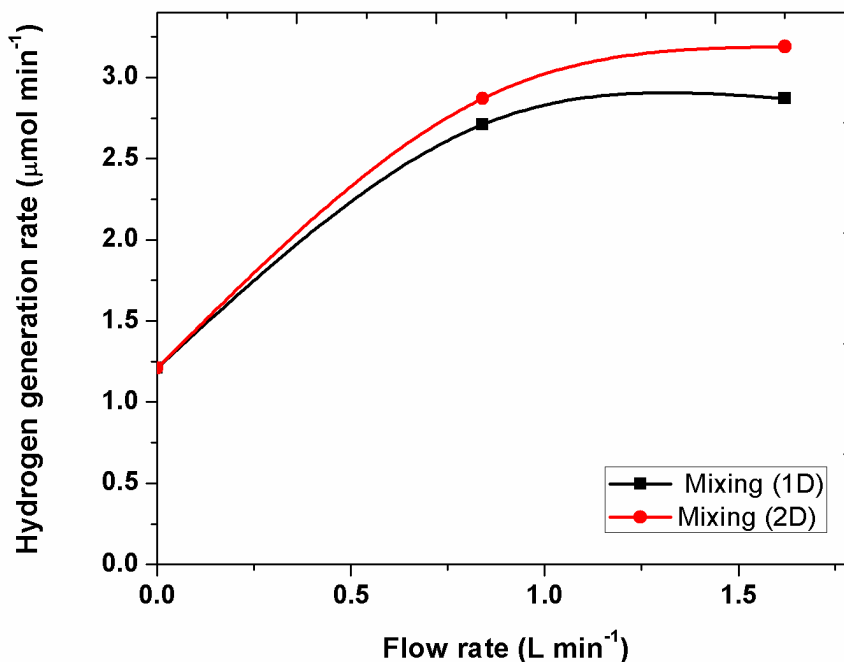


**Figure 4.21 Effect of flow rate on H<sub>2</sub> generation for both uni- and bi-directional mixing.** (Experimental conditions: EY-TiO<sub>2</sub>/Pt(0.25%) = 1 g L<sup>-1</sup>, [TEOA] = 0.25 M, I<sub>solar</sub> = 100 mW cm<sup>-2</sup>, pH = 7, N<sub>2</sub> saturated, pre-sonicated).

By increasing the flow rate from zero to 0.84 L min<sup>-1</sup>, rate of hydrogen generation increased by 2.2 and 2.4 times for uni- and bi-directional flows respectively. With further increment of flow rate to 1.62 L min<sup>-1</sup> the improvement of hydrogen generation was only 6 % and 11 % for uni- and bi-directional flows respectively. Bi-direction flow seemed to be slightly better than uni-directional flow because of superior mixing, which could be

achieved during the switching of inlet and outlet positions of the reactor via pump controller. In case of bi-direction flow we observed a maximum of 11 % increment in hydrogen generation rate in comparison with uni-directional flow. Again, the rates of hydrogen generation in flow reactor were compared with the conventional batch reactor data, and 17 - 23 % improvement in hydrogen generation rate for flow reactor was observed. We anticipated even better results with flow reactor, which were not achieved so far. For this reason detailed hydrodynamic study of the flow reactor was performed by solving momentum equations using commercial software package FUEENT.

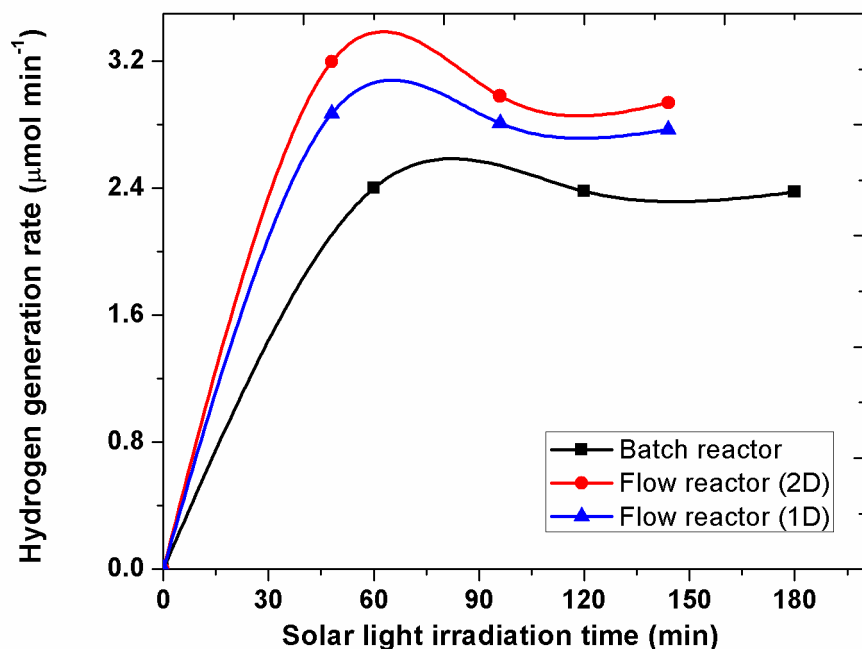


**Figure 4.22 Comparison of  $\text{H}_2$  generation rate in batch and flow reactor.**

(Experimental conditions:  $\text{EY-TiO}_2/\text{Pt}(0.25\%) = 1 \text{ g L}^{-1}$ ,  $[\text{TEOA}] = 0.25 \text{ M}$ ,  $I_{\text{solar}} = 100 \text{ mW cm}^{-2}$ ,  $\text{pH} = 7$ ,  $\text{N}_2$  saturated, pre-sonicated, batch reactor = 500 rpm, flow reactor =  $1.62 \text{ L min}^{-1}$ ).

### 4.3.9 Modification of flow reactor by hydrodynamics study

Computational fluid dynamics (CFD) is useful tool to investigate the hydraulics in chemical reactors. CFD provides detailed information on the flow and mixing in such system.<sup>48</sup> It is also helpful for the design and optimization of the stirred reactor,<sup>49, 50</sup> and has been widely used in the analysis of the reactor characterization in various applications.<sup>51, 52</sup> Here, we have used a commercial code ANSYS FLUENT 12.1 (FLUENT Inc.) to simulate our flow reactor for solar hydrogen generation.

Hence, in the present case, the flow has been modeled in three-dimensions for the prediction of the velocity field. The continuity and Navier-Stokes equations for an incompressible, constant viscosity liquid can be written as follows:

Continuity equation:

$$\frac{\partial \rho}{\partial t} + \nabla \cdot (\rho \vec{v}) = 0 \quad (4.6)$$

Momentum conversion equation:

$$\frac{\partial}{\partial t} (\rho \vec{v}) + \nabla \cdot (\rho \vec{v} \vec{v}) = -\nabla p + \nabla \cdot (\mu [(\nabla \vec{v} + \nabla \vec{v}^T)]) + \rho \vec{g} \quad (4.7)$$

Where,  $p$  is the static pressure,  $\mu$  is dynamic viscosity and  $\rho \vec{g}$  is the gravitational body force.

Grid preparation:

The geometry of the reactor was modeled by using Gambit v.2.4.6 to draw and describe the geometrical properties of the reactor which is of 10 cm diameter and 6 cm height. It has two inlets and two outlets of 0.015 cm diameter. Pump performance curve was obtained experimentally to determine the mass flow at the inlet of the reactor and pressure outlet condition was set at the outlet of the reactor to be 10000 Pa based on the pump technical information. We located dead zones (Figure 4.23) at the middle of the

reactor indicated with deep blue color. The presence of dead zones was also confirmed by particle tracking method.

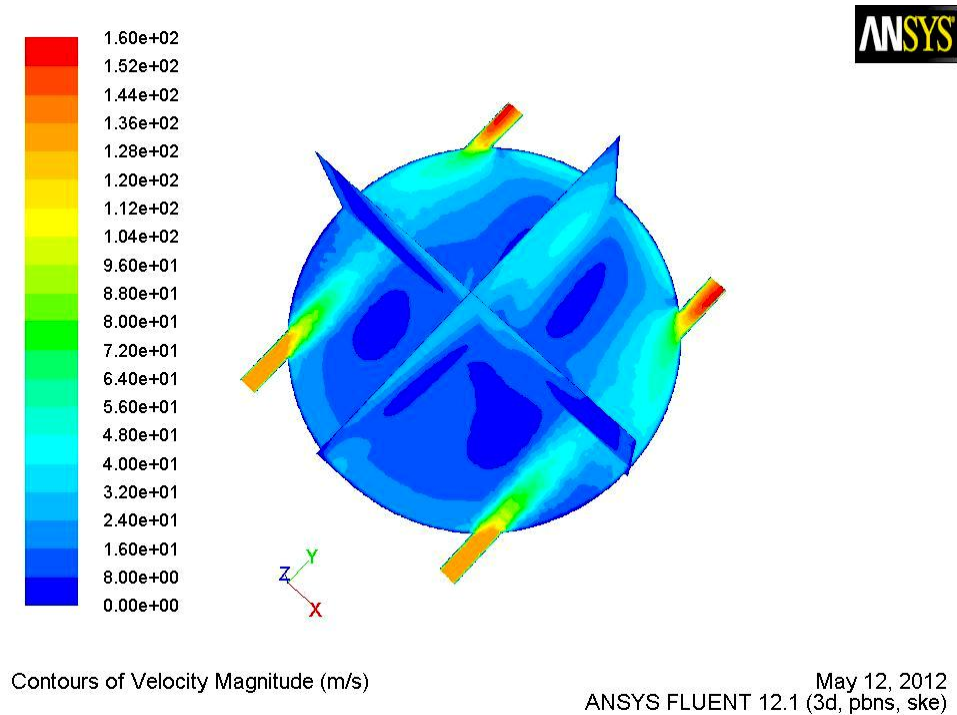


**Figure 4.23 Flow pattern inside the flow reactor**

To overcome this problem a special baffle needs to be introduced at the middle of the reactor. There are 36 holes in the baffle arranged in a systematic fashion to create turbulences in the reactor. In this arrangement we were able to eliminate those dead zones in the reactor which is also confirmed by particle tracking. Details about the baffle, improved flow pattern, and particle tracking diagrams are provided in Appendix G.

## 4.4 Conclusions

From the discussion presented in this chapter, the following conclusions can be stated.

i) DRS supported the visible light activity of EY-TiO<sub>2</sub>/Pt. TiO<sub>2</sub> was mostly in anatase form and with Pt loading the surface area was not changed. FTIR results suggested about the ester like linkage with EY and TiO<sub>2</sub> surface in the photocatalyst. EDX results reported the presence of Pt metal on TiO<sub>2</sub> surface.

ii) Different parameters showed significant effect on hydrogen generation. Neutral pH, 0.25 wt% of Pt on TiO<sub>2</sub>, photocatalyst mass of 1-1.3 g L<sup>-1</sup> were achieved as optimum levels for sacrificial hydrogen generation in solar and visible light.

iii) Photocatalyst immobilization was not successful over slurry based photocatalytic hydrogen generation. This was due to insufficient active sites and the influence of internal mass transfer.

iv) EY can incorporate visible light activity in both TiO<sub>2</sub> and TiO<sub>2</sub>/Pt. In solar light, hydrogen generation rate increased by 1.4 and 1.2 times by EY sensitization on TiO<sub>2</sub> and TiO<sub>2</sub>/Pt respectively.

v) With the incorporation of Pt a huge improvement in hydrogen generation rate was achieved compared to EY-TiO<sub>2</sub> alone in visible light. In solar light, platinum loading on both TiO<sub>2</sub> and EY-TiO<sub>2</sub> provided 4.7 and 4.1 times increment in hydrogen generation respectively.

vi) EY to TiO<sub>2</sub>/Pt mass ratio was shown to a crucial parameter for hydrogen generation. We obtained an optimum mass ratio (EY:TiO<sub>2</sub>/Pt) of 1:10 and 1:13.3 in visible and solar light respectively.

vii) Concentration of TEOA also played a major role during sacrificial hydrogen generation. Hydrogen generation rate varied as a function of TEOA concentration and it followed Langmuir-type isotherm.

viii) The reaction mechanisms in solar and visible light were different, although in both cases formaldehyde was detected as an intermediate product. However, in solar light, formaldehyde was oxidized by  $h^+/HO^\bullet$  to produce hydrogen.

ix) Light intensity is also an important parameter in photocatalytic hydrogen generation. The optimum intensity was  $100 \text{ mW cm}^{-2}$  (1sun).

x) Recombination of  $e^-/h^+$  or  $e^-/EY^+$  were determined through PL study, which illustrated the higher recombination rates in case of visible light compared to that of solar and UV light.

xi) Study in flow reactor showed positive effect of pre-sonication, increased flow rate and bi-directional mixing mode in solar hydrogen generation. Both uni- and bi-direction mixing at a flow rate of  $1.62 \text{ L min}^{-1}$  showed higher hydrogen generation rates compared to the batch reactor.

xii) The flow pattern inside the flow reactor was described using FLUENT which revealed the presence of dead zones in the middle of the reactor.

## 4.5 References

1. Fujishima, A., Electrochemical photolysis of water at a semiconductor electrode. *Nature* **1972**, 238, 37-38.
2. Domen, K.; Kudo, A.; Onishi, T., Mechanism of photocatalytic decomposition of water into H<sub>2</sub> and O<sub>2</sub> over NiO-SrTiO<sub>3</sub>. *Journal of Catalysis* **1986**, 102, (1), 92-98.
3. Kudo, A.; Kato, H., Photocatalytic decomposition of water into H<sub>2</sub> and O<sub>2</sub> over novel photocatalyst K<sub>3</sub>Ta<sub>3</sub>Si<sub>2</sub>O<sub>13</sub> with pillared structure consisting of three TaO<sub>6</sub> chains. *Chemistry Letters* **1997**, 26, (9), 867-868.
4. Wrighton, M. S.; Ellis, A. B.; Wolczanski, P. T.; Morse, D. L.; Abrahamson, H. B.; Ginley, D. S., Strontium titanate photoelectrodes. Efficient photoassisted electrolysis of water at zero applied potential. *Journal of the American Chemical Society* **1976**, 98, (10), 2774-2779.
5. Wagner, F. T.; Somorjai, G. A., Photocatalytic hydrogen production from water on Pt-free SrTiO<sub>3</sub> in alkali hydroxide solutions. *Nature (London, United Kingdom)* **1980**, 285, 559-560.
6. Lehn, J. M.; Sauvage, J. P.; Ziessel, R.; Hilaire, L., Water photocatalysis by UV irradiation of rhodium loaded strontium-titanate catalysts-relation between catalytic activity and nature of the deposit from combined photolysis and ESCA studies. *Israel Journal of Chemistry* **1982**, 22, (2), 168-172.
7. Bulatov, A. V.; Khidekel, M. L., Decomposition of water under the effect of UV radiation in the presence of platinized titanium dioxide. *Russian Chemical Bulletin* **1976**, 25, (8), 1794.
8. Sato, S.; White, J. M., Photodecomposition of water over Pt/TiO<sub>2</sub> catalysts. *Chemical Physics Letters* **1980**, 72, (1), 83-86.
9. Lee, J. S., Photocatalytic water splitting under visible light with particulate semiconductor catalysts. *Catalysis Surveys from Asia* **2005**, 9, (4), 217-227.
10. Ni, M.; Leung, M. K. H.; Leung, D. Y. C.; Sumathy, K., A review and recent developments in photocatalytic water-splitting using TiO<sub>2</sub> for hydrogen production. *Renewable and Sustainable Energy Reviews* **2007**, 11, (3), 401-425.
11. Abe, R.; Sayama, K.; Sugihara, H., Effect of Water/Acetonitrile Ratio on Dye-Sensitized Photocatalytic H<sub>2</sub> Evolution under Visible Light Irradiation. *Journal of Solar Energy Engineering* **2005**, 127, 413-416.



12. Donghua, P.; Jingfei, L., Development of Visible Light-Responsive Sensitized Photocatalysts. *International Journal of Photoenergy* **2012**, Article ID 262831, doi:10.1155/2012/262831.
13. Pan, B. Y. K.; Yen, T. F.; Chen, J. R. Treatment of wastewater containing citric acid and triethanolamine. **1992**.
14. West, R. J.; Gonsior, S. J., Biodegradation of triethanolamine. *Environmental Toxicology and Chemistry* **1996**, 15, (4), 472-480.
15. Abe, R.; Hara, K.; Sayama, K.; Domen, K.; Arakawa, H., Steady hydrogen evolution from water on Eosin Y-fixed TiO<sub>2</sub> photocatalyst using a silane-coupling reagent under visible light irradiation. *Journal of Photochemistry and Photobiology A: Chemistry* **2000**, 137, (1), 63-69.
16. Zhang, X.; Jin, Z.; Li, Y.; Li, S.; Lu, G., Photocatalytic hydrogen generation over Eosin Y-Sensitized TS-1 zeolite. *Applied Surface Science* **2008**, 254, (15), 4452-4456.
17. Zhang, X.; Jin, Z.; Li, Y.; Li, S.; Lu, G., Visible-light-induced hydrogen production over Pt-Eosin Y catalysts with high surface area silica gel as matrix. *Journal of power sources* **2007**, 166, (1), 74-79.
18. Kang, S. Z.; Chen, L.; Li, X.; Mu, J., Composite photocatalyst containing Eosin Y and multiwalled carbon nanotubes loaded with CuO/NiO: Mixed metal oxide as an active center of H<sub>2</sub> evolution from water. *Applied Surface Science* **2012**, 258, (16), 6029-6033.
19. Li, Q.; Chen, L.; Lu, G., Visible-light-induced photocatalytic hydrogen generation on dye-sensitized multiwalled carbon nanotube/Pt catalyst. *Journal of Physical Chemistry C* **2007**, 111, (30), 11494-11499.
20. Li, Q.; Lu, G., Visible-light driven photocatalytic hydrogen generation on Eosin Y-sensitized Pt-loaded nanotube Na<sub>2</sub>Ti<sub>2</sub>O<sub>4</sub>(OH)<sub>2</sub>. *Journal of Molecular Catalysis A: Chemical* **2007**, 266, (1), 75-79.
21. Sreethawong, T.; Junbua, C.; Chavadej, S., Photocatalytic H<sub>2</sub> production from water splitting under visible light irradiation using Eosin Y-sensitized mesoporous-assembled Pt/TiO<sub>2</sub> nanocrystal photocatalyst. *Journal of Power Sources* **2009**, 190, (2), 513-524.
22. Li, Y.; Xie, C.; Peng, S.; Lu, G.; Li, S., Eosin Y-sensitized nitrogen-doped TiO<sub>2</sub> for efficient visible light photocatalytic hydrogen evolution. *Journal of Molecular Catalysis A: Chemical* **2008**, 282, (1), 117-123.
23. Chowdhury, P.; Goma, H.; Ray, A. K., Factorial design analysis for dye-sensitized hydrogen generation from water. *International Journal of Hydrogen Energy* **2011**, 36, (21), 13442-13451.

24. Chowdhury, P.; Moreira, J.; Gomaa, H.; Ray, A. K., Visible Solar Light Driven Photocatalytic Degradation of Phenol with Dye-sensitized TiO<sub>2</sub>: Parametric and Kinetic Study. *Industrial & Engineering Chemistry Research* **2012**, 51, (12), 4523-4532.
25. Chen, H. H.; Anbarasan, R.; Kuo, L. S.; Chen, P. H., A novel report on Eosin Y functionalized MWCNT as an initiator for ring opening polymerization of  $\epsilon$ -caprolactone. *Materials Chemistry and Physics* **2011**, 126, 584-590.
26. Wang, Z. S.; Sayama, K.; Sugihara, H., Efficient eosin Y dye-sensitized solar cell containing Br<sup>-</sup>/Br<sup>3-</sup> electrolyte. *Journal of Physical Chemistry B* **2005**, 109, (47), 22449-22455.
27. Schiavello, M., *Heterogeneous photocatalysis*. John Wiley & Sons: **1997**; Vol. 3, p 87-107.
28. Sreethawong, T.; Yoshikawa, S., Enhanced photocatalytic hydrogen evolution over Pt supported on mesoporous TiO<sub>2</sub> prepared by single-step sol-gel process with surfactant template. *International Journal of Hydrogen Energy* **2006**, 31, (6), 786-796.
29. Mills, A.; Hunte, S. L., An overview of semiconductor photocatalysis. *Journal of Photochemistry and Photobiology-Chemistry Section* **1997**, 108, (1), 1-36.
30. Lu, M. C.; Roam, G. D.; Chen, J. N.; Huang, C. P., Factors affecting the photocatalytic degradation of dichlorvos over titanium dioxide supported on glass. *Journal of Photochemistry and Photobiology A: Chemistry* **1993**, 76, (1), 103-110.
31. Kalyanasundaram, K.; Kiwi, J.; Gratzel, M., Hydrogen evolution from water by visible light, a homogeneous three component test system for redox catalysis. *Helvetica Chimica Acta* **1978**, 61, (7), 2720-2730.
32. Badawy, M. I.; Ghaly, M. Y.; Ali, M. E. M., Photocatalytic hydrogen production over nanostructured mesoporous titania from olive mill wastewater. *Desalination* **2011**, 267, (2), 250-255.
33. Daskalaki, V. M.; Kondarides, D. I., Efficient production of hydrogen by photo-induced reforming of glycerol at ambient conditions. *Catalysis Today* **2009**, 144, (1-2), 75-80.
34. Tang, Q.; Lin, J.; Wu, Z.; Wu, J.; Huang, M.; Yang, Y., Preparation and photocatalytic degradability of TiO<sub>2</sub>/polyacrylamide composite. *European Polymer Journal* **2007**, 43, (6), 2214-2220.
35. Larson, R. A.; Stackhouse, P. L.; Crowley, T. O., Riboflavin tetraacetate: a potentially useful photosensitizing agent for the treatment of contaminated waters. *Environmental Science & Technology* **1992**, 26, (9), 1792-1798.

36. Shukla, K. S.; Mathur, P. C.; Bansal, O. P., Oxidation kinetics of triethanolamine by alkaline hexacyanoferrate (III). *Journal of Inorganic and Nuclear Chemistry* **1973**, 35, (4), 1301-1307.
37. Naman, S. A.; Gratzel, M., Visible-light generation of hydrogen from hydrogen sulphide in aqueous solutions of ethanolamines containing vanadium sulphide dispersions. *Journal of Photochemistry and Photobiology A: Chemistry* **1994**, 77, (2-3), 249-253.
38. Yin, Z.; Li, Y.; Peng, S.; Lu, G.; Li, S., Photocatalytic hydrogen generation in the presence of ethanolamines over Pt/TiO<sub>2</sub>. *Journal of Molecular Catalysis (China)* **2007**, 2.
39. Li, Y.; Xie, Y.; Peng, S.; Lu, G.; Li, S., Photocatalytic hydrogen generation in the presence of chloroacetic acids over Pt/TiO<sub>2</sub>. *Chemosphere* **2006**, 63, (8), 1312-1318.
40. Ray, A. K.; Beenackers, A. A. C. M., Novel swirl-flow reactor for kinetic studies of semiconductor photocatalysis. *AIChE Journal* **1997**, 43, (10), 2571-2578.
41. Shimidzu, T.; Iyoda, T.; Koide, Y., An advanced visible-light-induced water reduction with dye-sensitized semiconductor powder catalyst. *Journal of the American Chemical Society* **1985**, 107, (1), 35-41.
42. Chen, D.; Li, F.; Ray, A. K., External and internal mass transfer effect on photocatalytic degradation. *Catalysis today* **2001**, 66, (2-4), 475-485.
43. Gomaa, H.; Al Taweel, A. M., Dynamic analysis of mass transfer at vertically oscillating surfaces. *Chemical Engineering Journal* **2004**, 102, (1), 71-82.
44. Mackley, M. R.; Stonestreet, P., Heat transfer and associated energy dissipation for oscillatory flow in baffled tubes. *Chemical Engineering Science* **1995**, 50, (14), 2211-2224.
45. Gomaa, H.; Al Taweel, A. M.; Landau, J., Mass transfer enhancement at vibrating electrodes. *Chemical Engineering Journal* **2004**, 97, (2), 141-149.
46. Blel, W.; Le Gentil-Lelièvre, C.; Bénézech, T.; Legrand, J.; Legentilhomme, P., Application of turbulent pulsating flows to the bacterial removal during a cleaning in place procedure. Part 1: Experimental analysis of wall shear stress in a cylindrical pipe. *Journal of Food Engineering* **2009**, 90, (4), 422-432.
47. Chowdhury, P.; Viraraghavan, T., Sonochemical degradation of chlorinated organic compounds, phenolic compounds and organic dyes-A review. *Science of the Total Environment* **2009**, 407, (8), 2474-2492.
48. Wols, B. A.; Shao, L.; Uijtewaal, W. S. J.; Hofman, J.; Rietveld, L. C.; Van Dijk, J. C., Evaluation of experimental techniques to validate numerical computations of the

hydraulics inside a UV bench-scale reactor. *Chemical Engineering Science* **2010**, 65, (15), 4491-4502.

49. Stamou, A. I., Improving the hydraulic efficiency of water process tanks using CFD models. *Chemical Engineering and Processing: Process Intensification* **2008**, 47, (8), 1179-1189.

50. Torre, J. P.; Fletcher, D. F.; Lasuye, T.; Xuereb, C., Single and multiphase CFD approaches for modelling partially baffled stirred vessels: Comparison of experimental data with numerical predictions. *Chemical Engineering Science* **2007**, 62, (22), 6246-6262.

51. Darelus, A.; Rasmuson, A.; van Wachem, B.; Niklasson Bjorn, I.; Folestad, S., CFD simulation of the high shear mixing process using kinetic theory of granular flow and frictional stress models. *Chemical Engineering Science* **2008**, 63, (8), 2188-2197.

52. Pareek, V. K.; Cox, S. J.; Brungs, M. P.; Young, B.; Adesina, A. A., Computational fluid dynamic (CFD) simulation of a pilot-scale annular bubble column photocatalytic reactor. *Chemical Engineering Science* **2003**, 58, (3-6), 859-865.

## Chapter 5

### 5 Sacrificial Hydrogen Generation from Formaldehyde with TiO<sub>2</sub>/Pt Photocatalyst in Solar Radiation

#### 5.1 Introduction

Hydrogen production from a renewable source is a dream project of the 21<sup>st</sup> century. Photocatalytic water splitting technique has the potential for renewable hydrogen production from water.<sup>1</sup> However water splitting is not an easy task because of two main reasons namely, (i) very high positive free energy change ( $\Delta G^0 = 237 \text{ KJ mol}^{-1}$ ), and (ii) rapid reverse reaction. Water splitting being an endothermic reaction demands energy that is equal to enthalpy change ( $\Delta H$ ) required to split water into hydrogen and oxygen;  $\Delta G$  as a useful work and  $T\Delta S$  as a thermal energy.<sup>2, 3</sup> Sacrificial agents can be used as electron donor during the photocatalytic reaction process, to achieve a much higher hydrogen production rate by reacting irreversibly with the oxygen formed, photo-induced hole, or OH<sup>•</sup> radicals, to prevent backward reaction between produced H<sub>2</sub> and O<sub>2</sub> or hindering the recombination of photo-induced electrons and holes<sup>4</sup>

Organic pollutants can perform the role of electron donors, thereby can reduce the hydrogen production costs while at the same time can serve the dual role of hydrogen production as well as organic degradation. The chosen sacrificial agent should be inexpensive compared to the hydrogen produced to make the process a feasible one. Wastewater containing organic pollutants can be considered as suitable electron donor for this purpose. There are only few reports that demonstrate the involvement of organic pollutants as sacrificial electron donor for such system<sup>4-8</sup> Moreover TiO<sub>2</sub> photocatalyst has inherent electron donation ability for hydrogen production. Hence, the electron donor should have higher efficiency and stability.

In common photocatalytic degradation system, TiO<sub>2</sub> catalyst shows very good results under UV light.<sup>9</sup> The only exception is the involvement of oxygen during reaction. In

photodegradation process,  $O_2$  acts as an electron donor and produce superoxide ion which finally produce  $OH^\bullet$  radical.<sup>10</sup> If oxygen is present in the reaction system, then during photocatalytic water splitting it would compete with  $H^+$  ion for electron. Therefore, presence of oxygen in water splitting system is not advisable.

$TiO_2$  can produce hydrogen from water and different sacrificial agents but the efficiency is not significant; the system has considerable electron/hole recombination problem. This problem was addressed by the use of noble metal co-catalyst in trace amount on  $TiO_2$  catalyst surface.<sup>11</sup> Platinum loaded  $TiO_2$  catalyst has highest potential for hydrogen generation as shown by Li et al.<sup>4</sup>

Formaldehyde is a major volatile organic compound commonly found in the indoor environment emitted from building, furnishing materials and consumer products. It can also be found in gas phase and wastewater as pollutant which can be oxidized under UV radiation with  $TiO_2$ .<sup>12-15</sup>

Formaldehyde is used in many industries such as adhesive and glue manufacturing, production of synthetic resin, chemical and petroleum industry, paper industry, textile and wood processing, disinfectant and preservative production etc. These industries generate wastewater having variable concentration of formaldehyde.<sup>16</sup> Again the concentration of formaldehyde in effluents generated from many chemical industries ranges from 3 to 10 g  $L^{-1}$ .<sup>17</sup> Formaldehyde is toxic and has several health problems for humans. Thus, formaldehyde can seriously harm human health and impose ecological problems on the environment.<sup>16</sup>

Numerous organic compounds have been used as electron donors for photocatalytic hydrogen generation, namely, carboxylic acids, alcohols, carbohydrates, hydrocarbons, artificial high polymers.<sup>4, 11, 18</sup> There are very limited studies done on formaldehyde as sacrificial agent for hydrogen generation.<sup>19</sup> Moreover, all studies primarily use UV lamps as light sources.

In our previous work with triethanolamine electron donor, formaldehyde was detected as a major intermediate product under both solar and visible light driven hydrogen generation. So a detailed study on the photocatalytic behavior of formaldehyde for sacrificial hydrogen generation was necessary for better understanding of the process.

In this present work, we have used simulated solar light for degradation and simultaneous hydrogen generation from formaldehyde. The photocatalytic activity of TiO<sub>2</sub>/Pt catalyst produced by solar photo-deposition method was studied under both visible and solar irradiation. Effect of different basic parameters such as platinum content on TiO<sub>2</sub>, solution pH, initial concentration of formaldehyde, catalyst concentration and light intensity were systematically studied to understand the qualitative and quantitative effects as well as overall mechanism of the process.

## 5.2 Experimental

### 5.2.1 Reagents

All reagents were of analytical grade and used without further treatment. Aeroxide TiO<sub>2</sub> P25 (80-20 % anatase to rutile) from Evonik Degussa Corporation was used as catalyst. Formaldehyde solution (36.5%) from Sigma-Aldrich was used as sacrificial agent. Hydrogen hexachloroplatinate (IV) solution (8 wt %) was also purchased from Sigma-Aldrich Canada Ltd. Ultra pure water (18 MΩ) was prepared from an in-house EASYPure<sup>®</sup> RODI system (Thermo Scientific, Canada).

### 5.2.2 Preparation and characterization of photocatalyst

Platinum loading of the TiO<sub>2</sub>-P25 catalyst was performed by solar photo-deposition method following a modified version of previously reported by Chowdhury et al.<sup>20</sup> TiO<sub>2</sub> powder was mixed with required volume of 0.08 % hexacholoplatinic acid solution (corresponding to 0.25 %, 1 %, 1.3 %, 1.8 % nominal loading) and ethanol, and then it was sonicated for 5 min. A 90:10 volume ratio of water and ethanol was taken. Excess ethanol was used to supply enough sacrificial agents as hole (h<sup>+</sup>) scavenger to ensure complete reduction of Pt (IV). Then, the reaction mixture was placed under the solar

simulator (AM 1.5G filter, 1 Sun) for 3 h under vigorous stirring. As time progressed, the solution became off white color. After filtering and washing with water, the powder was dried at 150 °C for 2 h and milled in a mortar. Pure TiO<sub>2</sub> has a bulky nature which is totally lost after it undergoes photo-deposition process. It also loses its milky white color and turns into light grey.

Phase composition and the degree of crystallinity in the samples were determined by X-ray diffraction (XRD). The XRD data were obtained using a Rigaku–MiniFlex II, powder diffractometer (Japan), using CuK $\alpha$  ( $\lambda$  for K $\alpha$  = 1.54059 Å) over the desired 2 $\theta$  range with step width of 0.05°.

DRS (diffuse reflectance spectra) were recorded on a Shimadzu UV-VIS-NIR spectrophotometer (UV-3600) equipped with an integrating sphere using BaSO<sub>4</sub> as reference. Both absorbance and diffuse reflectance spectra were recorded for all samples.

### 5.2.3 Light sources

Experiments were performed under both solar and visible light. The simulated solar light was generated using solar simulator (Model: SS1KW, Sciencetech, ON, Canada with a 1000-W Xe arc lamp and an AM 1.5G filter). It produces identical simulated sunlight (1 Sun) of 100 mW cm<sup>-2</sup> at full power that matches the global solar spectrum at sea level. To generate only visible light, a UV cut-off filter (Omega optical, USA:  $\lambda > 420$  nm) was used. Spectral analysis of the irradiation from solar simulator was performed with StellarNet EPP2000C-25LT16 spectrometer.

### 5.2.4 Photocatalytic hydrogen generation

Photocatalytic reactions were carried out in a gas tight 530 mL Pyrex glass reactor with a flat transparent window at the top for illumination (details in Appendix C). The catalyst powder (TiO<sub>2</sub>/Pt) was suspended in 100 mL of formaldehyde solution (40 ppm to 4600 ppm) after pH adjustment with either 1:1 HCl or 0.1 M NaOH solution. The catalyst suspension was dispersed for 5 min in an ultrasonic bath and then the system was degassed by bubbling ultra pure nitrogen gas for about 40 min. Continuous stirring was



performed using magnetic stirrer (500 rpm). The photocatalyst was irradiated with a solar simulator from the top.

The gas sampling port in the reactor was sealed with a silicone rubber septum, and sampling was made intermittently through the septum during the experiments. The gas mixture was analyzed by Shimadzu GC 2014 with HeyeSep D packed column: 10 m length, 2 mm ID, 2  $\mu\text{m}$  film thickness and thermal conductivity detector (TCD). Ultra pure  $\text{N}_2$  gas was used as carrier gas.

## 5.3 Results and Discussion

### 5.3.1 Characterization of $\text{TiO}_2/\text{Pt}$ photocatalyst

XRD of bare  $\text{TiO}_2$  P25 and platinum loaded (0.25 %)  $\text{TiO}_2$  is shown in Figure 5.1. Inclusion of platinum metal onto  $\text{TiO}_2$  P25 did not alter the phase composition of the  $\text{TiO}_2$ . The XRD pattern in term of position and width of the peaks was similar to the standard crystal structure of  $\text{TiO}_2$  as described in our earlier studies.<sup>10</sup>

Diffuse reflectance spectra (DRS) of  $\text{TiO}_2$  and platinum loaded  $\text{TiO}_2$  are shown in Figure 5.2. With the incorporation of Pt metal, the peak little bit shifts toward visible region, and the band-gap changed from 3.04 eV to 2.95 eV.

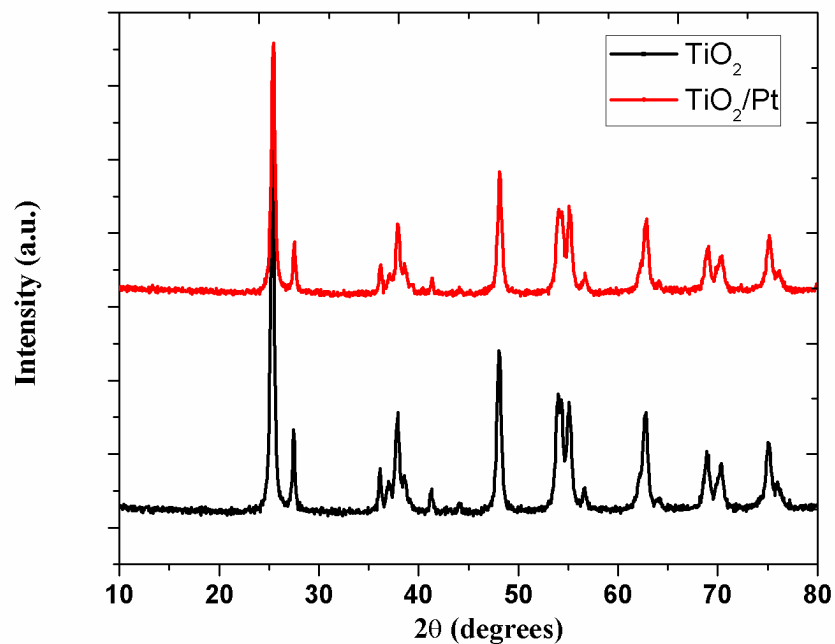


Figure 5.1 XRD for  $\text{TiO}_2$  and  $\text{TiO}_2/\text{Pt}$  photocatalysts.

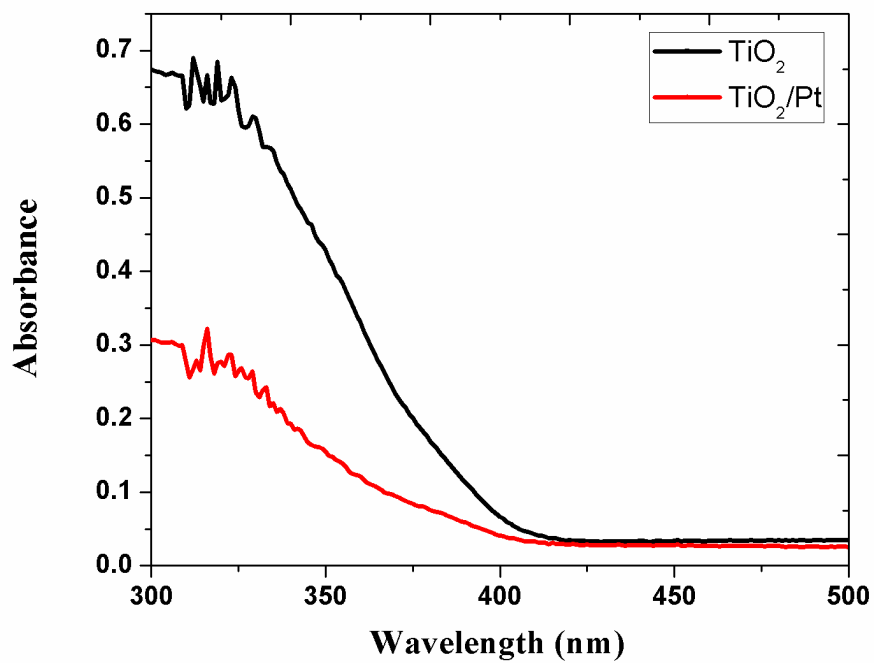


Figure 5.2 DRS for  $\text{TiO}_2$  and  $\text{TiO}_2/\text{Pt}$  photocatalysts.

### 5.3.2 Effect of platinum deposition on the photocatalytic activity of TiO<sub>2</sub>

Photocatalytic activity increased significantly with the incorporation of platinum metal on TiO<sub>2</sub> catalyst via solar photo-deposition method as shown in Figure 5.3. The rate of hydrogen generation increased from 0.34 μmol min<sup>-1</sup> to 2.28 μmol min<sup>-1</sup> with 1.0 % nominal loading of platinum. In order to determine the optimum dose of platinum, the loading was varied between 0 and 1.8 %. The rate of hydrogen generation increased rapidly up to 0.25 % platinum loading but then gradually dropped with further increment. Platinum metal as a dopant slightly reduced the band-gap of TiO<sub>2</sub>, but still could not initiate hydrogen generation under visible range of solar light. However, a significant enhancement of hydrogen generation was observed with the incorporation of platinum on TiO<sub>2</sub> surface under solar light as shown in Table 5.1. Higher platinum loading beyond optimum dose showed negative effect in hydrogen generation. This may be due to the decrease in adsorption sites of formaldehyde on TiO<sub>2</sub> and increase of UV light scattering during photocatalytic reaction.<sup>4</sup>

**Table 5.1 Effect of Pt deposition on TiO<sub>2</sub> P25**

<b>Photocatalyst</b>	<b>Hydrogen generation (μmol g<sup>-1</sup>)</b>
TiO <sub>2</sub> P25	541
TiO <sub>2</sub> /Pt (0.25 %)	4590

According to Linsebigler et al.<sup>21</sup> dispersed Pt metal on TiO<sub>2</sub> surface forms a Schottky barrier at the metal/semiconductor interface. This actually reduces the electron/hole recombination rate, and thereby, improves charge separation efficiency. Platinum metal on TiO<sub>2</sub> surface basically “pump” the photogenerated electron from TiO<sub>2</sub> to the adsorbed species, and thus hinder the possibility of their recombination with holes. In addition, platinum metal particle on TiO<sub>2</sub> improves reaction kinetics by decreasing the overpotential for hydrogen evolution.<sup>22, 23</sup>

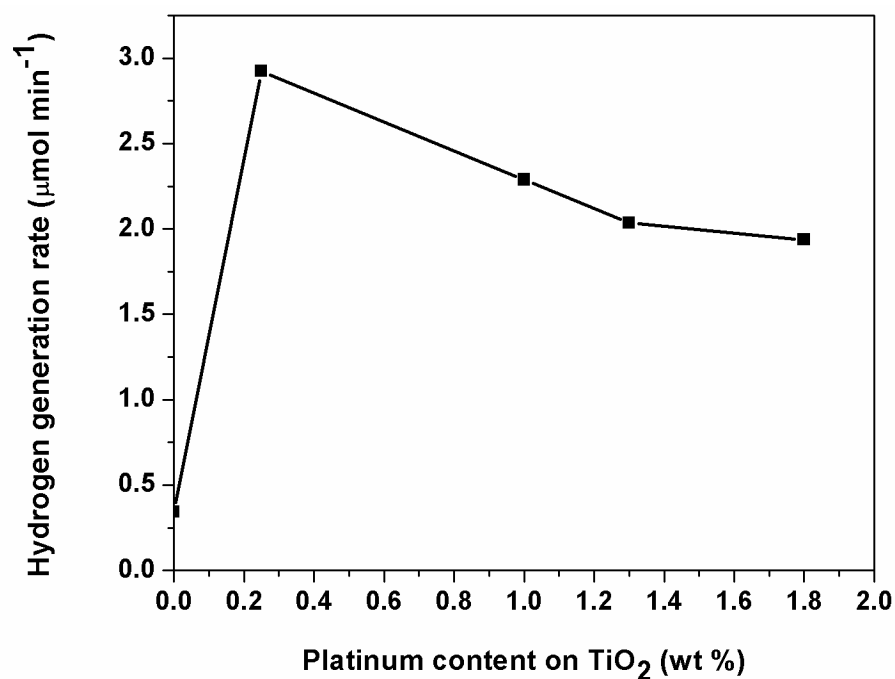


**Figure 5.3 Hydrogen generation rate versus platinum weight percent on TiO<sub>2</sub>.**  
 (Experimental conditions: [HCHO] = 0.1332 M, pH 6.7, [TiO<sub>2</sub>/Pt] = 1 g L<sup>-1</sup>, I<sub>Solar</sub> = 100 mW cm<sup>-2</sup>, N<sub>2</sub> saturated, pre-sonicated).

### 5.3.3 Effect of catalyst loading

To explore the effects of catalyst loading on hydrogen generation, a series of batch experiments were performed with TiO<sub>2</sub>/Pt (0.25 %) catalyst, in which the catalyst loading was varied between 0.2 and 1.9 g L<sup>-1</sup>. In all cases we have used natural pH (6.7) and all other parameters such as initial concentration of formaldehyde, platinum content on TiO<sub>2</sub> and light intensity were kept identical. TiO<sub>2</sub>/Pt has no visible light activity, and thus only solar-UV light was utilized during degradation of formaldehyde as well as generation of hydrogen. The rate of hydrogen production (r<sub>1</sub>) is shown in Figure 5.4, as a function of catalyst loading (g L<sup>-1</sup>). The rate increased with catalyst loading, but not linearly, in particular at low catalyst loadings, as would be expected.

The rate of hydrogen generation increased initially up to 1 g L<sup>-1</sup> then reached a plateau. This can be explained by the concept of active sites. At a low concentration of

photocatalyst slurry the photocatalytic reaction is mainly controlled by active sites which are accessible for adsorption of light and reactant.<sup>5, 24</sup> With gradual increment of photocatalyst slurry concentration, the solution turbidity increases, which thereby increases the UV light scattering. Moreover, the increased UV light scattering by suspended photocatalyst significantly reduces the UV transmission resulting in poor photocatalytic hydrogen generation. This observed phenomenon can be rationalized in terms of the availability of illuminated active sites on the TiO<sub>2</sub> surfaces, absorption and the penetration depths of light into the suspension. Hence, the rate of H<sub>2</sub> production per unit mass of catalyst ( $r_2$ ) decreases with the increase in catalyst loading<sup>25</sup>, as shown in Figure 5.4.

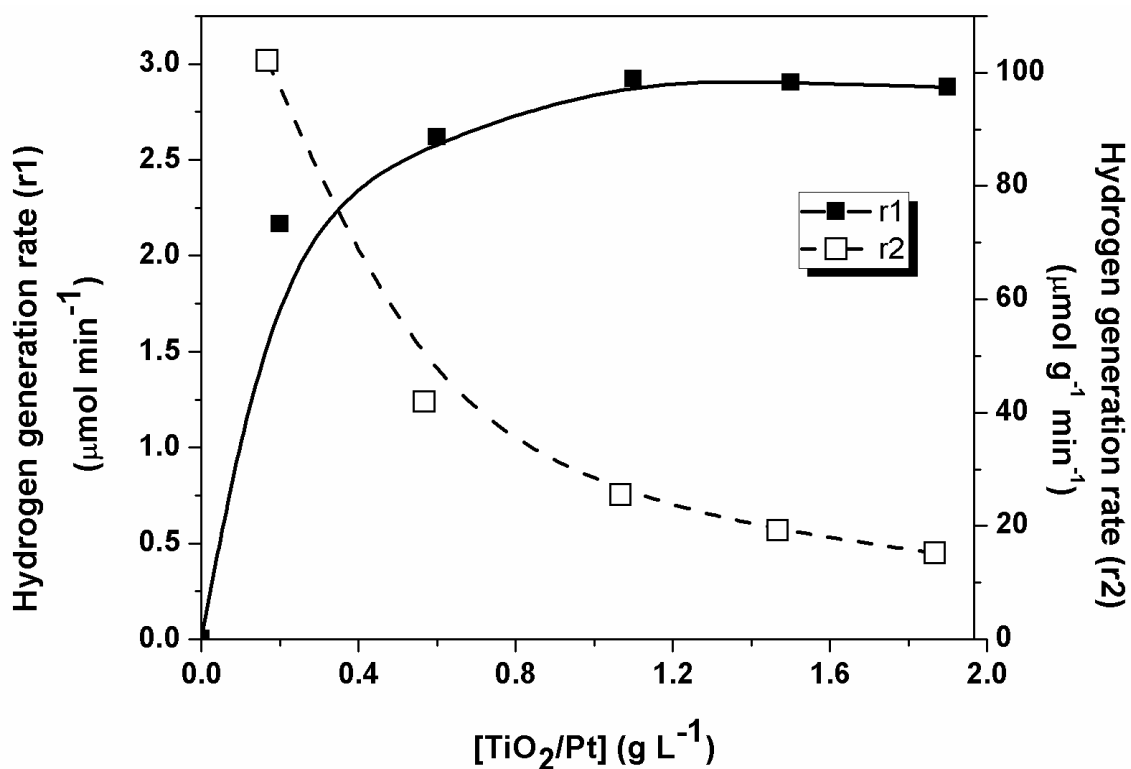


**Figure 5.4** Effect of catalyst concentration on the rate of hydrogen generation (r1); rate per unit mass of catalyst (r2). (Experimental conditions: [HCHO] = 0.1332 M, pH 6.7, Pt in TiO<sub>2</sub> = 0.25 %, I<sub>Solar</sub> = 100 mW cm<sup>-2</sup>, N<sub>2</sub> saturated, pre-sonicated).

### 5.3.4 Effect of initial pH of formaldehyde solution

Solution pH has a very significant influence in the photocatalytic reaction that takes place on TiO<sub>2</sub>/Pt surface. In aqueous slurry of TiO<sub>2</sub> the catalyst surface is embraced with plenty of hydroxyl groups and thus the ionization of TiO<sub>2</sub> is greatly affected by solution pH.



The point of zero charge (pzc) of pure Degussa P25 TiO<sub>2</sub> is in between 5.6 and 6.8,<sup>10, 26</sup> which can be slightly altered by the presence of trace amount of platinum deposits as per Pichat.<sup>27</sup>

Sun et al.<sup>28</sup> proposed plausible reaction mechanism for photocatalytic oxidation of gaseous formaldehyde in oxygen atmosphere where formation of superoxide anion or hydroxyl radical was mentioned as the heart of photo-oxidation process. In our case, the reactions were performed in N<sub>2</sub> atmosphere which totally eliminates the possibility of formation of superoxide ions. Thus, the active species would be only hydroxyl radical produced by the reaction of positive hole (h<sup>+</sup>) with water and hydroxyl groups absorbed on the TiO<sub>2</sub> surface. During the photocatalytic oxidation of formaldehyde on the TiO<sub>2</sub>/Pt, the formaldehyde is adsorbed on the hydroxyl groups on the catalyst surface via hydrogen bonding as shown in Figure 5.5. In presence of solar light irradiation, the formaldehyde is rapidly converted to formate species.

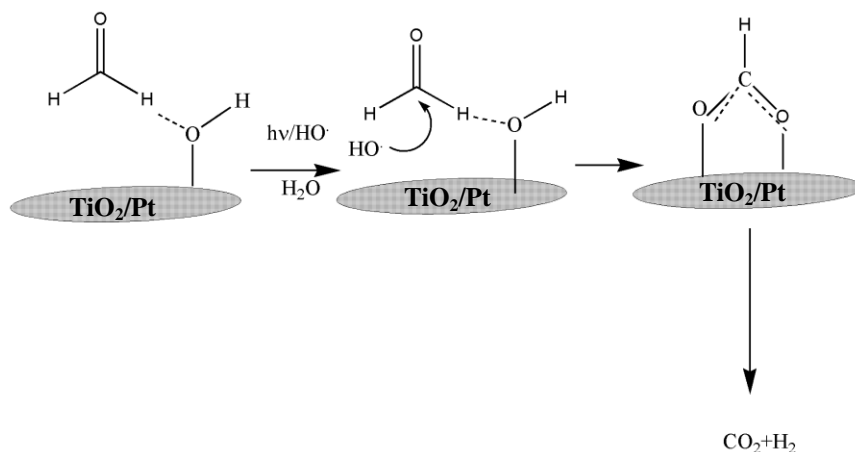


**Figure 5.5** Photocatalytic reaction of formaldehyde on TiO<sub>2</sub>/Pt surface

Under acidic pH, the degradation of formaldehyde producing hydrogen was lower compared to natural and alkaline pH (Figure 5.6). This could be explained by the fact of linkage of formaldehyde on  $\text{TiO}_2$  surface via hydrogen bonding, which was favored by negative surface charge of  $\text{TiO}_2$  at  $\text{pH} \geq 6.2$  (average point of zero charge of Degussa P25  $\text{TiO}_2$ ). The above phenomenon is quite opposite compared to the hydrogen generation from formic acid, acetic acid and oxalic acid,<sup>4</sup> where acidic pH is considered as the best pH for hydrogen generation.

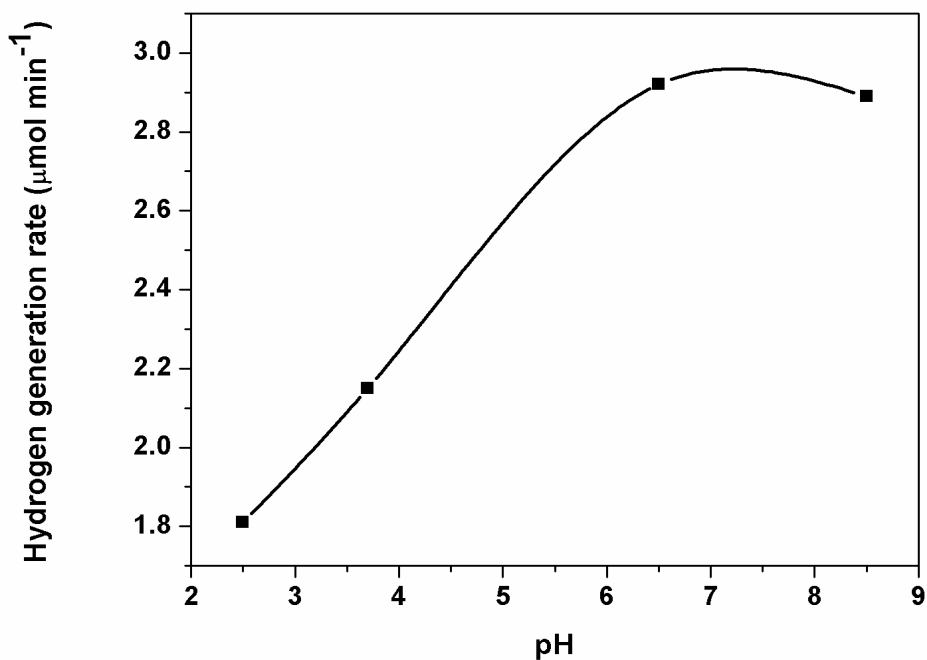


**Figure 5.6. Effect of initial pH of formaldehyde solution on the rate of hydrogen generation.** (Experimental conditions:  $[\text{HCHO}] = 0.1332 \text{ M}$ ,  $[\text{TiO}_2/\text{Pt}(0.25 \%) ] = 1 \text{ g L}^{-1}$ ,  $I_{\text{Solar}} = 100 \text{ mW cm}^{-2}$ ,  $\text{N}_2$  saturated, pre-sonicated).



### 5.3.5 Effect of initial concentration of formaldehyde

Formaldehyde molecule reacts with the photo-generated hole and/or hydroxyl radical and degrade to different compounds, Thus, the concentration of formaldehyde continuously changes reaction progresses. To determine the effect of initial concentration of formaldehyde on hydrogen generation, we have chosen 60 minutes time duration of experiment to compare the production of hydrogen as the change of reactant and/or product can be well determined during this time interval. Figure 5.7 describes the effect of initial formaldehyde concentration on the rate of hydrogen evolution. A significant improvement of hydrogen generation was observed with an increase in the concentration of formaldehyde. However, the hydrogen generation rate was found almost independent after 0.1332 M (4000 mg L<sup>-1</sup>) of formaldehyde concentration. Therefore, the rate varied as a function of formaldehyde concentration according to Langmuir-type equation as described below.<sup>4, 11</sup>

$$r = \frac{dC_{H_2}}{dt} = \frac{kKC_o}{1 + KC_o} \quad (5.1)$$

Where, r is the initial rate of hydrogen generation, k the reaction rate constant, and K the adsorption constant of formaldehyde on to TiO<sub>2</sub>/Pt photocatalyst. By fitting the above equation with experimental data (Figure 5.7), the values obtained for k = 2.3598 x 10<sup>-6</sup> mol min<sup>-1</sup> and K= 17.73 M<sup>-1</sup>.

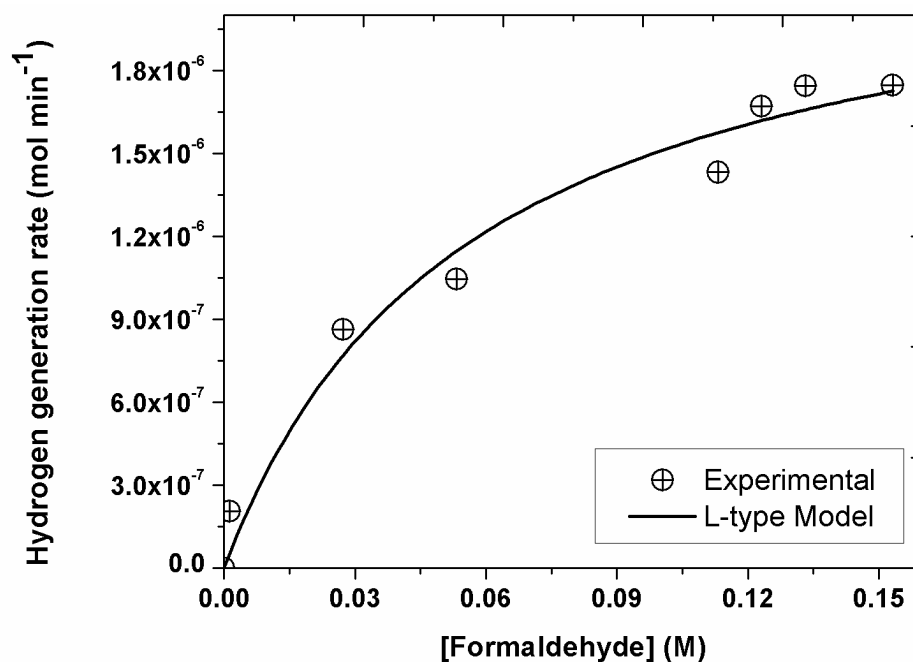


**Figure 5.7.** Effect of initial concentration of formaldehyde solution on the rate of hydrogen generation (both experimental rate and Langmuir type model rate). (Experimental conditions: pH 6.7-7.2, [TiO<sub>2</sub>/Pt]=1 g L<sup>-1</sup>, I<sub>Solar</sub>=100 mW cm<sup>-2</sup>, N<sub>2</sub> saturated, pre-sonicated).

### 5.3.6 Effect of light intensity

The main objective behind the optimization of different parameters such as photocatalyst dose, initial concentration of formaldehyde and/or the amount of noble metal (Pt) were to enhance the effective utilization of light energy. However, if the effect of light intensity on hydrogen is not wisely selected, a large portion of photons will be misused to heat up the system. This will also make our parameter optimization study ineffective. When higher light intensity causes energy waste instead of enhanced hydrogen generation, it would result in meaningless increase of cost.

We have studied the effect of solar light intensity in the range of 30 mW cm<sup>-2</sup> to 100 mW cm<sup>-2</sup>. The reaction rate constant  $k$ , followed power-law dependence on light intensities.

The hydrogen generation rate constants were evaluated as a function of solar light intensity, keeping all other parameters fixed. In solar radiation, the data fitted well with the power law model ( $k(I)=aI^b$ ) with  $a= 1.4266 \times 10^{-6}$ ,  $b=1.42$  and  $R^2 =0.999$  (Figure 5.8).

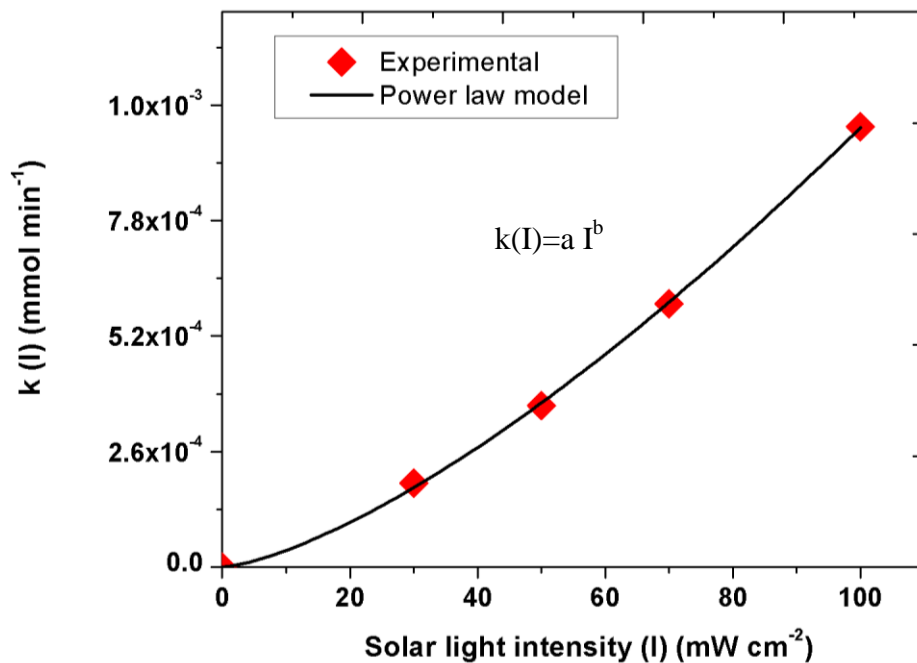


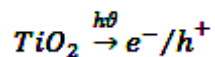
**Figure 5.8 Effect of light intensity on the rate of hydrogen generation.**

(Experimental conditions: [HCHO] = 0.1332 M, pH 6.7, [TiO<sub>2</sub>/Pt (0.25 %)] = 1 g L<sup>-1</sup>, I<sub>Solar</sub> = 100 mW cm<sup>-2</sup>, N<sub>2</sub> saturated, pre-sonicated).

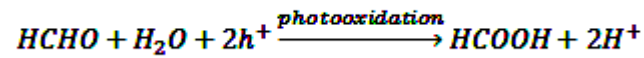
## 5.4 Reaction Mechanism

The major oxidative and reductive processes in the photodegradation of formaldehyde in aerated system with TiO<sub>2</sub> can be written as follows:<sup>12</sup>

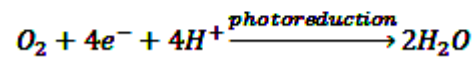
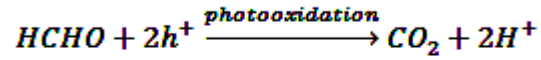
Step 1.



Step 2.

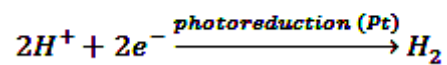
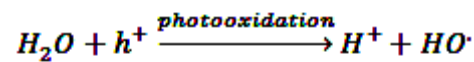
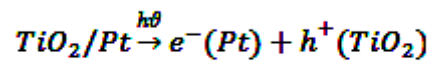


Step 3.



In absence of -oxygen (nitrogen atmosphere) the reaction mechanism slightly differs with TiO<sub>2</sub>/Pt photocatalyst.<sup>29</sup>

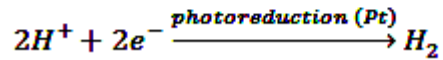
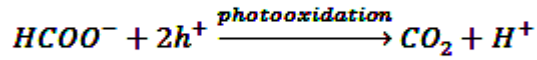
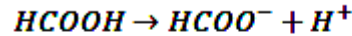
Step 1.



Step 2.



Step 3.



## 5.5 Apparent Quantum Yield

Apparent quantum yield can be calculated using the formula stated by Shimidzu et al.<sup>30</sup>

The quantum yield ( $\phi$ ) will certainly be higher than the apparent quantum yield, as the adsorbed photons are a certain fraction of the incident photons.

$$\begin{aligned} \phi > \text{apparent quantum yield, } \phi_{H_2} (\%) &= \frac{\text{number of } e^- \text{ or } h^+}{\text{number of incident photons}} \times 100 \\ &= \frac{\text{number of } H_2 \text{ molecule evolved}}{\text{number of incident photons}} \times 100 \end{aligned}$$

(5.2)

Considering full solar spectrum (300-650 nm) the apparent quantum yield was 1.24 %. However, TiO<sub>2</sub>/Pt photocatalyst utilized only UV light range for photocatalytic reaction. Therefore, we recalculated the apparent quantum yield with only UV radiation portion (300-388) and found much higher apparent quantum yield (10.91 %).

## 5.6 Conclusions

Results of the present study show that aqueous solution of formaldehyde under unaerated conditions produce hydrogen with the use of TiO<sub>2</sub>/Pt photocatalyst in solar radiation. With the incorporation of platinum metal onto TiO<sub>2</sub> the band gap energy lowered by 0.09 eV, but no photocatalytic activity was observed for hydrogen generation in visible light ( $\lambda > 420$  nm). Formaldehyde in solution acts as an electron donor and h<sup>+</sup>/O<sub>2</sub> scavenger, thereby suppresses the e<sup>-</sup>/h<sup>+</sup> recombination and H<sub>2</sub>/O<sub>2</sub> backward reaction. Therefore, degradation of formaldehyde and hydrogen production takes place simultaneously with high apparent quantum yield (10.91 %). Photocatalytic hydrogen generation from formaldehyde was very much influenced by solution pH, platinum content (wt%) on TiO<sub>2</sub>, catalyst concentration, light intensity, and initial formaldehyde concentration. The optimum conditions achieved for this study are given as follows: i) Isolar - 1sun, ii) platinum content – 0.25 wt%, iii) catalyst concentration – 1 g L<sup>-1</sup>, and iv) pH- neutral to alkaline. The proposed Langmuir-type model fits well with the experimental data for hydrogen generation at different initial concentration of formaldehyde.

## 5.7 References

1. Ni, M.; Leung, M. K. H.; Leung, D. Y. C.; Sumathy, K., A review and recent developments in photocatalytic water-splitting using TiO<sub>2</sub> for hydrogen production. *Renewable and Sustainable Energy Reviews* **2007**, 11, (3), 401-425.
2. Wu, N. L.; Lee, M. S., Enhanced TiO<sub>2</sub> photocatalysis by Cu in hydrogen production from aqueous methanol solution. *International Journal of Hydrogen Energy* **2004**, 29, (15), 1601-1605.
3. Yasushi, T., Thermodynamics of water splitting, in energy carriers and conversion systems. In *Encyclopedia of Life Support Systems (EOLSS)*, Ohta., T., Ed. **2006**; pp 1-5.
4. Li, Y.; Lu, G.; Li, S., Photocatalytic hydrogen generation and decomposition of oxalic acid over platinized TiO<sub>2</sub>. *Applied Catalysis A: General* **2001**, 214, (2), 179-185.
5. Badawy, M. I.; Ghaly, M. Y.; Ali, M. E. M., Photocatalytic hydrogen production over nanostructured mesoporous titania from olive mill wastewater. *Desalination* **2011**, 267, (2), 250-255.
6. Patsoura, A.; Kondarides, D. I.; Verykios, X. E., Photocatalytic degradation of organic pollutants with simultaneous production of hydrogen. *Catalysis Today* **2007**, 124, (3), 94-102.
7. Patsoura, A.; Kondarides, D. I.; Verykios, X. E., Enhancement of photoinduced hydrogen production from irradiated Pt/TiO<sub>2</sub> suspensions with simultaneous degradation of azo-dyes. *Applied Catalysis B: Environmental* **2006**, 64, (3), 171-179.
8. Hashimoto, K.; Kawai, T.; Sakata, T., Photocatalytic reactions of hydrocarbons and fossil fuels with water. Hydrogen production and oxidation. *The Journal of Physical Chemistry* **1984**, 88, (18), 4083-4088.
9. Chen, D.; Ray, A. K., Photodegradation kinetics of 4-nitrophenol in TiO<sub>2</sub> suspension. *Water Research* **1998**, 32, (11), 3223-3234.
10. Chowdhury, P.; Moreira, J.; Gomaa, H.; Ray, A. K., Visible Solar Light Driven Photocatalytic Degradation of Phenol with Dye-sensitized TiO<sub>2</sub>: Parametric and Kinetic Study. *Industrial & Engineering Chemistry Research* **2012**, 51, (12), 4523-4532.
11. Li, Y.; Xie, Y.; Peng, S.; Lu, G.; Li, S., Photocatalytic hydrogen generation in the presence of chloroacetic acids over Pt/TiO<sub>2</sub>. *Chemosphere* **2006**, 63, (8), 1312-1318.
12. Noguchi, T.; Fujishima, A.; Sawunyama, P.; Hashimoto, K., Photocatalytic degradation of gaseous formaldehyde using TiO<sub>2</sub> film. *Environmental Science & Technology* **1998**, 32, (23), 3831-3833.

13. Lam, R. C. W.; Leung, M. K. H.; Leung, D. Y. C.; Vrijmoed, L. L. P.; Yam, W. C.; Ng, S. P., Visible-light-assisted photocatalytic degradation of gaseous formaldehyde by parallel-plate reactor coated with Cr ion-implanted TiO<sub>2</sub> thin film. *Solar Energy Materials and Solar Cells* **2007**, 91, (1), 54-61.
14. Ching, W. H.; Leung, M.; Leung, D. Y. C., Solar photocatalytic degradation of gaseous formaldehyde by sol-gel TiO<sub>2</sub> thin film for enhancement of indoor air quality. *Solar Energy* **2004**, 77, (2), 129-135.
15. Zhang, X.; Liu, Q., Visible-light-induced degradation of formaldehyde over titania photocatalyst co-doped with nitrogen and nickel. *Applied Surface Science* **2008**, 254, (15), 4780-4785.
16. Glancer-Soljan, M.; Soljan, V.; Dragicevic, T. L.; Cacic, L., Aerobic degradation of formaldehyde in wastewater from the production of melamine resins. *Food Technology and Biotechnology* **2001**, 39, (3), 197-202.
17. Moussavi, G.; Yazdanbakhsh, A.; Heidarizad, M., The removal of formaldehyde from concentrated synthetic wastewater using O<sub>3</sub>/MgO/H<sub>2</sub>O<sub>2</sub> process integrated with the biological treatment. *Journal of Hazardous Materials* **2009**, 171, (1-3), 907-913.
18. Sakata, T., Photocatalysis of irradiated semiconductor surfaces: its application to water splitting and some organic reactions. *Journal of Photochemistry* **1985**, 29, 205-215.
19. Li, Y.; Lu, G.; Li, S., Photocatalytic production of hydrogen in single component and mixture systems of electron donors and monitoring adsorption of donors by in situ infrared spectroscopy. *Chemosphere* **2003**, 52, (5), 843-850.
20. Chowdhury, P.; Gomaa, H.; Ray, A. K., Factorial design analysis for dye-sensitized hydrogen generation from water. *International Journal of Hydrogen Energy* **2011**, 36, (21), 13442-13451.
21. Linsebigler, A. L.; Lu, G.; Yates Jr, J. T., Photocatalysis on TiO<sub>2</sub> surfaces: principles, mechanisms, and selected results. *Chemical Reviews* **1995**, 95, (3), 735-758.
22. Duonghong, D.; Borgarello, E.; Graetzel, M., Dynamics of light-induced water cleavage in colloidal systems. *Journal of the American Chemical Society* **1981**, 103, (16), 4685-4690.
23. Bard, A. J., Design of semiconductor photoelectrochemical systems for solar energy conversion. *Journal of Physical Chemistry* **1982**, 86, (2), 172-177.
24. Daskalaki, V. M.; Kondarides, D. I., Efficient production of hydrogen by photo-induced reforming of glycerol at ambient conditions. *Catalysis Today* **2009**, 144, (1-2), 75-80.



25. Karakitsou., K. E.; Verykios., X. E., Influence of Catalyst Parameters and Operational Variables on the Photocatalytic Cleavage of Water. *Journal of Catalysis* **1992**, 134, 629-643.
26. Lu, M. C.; Roam, G. D.; Chen, J. N.; Huang, C. P., Factors affecting the photocatalytic degradation of dichlorvos over titanium dioxide supported on glass. *Journal of Photochemistry and Photobiology A: Chemistry* **1993**, 76, (1), 103-110.
27. Pichat, P., Surface properties, activity and selectivity of bifunctional powder photocatalysts. *New Journal of Chemistry* **1987**, 11, 135-7401.
28. Sun, S.; Ding, J.; Bao, J.; Gao, C.; Qi, Z.; Li, C., Photocatalytic oxidation of gaseous formaldehyde on TiO<sub>2</sub>: an in situ DRIFTS study. *Catalysis Letters* **2010**, 137, (3), 239-246.
29. Miwa, T.; Kaneco, S.; Katsumata, H.; Suzuki, T.; Ohta, K.; Chand Verma, S.; Sugihara, K., Photocatalytic hydrogen production from aqueous methanol solution with CuO/Al<sub>2</sub>O<sub>3</sub>/TiO<sub>2</sub> nanocomposite. *International Journal of Hydrogen Energy* **2010**, 35, (13), 6554-6560.
30. Shimidzu, T.; Iyoda, T.; Koide, Y., An advanced visible-light-induced water reduction with dye-sensitized semiconductor powder catalyst. *Journal of the American Chemical Society* **1985**, 107, (1), 35-41.

## Chapter 6

# 6 Visible-Solar-Light-Driven Photocatalytic Degradation of Phenol with Dye-Sensitized TiO<sub>2</sub>: Parametric and Kinetic Study

## 6.1 Introduction

Solar energy is an abundant resource; the sun generates its energy through a thermonuclear process that converts hydrogen to helium every second. The process creates heat and electromagnetic radiation including visible, infrared, and ultraviolet radiation. Earth receives approximately  $1.5 \times 10^{18}$  kWh per year from solar energy, which is close to 28000 times the total annual world energy consumption.<sup>1</sup>

Heterogeneous photocatalysis is a technology in which a photoexcitable solid catalyst is continuously illuminated with light with an energy greater than the band gap of the semiconductor and electron/hole ( $e^-/h^+$ ) pairs are generated inside the semiconductor.<sup>2,3</sup> If an  $e^-/h^+$  pair does not recombine, it can migrate to the surface of the solid catalyst and participate in the degradation (oxidation or reduction) of pollutants.<sup>4</sup>

Phenol and phenolic compounds are toxic pollutants that can be found mainly in wastes from petroleum manufacture, coke ovens, paint stripping operations, and so on.<sup>5</sup> Photocatalytic degradation of phenol with the UV/TiO<sub>2</sub> system has been reported by several authors.<sup>4,6-8</sup>

In the solar spectrum, the range of wavelengths is broad, spanning from 250 to 2500 nm, but only 3.5–8 % of it is in the UV range.<sup>1</sup> Hence, TiO<sub>2</sub> can make use of only a small fraction of solar light for such photodegradation. This problem can be solved only by extending the light absorption capacity of TiO<sub>2</sub> catalysts.

Semiconductor photocatalysts can be modified to expand their photoresponse to the visible region for phenol degradation in several ways, including doping with cations/anions<sup>9-15</sup> or coupling with another small-band-gap semiconductor.<sup>16</sup> Most of

these methods, however, are quite expensive and time-consuming. Dye sensitization, on the other hand, is a new and simpler method that can extend TiO<sub>2</sub> activation to wavelengths longer than those corresponding to its band gap.

The dye-sensitization technique has been reported as an innovative technology that could play an important role in developing efficient and cost-effective semiconductor photocatalyst in the near future.<sup>17</sup> Solar cell applications based on dye-sensitized TiO<sub>2</sub> are among the most popular and successful methods to date<sup>18-21</sup> and have also been applied to visible light-induced detoxification of pollutants.<sup>22</sup> Dye sensitization begins with electron injection from the excited dye into the conduction band (CB) of TiO<sub>2</sub>, followed by interfacial electron transfer.<sup>23-27</sup>

In a dye-sensitized system, the main problem is the oxidation of adsorbed dye molecules with HO• radicals.<sup>28,29</sup> Inclusion of an additional electron donor might be helpful for the dye regeneration process, as reported for the dye-sensitized hydrogen generation process.<sup>30</sup>

Recombination of charge carriers (e<sup>-</sup>/dye<sup>+</sup>) is also responsible for low dye-sensitization activity, as it reduces the electron transfer to the conduction band of the semiconductor. Many authors have reported increased photocatalytic activities for metal-loaded titanium dioxide for the photodegradation of organic compounds.<sup>31-33</sup> Moreover, the presence of trace amounts of platinum metal was found to be beneficial in dye-sensitized hydrogen generation, as platinum reduces the recombination of cation/anion pairs.<sup>30</sup>

Different dyes (thionine, eosin Y, rhodamine B, methylene blue, Nile blue A, and safranin O) have been studied with TiO<sub>2</sub> catalysts for the degradation of pollutants under visible light.<sup>34,35</sup> Eosin Y dye has shown very good potential for the degradation of phenolic compounds.<sup>28</sup>

In this work, we employed eosin Y-sensitized platinum loaded TiO<sub>2</sub> catalyst with triethanolamine electron donor for the degradation of phenol under visible solar light. This photocatalytic system is successful for hydrogen generation under nitrogen

atmosphere but has not yet been applied for phenol degradation under aerated (or O<sub>2</sub>) systems. According to our knowledge, no study has yet been performed with such a system for phenol degradation under visible solar light. There is also inadequate information on the kinetics of this system.

The main objective of this investigation was to understand the dye-sensitization mechanism for phenol degradation under visible solar light. Parametric studies of (i) platinum cocatalyst, (ii) triethanolamine as electron donor, (iii) solution pH, (iv) light intensity, and (v) catalyst amount, as well as reaction kinetics for phenol photodegradation, were investigated.

## 6.2 Experimental Section

### 6.2.1 Materials

All reagents were of analytical grade and were used without further treatment. Aeroxide TiO<sub>2</sub> P25 (80 %:20 % anatase/rutile) from Evonik Degussa Corporation was used as the catalyst. Eosin Y dye (99.0 %, Sigma-Aldrich Canada Ltd.) was used as the sensitizer for TiO<sub>2</sub>; triethanolamine (98.0 %) and hydrogen hexachloroplatinate (IV) solution (8 wt %) were also purchased from Sigma-Aldrich Canada Ltd. Ultrapure water (18 MΩ) was prepared from an in-house EASYPure RODI system (Thermo Scientific, Ontario, Canada). Phenol (99.0 %) was purchased from Sigma-Aldrich Canada Ltd. and used to make standards and aqueous solutions for the photocatalytic reactions.

### 6.2.2 Instruments

Simulated air mass (AM) 1.5 solar light was generated using a solar simulator (model SS1KW, Sciencetech, Ontario, Canada, with a 1000-W Xe arc lamp and an AM 1.5G filter). It produced identical simulated 1-sun irradiance of 100 mW cm<sup>-2</sup> at full power that matched the global solar spectrum at sea level. Spectral analysis of their radiation from the solar simulator with a StellarNet EPP2000C-25LT16 spectrometer for UV–vis-NIR spectroscopy showed 6.5 % UV, 64.5 % visible, and the rest NIR light.

The quantification analyses of phenol and aromatic components were performed in a Shimadzu high-performance liquid chromatography (HPLC) prominence LC 20AB instrument with an SIL-20AC.HT auto sampler and a CTO-0AC column oven with an SPD-M20A diode array detector. An Altima HP C18 column (5  $\mu\text{m}$   $\times$  150 mm  $\times$  4.6 mm, lot 50198212) and a mobile phase of methanol and water (MiliQ water) 67/33% v/v at a flow rate of 0.5 ml min<sup>-1</sup> were used. The temperature of the column oven was kept at 25°C throughout the analysis. The wavelengths of analyses for phenol and reaction intermediates catechol [para-dihydroxybenzene (p-DHB)], hydroquinone (o-DHB), and 1,4-benzoquinone (1,4-BQ) were done at 270, 290, 275, and 255 nm, respectively. The injection volume for all samples was 5  $\mu\text{L}$ . An integrating sphere was utilized to measure the diffuse reflectance absorption spectra of the catalyst. pH measurements were carried out using a pH meter (780-Metrohm Ltd.).

### 6.2.3 Synthesis of eosin Y-sensitized TiO<sub>2</sub>/Pt photocatalyst

Platinum was loaded on TiO<sub>2</sub> catalyst by a solar photo deposition method. TiO<sub>2</sub> powder was stirred in an aqueous ethanol solution (ethanol/water = 10/90 by volume) with hexachloroplatinate (IV) solution (H<sub>2</sub>PtCl<sub>6</sub>), the amount of which corresponded to platinum loadings of 0.25, 0.5, 0.75, and 1 wt %. Then, the solution was irradiated under the solar simulator (at 1 sun) for 3 h. Photoreduction of H<sub>2</sub>PtCl<sub>6</sub> (Pt<sup>IV</sup>) occurred, and highly dispersed Pt particles were deposited on the TiO<sub>2</sub> surface.<sup>36</sup> After being filtered and washed with water, the powder was dried at 150°C for 2 h and milled in a mortar.

Eosin Y dye (EY) was adsorbed onto TiO<sub>2</sub>/Pt by stirring 0.5 g of the catalyst powder in a mixture of EY and anhydrous ethanol solvent (4.6  $\times$  10<sup>-4</sup> M) at room temperature for 12 h in the dark. This was followed by filtration, washing with anhydrous ethanol, and drying at 100 °C for 2 h. The obtained sample was kept in the dark to avoid catalyst deactivation. The EY-sensitized TiO<sub>2</sub>/Pt photocatalyst showed a broad absorption from 410 to 640 nm.<sup>30</sup>

## 6.2.4 Photocatalytic phenol degradation

Photocatalytic reactions were carried out in a Pyrex glass reactor (600 mL) with a flat window at the top for illumination. Figure 6.1 shows a schematic diagram of the photocatalytic reactor (11 cm diameter, 6.3 cm height) used in this investigation. The catalyst powder (EY-TiO<sub>2</sub>/Pt) was suspended in 150 mL of phenol and triethanolamine (TEOA) solution (0–0.5 M) after pH adjustment with 1:1 HCl. The catalyst suspension was dispersed for 5 min in an ultrasonic bath, and then the system was kept in the dark for 60 min to achieve adsorption equilibrium. A sample of about 3 mL was taken after filtration with 0.2- $\mu$ m filter to determine its initial concentration prior to illumination. All experiments were performed by continuously bubbling air through the liquid phase to cover the catalyst surface with oxygen and keep it constant during the oxidation process. Continuous stirring was performed using a magnetic stirrer. The photocatalyst was irradiated from the top with a solar simulator. The light source was equipped with AM 1.5G filter, as well as a 420-nm cutoff filter (Omega Optical) to remove all of the UV light. The water layer above the catalyst itself acted as an IR filter. Liquid samples were collected at regular intervals and analyzed by HPLC for residual phenol, hydroquinone, catechol, and 1,4-benzoquinone.

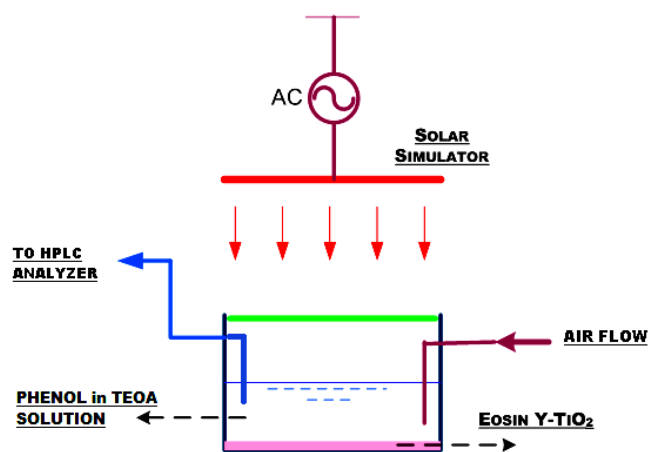


Figure 6.1 Photo-reactor for phenol degradation

## 6.3 Catalyst Characterization

### 6.3.1 Brunauer–Emmett–Teller (BET) method

As an approach to identify the surface area, pore size and the extent of porosity, a nitrogen adsorption–desorption isotherm was recorded. Figure 6.2 shows the representative Barrett–Joyner–Halenda (BJH) pore size distribution and adsorption–desorption isotherm plot (inset) of the EY-sensitized Pt-loaded TiO<sub>2</sub> catalyst. The adsorption isotherm has a hysteresis loop at high N<sub>2</sub> relative pressure ( $P/P_0 > 0.85$ ). The pore size distribution plot ( $dV/dD$  versus pore diameter) shows an average pore size of 1.7 nm. This implies the presence of a microporous structure. The determined BET surface area was found to be  $55 \text{ m}^2 \text{ g}^{-1}$ , which is comparable to that of P25 TiO<sub>2</sub> ( $50 \text{ m}^2 \text{ g}^{-1}$ ). This indicates that platinum loading and dye adsorption did not significantly affect the catalyst total surface area.

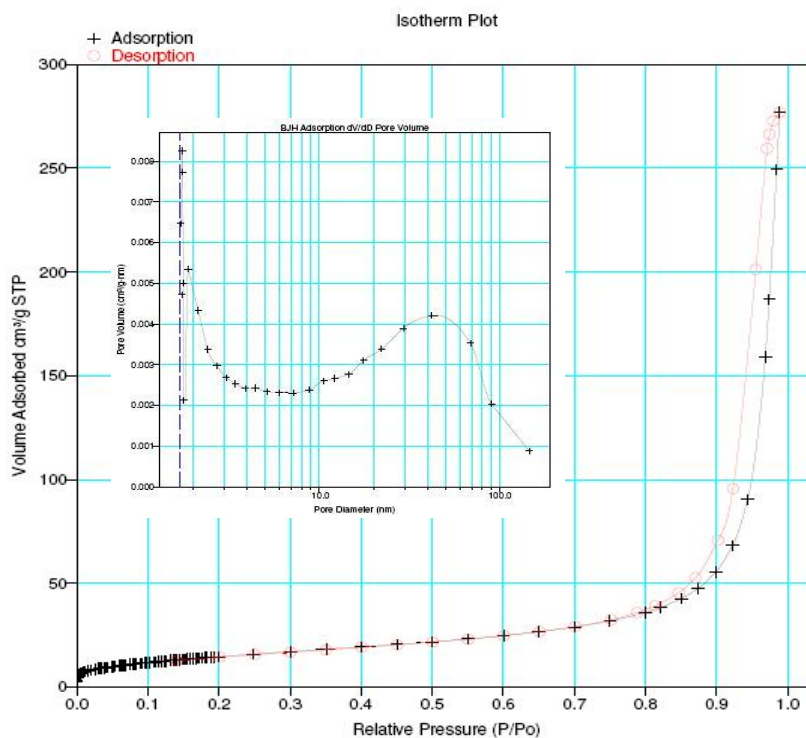


Figure 6.2 Isotherm plot (BJH pore size distribution)

### 6.3.2 X-ray diffraction (XRD)

Figure 6.3 shows the XRD pattern of the EY-TiO<sub>2</sub>/Pt sample at 0.5 wt % platinum loading. The XRD pattern was similar to the standard crystal structure of TiO<sub>2</sub>, with no diffraction peaks associated with Pt metal in the EY-TiO<sub>2</sub>/Pt sample. Hence, the metal sites are likely to be below the visibility limit of the X-ray analysis.<sup>37</sup> This suggests that the platinum loading process did not produce separate impurity phases and that the Pt nanoparticles can be considered as fully dispersed in the TiO<sub>2</sub> lattice. According to Choi et al.,<sup>38</sup> Ti (IV) ions can be substituted by Pt (IV) ions during platinum loading on to TiO<sub>2</sub> because of the similarity of their ionic radius [Pt (IV), 0.765 Å; Ti (IV), 0.745 Å]. However, Pt (II) ions could possibly be sited in the interstitial positions of the lattice instead of the Ti sites because of the relatively large size difference between the Pt (II) (0.94 Å) and Ti (IV) ions.

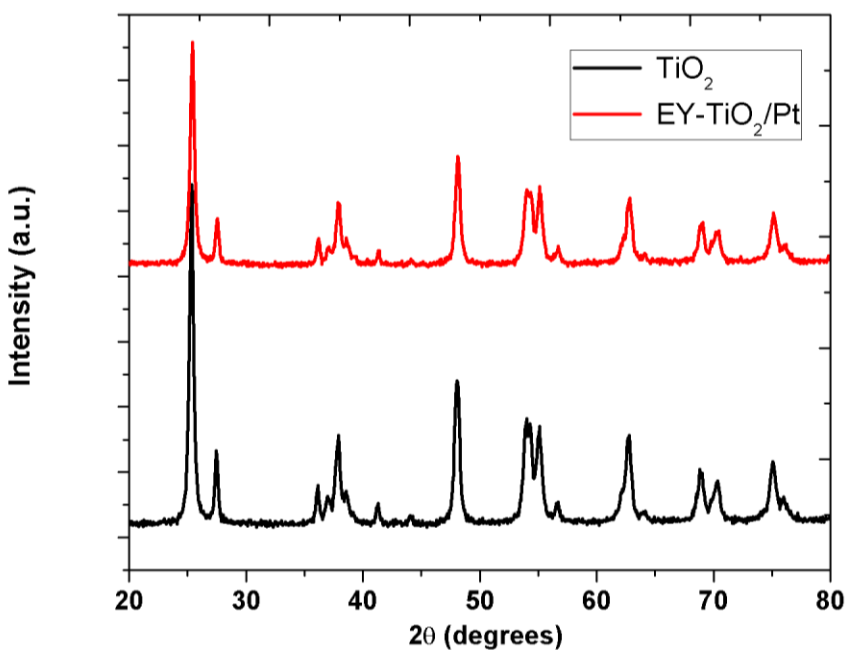
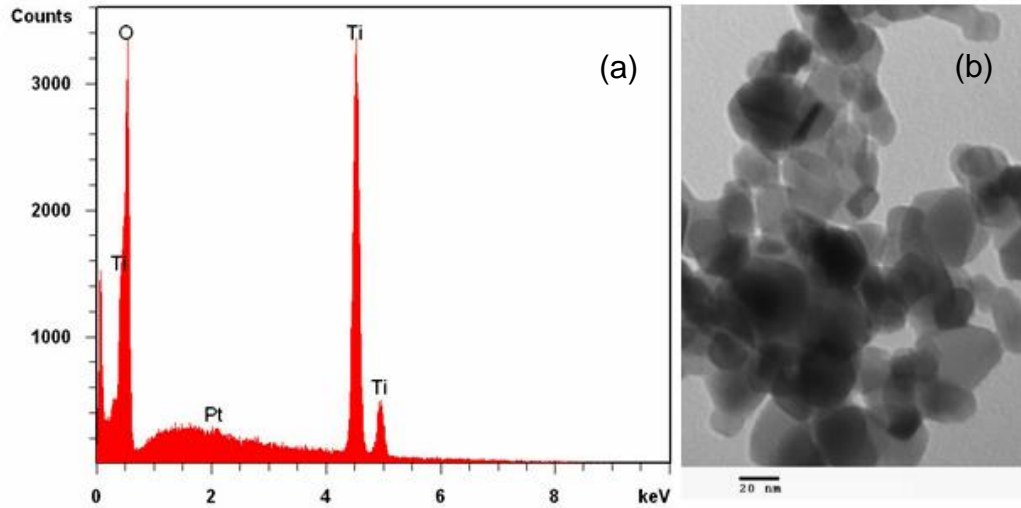


Figure 6.3 XRD image for TiO<sub>2</sub> and EY-TiO<sub>2</sub>/Pt catalysts.



### 6.3.3 Energy-dispersive X-ray (EDX) and Transmission and electron microscopy (TEM)

EDX analysis (Figure 6.4 (a)) revealed the presence of Pt metal in the EY-sensitized TiO<sub>2</sub> catalyst. The TEM (Figure 6.4 (b)) image clearly shows that the platinum nanoclusters are highly dispersed in the framework.



**Figure 6.4 (a) EDX image for EY-TiO<sub>2</sub>/Pt photocatalysts; (b) TEM image for EY-TiO<sub>2</sub>/Pt photocatalysts.**

### 6.3.4 Diffuse reflectance spectra (DRS)

Diffuse reflectance spectra (Figure 6.5) provide an indication of visible light activity of the EY-sensitized  $\text{TiO}_2/\text{Pt}$  catalyst. As can be seen, a broad spectrum of 450–600 nm is present. The catalyst has a band gap of 2.2 eV (average  $\lambda = 550$  nm).

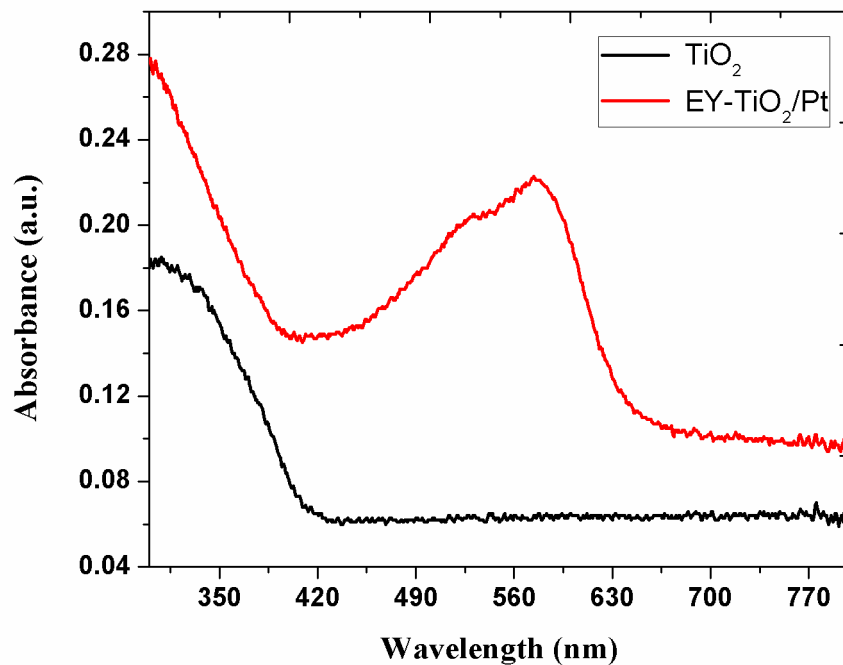
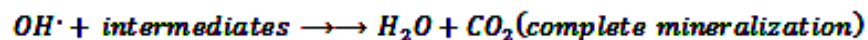
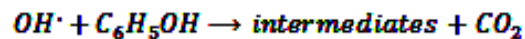
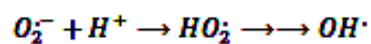
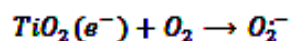
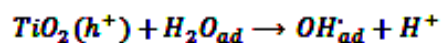
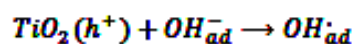
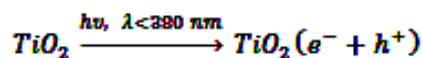


Figure 6.5 DRS image for  $\text{TiO}_2$  and EY- $\text{TiO}_2/\text{Pt}$  photocatalysts.

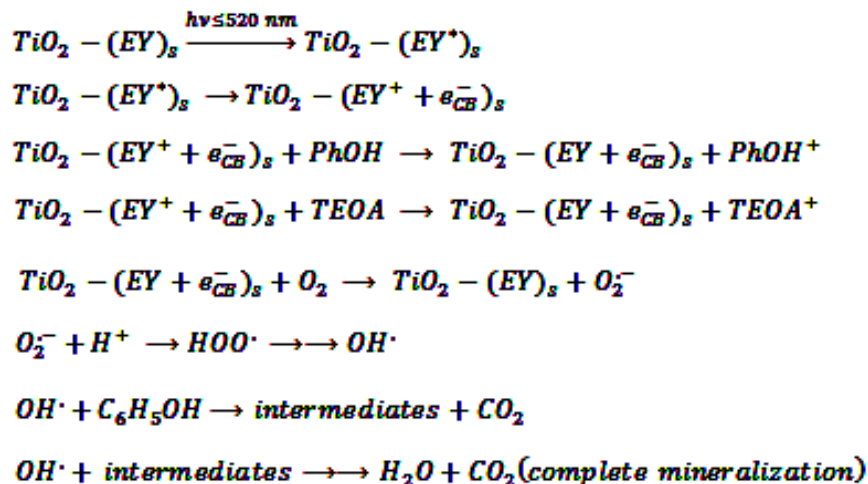
## 6.4 Reaction Mechanism and Kinetic Rate Expression

### 6.4.1 Reaction mechanism

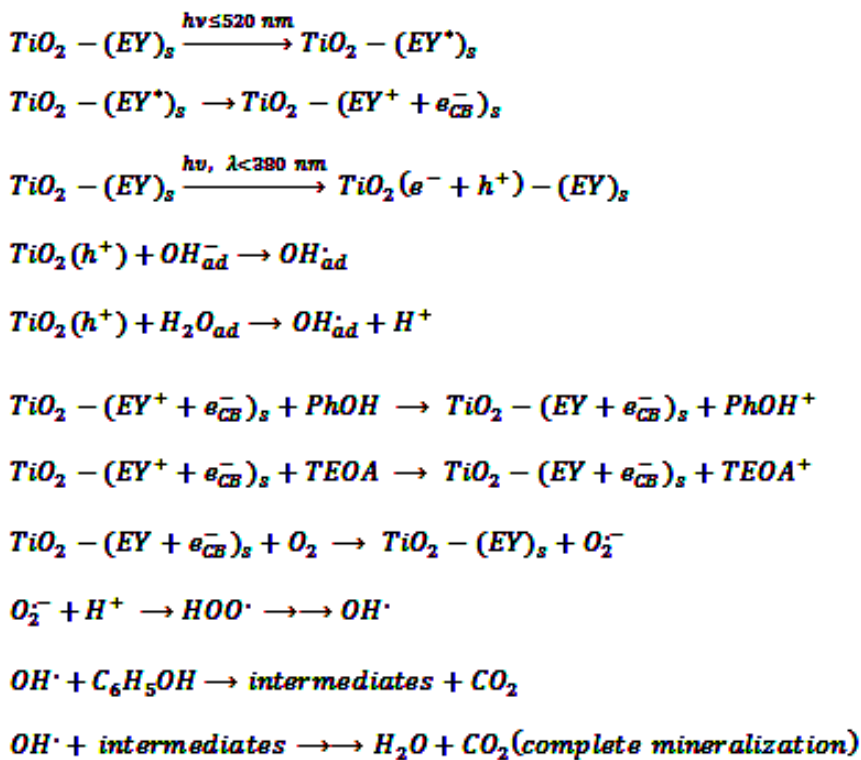
The degradation mechanism of phenol (PhOH) and its derivatives under UV light is described in the literature,<sup>7</sup> where hydroxyl radical (OH•) was reported to be the main oxidizing species. The mechanism is given by the reactions.



Dye-sensitized photodegradation of phenol (PhOH) under only visible light is initiated through excitation of the dye molecule from its ground state to the excited state, which finally facilitates electron transfer to the conduction band of the semiconductor (TiO<sub>2</sub>). The oxidized dye molecule (dye<sup>+</sup>) can interact with the pollutant (phenol), water, or an electron donor (e.g., TEOA) to return back to its ground state. A possible degradation reaction mechanism is described below.<sup>35,39</sup>



Because solar light contains both UV and visible radiation, the overall phenol degradation mechanism will be influenced by both types of radiation.<sup>39</sup>



The overall phenol degradation scheme is described in Figure 6.6.<sup>40</sup> In our case, we recognized superoxide ion as the active species because negligible phenol degradation was achieved under nitrogen atmosphere compared to degradation under oxygen (air) atmosphere. The formation of superoxide ion was also supported by the work of Vinu et al.<sup>28</sup> In our experiments, only catechol (p-DHB) and hydroquinone (o-DHB) were detected as intermediates, as indicated in Figure 6.7.

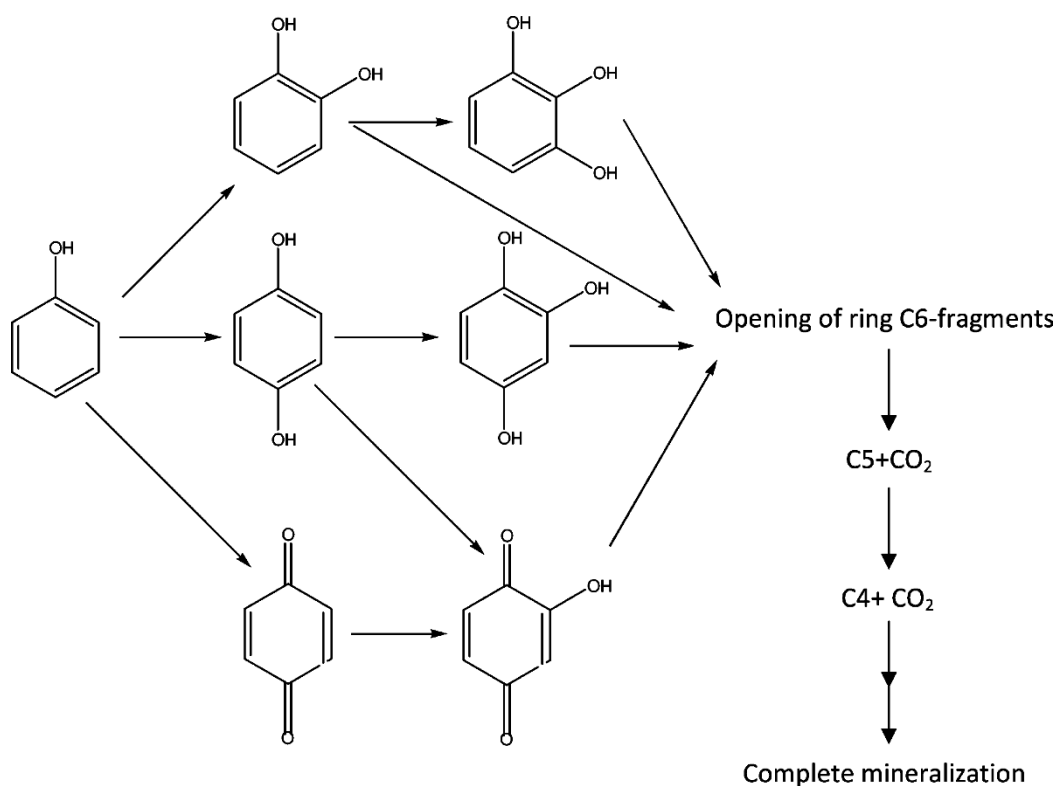


**Figure 6.6 Photo-degradation scheme of phenol under UV and visible photons.**

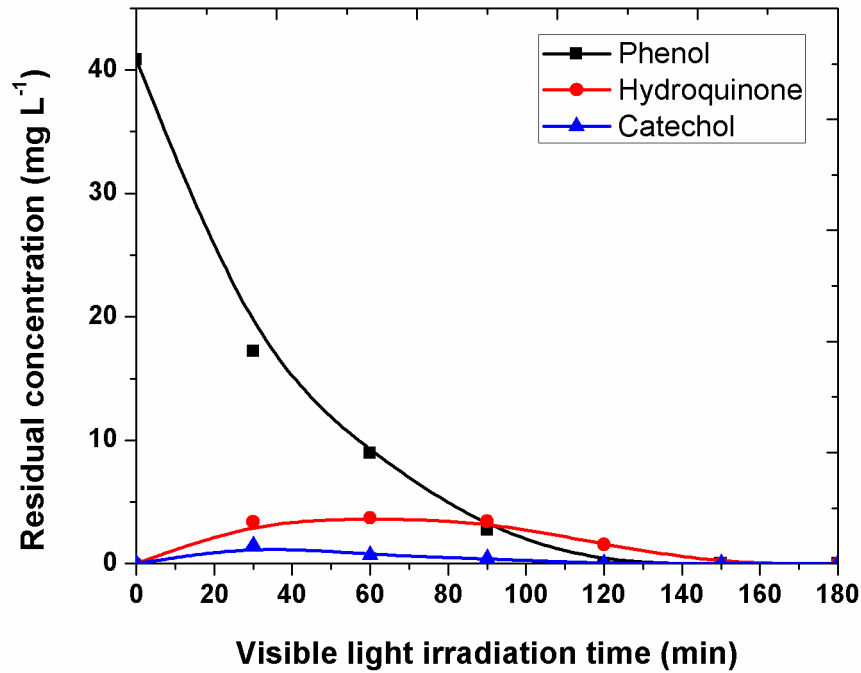


Figure 6.7 Residual concentration vs irradiation time plot for phenol and intermediates.

#### 6.4.2 Reaction kinetics

It has been demonstrated that bare TiO<sub>2</sub> catalyst is activated by light ( $\lambda < 380$  nm) and photodegradation of organic compounds occurs in presence of water saturated with dissolved oxygen. The primary step in UV photodegradation is the formation of e<sup>-</sup>/h<sup>+</sup> pairs within TiO<sub>2</sub> particles, whereas in dye-sensitized photodegradation under visible solar radiation, the dye molecule is first activated by visible light ( $\lambda > 420$  nm) and then injects electrons into the TiO<sub>2</sub> conduction band.<sup>34</sup> The kinetics of phenol degradation on TiO<sub>2</sub> can be described by a Langmuir–Hinshelwood equation as follows<sup>7</sup>:

$$-\frac{dC_{ph}}{dt} = \frac{W}{V} I \alpha \frac{k_r K_A C_{ph}^o}{1 + K_A C_{ph}^o} \quad (6.1)$$

Where,  $K_A$  is the adsorption equilibrium constant,  $k_r$  is the kinetic rate constant,  $I$  is the light intensity,  $\beta$  is a constant,  $V$  is the volume of the reaction mixture,  $W$  is the mass of catalyst, and  $C_{Ph}$  is the phenol concentration. The superscript 0 indicates the initial concentration. If we define the apparent kinetic constant as

$$k_{app} = \frac{W}{V} k_r K_A \quad (6.2)$$

Then, combining equation (6.1) and (6.2) gives

$$-\frac{dC_{ph}}{dt} = r_s = I \frac{\beta}{\alpha} \frac{k_{app} C_{ph}^0}{1 + K_A C_{ph}^0} \quad (6.3)$$

Equation (6.3) can be used to predict the kinetic parameters of phenol photodegradation at different irradiation intensities. Numerical details are discussed in section 6.6.

## 6.5 Parametric Study

### 6.5.1 Effect of mass of $TiO_2$

The effect of the amount of EY– $TiO_2$ /Pt catalyst on the removal of phenol was found to be significant. This finding confirms the positive influence of an increased number of photocatalyst active sites on the degradation kinetics. The variation in the degradation rate constant of phenol with the concentration of EY– $TiO_2$ /Pt was determined for the catalyst concentration range of 0.1–2.2 g L<sup>-1</sup>, as shown in Figure 6.8. The rate constant was found to increase with increasing concentration of catalyst and to approach a limiting value at high concentration. With an increase in catalyst mass, the total active surface area for light absorption increases, thereby increasing the number of hydroxyl and/or superoxide radicals. The limiting value mainly results from the following two factors: (i) aggregation of catalyst particles at high concentration causing a decrease in the number of surface active sites and (ii) an increase in opacity and light scattering of EY– $TiO_2$ /Pt

particles at high concentration leading to a decrease in the passage of irradiation through the sample. This is consistent with the results of other investigators.<sup>7</sup>

In this study, the initial rate was found to be proportional to the catalyst mass. However, above a certain catalyst concentration, the reaction rate became constant and independent of EY-TiO<sub>2</sub>/Pt. This limit corresponds to the maximum amount of catalyst in which all of the particles and the entire surface exposed were completely illuminated.<sup>7,41,42</sup> In our experiments, we used 0.8 g L<sup>-1</sup> as the optimum catalyst dosage for phenol degradation.

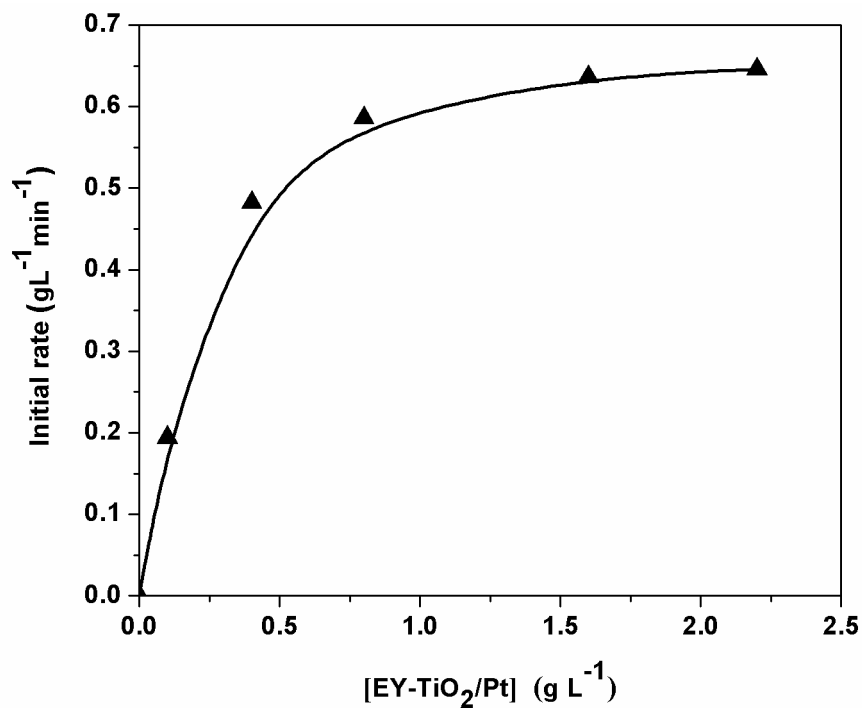


Figure 6.8 Initial phenol degradation rate vs catalyst dosage.



### 6.5.2 Effect of Pt content on TiO<sub>2</sub>

Noble-metal clusters on TiO<sub>2</sub> mainly accelerate the formation of superoxide anion (O<sub>2</sub><sup>•-</sup>) and also reduce the recombination of e<sup>-</sup>/dye<sup>+</sup> pairs by scavenging the electrons in the conduction band of TiO<sub>2</sub>.<sup>37</sup> Because platinum has the highest work function among metals, it is used extensively as a cocatalyst.<sup>43</sup> We found a significant effect of the Pt loading on phenol degradation. EY-sensitized TiO<sub>2</sub> without Pt metal can degrade phenol under visible light, but with the incorporation of 0.5 % Pt on TiO<sub>2</sub>, the degradation rate increases from 67 % to 100 % after 90 min of irradiation. Increasing the Pt content on the TiO<sub>2</sub> surface enhances the rate of photocatalytic degradation, as shown in Figure 6.9. In our experiments, we used different Pt contents between 0 % and 1.0 % and found improved degradation up to 0.5 % Pt content. Based on this finding, we used a 0.5 % Pt concentration as the optimum dose throughout this investigation. High metal loading can have a negative effect because it can behave as an e<sup>-</sup>/h<sup>+</sup> recombination center, as stated by Ni et al.<sup>17</sup> Accelerated e<sup>-</sup>/h<sup>+</sup> recombination by few transition metal loading was also reported by Ikeda et al.<sup>44</sup> Another reason might be that a high Pt dose could result in a decrease in phenol molecule adsorption sites, as well as an increase in the scattering of light and a decrease in its absorption by TiO<sub>2</sub>-(EY)s.<sup>43</sup>

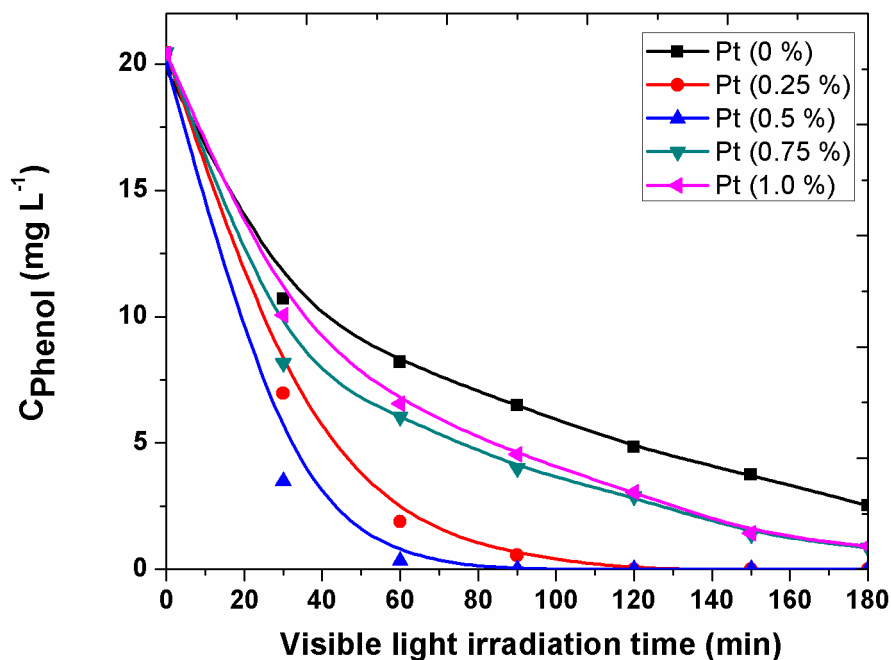
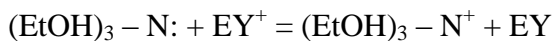


Figure 6.9 Residual phenol vs irradiation time plot at different platinum (wt %) on TiO<sub>2</sub>.

### 6.5.3 Effect of initial triethanolamine (TEOA) concentration

The role of TEOA can be viewed in light of its dual function because it could quench the oxidized form of the dye (EY<sup>+</sup>) or extend its lifetime in the photosensitized system, thereby providing efficient phenol degradation.<sup>45</sup> We performed our experiments from 0 to 0.5 M TEOA concentration and found an optimum dose of 0.2 M for phenol degradation at pH 7.0, as shown in Figure 6.10. TEOA solution itself is alkaline in nature and also can act as a buffer solution during phenol degradation. The oxidized dye species (EY<sup>+</sup>) can interact with both TEOA and phenol (or PhO<sup>-</sup>), and thus, a high TEOA concentration could slightly reduce the phenol degradation rate. The electron donor (TEOA) is used up through an irreversible oxidation that manifests itself in gradual darkening of the solution with time



TEOA exists more in a protonated form at pH 5 as compared to pH 9, where it is more deprotonated, and both forms exist at pH 7. The protonated form is a worse electron donor than the neutral form. Deprotonation of  $\text{TEOA}^+$  is a base-catalyzed reaction; its rate depends not only on the pH but also on the concentration of TEOA, which itself can act as a proton acceptor.<sup>46</sup>

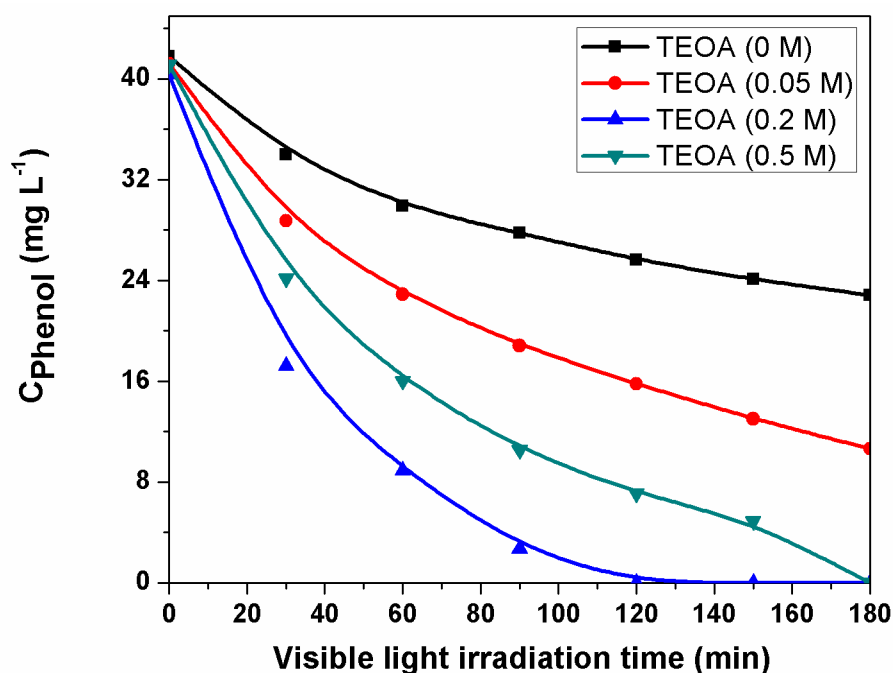


Figure 6.10 Residual phenol vs irradiation time plot at different concentration of TEOA.

#### 6.5.4 Effect of initial concentration of phenol

Initial pollutant concentration is crucial parameter in any water treatment process, and it is necessary to investigate its effect on the process performance. In this investigation, different concentration profiles were observed during the degradation of different starting

initial phenol concentrations. Between 54% and 100% of the phenol was degraded in 3 h by the EY modified  $\text{TiO}_2/\text{Pt}$  photocatalyst for initial phenol concentrations between 20 and 100  $\text{mg L}^{-1}$  (ppm), at a pH of 7.0 and a light intensity of  $100 \text{ mW cm}^{-2}$  (Figure 6.11). After 1 h, 98%, 78%, 56%, and 31% phenol degradations were achieved for initial phenol concentrations of 20, 40, 60, and 100  $\text{mg L}^{-1}$ , respectively. The time required afterward for the complete degradation of the aqueous phenol solution increased with increasing initial phenol concentration. This result can be explained by the fact that, at high initial phenol concentration, the quantity of phenol adsorbed on the EY- $\text{TiO}_2/\text{Pt}$  surface increases, which can suppress  $\text{HO}^\bullet$  radical formation through the decrease in the active sites for the adsorption of superoxide ions. Moreover, a high phenol concentration in the aqueous phase reduces the catalyst illumination and, thereby, photon absorption by the catalyst, resulting in a considerable decrease in phenol degradation. The apparent rate constant  $k_{\text{app}}$  ( $\text{min}^{-1}$ ) decreased with increasing initial concentration of phenol when the other parameters were kept unchanged. Therefore, the degradation rate was found to be pseudo-first-order with respect to the phenol concentration within the experimental range.

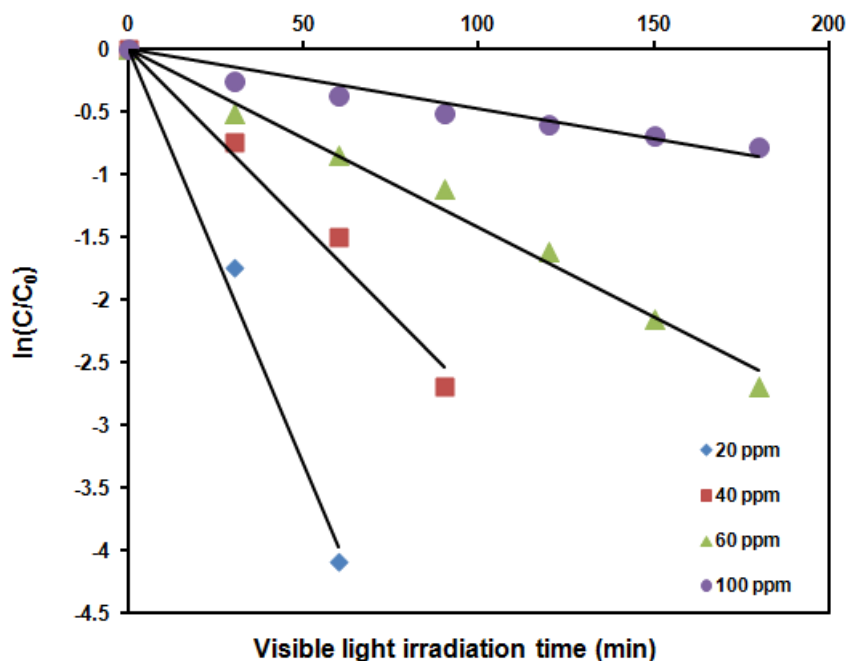


Figure 6.11 Initial phenol conc. vs irradiation time plot.

### 6.5.5 Effect of pH

In heterogeneous photocatalysis, if the photodegradation takes place on a catalyst surface, then pH plays a major role. The point of zero charge (pzc) for TiO<sub>2</sub> is about 6.8 at zero surface charge.<sup>7</sup> Hence, at alkaline pH (pH 9.0), the TiO<sub>2</sub> surface is negatively charged, and at acidic pH (pH 5.0), the surface is positively charged. Therefore, the pH value has a significant effect on the adsorption–desorption properties at the EY–TiO<sub>2</sub>/Pt surface



There was a drop in pH value from 7.0 to 6.3 during the 3 h experiment, which indicates the formation of acidic compounds during the reaction. However, we did not analyze for those acidic intermediates in this study. The acidic intermediates seem to be the most difficult compounds to be mineralized according to Mantzavinos et al.<sup>47</sup> Other intermediates such as aromatics (1,4-benzoquinone, hydroquinone, and catechol) that result from the reaction of hydroxyl radicals with phenol at the initial stage of the reaction undergo further photocatalytic oxidation to yield highly polar products such as aldehyde and carboxylic acid. We identified hydroquinone and catechol as intermediates (Figure 6.7) but detected no 1,4-benzoquinone. The aromatic intermediates disappeared some minutes after the disappearance of phenol. After reaching a maximum, the acids decreased with increasing reaction time, and at the end of the degradation process, phenol was completely mineralized to CO<sub>2</sub> and H<sub>2</sub>O.<sup>48</sup>

The effect of pH on the degradation of phenol is shown in Figure 6.12. The results indicate that pH has a significant effect at both low and high pH values where photodegradation rates are quite low. At pH 5.0, only 28 % phenol degradation was observed, which was quite similar to that at pH 9 (31 % degradation). At pH 9.0, EY–TiO<sub>2</sub>/Pt coagulates, and some of the dye leaches into the solution, imparting a pink

color to the solution. The optimum pH value for the degradation is 7.0, which gave 100 % phenol degradation after 2 h under similar experimental conditions.

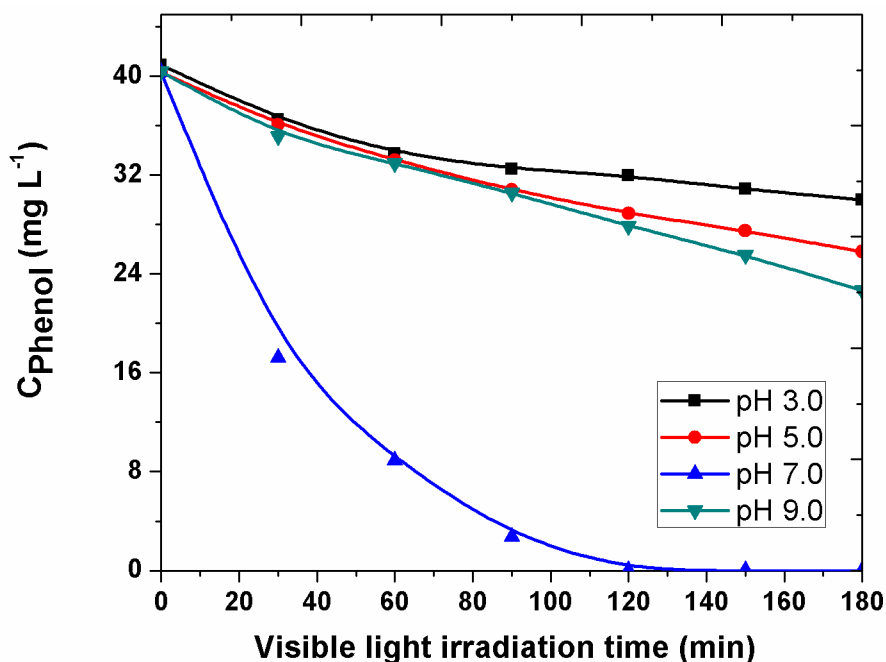
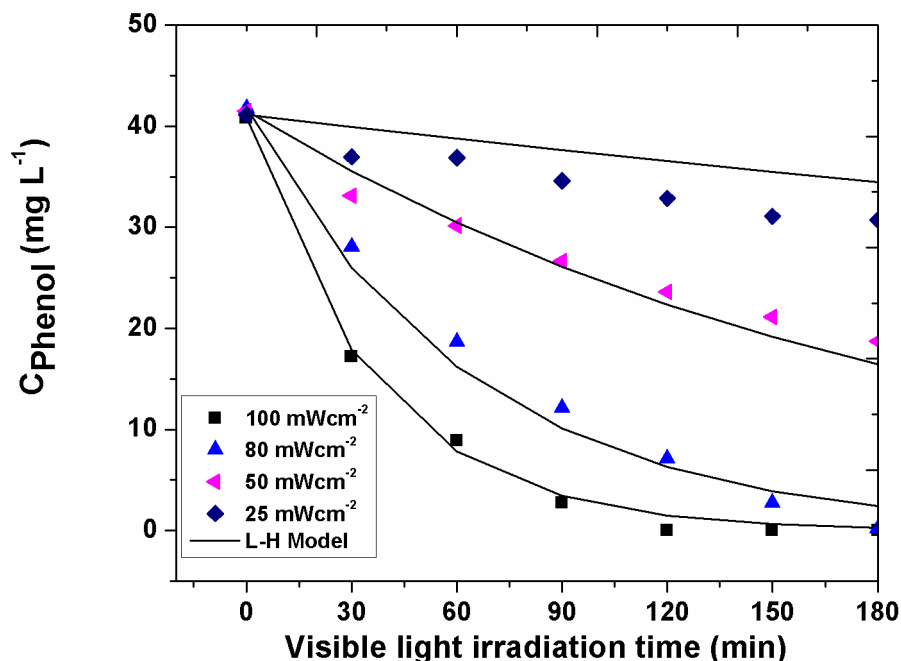


Figure 6.12 Residual phenol vs irradiation time plot at different solution pH.

### 6.5.6 Effect of light intensity

The incident light intensity is expected to be one of the rate-controlling parameters. To illustrate this effect, experiments were carried out at four different levels of incident light intensity, and the degradation rates at different times are reported in Figure 6.13. Previous studies on UV photodegradation have shown that the reaction rate increases with the square root of intensity at high intensity levels when mass-transfer limitations are not reached.<sup>7</sup> At sufficiently low levels of illumination (catalyst-dependent), on the other hand, the degradation rate is first-order in intensity.



**Figure 6.13 Phenol photo-degradation profiles at different irradiation intensities for both experimental and model plots.**

## 6.6 Phenol Degradation Kinetics

The photocatalytic degradation kinetics of many organic substrates have been analyzed in terms of Langmuir–Hinshelwood (L–H) rate equations.<sup>7,49,50</sup> Mostly in the literature, the L–H equation has been applied to describe the initial rate of degradation at time zero as a function of the initial substrate concentration. Less often, the L–H rate equation has been combined with the material, radiation, and momentum balance equations of the reactor to yield the dynamic or steady state behavior of the system.<sup>51–53</sup> An accurate degradation kinetic expression is very useful for the design, scale-up, and optimization of photocatalytic reactors and, therefore, for the development of photocatalytic degradation technology for industrial water treatment. In this study, a series of experiments was carried out for phenol degradation at pH 7.0, 40 ppm phenol concentration, and 0.8 g L<sup>-1</sup> EY–TiO<sub>2</sub>/Pt loading. As mentioned in sections 5.2 and 5.3, the optimum platinum

content and TEOA concentration were determined to be 0.5 % and 0.2 M, respectively. The light intensity was varied from 25 to 100 mW cm<sup>-2</sup>.

Mechanistic studies of photocatalytic degradation of phenol and its derivatives suggest a kinetic rate equation in the form of a modified L-H rate equation, given by the expression:

$$r_s = I_\alpha^\beta \frac{K_{app} C_{Ph}^0}{1 + K_A C_{Ph}^0} \quad (6.4)$$

Based on a parameter estimation using the experimental data, the values of  $\beta$ ,  $K_{app}$ , and  $K_A$  were obtained for the degradation of phenol at different irradiation intensities. Kinetics constants and their correlation coefficients are reported in Tables 6.1 and 6.2, respectively.

**Table 6.1 Kinetics constant values**

Constant	Value	Unit
$k_{app}$	$8.024 \times 10^{-6}$	min <sup>-1</sup>
$K_A$	0.134	ppm <sup>-1</sup>
$\beta$	2.147	-
error	93.85	
$r^2$	0.998	

**Table 6.2 Correlation coefficient values**

	$k_{app}$	$K_A$	$\beta$
$k_{app}$	1	0.9772	0.1101
$K_A$	0.9772	1	0.1259
$\beta$	0.1101	0.1259	1

The goodness of the model fit with the experimental data is reported in Figure 6.13. The kinetic equation can predict the concentration of phenol photodegradation during the entire degradation process and at different irradiation intensities at a pH value of 7.0 and an EY- TiO<sub>2</sub>/Pt concentration of 0.8 g L<sup>-1</sup>. Therefore, this model equation is meaningful. Table 3 presents a comparison between experimental phenol concentrations and the



model predictions at 100 mW cm<sup>-2</sup> light intensity. Good agreement between the experimental and predicted values was found for all cases.

**Table 6.3 Comparison between experimental phenol concentration and model prediction values at 100 mWcm<sup>-2</sup>**

<b>Irradiation time (min)</b>	<b>[Phenol] (mg L<sup>-1</sup>)</b>	<b>[Phenol]<sub>model</sub> (mg L<sup>-1</sup>)</b>	<b>Error</b>
0	40.8393	40.8393	0
30	17.2168	19.6152	5.7522
60	8.9238	9.4212	0.2474
90	2.7224	4.5250	3.2494
120	0	2.1734	4.7235
150	0	1.0439	1.0896
180	0	0.5014	0.2513
		Σerror	15.3136

## 6.7 Conclusions

Dye-sensitized photocatalysis was shown to be an efficient method for phenol degradation under visible solar light. The process involves electron transfer to the conduction band of  $\text{TiO}_2$  initiated by eosin Y dye sensitization under visible solar light. Eosin Y dye-sensitized  $\text{TiO}_2/\text{Pt}$  exhibited good visible light activity, as the band-gap energy dropped upon dye sensitization. The photogenerated electrons have a high oxidation potential and produce superoxide ( $\text{O}_2^{\bullet-}$ ) ions followed by  $\text{HO}^\bullet$ , which subsequently proceeds to the complete mineralization of phenol and other intermediates. Several reaction parameters were studied, and it was found that the catalyst dosage, solution pH, sacrificial electron-donor concentration, Pt content (wt %) on  $\text{TiO}_2$ , light intensity, and initial concentration of phenol mainly control the rate of phenol degradation. In this work, the optimum conditions for achieving maximum efficiency were established. A parametric study revealed that a high visible solar light intensity ( $80\text{--}100 \text{ mW cm}^{-2}$ ), moderate catalyst loading ( $0.8\text{--}1.0 \text{ g L}^{-1}$ ), low platinum content ( $0.25\text{--}0.5 \text{ wt } \%$ ) on  $\text{TiO}_2$ , moderate sacrificial electron-donor (TEOA) concentration ( $0.2 \text{ M}$ ), neutral pH ( $7.0$ ), and low initial phenol concentration advanced the photodegradation of phenol. At optimum conditions, 100 % phenol degradation was achieved in less than 2 h. Platinum loading and dye adsorption did not significantly affect the catalyst surface area, as is evident from BET data. With 0.5 % platinum incorporation on  $\text{TiO}_2$ , approximately 33 % improvement in photodegradation was achieved, which demonstrates the importance of the noble metal in the dye-sensitized photodegradation of phenol. The proposed L–H kinetic model is able to fit the experimental data for phenol degradation on EY– $\text{TiO}_2/\text{Pt}$  at different irradiation intensities. Experimental results were obtained at optimum conditions of catalyst loading, sacrificial electron-donor concentration, pH, and platinum content (wt %). Parameter optimization allowed for the application of a kinetic constant and absorption constant for a wide range of irradiation intensities.

## 6.8 References

1. Galvez, J. B.; Rodriguez, S. M., Solar Detoxification. *UNESCO Document* **2003**; p 19.
2. Hodes, G.; Gratzel, M., Photoelectrochemistry at semiconductor electrodes and small particles: A comparative study. *New Journal of Chemistry* **1984**, 8, (8-9), 509-520.
3. Ollis, D. F., Contaminants degradation in water. *Environmental Science & Technology* **1985**, 19, (6), 480-484.
4. Trillas, M.; Pujol, M.; Domenech, X., Phenol photodegradation over Titanium Dioxide. *Journal of Chemical Technology & Biotechnology* **1992**, 55, (1), 85-90.
5. Alemany, L. J.; Pardo, E.; Martin, F.; Galan-Fereres, M.; Blasco, J. M., Photodegradation of phenol in water using silica-supported titania catalysts. *Applied Catalysis B: Environmental* **1997**, 13, (3-4), 289-297.
6. Augugliaro, V.; Palmisano, L.; Sclafani, A.; Minero, C.; Pelizzetti, E., Photocatalytic degradation of phenol in aqueous titanium dioxide dispersions. *Toxicological and Environmental Chemistry* **1988**, 16, (2), 89-109.
7. Chen, D.; Ray, A. K., Photocatalytic kinetics of Phenol and its derivatives over UV radiation TiO<sub>2</sub>. *Applied Catalysis B: Environmental* **1999**, 23, (2-3), 143-157.
8. Ortiz-Gomez, A.; Serrano-Rosales, B.; Salaices, M.; de Lasa, H., Photocatalytic oxidation of Phenol: Reaction Network, kinetics modelling and Parameter Estimation. *Industrial & Engineering Chemistry Research* **2007**, 46, (23), 7394-7409.
9. Wang, Z.; Cai, W.; Hong, X.; Zhao, X.; Xu, F.; Cai, C., Photocatalytic degradation of phenol in aqueous nitrogen-doped TiO<sub>2</sub> suspensions with various light sources. *Applied Catalysis B: Environmental* **2005**, 57, (3), 223-231.

10. Kosowska, B.; Mozia, S.; Morawski, A. W.; Grzmil, B.; Janus, M.; Kalucki, K., The preparation of TiO<sub>2</sub>-nitrogen doped by calcinations of TiO<sub>2</sub>. xH<sub>2</sub>O under ammonia atmosphere for visible light photocatalysis. *Solar Energy Materials and Solar Cells* **2005**, 88, (3), 269-280.
11. Rehman, S.; Ullah, R.; Butt, A. M.; Gohar, N. D., Strategies of making TiO<sub>2</sub> and ZnO visible light active. *Journal of Hazardous Materials* **2009**, 170, (2), 560-569.
12. Gorska, P.; Zaleska, A.; Hupka, J., Photodegradation of phenol by UV/TiO<sub>2</sub> and Vis/N, C-TiO<sub>2</sub> processes: Comparative mechanistic and kinetic studies. *Separation and Purification Technology* **2009**, 68, (1), 90-96.
13. Ling, Q.; Sun, J.; Zhou, Q.; Ren, H.; Zhao, Q., Visible-light-driven titania/silica photocatalyst co-doped with boron and ferrum. *Applied Surface Science* **2008**, 254, (21), 6731-6735.
14. Ling, Q.; Sun, J.; Zhou, Q., Preparation and characterization of visible-light driven titania photocatalyst co-doped with boron and nitrogen. *Applied Surface Science* **2008**, 254, (10), 3236-3241.
15. Long, M.; Cai, W.; Cai, J.; Zhou, B.; Chai, X.; Wu, Y., Efficient photocatalytic degradation of phenol over Co<sub>3</sub>O<sub>4</sub>/BiVO<sub>4</sub> composite under visible light irradiation. *Journal of Physical Chemistry B* **2006**, 110, (41), 20211-20216.
16. Nahar, M. S.; Hasegawa, K.; Kagaye, S., Photocatalytic degradation of phenol by visible light-responsive iron doped TiO<sub>2</sub> and spontaneous sedimentation of the TiO<sub>2</sub> particles. *Chemosphere* **2006**, 65, (11), 1976-1982.
17. Ni, M.; Leung, M. K. H.; Leung, D. Y. C.; Samathy, L. K., A review and recent developments in photocatalytic water splitting using TiO<sub>2</sub> for hydrogen production. *Renewable and Sustainable Energy Reviews* **2007**, 11, (3), 401-425.

18. O'Regen, B.; Gratzel, M., A low cost high efficiency solar cell based on dye-sensitized colloidal TiO<sub>2</sub>-films. *Nature* **1991**, 353, (6364), 737-740.
19. Bach, U.; Lupo, D.; Comte, P.; Moser, J. E.; Weissortel, F.; Salbeck, J.; Spreitzer, H.; Gratzel, M., Solid-state dye-sensitized mesoporous TiO<sub>2</sub> solar cell with high photon to electron conversion efficiencies. *Nature* **1998**, 395, (6702), 583-585.
20. Karuppuchamy, S.; Nonomura, K.; Yoshida, T.; Sugiura, T.; Minoura, H., Cathodic electrodeposition of oxide semiconductor thin films and their application to dye-sensitized solar cells. *Solid State Ionics* **2002**, 151, (1), 19-27.
21. Mane, R. S.; Lew, W. J.; Pathan, H. M.; Han, S. H., Nanocrystalline TiO<sub>2</sub>/ZnO Thin Film: Fabrication and Application to dye-sensitized Solar Cells. *Journal of Physical Chemistry B* **2005**, 109, (51), 24254-24259.
22. Zhao, J.; Chen, C.; Ma, W., Photocatalytic degradation of organic pollutants under visible light irradiation. *Topics in Catalysis* **2005**, 35, (3), 269-278.
23. Ellingson, R. J.; Asbury, J. B.; Ferrere, S.; Ghosh, H. N.; Sprague, J. R.; Lian, T.; Nozik, A. J., Dynamics of Electron Injection in Nanocrystalline Titanium Dioxide Films Sensitized with [Ru(4, 4'-dicarboxy-2,2' bipyridine)<sub>2</sub> (NCS)<sub>2</sub>] by Infrared Transient Absorption. *Journal of Physical Chemistry B* **1998**, 102, (34), 6455-6458.
24. Galoppini, E., Linkers for anchoring sensitizers to semiconductor nanoparticles. *Coordination Chemistry Reviews* **2004**, 248, (13), 1283-1297.
25. Gratzel, M., Solar Energy Conversion by Dye-Sensitized Photovoltaic Cells. *Inorganic Chemistry* **2005**, 44, (20), 6841-6851.
26. Duncan, W. R.; Prezhdo, O. V., Theoretical Studies of Photoinduced Electron Transfer in Dye-sensitized TiO<sub>2</sub>. *Annual Review Physical Chemistry* **2007**, 58, 143-184.
27. Kim, W.; Tachikawa, T.; Majima, T.; Choi, W., Photocatalysis of Dye-Sensitized TiO<sub>2</sub> Nanoparticles with Thin Overcoat of Al<sub>2</sub>O<sub>3</sub>: Enhanced Activity for H<sub>2</sub> Production

and Dechlorination of  $\text{CCl}_4$ . *Journal of Physical Chemistry C* **2009**, 113, (24), 10603-10609.

28. Vinu, R.; Polisetti, S.; Madras, G., Dye sensitized visible light degradation of phenolic compounds. *Chemical Engineering Journal* **2010**, 165, (3), 784-797.

29. Qin, G.; Wu, Q.; Sun, Z.; Wang, Y.; Luo, J.; Xue, S., Enhanced photoelectron-catalytic degradation of phenols with bifunctionalized dye-sensitized  $\text{TiO}_2$  film. *Journal of Hazardous Materials* **2012**, 199-200, 226-232.

30. Chowdhury, P.; Goma, H.; Ray, A. K., Factorial design analysis for dye-sensitized hydrogen generation from water. *International Journal of Hydrogen Energy* **2011**, 36, (21), 13442-13451.

31. Suri, R. P. S.; Liu, J.; Hand, D. W.; Crittenden, J. C.; Perram, D. L.; Mullnis, M. E., Heterogeneous photocatalytic oxidation of hazardous organic contaminants in water. *Water Environment Research* **1993**, 65, (5), 665-673.

32. Bickley, R. I.; Gonzalez-Carreno, T.; Gonzalez-Elipé, A. R.; Munuera, G.; Palmisano, L., Characterization of Iron/Titanium Oxide Photocatalysts Part 2-surface studies. *Journal of Chemical Society, Faraday Transactions* **1994**, 90, (15), 2257-2264.

33. Sadeghi, M.; Liu, W.; Zhong, T. G.; Stavropoulos, P.; Levy, B., Role of photoinduced charge carrier separation distance in heterogeneous photocatalysis oxidative degradation of  $\text{CH}_3\text{OH}$  vapor in contact with Pt- $\text{TiO}_2$  and confirmed  $\text{TiO}_2$ - $\text{Fe}_2\text{O}_3$ . *Journal of Physical Chemistry* **1996**, 100, (50), 19466-19474.

34. Chatterjee, D.; Mahata, A.; Demineralization of organic pollutants on the dye-modified  $\text{TiO}_2$  semiconductor particulate system using visible light. *Applied Catalysis B: Environmental* **2001**, 33, (2), 119-125.

35. Chatterjee, D.; Dasgupta, S.; Rao, N. N., Visible light assisted photodegradation of halocarbons on the dye modified TiO<sub>2</sub> surface using visible light. *Solar Energy Materials and Solar Cells* **2006**, 90, (7), 1013-1020.
36. Abe, R.; Sayama, K.; Arakawa, H., Dye-sensitized photocatalysts for efficient hydrogen production from aqueous I<sup>-</sup> solution under visible light irradiation. *Journal of Photochemistry and Photobiology A: Chemistry* **2004**, 166, (1), 115-122.
37. Sakthivel, S.; Shankar, M. V.; Palanichamy, M.; Arabindoo, B.; Bahnemann, D. W.; Murugesan, V., Enhancement of Photocatalytic activity by metal adsorption: Characterization and photonic efficiency of Pt, Au and Pd deposited on TiO<sub>2</sub> catalyst. *Water Research* **2004**, 38, (13), 3001-3008.
38. Choi, J.; Park, H.; Hoffmann, M. R., Effects of single metal-ion doping on the visible-light photo reactivity of TiO<sub>2</sub>. *Journal of Physical Chemistry C* **2010**, 114, (2), 783-792.
39. Chakrabarti, S.; Chaudhuri, B.; Bhattacharjee, S.; Das, P.; Dutta, B. K., Degradation mechanism and kinetic model for photocatalytic oxidation of PVC-ZnO composite film in presence of a sensitizing dye and UV radiation. *Journal of Hazardous Materials* **2008**, 154, (1-3), 230-236.
40. Bhatkhande, D. S.; Pangarkar, V. G.; Beenackers, A. A., Photocatalytic degradation for environmental applications – a review. *Journal of Chemical Technology and Biotechnology* **2001**, 77, (1), 102-116.
41. Laoufi, N. A.; Tassalit, D.; Bentahar, F., The degradation of phenol in water solution by TiO<sub>2</sub> photocatalysis in a helical reactor. *Global NEST Journal* **2008**, 10, (3), 404-418.
42. Moreira, J.; Serrano, B.; Ortiz, A.; de Lasa, H., Evaluation of photon absorption in an aqueous TiO<sub>2</sub> slurry reactor using Monte Carlo Simulation and macroscopic Balance. *Industrial & Engineering Chemistry Research* **2010**, 49, (21), 10524-10534.

43. Li, Y.; Lu, G.; Li, S., Photocatalytic hydrogen generation and decomposition of oxalic acid over platinised TiO<sub>2</sub>. *Applied Catalysis A: General* **2001**, 214, (2), 179-185.
44. Ikeda, S.; Sugiyama, N.; Pal, B.; Marci, G.; Palmisano, L.; Noguchi, H.; Uosaki, K.; Ohtani, B., Photocatalytic activity of transition metal loaded titanium (IV) oxide powders suspended in aqueous solutions: correlation with electron-hole recombination kinetics. *Physical Chemistry Chemical Physics* **2001**, 3, (2), 267-273.
45. Zhang, X.; Jin, Z.; Li, Y.; Li, S.; Lu, G., Visible light induced hydrogen production over Pt-Eosin Y catalyst with high surface area silica gel as matrix. *Journal of Power Sources* **2007**, 166, (1), 74-79.
46. Kalyanasundaram, K.; Kiwi, J.; Gratzel, M., Hydrogen evolution from water by visible light, a homogeneous three component test system for redox catalysis. *Helvetica Chimica Acta* **1978**, 61, (7), 2720-2730.
47. Mantzavinos, D.; Hellenbrand, R.; Livingston, A. G., Metcalf, I. S., Catalytic wet oxidation of p-coumaric acid: Partial oxidation intermediates, reaction pathways and catalyst leaching. *Applied Catalysis B: Environmental* **1996**, 7, (3-4), 379-396.
48. Okamoto, K. I.; Yamamoto, Y.; Tanaka, H.; Tanaka, M.; Itaya, A., Heterogeneous photocatalytic decomposition of phenol over TiO<sub>2</sub> powder. *Bulletin of the Chemical Society of Japan* **1985**, 58, (7), 2015-2022.
49. Gora, A.; Toepfer, B.; Puddu, V.; Li Puma, G., Photocatalytic oxidation of herbicides in single component and multicomponent systems: Reaction kinetics analysis. *Applied Catalysis B: Environmental* **2006**, 65, (1), 1-10.
50. Hoffmann, M. R.; Martin, S. T.; Choi, W.; Bahnemann, D. W., Environmental Applications of Semiconductor Photocatalysis. *Chemical Reviews* **1995**, 95, (1), 69-96.



51. Puma, G. L.; Yue, P. L., Photocatalytic oxidation of chlorophenols in single-component and multicomponent systems. *Industrial & Engineering Chemistry Research* **1999**, 38, (9), 3238-3245.
52. Zalazar, C. S.; Romero, R. L.; Martin, C. A.; Cassano, A. E., Photocatalytic intrinsic reaction kinetics I: Mineralization of dichloroacetic acid. *Chemical Engineering Science* **2005**, 60, (19), 5240-5254.
53. Zhang, F.; Zhao, J.; Shen, T.; Hidaka, H.; Pelizzetti, E.; Serpone, N., TiO<sub>2</sub>-assisted photodegradation of dye pollutants II: Adsorption and degradation kinetics of eosin in TiO<sub>2</sub> dispersion under visible light irradiation. *Applied Catalysis B: Environmental* **1998**, 15, (1-2), 147-156.

## Chapter 7

### 7 Conclusions and Recommendations

This Ph.D. dissertation illustrates a research study on the application of solar and visible light photocatalysis for sacrificial hydrogen generation and water detoxification with chemically modified TiO<sub>2</sub>. Dye sensitization technique is applied to modify the photocatalytic activity of TiO<sub>2</sub> in the solar and visible light spectrum. Reaction kinetics, parametric studies and well as reaction mechanism are performed for sacrificial hydrogen generation and water detoxification. The basic aspiration is to recognize the applicability of TiO<sub>2</sub> based photocatalysts under solar light that is abundant and available free of cost.

The potential of eosin Y-sensitized platinum loaded TiO<sub>2</sub> photocatalyst was established for sacrificial hydrogen generation as well as phenol degradation in presence of triethanolamine as electron donor. A solar simulator was used as light source which provided UV, visible and complete solar spectra with the help of different optical filters. Several analytical instruments such as Gas Chromatography (equipped with a TCD), High Performance Liquid Chromatography (HPLC), UV-Vis-NIR spectrophotometer, QuantaMaster<sup>TM</sup> 40, HACH spectrophotometer, StellarNet EPP2000C-25LT16 spectrometer, were employed for quantification of H<sub>2</sub>, analysis of phenol and its intermediate, analysis of eosin Y and triethanolamine, photoluminescence measurement, quantification of formaldehyde, and for measuring photon fluxes, respectively.

#### 7.1 Major Contributions

The following are the significant contributions of this Ph.D. research.

- Most of the studies were done at low intensity range with 300-400 W lamps. Effect of different light intensities on hydrogen generation was verified in this report, which was a necessary step for utilization of natural solar light. Apparent quantum yields at different light intensities were also evaluated. Individual effect of UV and visible spectra were determined for

hydrogen generation, and the correlation between UV, visible, and solar light irradiation for hydrogen generation was also evaluated.

- ❑ Photoluminescence (PL) spectroscopy was used to verify the electron/hole recombination process, which was correlated with UV, visible and solar light at different light intensities.
- ❑ With triethanolamine as electron donor, formaldehyde was detected in solar and visible light. The hydrogen generation process in solar light was a combination of band gap excitation and dye sensitization that was confirmed by estimating residual concentration of formaldehyde.
- ❑ Detailed study was performed with formaldehyde for photocatalytic hydrogen generation. The heterogeneous rate of hydrogen generation was well fitted with a Langmuir type model.
- ❑ To overcome the mass transfer limitation, a flow reactor was designed which utilized a peristaltic pump with controller to generate both uni- and bi-directional flows. Effects of sonication, flow rate and flow direction on hydrogen generation were established.
- ❑ Solar light based platinum photo-deposition method was introduced for the first time, which should saved energy and cost. This method showed excellent efficiency for both H<sub>2</sub> generation and phenol degradation.
- ❑ Statistical analysis was performed using design of experiment for hydrogen generation using eosin Y-sensitized TiO<sub>2</sub>/Pt. This method provided a quantitative assessment of the principal factors and effects that influenced hydrogen generation performance.
- ❑ Phenol degradation was studied for the first time with this new photocatalyst in presence of triethanolamine. The photogenerated electrons have a high oxidation potential and produce superoxide (O<sub>2</sub><sup>•-</sup>)

ions followed by  $\text{HO}^\bullet$ , which subsequently proceeds to complete degradation of phenol and other intermediates.

## 7.2 Other Key Contributions

- ❑ Diffuse reflectance spectra supported the visible light activity of eosin Y – sensitized Pt loaded  $\text{TiO}_2$ . X-ray diffraction spectra confirmed that  $\text{TiO}_2$  was mostly in anatase form, and with Pt loading the surface area did not change. FTIR results suggested the presence of ester like linkage with eosin Y and  $\text{TiO}_2$  surface in the photocatalyst. EDX results reported the presence of Pt metal on  $\text{TiO}_2$  surface.
- ❑ Based on factorial design analysis, solution pH and light irradiation time showed positive effects on hydrogen generation whereas Pt content (wt %) showed negative effect on hydrogen generation. Eosin Y and triethanolamine concentration have shown moderate positive effects on hydrogen generation although their interaction effect was insignificant compared to other parameters.
- ❑ Neutral pH, 0.25 wt % of Pt on  $\text{TiO}_2$ , photocatalyst mass of 1-1.3  $\text{g L}^{-1}$  were achieved as optimum levels for sacrificial hydrogen generation in solar and visible light. Hydrogen generation rate varied as a function of triethanolamine concentration according to Langmuir-type isotherm.
- ❑ In solar light, hydrogen generation rate increased by 1.4 and 1.2 times by sensitization with eosin Y on  $\text{TiO}_2$  and  $\text{TiO}_2/\text{Pt}$  respectively. An additional improvement of 4.7 and 4.1 times in hydrogen generation was achieved by Pt loading on both  $\text{TiO}_2$  and EY- $\text{TiO}_2$  respectively. With the incorporation of Pt a huge improvement in hydrogen generation rate was achieved compared to eosin Y-sensitized  $\text{TiO}_2$  alone in visible light.

- ❑ Eosin Y to TiO<sub>2</sub>/Pt mass ratio was shown to be a key parameter for hydrogen generation. Optimum mass ratios (EY : TiO<sub>2</sub>/Pt) of 1:10 and 1:13.3 were obtained in visible and solar light respectively.
- ❑ The reaction mechanisms for sacrificial hydrogen generation in solar and visible light were quite different. In visible light, dye sensitization mechanism worked whereas in solar light both band gap excitation and dye sensitization mechanism operated simultaneously. In both cases formaldehyde was detected as an intermediate product. In solar light, formaldehyde was oxidized by h<sup>+</sup>/OH<sup>•</sup> to produce hydrogen, whereas in visible light formaldehyde was not oxidized any further.
- ❑ Recombination of e<sup>-</sup>/h<sup>+</sup> and/or e<sup>-</sup>/oxidized eosin Y (EY<sup>+</sup>) were determined through photoluminescence (PL) study, which illustrated the higher recombination rates in case of visible light compared to that of solar and UV light. The recombination rate increased with light intensity upon which depend the apparent quantum yields (QY). With the increase of light intensity QY was gradually dropped, which was also supported by the PL spectra.
- ❑ A pulsating flow reactor was used for the hydrodynamic study of solar hydrogen generation. It confirmed the positive effect of pre-sonication, increased flow rate and bi-directional mixing mode in solar hydrogen generation.
- ❑ Photocatalytic hydrogen generation from formaldehyde was affected by solution pH, Pt content (wt %) on TiO<sub>2</sub>, catalyst concentration, light intensity, and initial formaldehyde concentration. The optimum conditions were achieved as follows: i) I<sub>solar</sub> - 1sun (100 mW cm<sup>-2</sup>), ii) platinum content – 0.25 wt%, iii) catalyst concentration – 1 g L<sup>-1</sup>, and iv) pH-neutral to alkaline. The proposed Langmuir-type model fitted well with

the experimental data for hydrogen generation at different initial concentrations of formaldehyde. Degradation of formaldehyde and hydrogen production took place simultaneously with high apparent quantum yield (10.91 %).

- Eosin Y-sensitized photocatalysis was shown to be an efficient method for phenol degradation under visible solar light. A parametric study revealed that a high visible solar light intensity (80–100 mW cm<sup>-2</sup>), moderate catalyst loading (0.8–1.0 g L<sup>-1</sup>), low platinum content (0.25–0.5 wt %) on TiO<sub>2</sub>, moderate sacrificial electron-donor (triethanolamine) concentration (0.2 M), neutral pH (7.0), and low initial phenol concentration enhanced the photodegradation of phenol. At optimum conditions, 100 % phenol degradation was achieved in less than 2 h. The proposed L–H kinetic model was able to fit the experimental data for phenol degradation on eosin Y-sensitized TiO<sub>2</sub>/Pt at different irradiation intensities.

### 7.3 Recommendations for Future Work

Following are the recommendations for further studies:

- ❖ Detailed study for solar photo-deposition method is required to be performed for further improvement of the photocatalyst.
- ❖ Preliminary hydrodynamic study using FLUENT showed dead zones in the flow reactor. Efforts were made to eliminate those dead zone using baffles inside the reactor as described in Appendix G. More systematic computational fluid dynamics study is required for better reactor design.
- ❖ Fractional factorial design approach can be used to include a large number of parameters for statistical design analysis.

- ❖ Since triethanolamine was present in the system during phenol degradation, initial TOC values were quite high. To achieve complete mineralization, longer duration needs to be considered in future research.
- ❖ Since phenol degradation was studied in visible light only, the use of complete solar spectra for phenol degradation need to be explored in future studies.
- ❖ A better IR filter should be used to remove IR that heats up the system.
- ❖ Natural dye can be extracted and used for dye-sensitization of TiO<sub>2</sub>/Pt photocatalyst.

## APPENDIX

### A. Appendix A: Dye Absorption Spectra

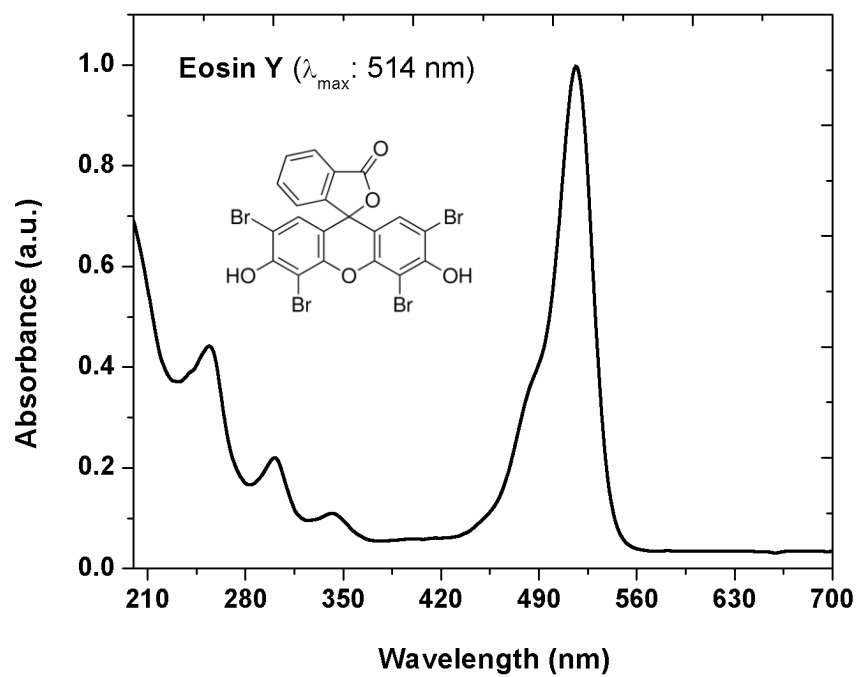


**Figure A.1** UV-vis absorption spectrum of  $9.65 \times 10^{-3}$  mM Eosin Y in aqueous solution



## B. Appendix B: Calibration Plot –H<sub>2</sub> Gas

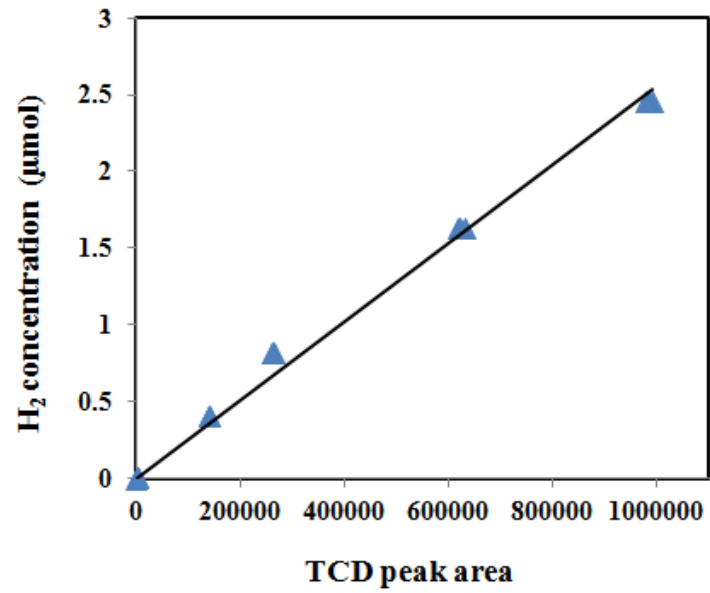


Figure B.1 TCD calibration curve for hydrogen

$$Y_{\text{H}_2} = 3 \times 10^{-6} X \quad (\text{B.1})$$

where,  $Y_{\text{H}_2}$  is the hydrogen concentration ( $\mu\text{mol}$ ) and  $X$  is the TCD peak area.

Equation B.1 reports the equation for the calibration curve that was obtained from the GC/TCD data with a  $R^2$  value of 0.993.

**Calculation of total H<sub>2</sub> generation:**

- mole fraction is calculated from the GC calibration curve.
- then the following formulae are used for the calculation of total amount of hydrogen in the reactor:

$$n_{H_2} = \frac{P_{H_2} V_{H_2}}{RT} \quad (\text{B.2})$$

$$P_{H_2} = x_{H_2} \times P \quad (\text{B.3})$$

where,  $n_{H_2}$  is number of moles of hydrogen,  $P$  is the total pressure of the reactor; the hydrogen will instantaneously occupy the overhead volume of the reactor in a well mixed system.  $R$  is universal gas constant ( $8.314 \text{ N m mol}^{-1} \text{ K}^{-1}$ ) and  $T$  is temperature (K).

## C. Appendix C: Details of Photoreactors

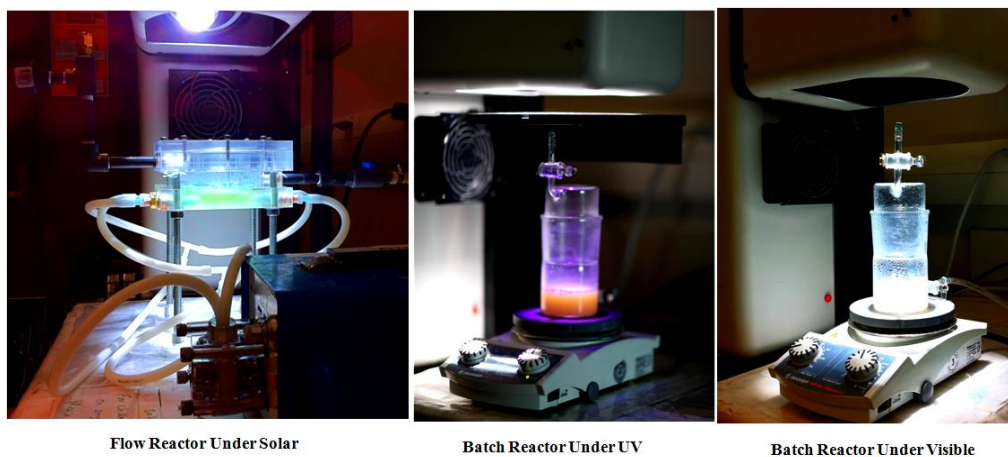


**Figure C.1 Batch and flow reactor configuration under different light sources.**

i) Batch reactor used in sacrificial hydrogen generation from triethanolamine (Chapter-4) and formaldehyde (Chapter-5):

Total volume = 530 mL; Illumination from the top through 6.5 cm diameter. Magnetic stirrer was used for mixing. Reaction mixture volume = 100 mL. System was saturated with N<sub>2</sub> gas.

ii) Flow reactor used in sacrificial hydrogen generation from triethanoamine (Chapter-4):

Total volume = 500 mL; Illumination from the top through 9 cm diameter. Peristaltic pump was used for mixing with a maximum flow of 1.62 L min<sup>-1</sup>. Reaction mixture volume = 200 mL. System was saturated with N<sub>2</sub> gas.

**Flow reactor diagram (Chapter-4):**

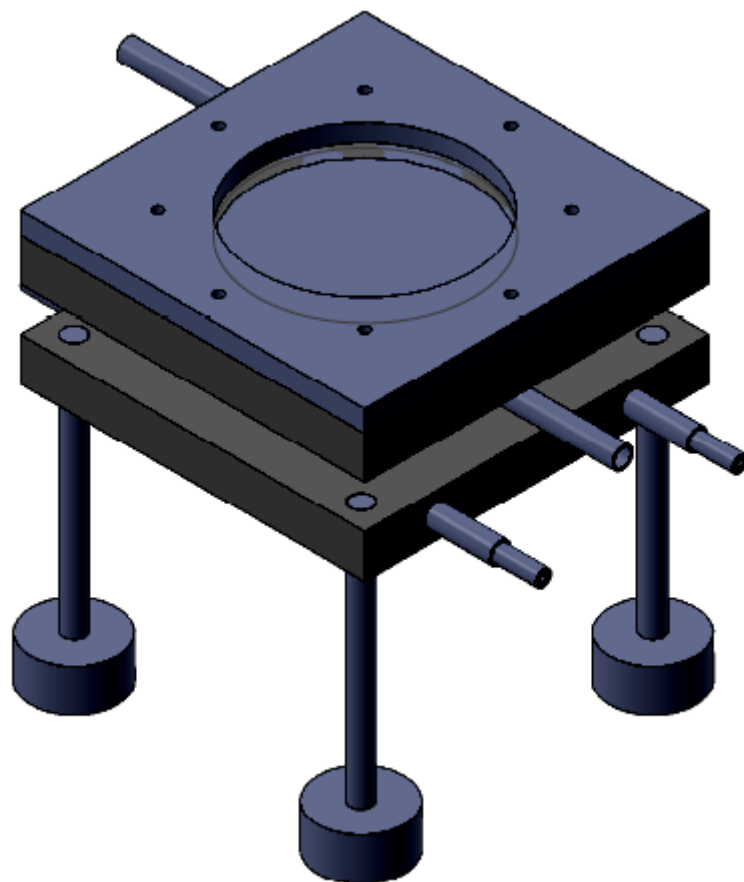


**Figure C.2 Flow reactor for sacrificial hydrogen generation**

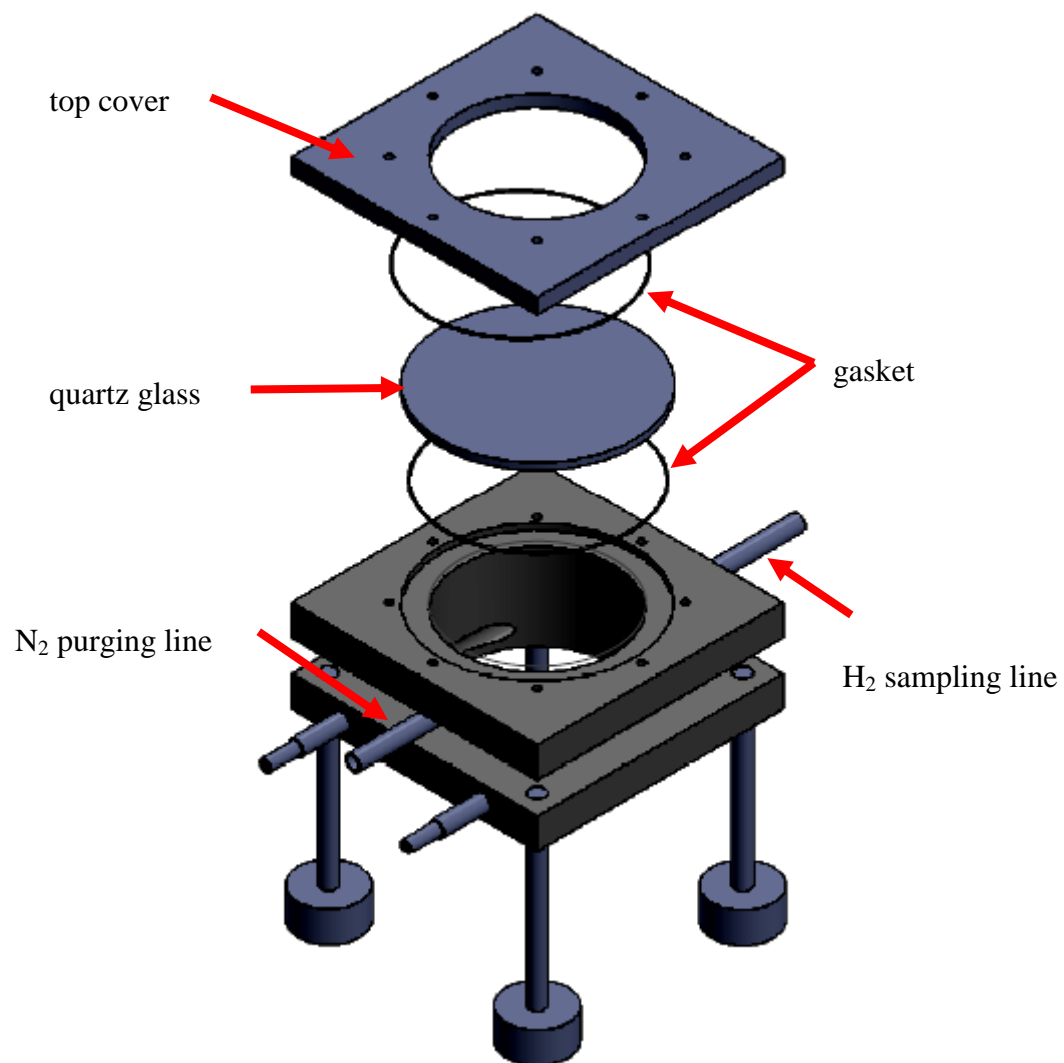


**Figure C.3 Flow reactor exploded view**

## D. Appendix D: Eosin Y Degradation under Different Light Sources

### 1. Effect of light sources on Eosin Y degradation:

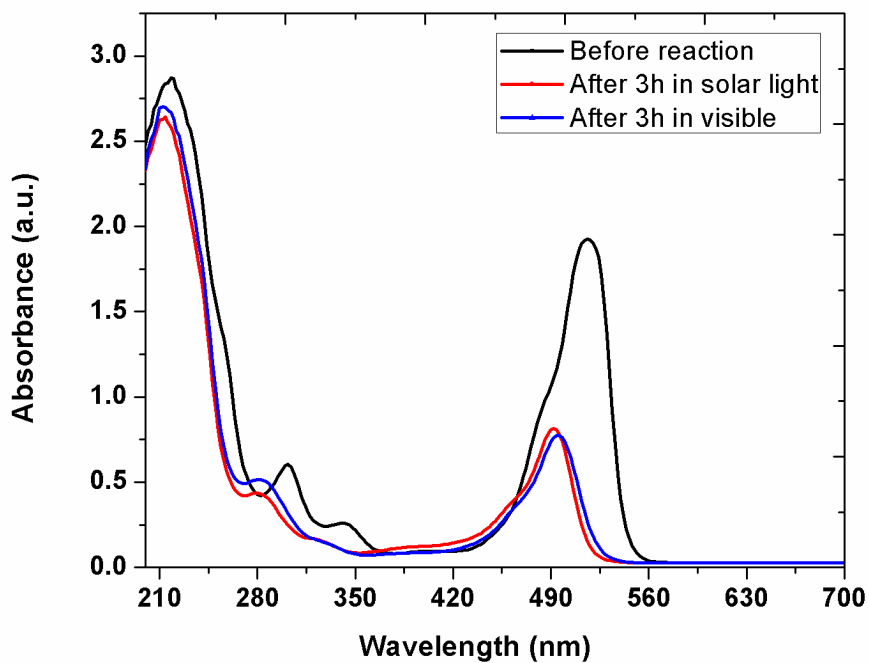


**Figure D.1 Eosin Y degradation under solar and visible light.**

Experimental conditions:  $[EY]=3.86 \times 10^{-2}$  mM,  $I=100$  mW  $\text{cm}^{-2}$ ,  
 $[TEOA]=0.25$  M.

## 2. Effect of UV, visible and solar light intensity on Eosin Y degradation:

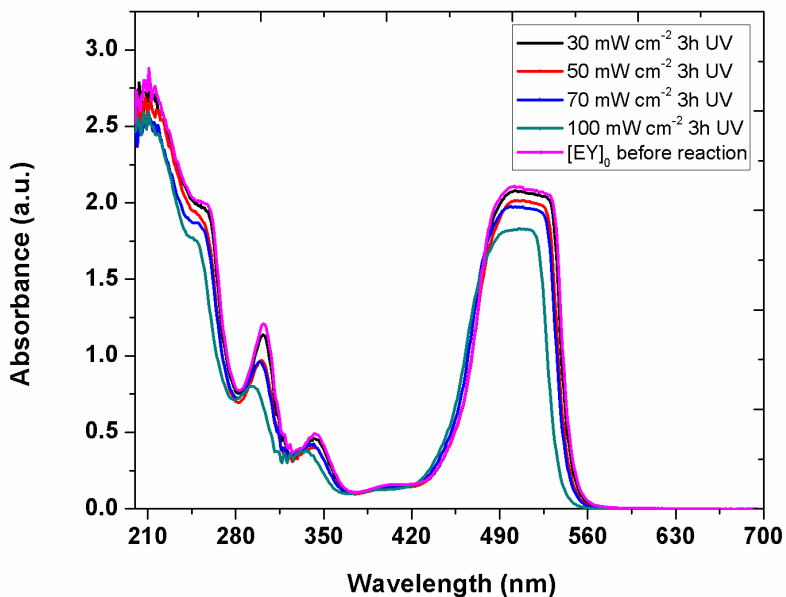


Figure D.2 Effect of UV light intensity on Eosin Y degradation.

Experimental conditions: [EY]= $7.72 \times 10^{-2}$  mM, [TEOA]=0.25 M.

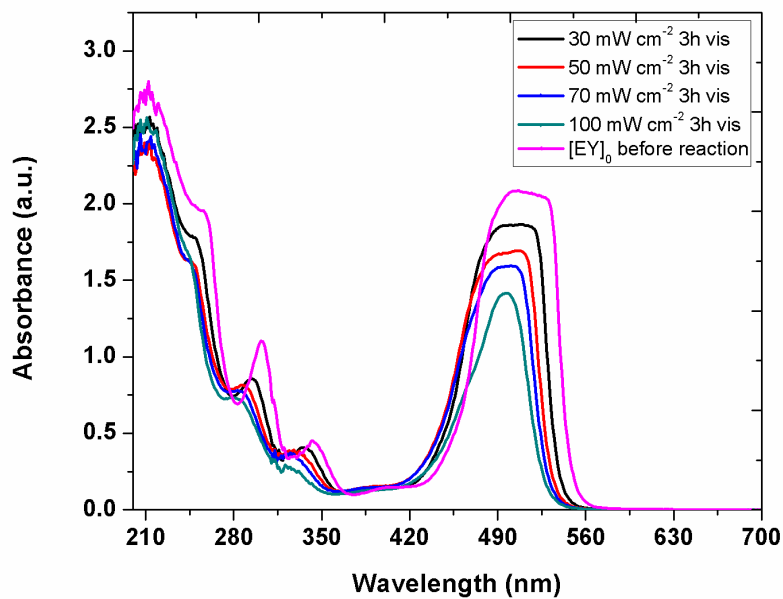
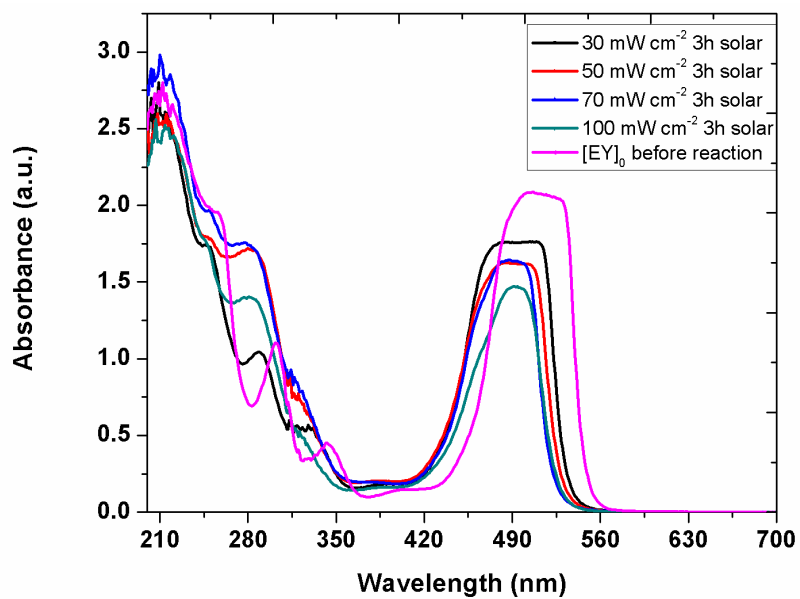


Figure D.3 Effect of visible light intensity on Eosin Y degradation.

Experimental conditions: [EY]= $7.72 \times 10^{-2}$  mM, [TEOA]=0.25 M.



**Figure D.4 Effect of solar light intensity on Eosin Y degradation.**  
Experimental conditions: [EY]= $7.72 \times 10^{-2}$  mM, [TEOA]=0.25 M.



## E. Appendix E: Light Spectra of Solar Simulator

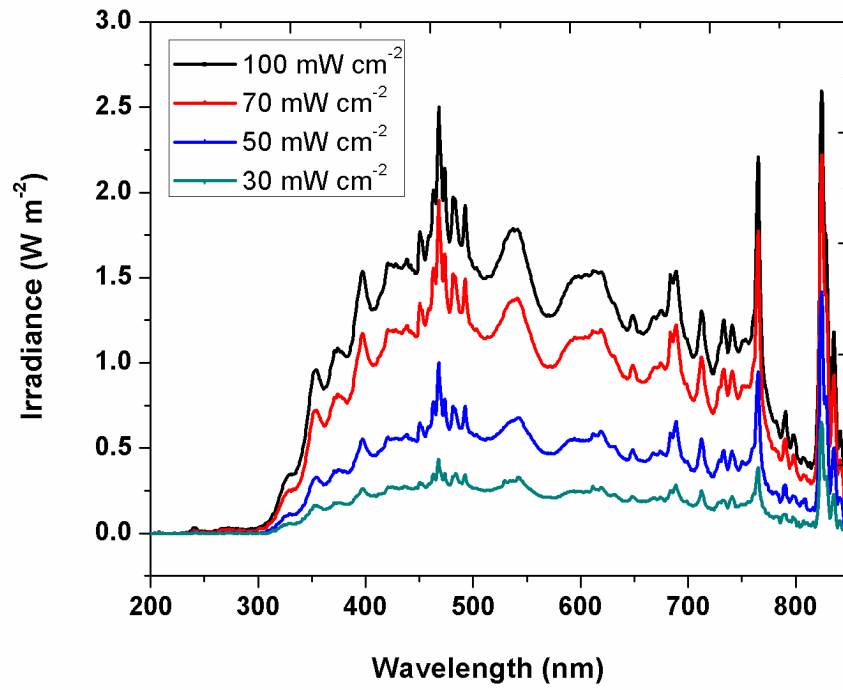
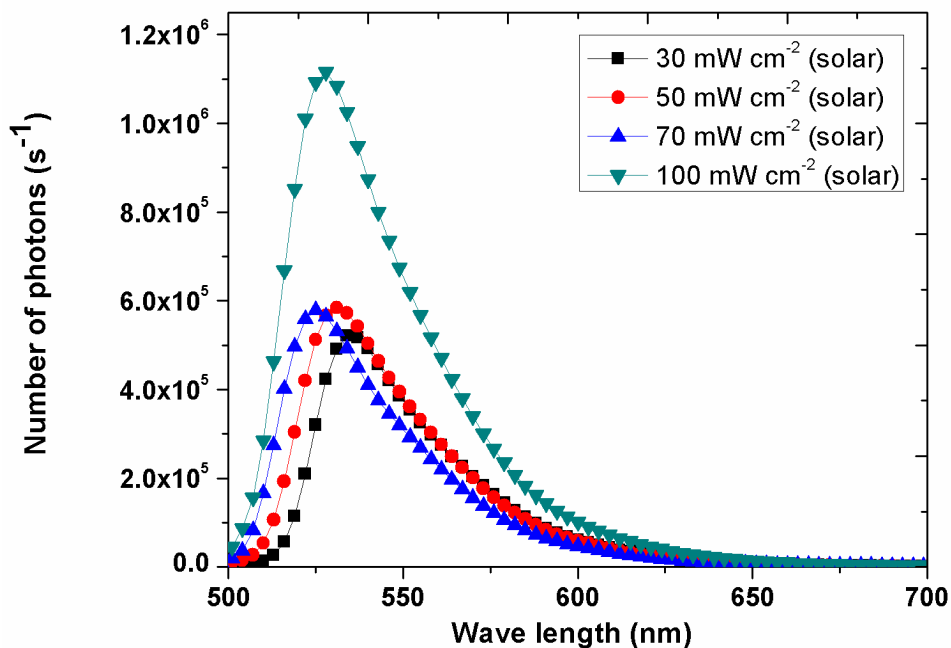


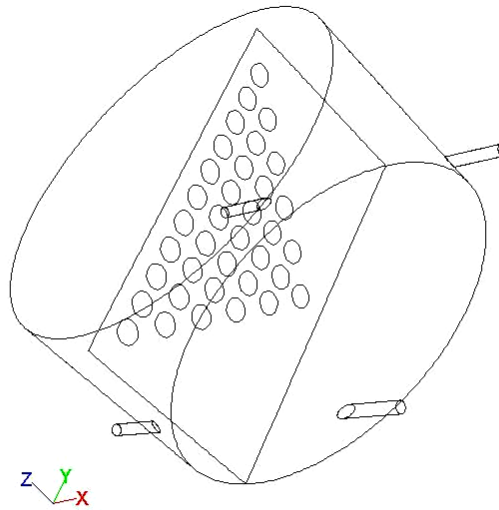
Figure E.1 Solar simulator light spectra at different intensities.

## F. Appendix F: PL Spectra under UV, Visible and Solar light



**Figure F.1** PL spectra EY-TiO<sub>2</sub>/Pt catalyst solution at different solar light intensities showing higher e<sup>-</sup>/h<sup>+</sup> recombination rate at higher light intensities. Experimental conditions: [EY]=7.72 x 10<sup>-2</sup> mM, [TEOA]=0.25 M. EY-TiO<sub>2</sub>/Pt (0.25 %)= 1g L<sup>-1</sup>.

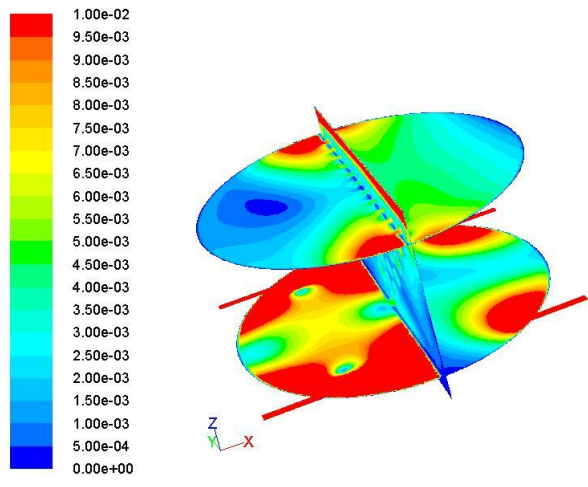
## G. Appendix G: Flow Reactor Modifications



Mesh

May 12, 2012  
ANSYS FLUENT 12.1 (3d, pbns, ske)

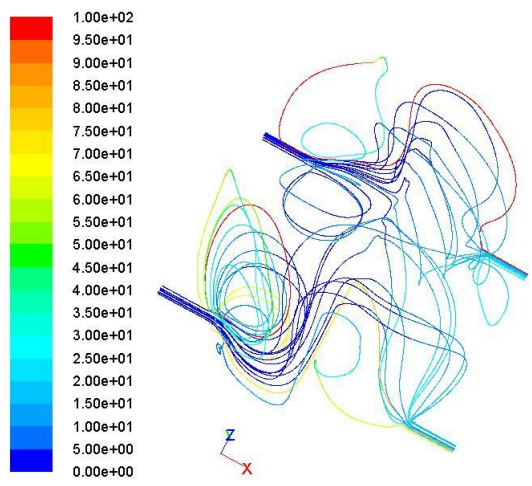
**Figure G.1 Proposed modified flow reactor with baffle.**



Contours of Velocity Magnitude (m/s)

May 12, 2012  
ANSYS FLUENT 12.1 (3d, pbns, ske)

**Figure G.2 Modified flow reactor with minimum dead zones.**



Particle Traces Colored by Particle Residence Time (s)

May 13, 2012  
ANSYS FLUENT 12.1 (3d, pbns, ske)

**Figure G.3 Particle tracking for modified flow reactor.**

## H. Appendix H: Calibration Curves for Phenol

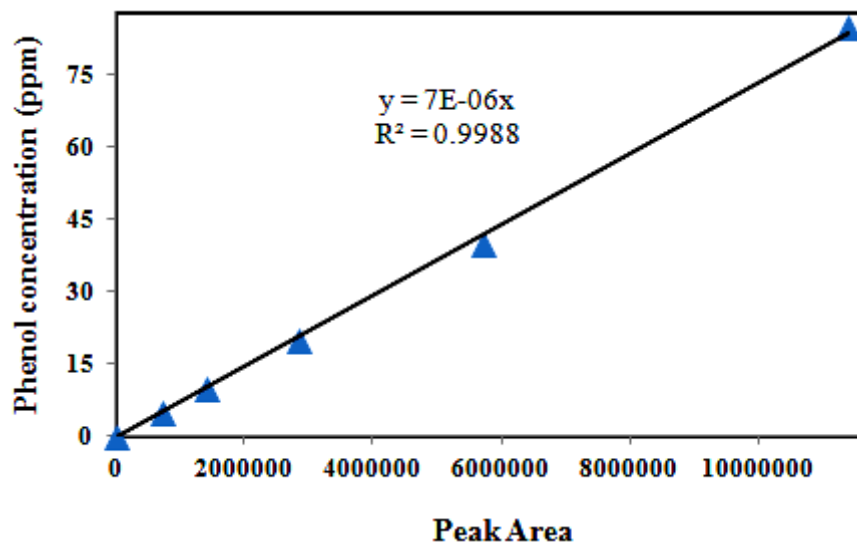


Figure H.1 Calibration curve for aqueous solution of phenol.

# I. Appendix I: Copyright Informations

Chapter-1 copyright permission:



**International Journal of Hydrogen Energy**

5794 SW 40<sup>th</sup> St. # 303, Miami, FL 33155, U.S.A.



11 June 2012

To: Pankaj Chowdhury [REDACTED]

Cc: Emre A. Veziroglu [REDACTED]

Subject: Copyright PermissionDear Pankaj:

Thank you very much for your email of 9 June 2012. In accordance with your request, we hereby give you permission to use the following figure in your Thesis/Dissertation:

Figure 1. Global energy system transition, 1850-2150

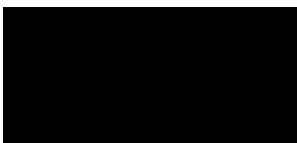
Article Title: Hydrogen futures: toward a sustainable energy system

Author: Seth Dunn

Source: International Journal of Hydrogen Energy, Volume 27 (2002), Pages 235-264.

Wishing you all the best in your endeavors, I remain

Sincerely yours,



T. Nejat Veziroglu

Founding Editor-in-Chief, International Journal of Hydrogen Energy

## Chapter-2 copyright permission:



# RightsLink®

[Home](#)[Account Info](#)[Help](#)

**Title:** Linkers for anchoring sensitizers to semiconductor nanoparticles  
**Author:** Elena Galoppini  
**Publication:** Coordination Chemistry Reviews  
**Publisher:** Elsevier  
**Date:** July 2004  
Copyright © 2004, Elsevier

Logged in as:  
PANKAJ CHOWDHURY  
Account # :  
3000538883

[LOGOUT](#)

### Order Completed

Thank you very much for your order.

This is a License Agreement between PANKAJ CHOWDHURY ("You") and Elsevier ("Elsevier"). The license consists of your order details, the terms and conditions provided by Elsevier, and the [payment terms and conditions](#).

[Get the printable license.](#)

License Number	2919221194278
License date	May 31, 2012
Licensed content publisher	Elsevier
Licensed content publication	Coordination Chemistry Reviews
Licensed content title	Linkers for anchoring sensitizers to semiconductor nanoparticles
Licensed content author	Elena Galoppini
Licensed content date	July 2004
Licensed content volume number	248
Licensed content issue number	13-14
Number of pages	15
Type of Use	reuse in a thesis/dissertation
Portion	figures/tables/illustrations
Number of figures/tables /illustrations	1
Format	both print and electronic
Are you the author of this Elsevier article?	No
Will you be translating?	No
Order reference number	
Title of your thesis/dissertation	Solar and Visible Light Driven Photocatalysis for Sacrificial Hydrogen Generation and Water Detoxification with Chemically Modified TiO <sub>2</sub>
Expected completion date	Aug 2012
Estimated size (number of pages)	180
Elsevier VAT number	GB 494 6272 12
Permissions price	0.00 USD
VAT/Local Sales Tax	0.0 USD / 0.0 GBP
Total	0.00 USD

[ORDER MORE...](#)[CLOSE WINDOW](#)

Copyright © 2012 [Copyright Clearance Center, Inc.](#) All Rights Reserved. [Privacy statement](#). Comments? We would like to hear from you. E-mail us at [customercare@copyright.com](mailto:customercare@copyright.com)

**ELSEVIER LICENSE  
TERMS AND CONDITIONS**

May 31, 2012

---

---

This is a License Agreement between PANKAJ CHOWDHURY ("You") and Elsevier ("Elsevier") provided by Copyright Clearance Center ("CCC"). The license consists of your order details, the terms and conditions provided by Elsevier, and the payment terms and conditions.

**All payments must be made in full to CCC. For payment instructions, please see information listed at the bottom of this form.**

Supplier	Elsevier Limited The Boulevard, Langford Lane Kidlington, Oxford, OX5 1GB, UK
Registered Company Number	1982084
Customer name	PANKAJ CHOWDHURY
Customer address	████████████████████ ████████████████████
License number	2919221194278
License date	May 31, 2012
Licensed content publisher	Elsevier
Licensed content publication	Coordination Chemistry Reviews
Licensed content title	Linkers for anchoring sensitizers to semiconductor nanoparticles
Licensed content author	Elena Galoppini
Licensed content date	July 2004
Licensed content volume number	248
Licensed content issue number	13-14
Number of pages	15
Start Page	1283
End Page	1297
Type of Use	reuse in a thesis/dissertation
Portion	figures/tables/illustrations
Number of figures/tables /illustrations	1
Format	both print and electronic
Are you the author of this Elsevier article?	No
Will you be translating?	No
Order reference number	
Title of your thesis/dissertation	Solar and Visible Light Driven Photocatalysis for Sacrificial Hydrogen Generation and Water Detoxification with Chemically Modified TiO <sub>2</sub>



Expected completion date	Aug 2012
Estimated size (number of pages)	180
Elsevier VAT number	GB 494 6272 12
Permissions price	0.00 USD
VAT/Local Sales Tax	0.0 USD / 0.0 GBP
Total	0.00 USD
Terms and Conditions	

## INTRODUCTION

1. The publisher for this copyrighted material is Elsevier. By clicking "accept" in connection with completing this licensing transaction, you agree that the following terms and conditions apply to this transaction (along with the Billing and Payment terms and conditions established by Copyright Clearance Center, Inc. ("CCC"), at the time that you opened your Rightslink account and that are available at any time at <http://myaccount.copyright.com>).

## GENERAL TERMS

2. Elsevier hereby grants you permission to reproduce the aforementioned material subject to the terms and conditions indicated.

3. Acknowledgement: If any part of the material to be used (for example, figures) has appeared in our publication with credit or acknowledgement to another source, permission must also be sought from that source. If such permission is not obtained then that material may not be included in your publication/copies. Suitable acknowledgement to the source must be made, either as a footnote or in a reference list at the end of your publication, as follows:

“Reprinted from Publication title, Vol /edition number, Author(s), Title of article / title of chapter, Pages No., Copyright (Year), with permission from Elsevier [OR APPLICABLE SOCIETY COPYRIGHT OWNER].” Also Lancet special credit - “Reprinted from The Lancet, Vol. number, Author(s), Title of article, Pages No., Copyright (Year), with permission from Elsevier.”

4. Reproduction of this material is confined to the purpose and/or media for which permission is hereby given.

5. Altering/Modifying Material: Not Permitted. However figures and illustrations may be altered/adapted minimally to serve your work. Any other abbreviations, additions, deletions and/or any other alterations shall be made only with prior written authorization of Elsevier Ltd. (Please contact Elsevier at [permissions@elsevier.com](mailto:permissions@elsevier.com))

6. If the permission fee for the requested use of our material is waived in this instance, please be advised that your future requests for Elsevier materials may attract a fee.

7. Reservation of Rights: Publisher reserves all rights not specifically granted in the combination of (i) the license details provided by you and accepted in the course of this licensing transaction, (ii) these terms and conditions and (iii) CCC's Billing and Payment terms and conditions.

8. License Contingent Upon Payment: While you may exercise the rights licensed immediately upon issuance of the license at the end of the licensing process for the transaction, provided that you have disclosed complete and accurate details of your proposed use, no license is finally effective unless and until full payment is received from you (either by publisher or by CCC) as provided in CCC's Billing and Payment terms and conditions. If full payment is not received on a timely basis, then any license preliminarily granted shall be deemed automatically revoked and shall be void as if never granted. Further, in the event that you breach any of these terms and conditions or any of CCC's Billing and Payment terms and conditions, the license is automatically revoked and shall be void as if never granted. Use of materials as described in a revoked license, as well as any use of the materials beyond the scope of an unrevoked license, may constitute copyright infringement and publisher reserves the right to take any and all action to protect its copyright in the materials.

9. Warranties: Publisher makes no representations or warranties with respect to the licensed material.

10. Indemnity: You hereby indemnify and agree to hold harmless publisher and CCC, and their respective officers, directors, employees and agents, from and against any and all claims arising out of your use of the licensed material other than as specifically authorized pursuant to this license.

11. No Transfer of License: This license is personal to you and may not be sublicensed, assigned, or transferred by you to any other person without publisher's written permission.

12. No Amendment Except in Writing: This license may not be amended except in a writing signed by both parties (or, in the case of publisher, by CCC on publisher's behalf).

13. Objection to Contrary Terms: Publisher hereby objects to any terms contained in any purchase order, acknowledgment, check endorsement or other writing prepared by you, which terms are inconsistent with these terms and conditions or CCC's Billing and Payment terms and conditions. These terms and conditions, together with CCC's Billing and Payment terms and conditions (which are incorporated herein), comprise the entire agreement between you and publisher (and CCC) concerning this licensing transaction. In the event of any conflict between your obligations established by these terms and conditions and those established by CCC's Billing and Payment terms and conditions, these terms and conditions shall control.

14. Revocation: Elsevier or Copyright Clearance Center may deny the permissions described in this License at their sole discretion, for any reason or no reason, with a full refund payable to you. Notice of such denial will be made using the contact information provided by you. Failure to receive such notice will not alter or invalidate the denial. In no event will Elsevier or Copyright Clearance Center be responsible or liable for any costs, expenses or damage incurred by you as a result of a denial of your permission request, other than a refund of the amount(s) paid by you to Elsevier and/or Copyright Clearance Center for denied permissions.

#### **LIMITED LICENSE**

The following terms and conditions apply only to specific license types:

15. **Translation:** This permission is granted for non-exclusive world **English** rights only unless your license was granted for translation rights. If you licensed translation rights you may only translate this content into the languages you requested. A professional translator must perform all translations and reproduce the content word for word preserving the integrity of the article. If this license is to re-use 1 or 2 figures then permission is granted for non-exclusive world rights in all languages.

16. **Website:** The following terms and conditions apply to electronic reserve and author websites:

**Electronic reserve:** If licensed material is to be posted to website, the web site is to be password-protected and made available only to bona fide students registered on a relevant course if:

This license was made in connection with a course,

This permission is granted for 1 year only. You may obtain a license for future website posting,

All content posted to the web site must maintain the copyright information line on the bottom of each image,

A hyper-text must be included to the Homepage of the journal from which you are licensing at <http://www.sciencedirect.com/science/journal/xxxxx> or the Elsevier homepage for books at <http://www.elsevier.com> , and

Central Storage: This license does not include permission for a scanned version of the material to be stored in a central repository such as that provided by Heron/XanEdu.

17. **Author website** for journals with the following additional clauses:

All content posted to the web site must maintain the copyright information line on the bottom of each image, and

the permission granted is limited to the personal version of your paper. You are not allowed to download and post the published electronic version of your article (whether PDF or HTML, proof or final version), nor may you scan the printed edition to create an electronic version,

A hyper-text must be included to the Homepage of the journal from which you are licensing at <http://www.sciencedirect.com/science/journal/xxxxx> , As part of our normal production process, you will receive an e-mail notice when your article appears on Elsevier's online service ScienceDirect (www.sciencedirect.com). That e-mail will include the article's Digital Object Identifier (DOI). This number provides the electronic link to the published article and should be included in the posting of your personal version. We ask that you wait until you receive this e-mail and have the DOI to do any posting.

Central Storage: This license does not include permission for a scanned version of the material to be stored in a central repository such as that provided by Heron/XanEdu.

18. **Author website** for books with the following additional clauses:

Authors are permitted to place a brief summary of their work online only.

A hyper-text must be included to the Elsevier homepage at <http://www.elsevier.com>

All content posted to the web site must maintain the copyright information line on the bottom of each image

You are not allowed to download and post the published electronic version of your chapter, nor may you scan the printed edition to create an electronic version.

Central Storage: This license does not include permission for a scanned version of the

material to be stored in a central repository such as that provided by Heron/XanEdu.

19. **Website** (regular and for author): A hyper-text must be included to the Homepage of the journal from which you are licensing at <http://www.sciencedirect.com/science/journal/xxxxx>. or for books to the Elsevier homepage at <http://www.elsevier.com>

20. **Thesis/Dissertation**: If your license is for use in a thesis/dissertation your thesis may be submitted to your institution in either print or electronic form. Should your thesis be published commercially, please reapply for permission. These requirements include permission for the Library and Archives of Canada to supply single copies, on demand, of the complete thesis and include permission for UMI to supply single copies, on demand, of the complete thesis. Should your thesis be published commercially, please reapply for permission.

21. **Other Conditions**:

v1.6

**If you would like to pay for this license now, please remit this license along with your payment made payable to "COPYRIGHT CLEARANCE CENTER" otherwise you will be invoiced within 48 hours of the license date. Payment should be in the form of a check or money order referencing your account number and this invoice number RLNK500789777.**

**Once you receive your invoice for this order, you may pay your invoice by credit card. Please follow instructions provided at that time.**

**Make Payment To:**  
Copyright Clearance Center  
Dept 001  
P.O. Box 843006  
Boston, MA 02284-3006

**For suggestions or comments regarding this order, contact RightsLink Customer Support: [customercare@copyright.com](mailto:customercare@copyright.com) or +1-877-622-5543 (toll free in the US) or +1-978-646-2777.**

**Gratis licenses (referencing \$0 in the Total field) are free. Please retain this printable license for your reference. No payment is required.**

---

---

Chapter-3 copyright permission:



International Journal of Hydrogen Energy

5794 SW 40<sup>th</sup> St. # 303, Miami, FL 33155, U.S.A.



31 May 2012

To: Pankaj Chowdhury [REDACTED]

Cc: Emre A. Veziroglu [REDACTED]

Subject: Copyright Permission

Dear Pankaj:

Thank you very much for your email of 31 May 2012. In accordance with your request, we hereby give you permission to reuse the following article in your Thesis/Dissertation:

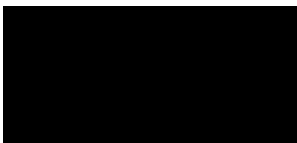
Title: Factorial design analysis for dye-sensitized hydrogen generation from water

Author: Pankaj Chowdhury et al

Source: International Journal of Hydrogen Energy, Volume 36, Issue 21, October 2011, Pages 13442–13451.

Wishing you all the best in your endeavors, I remain

Sincerely yours,



T. Nejat Veziroglu

Founding Editor-in-Chief, International Journal of Hydrogen Energy

Chapter-6 copyright permission:



RightsLink®

Home

Account  
Info

Help



ACS Publications  
High quality. High impact.

**Title:** Visible-Solar-Light-Driven  
Photocatalytic Degradation of  
Phenol with Dye-Sensitized TiO<sub>2</sub>:  
Parametric and Kinetic Study

Logged in as:  
PANKAJ CHOWDHURY  
Account #:  
3000538883

**Author:** Pankaj Chowdhury, Jesus  
Moreira, Hassan Gomaa, and  
Ajay K. Ray

LOGOUT

**Publication:** Industrial & Engineering  
Chemistry Research

**Publisher:** American Chemical Society

**Date:** Mar 1, 2012

Copyright © 2012, American Chemical Society

#### PERMISSION/LICENSE IS GRANTED FOR YOUR ORDER AT NO CHARGE

This type of permission/license, instead of the standard Terms & Conditions, is sent to you because no fee is being charged for your order. Please note the following:

- Permission is granted for your request in both print and electronic formats, and translations.
- If figures and/or tables were requested, they may be adapted or used in part.
- Please print this page for your records and send a copy of it to your publisher/graduate school.
- Appropriate credit for the requested material should be given as follows: "Reprinted (adapted) with permission from (COMPLETE REFERENCE CITATION). Copyright (YEAR) American Chemical Society." Insert appropriate information in place of the capitalized words.
- One-time permission is granted only for the use specified in your request. No additional uses are granted (such as derivative works or other editions). For any other uses, please submit a new request.

BACK

CLOSE WINDOW

Copyright © 2012 [Copyright Clearance Center, Inc.](#) All Rights Reserved. [Privacy statement.](#)  
Comments? We would like to hear from you. E-mail us at [customer@copyright.com](mailto:customer@copyright.com)

# Curriculum Vitae

## **PANKAJ CHOWDHURY**

### **Education**

**2012      PhD, Chemical Engineering**

The University of Western Ontario, London, ON, Canada.

Thesis: Solar and Visible Light Driven Photocatalysis for Sacrificial Hydrogen Generation and Water Detoxification with Chemically Modified TiO<sub>2</sub>.

**2004      Master of Technology, Chemical Engineering**

(Specialization in Petrochemicals and Refinery Engineering)

University of Calcutta, Kolkata, India.

**2002      Bachelor of Technology, Chemical Engineering**

University of Calcutta, Kolkata, India.

**1999      Bachelor of Science, Chemistry**

University of Calcutta, Kolkata, India.

### **Research and Professional Experience**

**2008 - 2012      NSERC Fellow and Graduate Research/Teaching Assistant**

Department of Chemical and Biochemical Engineering

The University of Western Ontario, London, ON, Canada.

**2007 - 2008      Graduate Research Assistant/Teaching Assistant**

Department of Environmental System Engineering

University of Regina, Regina, SK, Canada

**2004 - 2006      Research Engineer (Chemical and Environmental Engineering Division).**

Ballarpur Industries Ltd, Research and Development Centre, Gurgaon, India.

### Articles Published in Refereed Journals

- ❑ **Chowdhury, P.**, Moreira, J., Gomaa, H., Ray, A. K. (2012) Visible solar light driven photocatalytic degradation of phenol with dye-sensitized TiO<sub>2</sub>: parametric and kinetic study. *Industrial & Engineering Chemistry Research* 51 (12): 4523-4532. (Impact Factor: 2.237) (Cited in Scopus (1)).
- ❑ **Chowdhury, P.**, Gomaa, H., Ray, A. K. (2011) Factorial design analysis for dye-sensitized hydrogen generation from water. *International Journal of hydrogen Energy*. 36(21): 13442-13451. (Impact Factor: 4.053).
- ❑ **Chowdhury, P.**, Viraraghavan, T., Srinivasan, A. (2010) Biological treatment processes for fish processing wastewater – A review. *Bioresource Technology*. 101(2): 439-449. (Impact Factor: 4.365) (Cited in Scopus (6)).
- ❑ **Chowdhury, P.**, Viraraghavan, T. (2009) Sonochemical degradation of chlorinated organic compounds, phenolic compounds and organic dyes – A review. *Science of the Total Environment*. 407(8): 2474-2492. (Impact Factor: 2.905) (Cited in Scopus (24)).
- ❑ Naiya, T. K., **Chowdhury, P.**, Bhattacharya, A. K., Das, S. K. (2009) Saw dust and neem bark as low-cost natural biosorbent for adsorptive removal of Zn(II) and Cd(II) ions from aqueous solutions. *Chemical Engineering Journal*. 148(1): 68-79. (Impact Factor: 2.816) (Cited in Scopus (25)).
- ❑ Srinivasan, A., **Chowdhury, P.**, Viraraghavan, T. (2008) AIR STRIPPING IN INDUSTRIAL WASTEWATER TREATMENT, in Water and Wastewater Technologies, [Ed. Saravanamuthu (Vigi) Vigneswaran], in *Encyclopedia of Life Support Systems (EOLSS)*, Development under the Auspices of the UNESCO, Eolss Publishers, UK, [<http://www.eolss.net>].
- ❑ **Chowdhury, P.**, Gupta, P., Kumar, M., Bajpai, P. K., Varadhan, R. (2005) Study on Improving the Opacity of Paper Using Adjunct Filler Pigments. *IPPTA Journal*. 17(3): 57-62.



## Refereed Conference Proceedings

- ❑ **Chowdhury, P.**, Gomaa, H., Ray, A. K. Dye-sensitized photocatalyst – a breakthrough in green energy and environmental applications. AIChE annual conference, October 2011, Minneapolis, USA.
- ❑ **Chowdhury, P.**, Gomaa, H., Ray, A. K. Dyesensitized visible light photocatalysis for hydrogen production at 8<sup>th</sup> World Congress of Chemical Engineering, August 2009, Montreal, Canada.
- ❑ Viraraghavan, T., **Chowdhury, P.**, Recent Trends in Arsenic Removal Technologies at 2007 International Symposium on Environmental Science and Technology, November 2007, Beijing, China.

## Conference Presentations (non-refereed contribution)

- ❑ **Chowdhury, P.**, Gomaa, H., Ray, A. K. Behaviour of dye-sensitized photocatalyst under visible and solar radiation – A comparative study for hydrogen generation. 61<sup>st</sup> Canadian Conference of Chemical Engineering (CSCHE), October 2011, London, Canada.
- ❑ **Chowdhury, P.**, Gomaa, H., Ray, A. K. Solar hydrogen production via dye-sensitized photocatalysis. OCE Discovery conference, May 2011, Toronto, Canada.
- ❑ Ray, A. K., **Chowdhury, P.**, Gomaa, H. Hydrogen by water splitting from dye-sensitized photocatalysis. 60<sup>th</sup> Canadian Conference of Chemical Engineering (CSCHE), October 2010, Saskatoon, Canada.
- ❑ Chakrabarti, S. K., **Chowdhury, P.**, Chauhan, V. S. Understanding Surface Characteristics and Surface Chemistry for Printing Properties of Paper. Seminar on emerging application on surface science, November 2005, IIT Delhi, India.
- ❑ **Chowdhury, P.**, Gupta, P., Kumar, M., Bajpai, P. K., Varadhan, R. Study on Improving the Opacity of Paper Using Adjunct Filler Pigments. IPPTA Zonal Seminar, July 2005, Ahmedabad, India.
- ❑ **Chowdhury, P.**, Bhattacharya, A. K., Mandol, S. N. and Das, S. K. Removal of Zn(II) from wastewater using natural and synthetic adsorbents. First joint meeting of Indian Institute of Chemical Engineers (IICHe) and American Institute of Chemical Engineers (AIChE) (CHEMCON-2004), December 2004, Mumbai.

### **Poster Presentations (non-refereed contribution)**

- ❑ **Chowdhury, P.**, Malekshoar, G., Andalib, M., Ray, M., Zhu, J., Ray, A. K. Photocatalytic hydrogen production & water treatment under visible and solar light. OCE Discovery conference, May 2011, Toronto, Canada.
- ❑ **Chowdhury, P.**, Moreira, J., Ray, A. K., Gooma, H. Application of dye-sensitized photocatalyst in environmental detoxification. Water Innovation Forum: A competitive and Innovative Agricultural Sector, January 2011, London, Canada.

### **Scholarship and Awards**

- ❑ NSERC PDF 2012-2014.
- ❑ NSERC PGS D 2010-2012.
- ❑ Ontario Graduate Scholarship 2010 (declined)

### **Relevant Activities**

- ❑ Organized the 2nd annual Particle Technology Research Centre Conference (PTRC) held on July 9 - 10, 2009 and our departmental graduate symposium during May 2010 at The University of Western Ontario.
- ❑ Worked as editor for our graduate news letter for two terms.
- ❑ Worked as steward (2010-11) and served in TANB committee at GTA union, at The University of Western Ontario.
- ❑ Volunteered in organizing fund raising program for Myanmar disaster - May 2008 at University of Regina with Indian Student Association, University of Regina and Canadian Red Cross.
- ❑ Member of Indian Graduate Student Association at University of Western Ontario, London, ON.